Cortical Reorganisation and Tinnitus Following Restricted Peripheral Deafferentation in the Ferret: Targeting Neural Plasticity by Optogenetic Silencing



Joshua R Gold, B.Sc.

Merton College, University of Oxford

A thesis submitted for the degree of

Doctor of Philosophy

Michaelmas, 2015

For my family.

Cortical Reorganisation and Tinnitus Following Restricted Peripheral Deafferentation in the Ferret: Targeting Neural Plasticity by Optogenetic Silencing

Joshua R Gold, B.Sc.

Merton College, University of Oxford

A thesis submitted for the degree of Doctor of Philosophy

Michaelmas, 2015

Subjective tinnitus is the perception of a sound in the absence of an environmental source, and is thought to derive from maladaptive neuroplasticity that occurs following hearing impairment. However, the underlying structural and functional mechanisms remain unresolved. Our aims were thus to develop a model of trauma-induced tinnitus, and to investigate whether primary auditory cortex played a causal role.

We tested ferrets on a gap-in-noise detection task to assess auditory temporal processing, which is impaired in tinnitus and hearing loss. Ferrets displayed robust gap-detection performance, with sensitivity that varied with the frequency content and bandwidth of the acoustic carrier noise, as we also found in human subjects tested on a comparable task. This confirmed the ferret as a relevant model of auditory temporal processing.

To investigate hearing-loss-related neuroplasticity, ferrets underwent a partial, unilateral lesion of the spiral ganglion (SG), replicating aspects of otopathology described in tinnitus. Behaviourally, this lesion induced heterogeneous outcomes, with some ferrets displaying temporal processing impairments, and others showing post-lesion adaptation. These behavioural outcomes correlated with features of the auditory brainstem response, indicating a possible predisposition towards adaptation/maladaptation. Anatomical and physiological analysis of auditory cortical cells showed evidence for lesion-related central neuroplasticity that correlated with each animal's behavioural phenotype.

We finally sought to determine whether these cortical changes underpinned the behavioural changes described. The optogenetic protein Archaerhodopsin-T was expressed bilaterally in auditory cortical neurons of SG-lesioned ferrets, allowing suppression of neural spiking during behaviour. Only contralesional suppression mediated any substantive behavioural effects, improving the performance of animals with temporal processing impairments, and impairing performance in animals with post-lesion improvements. The mechanistic basis for these effects was shown, through physiological recordings, to derive from optogenetic enhancements in cortical temporal processing.

Together, these results suggest that primary auditory cortex plays an important role in mediating deafferentation-related neuroplasticity, suggesting possible strategies for remediation of the maladaptive processing potentially underpinning tinnitus in humans.

Acknowledgements

I would first and foremost like to thank my supervisors, Professors Victoria Bajo and Andrew King. Throughout this project, both have provided immeasurable support and guidance, for which I am endlessly grateful. Andy, for his careful eye and exceptional judgement, and from whom I could always expect a precision and clarity of thought I had not thought possible. Vicky, as the driving force behind this project, for her boundless energy, magnificent expertise, and remarkable patience, each of which I have benefited from during my time at Oxford, and for whom have the utmost respect and gratitude.

For his experimental wizardry and knowledge, I wish to thank Dr Fernando Nodal, without whom the work described here would not have been possible.

I wish to thank those who contributed to ferret behavioural testing: Vicky, Fernando, Dr Amy Hammond-Kenny, Dr Peter Keating, Daniel Kumpik, Fabien Peters, and Susan Spires. They each appreciate the struggles involved in the running of the ferrets, and without their involvement this project would have been unending.

Also, my thanks go to the Auditory Neuroscience Group as a whole. The quality of discussion and company was insuperable. In particular, I wish to thank my office-mates over the last few years, Dr Johannes Dahmen, Dr Peter Keating, Daniel Kumpik, and Sebastian Vasquez-Lopez, for some wonderful conversations and ideas, both intellectual and less so.

I am indebted to Action on Hearing Loss for awarding a studentship (S72_Bajo) that allowed me to undertake the work described in this thesis.

Finally, I must thank my family: my sister, Lucy, and my parents, Linda and Julian. Their love and support have been unlimited, and without them I would not have made it this far.

Contributions

Chapter 1

Portions of this chapter were previously published as *Gold JR, Bajo VM (2014) Insult-induced adaptive plasticity of the auditory system. Frontiers in Neuroscience, 8:1–31; doi: 10.3389/fnins.2014.00110.*

Chapter 2

Ferret Gap-in-Noise Detection: Hardware installed by Fernando Nodal (FN). Software written by FN and Peter Keating (PK). Behavioural training performed by Victoria Bajo (VB), Joshua Gold (JG), FN, Fabien Peters (FP), and Susan Spires (SS). Behavioural testing performed by VB, JG, Amy Hammond-Kenny (AHK), PK, Daniel Kumpik (DK), FN, FP, and SS.

Human Gap-in-Noise Detection: Hardware installed by JG and FN. Software adapted from ferret gap-detection paradigm by JG, DK, and FN. Testing conducted by VB, JG, and FN.

Auditory Brainstem Responses: Stimuli designed by JG, FP, and Jan Schnupp. Pilot data collected by FP and JG (not included in thesis). Thesis data collected by JG.

Lesion of the Spiral Ganglion: Surgeries performed by VB, JG, and FN. *Post mortem* cochleae removal performed by VB and JG. Histological processing and quantification of cochleae performed by David Furness (DF) (Keele University).

Optogenetic Implantation and Silencing of the Primary Auditory Cortex: Surgeries performed by VB, JG, and FN. Optogenetic viral vector constructs provided by Edward Boyden (Massachusetts Institute of Technology), and manufactured by UNC Vectorcore. Behavioural testing performed by VB, JG, AHK, FN, and SS.

Neurophysiological Recordings of Auditory Cortex: Surgeries and recordings performed by VB, JG, and FN. Stimuli designed by JG and FN.

Brain Anatomy: Perfusions, histological processing, and analysis and quantification performed by VB and JG.

Chapter 3

Data processing and analysis performed by JG, using MATLAB scripts written by JG and FN. Portions of this chapter were previously published as *Gold JR, Nodal FR, Peters F, King AJ, Bajo VM (2015) Auditory gap-in-noise detection behavior in ferrets and humans. Behavioral Neuroscience 129:473–490.*

Chapter 4

Data processing and analysis performed by JG. Fig.4-23(A, B) prepared by DF. Photomicrographs in Figs.4-24 to 4-29 prepared by VB.

Chapter 5

Data processing and analysis performed by JG. Fig.5-16 prepared by VB.

Table of Contents

1. General Introduction 1
1.1. Hearing Loss and the Mammalian Auditory System 1
1.2. Changes in Cochlear Function Following Peripheral Insult 7
1.3. Neurochemical and Structural Changes Induced by Auditory Damage 12
1.4. Changes in the Auditory Neuraxis 17
1.5. Insult-Mediated Changes in Neural Receptive Fields and Networks 27
1.6. The Functional and Behavioural Implications of Trauma-Driven Plasticity 34
1.7. Optogenetics and Manipulation of Brain Activity 39
1.8. Thesis Overview 41

2. Methods 44
Overview 44
2.1. Gap-in-Noise Detection Behaviour 47
2.2. Auditory Brainstem Responses (ABRs) 61
2.3. Lesion of the Spiral Ganglion 70
2.4. Optogenetic Implantation and Silencing of the Primary Auditory Cortex 74
2.5. Neurophysiological Recordings of Auditory Cortex 79
2.6. Brain Anatomy 90

3. Auditory Gap-in-Noise Detection Behaviour in Ferrets and Humans 93
3.1. Introduction 93
3.2. Results 97
3.3. Discussion 126

4. Behavioural and Physiological Effects of Lesioning the Ferret Spiral Ganglion – A Possible Model of Tinnitus? 134
4.1. Introduction 134
4.2. Results 138
4.3. Discussion 200

5. Optogenetic Silencing of the Ferret Auditory Cortex 221
5.1. Introduction 221
5.2. Results 225

5.3. Discussion 256

6. Discussion and Future Directions 265
6.1. Overview 265
6.2. Summary of Chapter Contents 267
6.3. Ongoing Work 271
6.4. Future Directions 273

A. Appendix 284

Bibliography 290

Abbreviations

I-VI: Cortical layers 1 - 6

A1: Primary Auditory Cortex

AAF: Anterior Auditory Field

ABR: Auditory Brainstem Response

AC: Auditory Cortex

ADF: Anterior Dorsal Field

AEG: Anterior Ectosylvian Gyrus

ANF: Auditory Nerve Fibre

ArchT: Archaerhodopsin-T

aROC: Area under ROC

AS: Ansinate Sulcus

ASG: Anterior Sigmoid Gyrus

AVF: Anterior Ventral Field

BBN: Broad Band Noise

BF: Best Frequency

BM: Basilar Membrane

C: Control animals

CAP: Compound Action Potential

CF: Characteristic Frequency

Cl/Cls: Claustrum

crs: Cruciate sulcus

D: Dorsal

DBS: Deep Brain Stimulation

DCIC: Dorsal Cortex of the IC

DCN: Dorsal Cochlear Nucleus

DPOAE: Distortion Product Oto-Acoustic Emission

DPSS: Diode-Pumped Solid State (Laser)

ec: Extracellular

ECoG: Electrocorticography

FRA: Frequency Response Area

GFP: Green Fluorescent Protein

HP: Hippocampus

I: Impaired animals

IC: Inferior Colliculus

ic: Intracellular

IEG: Immediate Early Gene

IHC: Inner Hair Cell

L: Lateral

LG: Lateral Gyrus

LGN: Lateral Geniculate Nucleus

LL: Lateral Lemniscus

LME: Linear Mixed Effects Statistical Model

MEG: Middle Ectosylvian Gyrus

MI: Mutual Information

MGB: Medial Geniculate Body

MRS: Magnetic Resonance Spectroscopy

MS: Medial Septum

NADPHd: reduced Nicotinamide Adenine Dinucleotide Phosphate diaphorase

NB: Nucleus Basalis

NBN: Narrow Band Noise

NeuN: Neuronal nuclear protein

NI: Not-Impaired animals

(n)NOS: (neuronal) Nitric Oxide Synthase

O: Onset Response

OB: Olfactory Bulb

OBG: Orbital Gyrus

OHC: Outer Hair Cell

P: Posterior

PAG: Periaqueductal Grey

PB: Phosphate Buffer

PBS: Phosphate-Buffered Saline

PEG: Posterior Ectosylvian Gyrus

PPF: Posterior Pseudosylvian Field

prs: Presylvian Sulcus

PS: Post-Stimulus Response

PSF: Posterior Suprasylvian Field

PSG: Posterior Sigmoid Gyrus

pss: Pseudosylvian Sulcus

PSTH: Peri-Stimulus Time Histogram

R: Right

Rf: Rhinal fissure

RI: Residual Inhibition

RLF: Rate Level Function

RMS: Root Mean Square

ROC: Receiver Operating Characteristic

RS: Residual Suppression

S: Sustained Response

S: Section number

SC: Superior Colliculus

SDT: Signal Detection Theory

SFR: Spontaneous Firing Rate

SG: Spiral Ganglion; SGC: SG Cell

SNR: Signal-to-Noise Ratio

SOC: Superior Olivary Complex

SSG: SupraSylvian Gyrus

sss: Suprasylvian Sulcus

STN: Sub-Thalamic Nucleus

Str: Striatum

tDCS: transcranial Direct Current Stimulation

V: Ventral

VCN: Ventral Cochlear Nucleus

VP: Ventral Posterior (Area)

Chapter 1

General Introduction

1.1 Hearing Loss and the Mammalian Auditory System

The adult mammalian auditory system displays a remarkable degree of plasticity, manifesting as changes in the central representation of sounds. Modulatory processes in the adult auditory brain are crucial in the performance and learning of ethologically relevant behaviours (Froemke and Martins, 2011; King et al., 2011), and are differentially affected during active and passive listening (Pienkowski and Eggermont, 2011). The changes observed in different contexts typically facilitate behavioural adaptation – for example, mammals may preferentially use monaural spectral cues during sound localisation, if raised with a sporadic conductive hearing loss (Keating et al., 2013, 2015). However, as previously reviewed (Salvi et al., 2000; Syka, 2002; Gold and Bajo, 2014), the changes that develop following a sensorineural

auditory insult may represent a unique assemblage, specific to damaged sensory input.

Hearing loss poses a significant burden to healthcare services globally, with the rate of hearing impairment approaching ~40% in older adult populations (Agrawal et al., 2008; Nondahl et al., 2011). This age-related hearing loss, or presbycusis, typically impairs sufferers' hearing for high frequency sounds, in both ears, with the predominant lesion affecting the stria vascularis and/or the auditory nerve (Schuknecht and Gacek, 1993). Aetiologically, the causes of presbycusis are certainly complex, though noise trauma early in life can exacerbate the risk of developing presbycusis (Kujawa and Liberman, 2006); concordantly, rates of insult-induced hearing impairment appear to be climbing among younger cohorts (Niskar et al., 2001). These epidemiological observations behove the investigation of the underlying mechanisms that might be responsible for the peripheral and central changes affecting normal auditory processing, which in day-to-day life can substantial impair speech perception and auditory scene analysis, for example.

A link between auditory disruption and tinnitus has long been appreciated (e.g. Axelsson and Sandh, 1985). Recently, suggestions that maladaptive neuroplasticity may be responsible for tinnitus, especially when no audiometric hearing loss is identifiable (Schaette and McAlpine, 2011), has sparked interest in the condition (Eggermont and Roberts, 2004). The instantiation of tinnitus represents a problem: both for its human sufferers, substantially decreasing quality of life in some patients (Lewis et al., 1994), since few effective treatments are available (Baguley et al., 2013; Langguth et al., 2013); but also for researchers investigating its underpinning

neurobiology, since little consensus has been reached about what induces and maintains tinnitus chronically (Kaltenbach, 2011; Knipper et al., 2013; Noreña and Farley, 2013; Roberts et al., 2013).

Herein this thesis finds its focus – to investigate how the brain responds to peripheral trauma in a behaviourally relevant fashion, and how to address the maladaptive neural processing that may underlie tinnitus, through targeted intervention in auditory brain regions effecting this abnormal neural activity. Much of the work described henceforth focuses upon activity in auditory cortex (AC), although there is a clear role for the auditory periphery and subcortical auditory system in the changes that take place following peripheral insult.

1.1.1 Overview of the mammalian auditory system

The mammalian auditory system is a marvel of biological function, capable of transducing small pressure fluctuations in the air into electrical signals that, ultimately, are interpreted sounds in our environment, physically characterised by particular frequencies and amplitudes, and perceived as varying in pitch, timbre, location, etc. (Schnupp et al., 2011). Prior to exploring how this system is affected by trauma, we shall provide a brief overview of its structure and function.

Functionally, the ear collects sound waves and directs them towards the point at which they can be converted into neuronal signals. The outer ear, or pinna, corrals sounds into the ear canal, inducing vibrations at the tympanic membrane, which in turn yield corresponding vibrations at cochlear oval window membrane, by way of the middle ear ossicles. At the oval window membrane's inner face, these vibrations

establish pressure variations in the fluid (perilymph)-filled chambers of the cochlear coil. The release of these pressure variations, via corresponding vibrations at the cochlear round window, necessitates the creation of longitudinal, travelling waves in the basilar membrane (BM), a tissue structure that subdivides the cochlea into upper and lower compartments. There is a basal-to-apical decrement in the BM's stiffness alongside a progressive increment in width, combined with an apical-to-basal inertial gradient in the cochlear perilymph. Thus, acoustic waveforms undergo a frequency decomposition along the cochlea's length, with different frequencies causing maximal vibrations at different locations logarithmically scaled along the BM's length (a so-called tonotopic organisation).

These vibrations are transduced into electrical signals by the cochlear hair cells (HCs), of which two kinds are present in mammals: inner (IHCs), and outer (OHCs), named according to their location in the organ of Corti relative to the cochlear modiolus. The vibrating BM, effecting up-and-down motions in the tonotopically appropriate HC population, leads to the back-and-forth movement of the HC stereocilia (Fig.1.1). This motion modulates the flow of K^+ cations down an electrical gradient into the HC (Schnupp et al., 2011). The accompanying depolarisation facilitates the release of glutamate from the IHC ribbon synapse, and so the afferent transmission of acoustic information in type-I auditory nerve fibres (ANFs). Membrane potential changes in OHCs, by contrast, engage a voltage-sensitive membrane-bound actuator protein called prestin, which is responsible for gain changes being imposed on the mechanical properties of the BM (Oliver et al., 2001). The corresponding type-II ANF population, albeit of lower density, and upon which OHCs synapse, putatively encode "auditory pain" information during exposure to

tissue-damaging noise (Flores et al., 2015). Both IHCs and OHCs, while exquisitely sensitive to sound-induced vibration of the BM, are also terribly fragile, and easily subject to damage.

Upon entering the brainstem by way of the spiral ganglion, ANFs make obligate synapses within the cochlear nucleus (CN), a lateral brainstem structure possessing two major divisions. The ventral cochlear nucleus (VCN) contains cells with a variety of response properties, projecting onwards predominantly to the superior olivary complex (SOC) (Schnupp et al., 2011). The dorsal cochlear nucleus (DCN), by contrast, possesses a cerebellar-like trilaminar structure, in which both auditory and non-auditory inputs are integrated and subject to synaptic plasticity (Oertel and Young, 2004; Tzounopoulos et al., 2004). Within the DCN, synapses are formed on projection cells from somatosensory and auditory sources (Shore and Zhou, 2006). Multisensory integration permits the modulation of auditory responses according to the mode of somatosensory input (Shore and Zhou, 2006): for example, rotation of the pinna and head can affect auditory receptive field properties (Young et al., 1995). The DCN sends outputs directly to the contralateral inferior colliculus (IC), containing multisensory-derived information (Jain and Shore, 2006).

From SOC, which receives information from both ears, and the dorsal and ventral nuclei of the lateral lemniscus (LL) and onwards to IC, projections are observed to follow two major routes. Outputs from the external nucleus and nucleus of the brachium of the IC enter the superior colliculus (SC), wherein a laminated structure contains multisensory representations of feature space in the organism's environment (Palmer and King, 1982; King, 2004). A large proportion of the IC's

outputs project rostrally to the medial geniculate body of the thalamus (MGB), a primary waypoint for projections to higher centres. The importance of the MGB is derived from its capacity to gate auditory information outflow towards AC (Banks and Smith, 2011). The outputs of MGB exist both as "core-type" thalamocortical fibres with narrowly frequency-tuned projections to primary fields of AC, from the ventral MGB; and as projections more broadly to both auditory and non-auditory regions of the telencephalon (e.g. lateral amygdala (Doron and LeDoux, 1999)) from the medial and dorsal divisions of MGB, which enter AC in layers I and V/VI in a "broad-brush" fashion (Harris and Shepherd, 2015).

The input profile of AC is largely consistent with other sensory cortices, displaying substantial thalamocortical inputs into layer IV, which houses a large population of intratelencephalic projection neurons that extend ipsilateral axonal arbours elsewhere in the forebrain (Harris and Shepherd, 2015) – by contrast, callosal projections are derived primarily from layers III and V (Fame et al., 2011). AC is notable for its apparent lack of canonical excitatory spiny stellate cells in layer IV, suggesting its intrinsic microcircuitry may differ from the better-studied somatosensory and visual cortices. AC also possesses large efferent projection cells within layer Vb, which send axons via the pyramidal tract to influence activity in the midbrain and brainstem. These projection neurons are integral in the adaptation of the mature auditory system to altered auditory space cues (Bajo et al., 2010b; Bajo and King, 2012). Layer V neurons also supply feedforward projections to MGB, predominantly the dorsal compartment (Rouiller and Welker, 1991). Efferent corticothalamic tracts originating in layer VI, terminate reciprocally within thalamic domains that gave rise to afferent projections within the same cortical column. These

corticothalamic projection neurons receive few thalamic or local inputs, instead gaining much of their excitatory drive from long-range higher-order synapses.

The functional architecture of AC fields in the ferret (*Mustelid putorius furo*) have been characterised over recent years. Mapping studies throughout the ectosylvian gyrus (EG) have identified the middle division (MEG) as the site of the core AC fields (primary, A1; and anterior auditory field, AAF) (Nelken et al., 2004; Bizley et al., 2005), organised tonotopically along the ventrorostral-dorsocaudal axis of MEG. A less clear tonotopy is seen in posterior fields within the posterior ectosylvian gyrus (posterior pseudosylvian, PPF; and posterior suprasylvian, PSF), corresponding in part with their putative higher-order computational function, and the frequency-specific intratelencephalic projections received therein from A1 (Bizley et al., 2015). In contrast, little-to-no tonotopic arrangement is seen in the major anterior field (anterior dorsal, ADF), which receives dispersed input from AAF, yet none from ventral MGB. A similar lack of tonotopy exists in fields AVF and VP, which are possibly homologous to belt/parabelt AC regions in other species. The higher AC regions of ferrets are proposed to mediate aspects of auditory cognition via connections with prefrontal cortical areas (Fritz et al., 2010; Atiani et al., 2014).

1.2 Changes in Cochlear Function Following Peripheral Insult

1.2.1 The anatomy of cochlear injury

The cochlear HC population, due to being located at the boundary between the peripheral and central auditory systems, is exquisitely sensitive to damage. Following an acutely induced acoustic overexposure (typically >100 dB SPL and >1 hr), the

degree of HC loss generally scales with the amplitude and duration of the insult. This usually manifests as extensive OHC death, with frequency-delimited loss of IHCs scaling with trauma severity (Spongr et al., 1992). Lesion patterns following similar exposure protocols are variable, however, with equivalent outer and inner hair cell degeneration (Dolan et al., 1975; Kiang et al., 1975), and consistent damage to basally-located OHCs and IHCs, occasionally observed regardless of the spectral content or duration of the acoustic trauma (Hawkins et al., 1976; Mulders et al., 2011).

Importantly, similarities have been observed between the effects of acute trauma and ageing. Age-related changes affect the cochlea in a stereotyped, multifactorial manner (Schuknecht, 1964; Schuknecht and Gacek, 1993; Ohlemiller, 2004), with the audiological features of presbycusis characterised by the pattern of cochlear pathology. According to Schuknecht, specific cochlear components/structures may undergo independent degradation, though ultimately these various pathologies appear to converge upon auditory neuropathy in the spiral ganglion (SG) (Keithley and Feldman, 1979; Cohen et al., 1990; Dazert et al., 1996; White et al., 2000; Engle et al., 2013; Viana et al., 2015). This common neuropathic endpoint, involving partial-to-complete peripheral deafferentation of HCs, is likely preceded by functional disturbance of the synaptic interface between SG afferents and IHCs (Stamataki et al., 2006; Sergeyenko et al., 2013).

Equivalent damage to the IHC-ANF interface has been observed in acute experimentally-induced hearing loss, with regions of IHC loss correlated with reactive swelling and peripheral deafferentation of an equivalent SG cell (SGC) population (Feng et al., 2012). The retraction of peripheral afferents following

trauma-mediated terminal swelling associates with disruption of the IHC ribbon synapse, a specialised glutamatergic structure necessary for synchronised auditory nerve activity (Buran et al., 2010). Under traumatic conditions, the ribbon synapse can cause an excitotoxic injury of ANFs (Puel et al., 1998; Pujol and Puel, 1999).

Ribbon synaptopathy may develop without overt IHC morphological disruption (Liu et al., 2013), and is possibly a predictable consequence of cochlear trauma (Rüttiger et al., 2013; Singer et al., 2013). Observations of ribbon synaptopathy following even mild acoustic overexposure (Maison et al., 2013) are compromising from a functional perspective, even if audiometric thresholds remain unchanged, since cochlear degeneration may have unwanted consequences at much later time points after the initial insult (Kujawa and Liberman, 2006, 2009; Sergeyenko et al., 2013; Viana et al., 2015) (Fig.1-1).

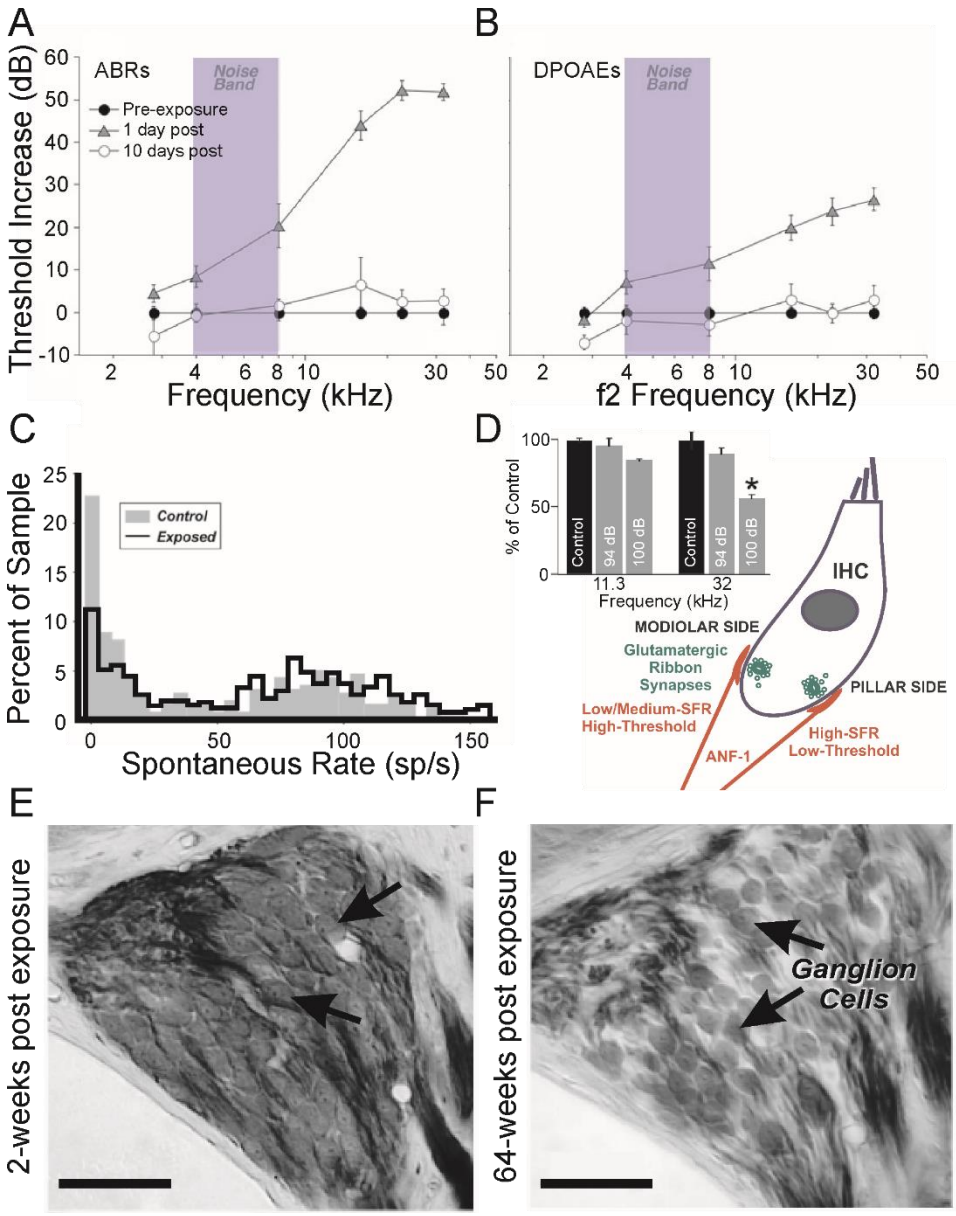

Figure 1-1: Peripheral Effects of Auditory Trauma. Peripheral thresholds measured using auditory brainstem responses (A) and distortion product otoacoustic emissions (B) following exposure to noise trauma (4-8 kHz, 106-109 dB SPL, 2h). Both are elevated 24 hrs following overexposure (triangles), however by >7 days thresholds have returned to normal (open circles). Modified with permission from Lin et al., (2011). C) The bimodal distribution of spontaneous rates in ANs of exposed animals shifts over a similar time course, leading to underrepresentation of trauma-affected type-1 auditory nerve fibres with spontaneous rates <20 spikes/second. Modified with permission from Furman et al. (2013). (D) These fibres synapse on the modiolar side of inner hair cells, and typically have a wide dynamic response range, allowing effective rate coding up to high stimulus intensities. In a mouse model of exposure (inset), high-threshold type-1 ANFs are reduced in the acoustic trauma region following traumatic exposure (8-16 kHz octave-band noise, 100 dB SPL), but not following a non-traumatic stimulus (94 dB SPL). Modified with permission from Hickox and Liberman, (2014). (E, F) Histological comparison between SG basal turns of mice in the short- (E) and long- (F) terms following trauma reveals that high-threshold response loss precipitates ongoing SGC apoptosis. Scale bars 50 μm. Modified with permission from Kujawa and Liberman, (2009).

1.2.2 The assessment and outcomes of peripheral trauma

Audiogram-based assessment is capable of detecting hearing loss defined in terms of OHC dysfunction and/or threshold elevation, and is used extensively to define the consequences of cochlear trauma in terms of "permanent" or "temporary" threshold shifts. Typically, this is via inspection of the auditory brainstem response (ABR) or ANF compound action potential (CAP), with distortion product otoacoustic emissions (DPOAEs) providing insight into OHC function. Despite their clinical utility, there is a concern regarding the reliance upon these tools exclusively. Long-term degeneration of SGCs develops in aged mice with intact IHCs and permanently raised ABR thresholds (Kujawa and Liberman, 2006); however, a type of insidious pathology has recently been characterised following an apparently limited, acute hearing loss, previously thought to have few ongoing peripheral ramifications (Fig.1-1).

Inspection of mouse cochleae without evidence of raised thresholds (on ABRs or DPOAEs), nor with any overt structural damage to OHC/IHC populations, revealed IHC-specific ribbon synaptopathy within 24 hours of acoustic trauma, manifesting as supra-threshold reductions in ABR amplitude at the affected cochleotopic frequencies (Kujawa and Liberman, 2009). Surprisingly, late-stage (>2 years) cochleography exposed ≤50% reduction of SGC density, regardless of the state of the organ of Corti. These findings were replicated in the guinea pig (Lin et al., 2011), and suggested to occur in humans (Viana et al., 2015), with experiments indicating that this "silent" afferent degeneration only affects ANFs encoding high-intensity stimuli (Furman et al., 2013), possibly underpinning the typical features of

presbycusis. Given the multifaceted peripheral sequelae of cochlear trauma, comprehensive evaluation of auditory afferent function must fully characterise the extent of cochlear pathology following auditory trauma, both clinically and experimentally (Ahlf et al., 2012; Dehmel et al., 2012a; Gu et al., 2012; Rüttiger et al., 2013; Lowe and Walton, 2015).

1.3 Neurochemical and Structural Changes Induced by Auditory Damage

1.3.1 Activity-related gene modulation

The expression of certain immediate early genes (IEGs), as a surrogate for neuronal metabolic state, has revealed time-varying modulation patterns in AC (Wallhäusser-Franke et al., 2003; Tan et al., 2007). Region-specific insult-induced changes in the expression of Arg3.1/Arc (activity-regulated gene/activity-regulated cytoskeleton-associated protein) have proved informative. Arg3.1/Arc mobilisation putatively occurs through brain-derived neurotrophic factor (BDNF)-mediated activation of the MEK-ERK signalling pathway (Ying et al., 2002). On examining the effects of acoustic trauma in the adult gerbil, Mahlke and Wallhäusser-Franke (2004) found that Arg3.1/Arc upregulation occurs in cortex only, with acoustic trauma yielding a non-layer-specific Arg3.1/Arc expression pattern in a tonotopically constrained manner, effectively matching the cochlear trauma profile.

More recently, trauma-exposed animals with demonstrable IHC ribbon synapse degradation were found to display Arg3.1/Arc mobilisation that was diminished, not enhanced (Tan et al., 2007; Rüttiger et al., 2013; Singer et al., 2013) (Fig.1-2). This bidirectional Arg3.1/Arc modulation is inversely correlated with the degree of BDNF

expression in the spiral ganglion, for periods spanning 3 hours to 6 days after acoustic exposure (Tan et al., 2007). In a similar experimental procedure, Arg3.1/Arc was downregulated in cerebral cortex for at least 14-30 days post-trauma (Rüttiger et al., 2013; Singer et al., 2013). Although the functional consequences of long-term up- or downregulation following auditory insults remain uncertain, Arg3.1/Arc is thought to play a key role in controlling AMPA-type glutamate receptor distribution during homeostatic plasticity (e.g. Shepherd et al., 2006; Bramham et al., 2010; Gao et al., 2010; Béïque et al., 2011).

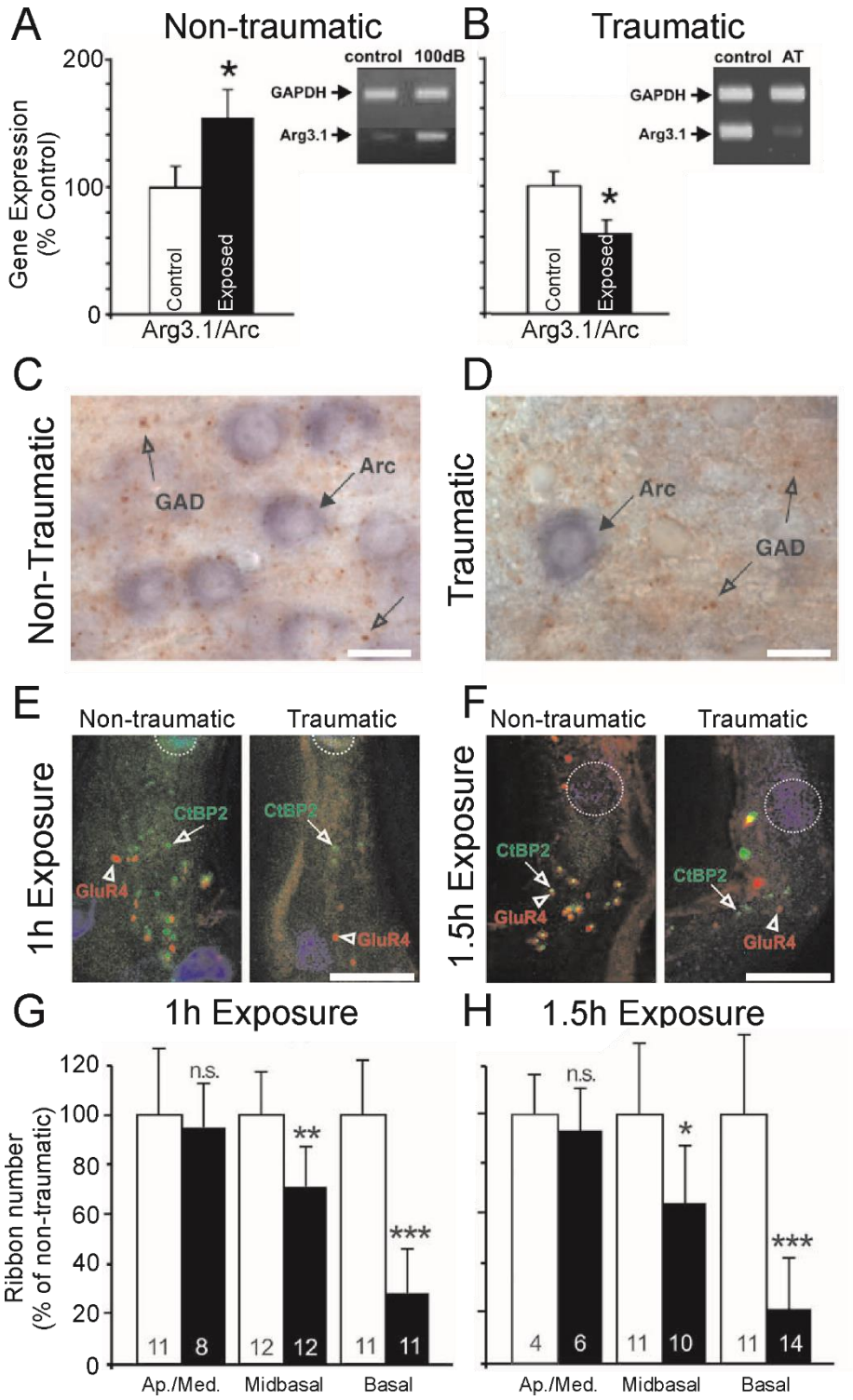

Figure 1-2: Changes in AC expression of Arg3.1/Arc and Cochlear Ribbon Synapse Density Related to the Degree of Acoustic Trauma. A) Following exposure to acoustic trauma that renders non-permanent threshold elevation (100 dB SPL, 2h), reverse-transcriptase polymerase chain reaction reveals Arg3.1/Arc is significantly upregulated in AC; (B) animals overexposed at 115-119dB SPL for 2h displayed downregulation of Arg3.1/Arc transcripts. Modified with permission from Tan et al., (2007). C, D) Immunohistochemical labelling of Arg3.1/Arc mRNA in AC of animals exposed to a

similar trauma (120 dB SPL, 2h). Glutamate decarboxylase puncta are also indicated. Modified with permission from Singer et al., (2013). Following acoustic overexposure for either (E) 1h or (F) 1.5h, staining for IHC ribbon synapses (CtBP2, green, open arrows) indicated a behaviourally-categorised subset of animals with reduction in ribbon synapse density, shown for the cochlear mid-basal turn. IHC nuclei are labelled with DAPI (blue, circled); glutamate receptor subunit GluR4 protein labelled (red, open arrowheads). Scale bars 10μm. G, H) For each exposure protocol, a subset of animals was categorised according to significant proportional reductions in midbasal and basal cochlear IHC ribbon synapse densities, relative to exposed animals without this pathology. Open bars = controls; filled bars = exposed. Numbers in each bar correspond to respective N. Modified with permission from Rüttiger et al., (2013).

1.3.2 Excitatory/Inhibitory signalling function

Given these changes in IEGs, significant alterations in glutamatergic function in AC might be expected after auditory insult. Changes in glutamatergic metabolism, however, have been well-documented only subcortically, such as the minor reduction of glutamate concentrations in MGB, IC and CN during presbycusis (Banay-Schwartz et al., 1989b). Cochlear ablation, by contrast, induces enhanced glutamate metabolism, as levels of glutamate and aspartate in CN correlate with the degree of cochlear damage (Godfrey et al., 2005, 2014). Work directed at such changes in the DCN has unveiled marked crossmodal reweighting: by assigning VGLUT subtypes 1 and 2 to auditory and non-auditory inputs, respectively (Zhou et al., 2007), Shore and colleagues revealed an upregulated representation of nonauditory afferents in the fusiform layer of DCN following cochlear trauma (Zeng et al., 2009, 2012).

By contrast, there is a better understanding of inhibitory changes which, alongside the reactive changes in glutamate release and signalling subcortically, may precipitate a disruption of excitatory/inhibitory homeostasis. Auditory insults affect inhibition early in the auditory pathway, failing to recover to pre-lesion levels in the AVCN (Hildebrandt et al., 2011). Similarly, reductions in the density of glycine-immunoreactive puncta (Asako et al., 2005) and glycine receptor subunit protein (Wang et al., 2009) have each been reported throughout CN. Such changes develop with altered strychnine binding and glycine metabolism in the ipsilateral CN and SOC (Suneja et al., 1998a, 1998b; Buras et al., 2006), suggestive of sustained post-deafening hyperexcitability (Potashner et al., 2000). Similarly, significant brainstem

inhibitory reductions have been reported in models of presbycusis (Banay-Schwartz et al., 1989a; Milbrandt et al., 1994).

Inhibitory disruptions, inducing disinhibitory effects, are well-described in the IC (reviewed in Caspary et al., 2008; Ouda and Syka, 2012), although comparable GABAergic dysregulation is seen cortically. GABA density reductions throughout AC appear to be co-determined by age and hearing loss, since GAD65 expression is reduced after acoustic trauma in younger adult animals (Yang et al., 2011). Despite the picture of post-traumatic auditory neurochemistry standing broadly incomplete, certain *characteristic* changes appear to occur regardless of insult type. An improved understanding of the neuropharmacological correlates of auditory trauma would be informative in the development of patient treatment regimens revolving around compensating for these changes (Schreiber et al., 2010; Mukherjea et al., 2011).

1.4 Changes in the Auditory Neuraxis

The neurochemical and molecular changes that develop after hearing loss, irrespective of its origin, appear to have a certain pattern that might be expected to impact upon activity within and throughout the auditory system and its encoding of acoustic stimuli. Therefore, we will examine the kinds of activity changes that develop at different levels of the auditory system.

1.4.1 Auditory Nerve Fibres

The activity of ANFs changes in response to various experimental insults. Under extremely damaging circumstances, some ANFs remain functionally normal, even if the likelihood of recording from an active fibre declines with the degree of IHC

damage (Wang et al., 1997). In such cases, functional normality is apparently contingent upon modification of the electrical properties of individual axons (Fryatt et al., 2011), and the survival of the OHC population. OHC survival, in particular, is necessary for maintaining sharp, low threshold tuning at the fibres' respective characteristic frequencies (CF) (the sound frequency at which the neuron responds at the lowest sound level presented) (Kiang et al., 1975; Dallos and Harris, 1978).

ANF response properties may be affected in other ways. By chronically monitoring the CAP for weeks, long term (≤5 weeks post-exposure) reductions in the maximum evoked CAP magnitude can be observed for chinchillas with selective IHC ablation (Qiu et al., 2000) (Fig.1-3). Since the CAP represents the summed activity of multiple fibres, reduction in the steepness (or gain) of the nerve's rate-level function (RLF) may ostensibly derive from either, or each, of two sources: a similar reduction in gain of the RLFs of individual fibres; or a graded loss of fibres, especially those encoding high-intensity sounds (Liberman, 1982; Taberner and Liberman, 2005).

By contrast, even with minimal cochlear trauma, such as that derived from an acoustically-induced "temporary" hearing loss, a frequency-selective deactivation of ANFs responsive up to high intensities may occur, causing a shift in the distribution of ensemble spontaneous activity toward higher firing rates (>20sp/s) (Furman et al., 2013) (Fig.1-1). This pattern of deafferentation has been associated with a depression in IHC ribbon synapse density, and also arises in presbycusis (Schmiedt et al., 1996). Thus, cochlear trauma is potentially linked with a degradation of high intensity coding (Wan et al., 2015), beginning at the level of the AN, despite possible threshold preservation.

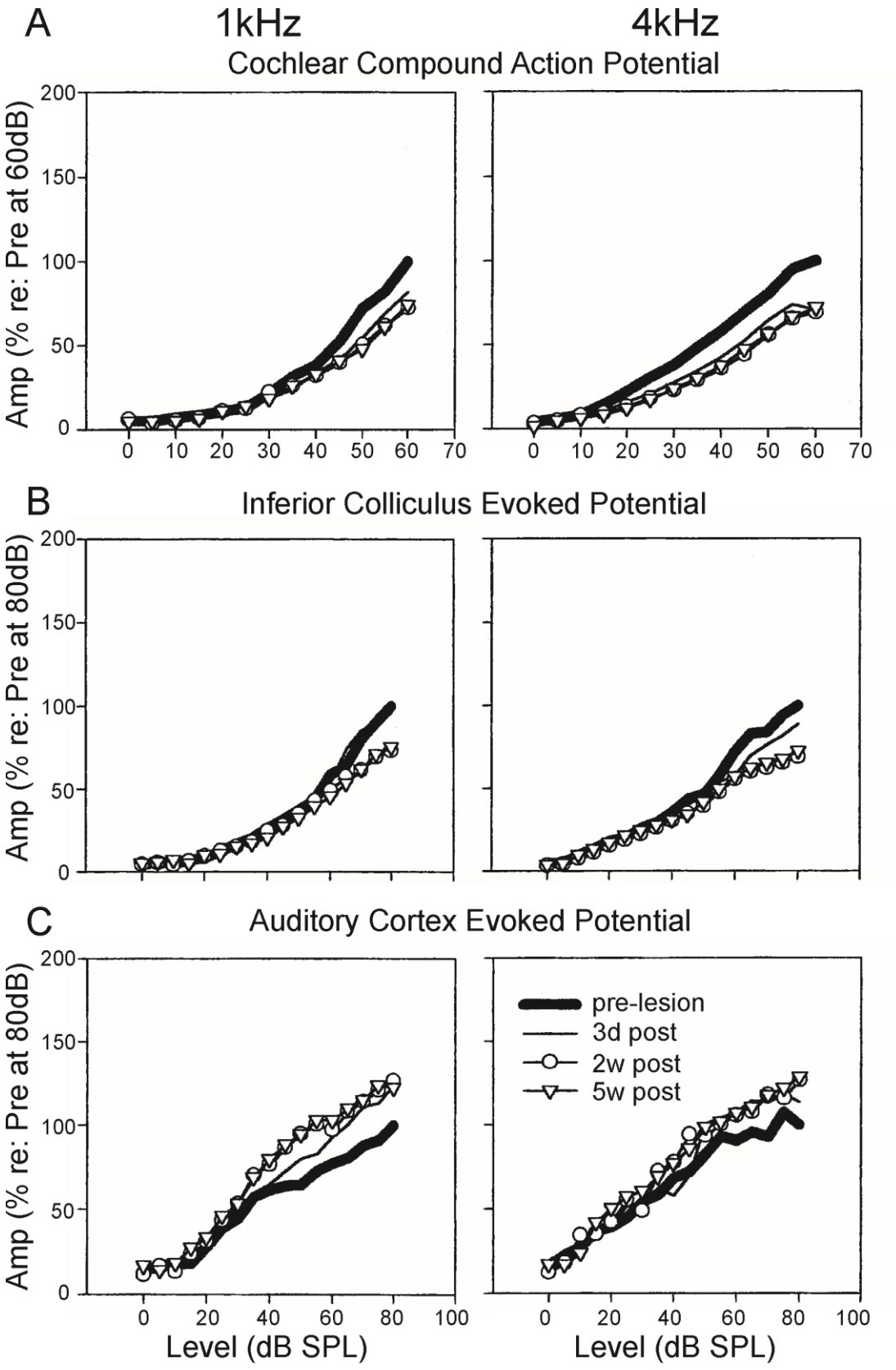
A
1kHz
4kHz
Cochlear Compound Action Potential
Amp (% re: Pre at 60dB)
200
150
100
50
0
0 10 20 30 40 50 60 70
B
Inferior Colliculus Evoked Potential
Amp (% re: Pre at 80dB)
C
Auditory Cortex Evoked Potential
pre-lesion
3d post
2w post
5w post
0 20 40 60 80 100
Level (dB SPL)

Figure 1-3 (previous page): Specific elevation of sound-evoked field potential amplitude vs. level after selective IHC ablation. Following systemic injection of carboplatin into chinchillas, the selective IHC lesion that develops was evaluated by chronic electrode implantation with measurement of evoked field response functions from the CAP (A), IC (B) and AC (C) in the awake animal in response to 1 kHz (left column) and 4 kHz (right column) pure tone stimulation. By recording prior to lesion induction (thick lines), and 3 days (thin lines), 2 weeks (circles) and 5 weeks (triangles) after lesioning, a maintained suppression of evoked response amplitudes was found in both the cochlea and the IC. Paradoxically, IHC ablation yielded a marked steepening of evoked response functions recorded from AC. Modified with permission from Qiu et al. (2000).

1.4.2 Ventral and Dorsal Cochlear Nucleus

As a major site of ANF afferent termination, CN neurons would be expected to display profound changes in activity, putatively compensating for the reduction in peripheral drive. Given the high spontaneous firing rates (SFRs) of ANFs, even the "silent" loss of high-threshold (low-SFR) fibres might profoundly affect the baseline activity of VCN cells, since SFRs of VCN cells may be fundamentally determined by ANF activity (Koerber et al., 1966).

The VCN might express post-lesion response enhancement through plastic remodelling. Following a partial cochlear lesion achieved mechanically or acoustically, a significant elevation of spontaneous discharge was observed (Vogler et al., 2011). By comparison, when identified units of VCN were recorded following permanent hearing loss, primary-like neurons in particular displayed diminished RLF gain, whereas non-primary chopper-type cells consistently exhibited monotonic steep RLFs (Cai et al., 2009).

As the other major subdivision of the cochlear nucleus, and one in receipt of both auditory and somatosensory inputs, neurons in DCN have been extensively investigated for changes in excitability under a variety of traumatic conditions. A significant spontaneous firing rate increase in DCN fusiform layer cells develops within a few (2-5) days following cochlear trauma, and persists for weeks thereafter (Kaltenbach and Afman, 2000; Finlayson and Kaltenbach, 2009).

1.4.3 Inferior Colliculus

At the level of the IC, the predictability of trauma-related neuronal excitability modulations is less concrete. SFR elevations have been characterised in the days-to-weeks following acoustic trauma (Dong et al., 2009; Mulders and Robertson, 2009; Manzoor et al., 2013; Robertson et al., 2013), complete cochlear deafferentation (Moore et al., 1997), and – acutely – after high-dose salicylate injection (Jastreboff and Sasaki, 1986; but see Ma et al., 2006). These SFR changes develop in a manner correlated with those cochlear regions displaying equivalent bandpassed CAP threshold increases, with IHC and/or OHC loss (Willott et al., 1988; Mulders et al., 2011).

Sectioning of the auditory nerve can normalise trauma-related hyperactivity in the IC central nucleus (CNIC) (Mulders and Robertson, 2009), as may lesioning the DCN (Manzoor et al., 2012). These data suggest that IC may chiefly adopt the evolved, persistent hyperactivity of the DCN (Zacharek et al., 2002; Zhang et al., 2006). Nevertheless, longer term observations have revealed that the IC may transition through a period of SFR lability prior to a more permanent acquisition of hyperactivity. By contrast with ipsilateral cochlear nerve lesions performed at 2-6 weeks after acoustic trauma, when auditory neurectomy was conducted at 8-12 weeks, IC hyperactivity remained (Mulders and Robertson, 2011). The dorsal cortex of IC, in particular, displays evidence of hearing loss-related hyperactivity when measured using functional imaging approaches (Holt et al., 2010) – as a major terminus for corticofugal projections, this may be important in the processing of cortically directed acoustic information. Overall, the IC displays compensatory hyperactivity in response to auditory trauma (Robertson et al., 2013).

1.4.4 Auditory Thalamus

Suprathreshold neural response latencies in MGB neurons are predominantly retained across a range of characteristic tuning frequencies following partial cochlear ablation (Kamke et al., 2003). Intriguingly, evidence from the Caspary group suggests a paradoxical increase of inhibition therein, with indications that noise trauma mediates a specifically extrasynaptic enhancement in tonic GABAergic transmission and burst-firing (Richardson et al., 2012; Sametsky et al., 2015), standing the MGB in contrast to other auditory centres.

1.4.5 Auditory Cortex

Based on the changes observed in subcortical nuclei, spontaneous activity and suprathreshold responses at the level of primary AC (A1) might be expected to be elevated. SFR increases in cortical units appear to manifest after acoustic overexposure (Noreña and Eggermont, 2003, 2006), though at a delay of a few hours after trauma, leading to sustained augmentation across A1 for at least 4 months (Seki and Eggermont, 2003; Engineer et al., 2011).

Following acoustic trauma, cross-correlation analysis revealed coincident enhancement of neural spiking synchrony. This elevation in synchrony was particularly prevalent in those regions that displayed some amount of threshold elevation post-traumatically (Noreña and Eggermont, 2006). Based on the observation that this aspect of neural activity was enhanced almost instantaneously following trauma (Noreña and Eggermont, 2003), and prior to the onset of SFR enhancements, correlated network spiking may be acting as a precursor to the ongoing plastic modulation of single cell and network response properties.

A greater proportion of monotonic RLFs are seen in cortical neurons tuned to frequencies outside those represented in the region of cortex responding to the lesioned region of the cochlea (Noreña et al., 2003) (this region of the auditory lemniscal pathway is termed the "lesion projection zone", or LPZ (Schmid et al., 1996; Calford, 2002)). This observation, alongside that of enhanced evoked responses (Engineer et al., 2011), indicates an increase in excitatory activity, possibly driven by a correlated inhibitory dysregulation (e.g. Rajan, 2001). Using single cell recordings from animals with noise-induced threshold elevations, Bao and colleagues have indicated that the mechanistic underpinnings of this putatively homeostatic reweighting may operate for both excitatory and inhibitory synaptic signalling (Yang et al., 2012). Whereas cells outside of the LPZ displayed proportional enhancement of excitatory and inhibitory activity, those neurons that underwent peripheral deafferentation instead displayed reweighting towards more excitatory responses (Yang et al., 2011) (Fig.1-4).

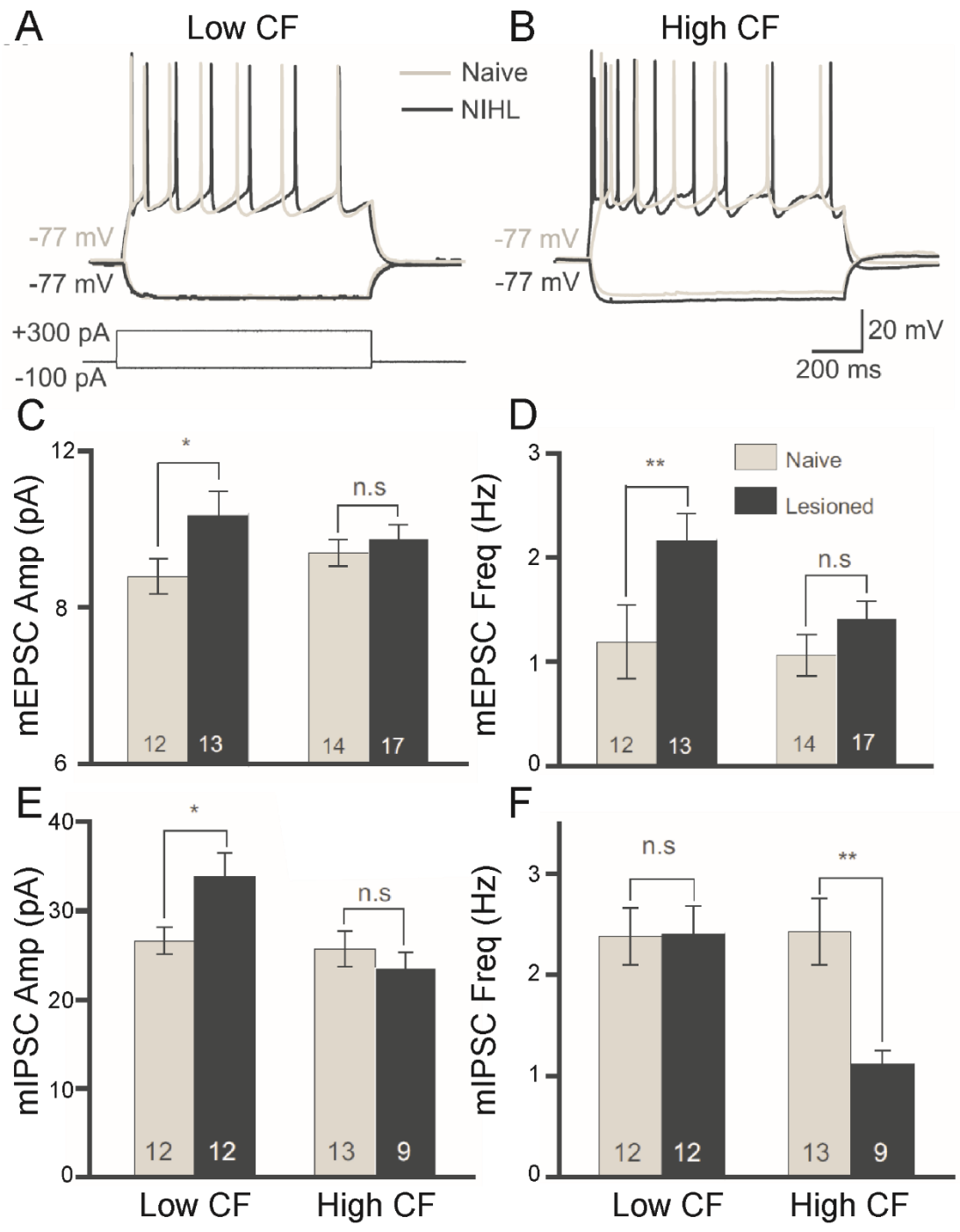

Figure 1-4: Cortical Excitatory/Inhibitory Balance is Differentially Modified by Acoustic Trauma. Following acoustic trauma (123 dB SPL, 4kHz, 7h), *in vitro* patch recordings from rat A1 layer 2/3 pyramidal neurons were performed to evaluate relative changes in excitability between neurons with low- or high-characteristic frequency (CF) tuning. In response to current pulse injection, low-CF neurons showed no enhancement in the number of spikes fired (A), whereas high-CF cells displayed elevated excitability (B). Modified with permission from Yang et al. (2012). There was a significant post-exposure increase in the amplitude (C) and frequency (D) of miniature excitatory postsynaptic currents (mEPSCs) in low-CF neurons only. Similar analysis revealed a significant trauma-driven elevation of miniature inhibitory postsynaptic currents (mIPSCs) amplitude in low-CF neurons (E),

whereas the frequency of mIPSCs was significantly depressed in high-CF cells (F). Modified with permission from Yang et al. (2011).

1.5 Insult-Mediated Changes in Neural Receptive Fields and Networks

Although the characteristics of neural activity throughout the auditory system are clearly modified following hearing loss, this does not indicate how sounds are actually encoded within neurons and neural ensembles: thus, we will now explore the representation of acoustic stimuli at the network level.

1.5.1 Frequency receptive field remapping

Among the earlier explorations of ensemble responses to deafferentation and trauma are the systematic characterisations conducted of the tonotopic remapping that develops following hearing loss. This phenomenon (reviewed in Calford, 2002; Irvine, 2007; Kilgard, 2012) involves the modification of cochlear tonotopy within a lemniscal auditory centre, such that there is an overrepresentation of one or more frequency bands – effectively to the exclusion of others. Pioneering work from Irvine and colleagues unveiled a systematic flattening of the A1 tonotopic map that was contralateral to partial cochlear damage (Fig.1-5) (Robertson and Irvine, 1989; Rajan et al., 1993). Similar high-frequency lesions of SG, induced chemically, may also result in tonotopic remapping, refined over the course of months to yield enhanced cortical representation of low frequency sounds (Schwaber et al., 1993; Kakigi et al., 2000) (Fig.1-5).

Interestingly, such adaptive remodelling may not be universal. In recordings from A1 in the short term, tonotopic remapping has been found to normalise over the course of a week post-trauma (Ahlf et al., 2012). Moreover, following a *low-frequency* permanent deafferentation, ipsi- and contralateral cortical tonotopies were found, by

6 months post-insult, to be brought back into register (in contrast with the remapping described above) (Cheung et al., 2009).

There exists the possibility that cortical remapping may be inherited, in part, from plasticity in afferent centres. Recordings made in the ventral division of MGB contralateral to the cochlear lesion certainly indicate the existence of putative tonotopic remapping therein (Kamke et al., 2003). These observations indicate the importance of thalamocortical circuitry in potentially mediating high-level remodelling of receptive fields after peripheral receptor organ damage, as distinct from simple rostral transmission of deafferented, occasionally silenced (Rajan and Irvine, 1998), projections.

As a point for comparison, the smooth, linear progression of tonotopy that exists along the dorsoventral axis of the IC's central nucleus was predictably flattened after a cochlear lesion, producing an expanded region in which the characteristic frequency of these IC neurons matched that of the lower edge of the LPZ (Irvine et al., 2003). However, there was a pronounced dichotomy among neurons, in terms of the stimulus intensity required to drive activity: although many neurons displayed markedly raised thresholds – akin to those observed in the VCN – others displayed driven onset activity at sound levels near control thresholds. While there exists the possibility of selective remodelling of neural connectivity, the fact that similar tuning patterns were observed within minutes-to-hours following high-frequency spiral ganglion lesions (Snyder et al., 2000, 2008; Snyder and Sinex, 2002) might suggest a release from inhibition of previously subthreshold inputs coding for frequencies below those affected by the hearing loss (Irvine et al., 2003; Izquierdo et al., 2008).

Notably, the tonotopic map in the DCN following partial cochlear lesion was similarly disrupted, with any remapping accompanied by raised thresholds indicative of residual responsivity, rather than plastic remodelling (Rajan and Irvine, 1998). As a general principle, it may be that tonotopic plasticity only emerges at levels above the auditory midbrain (encompassing some units in IC), though residual disinhibition is liable to affect the frequency coding of neurons throughout the central auditory system.

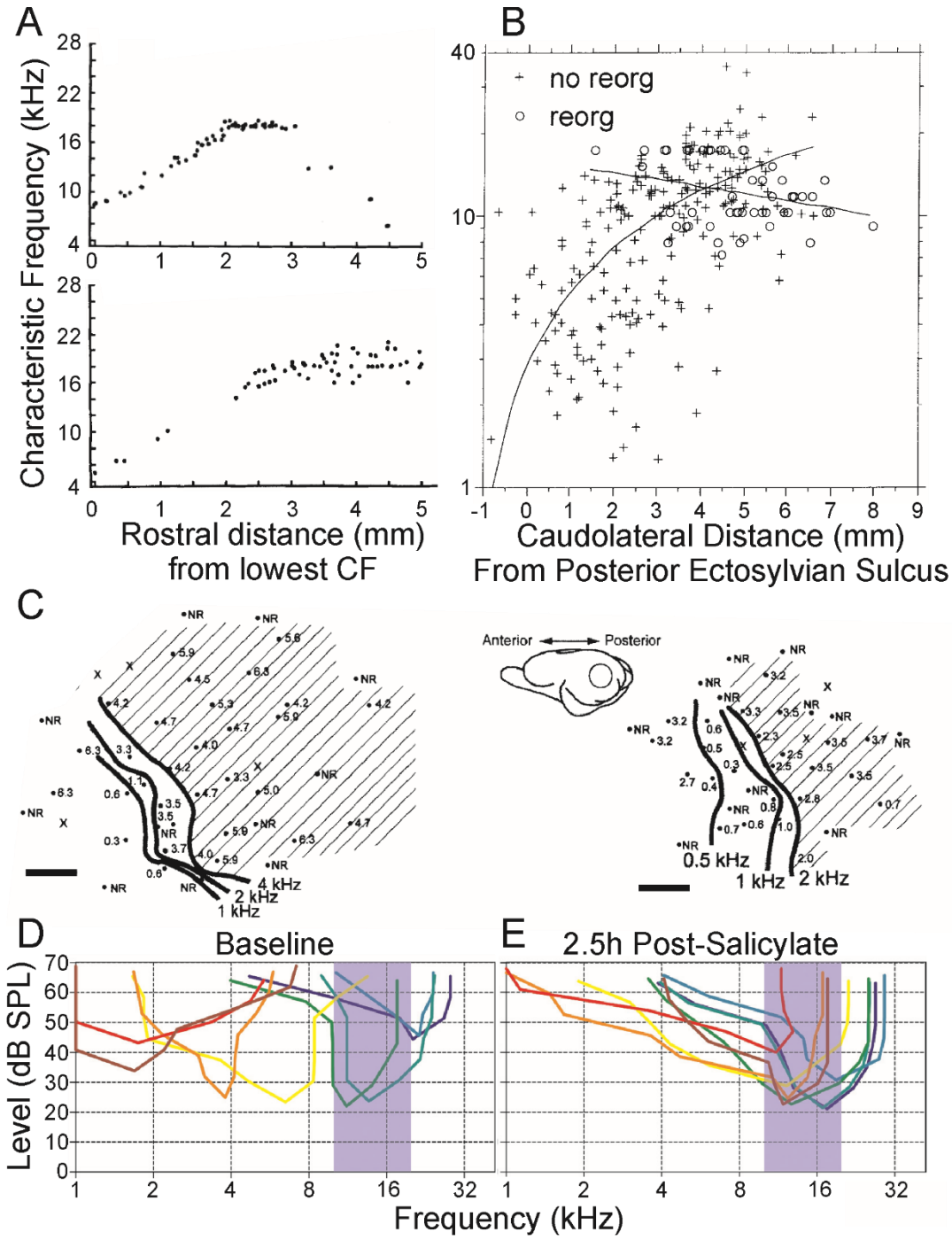

Figure 1-5: Remapping of the tonotopy in the A1 following a variety of peripheral insults. (A) A flattening of the linear progression of characteristic frequency (CF) tuning when units were recorded along the dorsoventral axis of A1 is observed following partial mechanical lesion of the cochlea in adult cats (individual subjects, upper and lower. Each datapoint represents a single unit CF. Modified with permission from (Rajan et al., 1993). (B) A similar flattening of tonotopic progression is demonstrated as a function of distance along the cortical surface dorsoventrally in adult cats exposed to narrowband-passed acoustic trauma, from reorganised (crosses) and non-reorganised (circles) cortical surface. Modified with permission from Seki and Eggermont, (2002). (C) In individual adult chinchillas (left, right) exposed to amikacin-induced basal cochlear hair cell lesions, there is a rearrangement of cortical responses with low characteristic frequencies in regions of the cortex

normally responsive at threshold to higher frequency stimuli (shaded region). Scale bars 1mm. Modified with permission from Kakigi et al., (2000). (D) When individual multiunits were isolated in the adult rat A1 (each unit is a different color), together spanning the hearing range of the animal, (E) systemic injection of salicylate (250 mg/kg intraperitoneal) produced a dynamic retuning of multiunits towards a CF range of 10-20 kHz by 2.5h after injection. Modified with permission from (Stolzberg et al., 2011).

1.5.2 Changes in properties of network responses to temporally complex stimuli

In the context of complex stimulus processing, more fundamental shifts in neural output may distort the representation or encoding of stimuli in "higher" cortical centres. Recordings in the rhesus monkey have highlighted an age-related loss of hierarchical abstraction across cortical fields. For example, in young monkeys the spatial sensitivity of neuronal responses is improved from A1 to the more secondary caudolateral field (area CL), whereas such refinement is absent in older animals (Juarez-Salinas et al., 2010). These effects derive from reductions in inhibition to off-target locations in both CL and A1 (yielding broader spatial receptive fields), as well as a reduction in onset latency in CL, suggesting that plasticity may selectively arise in the primate corticothalamic system, thus enhancing the representation of primary afferent stimuli in non-primary cortical fields (Engle and Recanzone, 2012). To the extent that such age-dependent cortical remodelling may have the capacity for normalisation, recent experiments have focussed on the effects of auditory-driven behavioural training. In one of these studies, aged rats displayed restoration of the tonotopic map found in A1, as well as in neuronal spectrotemporal response properties (de Villers-Sidani et al., 2010), possibly following recovery from maladaptive changes in the function of neurons that were parvalbumin-positive, a marker in cortex for fast-spiking inhibitory interneurons.

The suggestion that temporal processing deficits may endure at the level of the IC, having also been documented in the cochlear nuclei, is apparent even from ABR analysis, which provides a surrogate for synchronous network activation (Buchwald and Huang, 1975). Although no age-related differences were found during frequency-

modulated stimulation of collicular cells (Lee et al., 2002), aged animals showed abnormal sensitivity to background noise (Parthasarathy et al., 2010) and stimulus modulation depth (Parthasarathy and Bartlett, 2011) in the encoding of modulated sounds. In a similar fashion, neurometric gap-detection thresholds were significantly elevated in aged mice (Walton et al., 1998), particularly in those that displayed signs of presbycusis (Barsz et al., 2002). Clearly, presbycusis/ageing induces marked defects in the temporal coding capabilities of the central auditory system – whether these symptoms are liable to emerge following traumatic hearing loss is unclear, however.

1.5.3 Altered cross-modal sensitivity of the auditory system following trauma

Aside from displaying compromised acoustic responsivity, the bilaterally deafferented AC comprises a substantial proportion of neurons that exhibit salient responses to somatosensory inputs (Allman et al., 2009). However, the proportion displaying verifiable multisensory integration, under conditions of selectively preserved auditory input, is in fact diminished relative to control animals (Meredith et al., 2012). This is surprising, since it suggests that the consequences of hearing loss are unlikely to affect simply the central encoding of sounds, but moreover the ability of the brain to use those representations to construct a holistic depiction of objects in the organism's multisensory environment.

All the more interesting is that in related work from Shore and colleagues, an enhancement of somatosensory input into the DCN driven by traumatic threshold elevations has been described (Shore et al., 2008). This modified sensory afferent input in the DCN is accompanied by alterations of the typical stimulus timing-dependent

plasticity rules for bimodal integration during successive auditory/somatosensory stimulation (Dehmel et al., 2012b; Koehler and Shore, 2013a, 2013b) (Fig.1-6), generally producing a long-term enhancement of unimodal acoustically evoked activity. It is unclear how this multisensory enhancement in the brainstem is liable to affect auditory perception, but it remains possible that rather than acting adaptively, this abnormal recruitment of somatosensory drive may operate counteractively, further disrupting, rather than aiding, central auditory processing – indeed, crossmodal reorganisation has been cited as a possible impairment to cochlear implant rehabilitation outcomes (Kral and Sharma, 2012).

1.6 The Functional and Behavioural Implications of Trauma-Driven Plasticity

Clearly the auditory brain is grossly affected by deafferentation, with signs of abnormal function at the cellular, ensemble, and network levels that suggest the representation of acoustic stimuli is impacted beyond the simple effects of audiometric threshold elevation. A major point of inquiry in current auditory neuroscience thus seeks to explain how it is that (subjective) tinnitus, being the perception of an auditory stimulus in the absence of an environmental equivalent, may come about in the wake of auditory trauma of a variety of forms, and manifest in only a proportion of any tested cohort (e.g. Eggermont and Roberts, 2004; Roberts et al., 2010; Noreña and Farley, 2013). Concerns have also been raised regarding the capacity to behaviourally test for the presence/absence of abnormal positive percepts in animals (Eggermont, 2013; Lobarinas et al., 2013a; Gold and Bajo, 2014; Hickox and Liberman, 2014).

1.6.1 Hearing loss-induced behavioural threshold modulations

In lieu of OHC loss, audiometric thresholds are relatively well-preserved (Lobarinas et al., 2013b), whereas frequency discrimination is apparently reliant on effective preservation of IHCs (Nienhuys and Clark, 1978). The majority of peripherally-mediated insults probably affect one or both subtypes of HC, even where the subject's electrophysiologically characterised thresholds are normalised following trauma (Kujawa and Liberman, 2009). As such, the perceptual experience of an adult mammal subject might consequentially be affected in some fashion.

More recently, behavioural characterisation has focussed upon the evaluation of changes in temporal processing ability, primarily (though not exclusively) in the form of testing gap-detection thresholds following insult. Electrophysiological data have demonstrated that neurometric gap detection thresholds deteriorate with presbycusis (e.g. Recanzone et al., 2011) or acoustic trauma (Yin et al., 2008; Berger et al., 2014). Such neural changes appear to be behaviourally reflected by impairments in psychometric discrimination performance using gap-in-noise stimuli (Giraudi-Perry et al., 1982; Salvi and Arehole, 1985; Rybalko and Syka, 2005; Gold et al., 2013). Performance of these operant behavioural paradigms is certainly reliant upon the normal function of the central auditory system (Ison et al., 1991; Kelly et al., 1996; Threlkeld et al., 2008).

Additionally, a number of studies have leveraged various paradigms involving prepulse inhibition (PPI) of the acoustic startle response in small mammals. This behaviour is reflexive, and can be recorded in the absence of training. Suppression of the acoustic startle using a gap-in-noise prepulse (gap-mediated

prepulse inhibition of the acoustic startle reflex, or GPIAS) has been used to explore low-level temporal processing (Longenecker and Galazyuk, 2012; Lobarinas et al., 2013a; Hickox and Liberman, 2014), with evidence indicating correlations between the gap-startle state of an animal and markers of neuronal plasticity, found both cortically and subcortically (Engineer et al., 2011; Koehler and Shore, 2013a; Coomber et al., 2014). Given the extensive excitatory/inhibitory remodelling that is associated with ageing (Caspary et al., 2008), it is possibly unsurprising that GPIAS impairment has also been demonstrated in a mouse model of presbycusis; here, behavioural impairment was correlated with cortical inhibitory dysfunction (Llano et al., 2012).

1.6.2 Perceptual phantoms and proposed behavioural correlates

The search for methods that reliably identify a tinnitus-like percept in experimental animals represents a major current research topic. The existence of tinnitus is, by convention, categorically different from the perception of silence. It is thus not unreasonable that a popular approach has sought to detect the phantom percept using operant conditioning paradigms to measure behaviour (Jastreboff et al., 1988; Bauer and Brozoski, 2001; Heffner and Harrington, 2002; Guitton et al., 2003; Rüttiger et al., 2003; Yang et al., 2007, 2011; Sederholm and Swedberg, 2013). In these paradigms, a change in the animal's approach/avoidance behaviour following exposure to a tinnitus-inducing agent is inferred to indicate changes in the animal's actual perceptual state. Unfortunately, longitudinal measurements of each animal's auditory physiology were made rarely, preventing the correlation of behaviour with a more objective identifier of modified auditory function.

GPIAS has recently been suggested to have the potential for the behavioural interrogation of tinnitus (Turner et al., 2006, 2012), allowing researchers to couple behaviour with physiological and anatomical measurements within individual animals. This approach has yielded interesting and promising data regarding the behavioural correlates of neurophysiological modulation and has been validated using other tinnitus-like behavioural reporter paradigms (Bauer and Brozoski, 2001; Yang et al., 2007) (Fig.1-6). However, the likelihood that the technique acts as a reliable indicator of tinnitus proper remains under debate, not least due to the exclusively subcortical circuitry sufficient for the behaviour's expression (Eggermont, 2013; Gold and Bajo, 2014). This does not discount reflex-based paradigms as informative about the sub-cognitive encoding of acoustic stimuli, and how this is affected by hearing loss. However, the extent to which they might be applicable to human patients is questionable - for example, the frequency specificity of GPIAS is not replicated in human tinnitus patients (Fournier and Hébert, 2013), nor do such patients display detection deficits at the gap lengths typically used for GPIAS (Campolo et al., 2013).

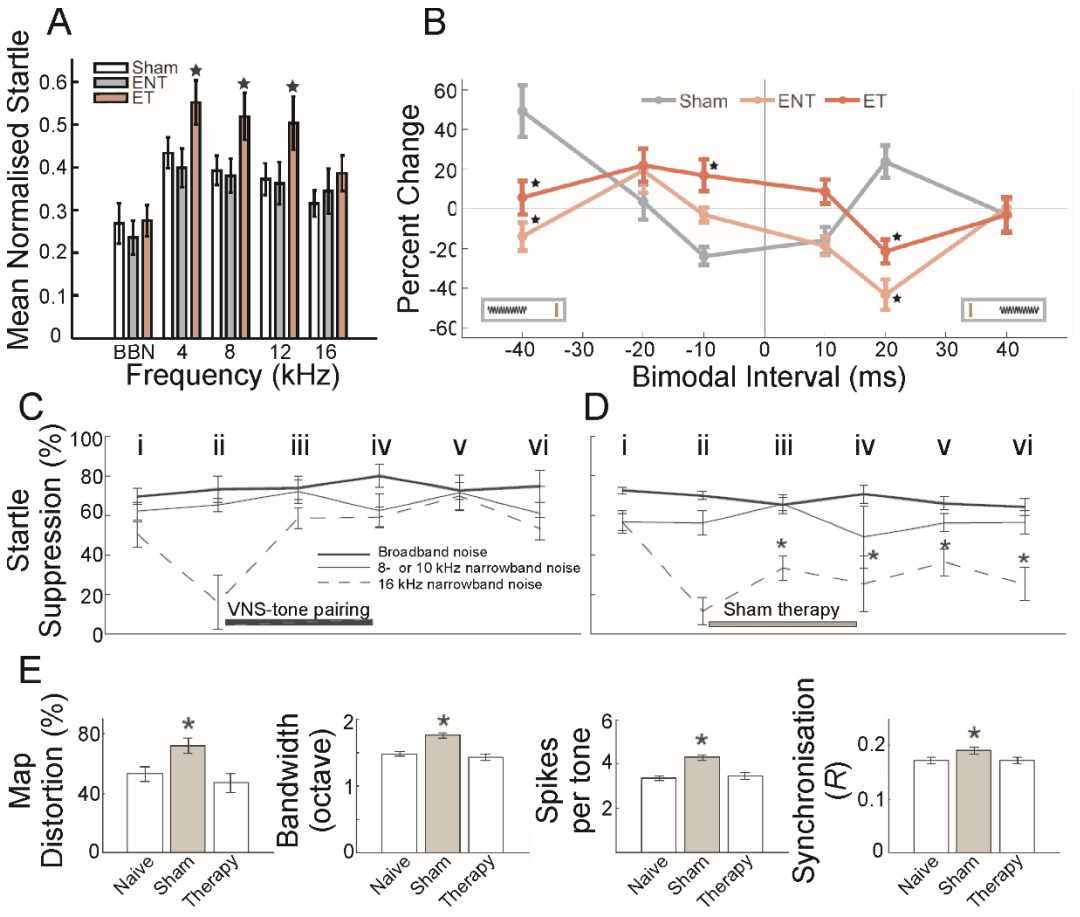

Figure 1-6: GPIAS in Rodents Indicates Neurobiological Changes Following Auditory Insult. A) In a cohort of adult guinea pigs, acoustic overexposure (1/4 octave band noise centred at 7 kHz, 93 dB SPL, 2 h; twice-exposed, separated by 6-8 weeks) yielded a subset of animals with decreased normalised GPIAS for 4-16 kHz bandwidths. Sham controls = white bars; GPIAS-unimpaired animals = grey bars; GPIAS-impaired animals = pink bars. Star = p<0.05 vs. other bars in the same frequency band. B) The animals displayed significantly different stimulus-timing dependent plasticity functions for bimodal somatosensory-auditory stimulation compared with both sham controls, and exposed but unimpaired animals. Sham = grey; GPIAS-unimpaired = pink; GPIAS-impaired = red. Modified with permission from Koehler and Shore (2013a). C-E) Following exposure to acoustic trauma (octave band noise centred at 16kHz, 115 dB SPL, 1h), adult rats underwent daily pairing of pure tones outside the 8-10 kHz bandwidth, either with vagal nerve stimulation (VNS) (C) or sham stimulation (D). VNS-tone pairing produced rapid and long-lasting remediation of GPIAS impairments for 8-10 kHz background masking; sham-tone pairing produced no improvement. Time points: i = before trauma; ii = 4 weeks post- exposure; iii = 10 days after initiation of VNS-tone or sham-tone pairing therapy; iv = 20 days after therapy initiation; v = 1 week post-therapy; vi = 3 weeks post-therapy. (E) VNS-tone pairing also normalised vs. control measurements, aspects of A1 neural activity that had been enhanced following trauma, including tonotopic map distortion, frequency receptive field bandwidth, evoked spike response number, and neural spike-timing synchrony. Leftmost bars = naive; middle bars (grey) = sham-tone pairing therapy; rightmost bars = VNS-tone pairing therapy. Asterisk = p<0.05 vs. controls. Modified with permission from Engineer et al., (2011).

Nevertheless, non-specific gap-detection deficits have been demonstrated among a subset of tinnitus patients (Fournier and Hébert, 2013), as have auditory processing impairments in encoding speech sounds (Moon et al., 2015). Such perceptual abnormalities affecting accurate temporal processing may comprise part of the tinnitus-like syndrome in animal models. However, behavioural paradigms are needed that carefully disentangle the presence of tinnitus itself from auditory processing deficits that may arise from auditory trauma, neuroplastic changes, or otherwise. These efforts may be aided by evaluating the causes underlying changes to neural gain and network spiking synchrony following some tinnitus-related insult, particularly with respect to rebalancing of excitatory/inhibitory signalling mechanisms (Knipper et al., 2013). However it is only recently that appropriate technologies have become available to engage such a putative rebalancing.

1.7 Optogenetics and Manipulation of Brain Activity

The recent development of light-neural interface technologies has facilitated experimental interventions that previously were impossible with electrical or pharmacological approaches, enabling neural structures to be targeted with greater spatial and temporal resolution than either of these older approaches (Fenno et al., 2011; Yizhar et al., 2011; Hausser, 2014; Grosenick et al., 2015). The field at present had its inception with Channelrhodopsin-2 (ChR2), a microbial light-sensitive opsin protein derived from *Chlamydomonas reinhardtii* that, upon blue light illumination, allows for high-density passage of cations into the neuron. This influx depolarises the cell membrane potential and so increases the rate of spiking (Nagel et al., 2003; Boyden et al., 2005).

In opposition to this activation approach, a separate class of opsins has emerged that allows direct neural silencing through cellular membrane potential hyperpolarisation. Whereas among channelrhodopsins the effector mechanism is largely channel-like, among silencing opsins two main approaches have been explored: in the first, a light-sensitive halorhodopsin derived from *Natromonas pharaonis* (NpHR) stably pumps chloride anions across the cell membrane (Zhang et al., 2007); in the second, the *Halorubrum sodomense* gene archaerhodopsin-3 (Arch) yielded very high (<900 pA) suppression currents when stimulated with green-yellow light, by pumping protons into the neuropil from the cellular interior (Chow et al., 2010). For both NpHR and Arch, additional improvements were later described: eNpHR was developed to account for earlier problems associated with loss-of-function at high NpHR expression levels (Gradinaru et al., 2010); and ArchT was created to facilitate higher (3-fold) light sensitivity *in vivo* compared with Arch (Han et al., 2011). During NpHR-mediated suppression, however, marked shifts in the Cl^- reversal potential were observed, substantially affecting cellular acidity (Raimondo et al., 2012). Thus, all else being equal, employing Arch-derived optogenetic technologies to achieve neural silencing seems more prudent, particularly if the aim is for longer-term experimental protocols to be tested.

By using animals expressing opsin genes in various brain regions, alongside optical fibre implantation and light illumination, interesting and marked changes in network and behavioural activity have been described, particularly in the auditory system. Optogenetic intervention has not only facilitated the description of both inter- (Rock and Apicella, 2015) and intra-hemispheric (Bajo et al., 2013; Hamilton et al., 2013; Znamenskiy and Zador, 2013; Schneider et al., 2014; Weible et al., 2014a, 2014b;

Xiong et al., 2015) pathways affecting activity in AC, and subcortically in the brainstem (Shimano et al., 2013) and auditory nerve (Hernandez et al., 2014), but also, in certain experiments, the behavioural effects of selective activation/inactivation of these very pathways. Pertinently, Weible and colleagues have begun to disentangle the mechanisms responsible for encoding temporally salient acoustic information in AC (Weible et al., 2014b). Also notable is work exploring the therapeutic potential of optogenetic intervention in the auditory system (Shimano et al., 2013; Hernandez et al., 2014) and more generally (Chow and Boyden, 2013).

1.8 Thesis Overview

This thesis aims to explore how the auditory system, and in particular AC, responds to a particular kind of peripheral insult (partially lesioning the SG), modelled on presbycusis (Viana et al., 2015). Initially, we pursued a behavioural paradigm that characterises the temporal processing capabilities of ferrets, and to determine whether these animals represent a good model for human auditory temporal processing. We then sought to determine the effects of the SG lesion across a range of analysis types, evaluating longitudinal shifts in behaviour, neurophysiology and neurochemistry. We aimed to identify physiological/anatomical markers that correlated with changes in behaviour, and to determine if this potential constellation of changes is similar to the maladaptive environment liable to occur in human hearing loss and tinnitus sufferers. Furthermore, this thesis investigates how optogenetic intervention in the perturbed AC might represent a translationally relevant approach for rescuing abnormal activity that disrupts the neuronal representation of acoustic stimuli, which may in turn affect acoustically driven perception and behaviour.

In Chapter 2, the experimental methodology will be described, encompassing the full breadth of approaches employed throughout the thesis.

In Chapter 3, we will describe a novel behavioural assay in ferrets – an operantly-trained gap-in-noise detection task allowing the investigation of the perceptual correlates of temporal processing in the auditory system (Gold et al., 2015). The paradigm was designed to allow the robust sampling the ferret's temporal perception at multiple time-points and under multiple treatment conditions, across a range of acoustic stimulus frequencies covering the ferret's physiological hearing range. An equivalent behavioural task was tested in a cohort of human subjects, enabling the verification of the ferret as a useful comparative model of auditory function.

Chapter 4 investigates how the auditory system is affected by, and adapts to, the introduction of a selective, unilateral lesion of the SG. Individual ferrets were assessed in their performance on gap-in-noise detection behaviour prior to and following SG lesion. In these animals, we measured ABRs pre-lesion, just after the lesion and at least 3 months later, to diagnostically determine the efficacy of the lesioning procedure, and any associated subcortical neuroplasticity. Neurophysiological multiunit data were obtained by recording bilaterally from ACs of these animals, using multichannel silicon arrays, to explore post-lesion neuronal effects in the AC, particularly the kinds of changes described above. Brain tissues were histologically analysed to explore changes in neurochemical markers associated with a maladaptive tinnitus-like state, including Arc and nitric oxide metabolism. Histological analysis of lesioned cochleae was undertaken in collaboration with the

Furness Laboratory at Keele University, to quantify SGC populations under light microscopy.

In Chapter 5, we explore the interventional capacity of optogenetically silencing the ACs, both unilaterally and bilaterally, following the SG lesion. Lesioned ferrets (and unlesioned controls) were tested on our gap-in-noise detection paradigm during selective silencing of auditory cortical activity. This was achieved in collaboration with the Boyden Laboratory at MIT, using a viral construct encoding ArchT (Han et al., 2011). The neurophysiology of AC in injected animals was evaluated using extracellular recordings combined with laser stimulation. Histological processing was conducted to determine the injection sites, and their projection profiles.

Finally, we will present a general discussion of the work presented throughout the thesis, future work suggested by our findings, and the possible clinical ramifications of our experiments.

Chapter 2

Methods

2 Overview

These experiments were conceived to evaluate the changes that develop following a partial hearing loss, which was designed to mimic that observed in hearing loss patients with tinnitus (see Chapter 1; Gold and Bajo, 2014). By monitoring individual animals longitudinally while probing auditory function and perception, we sought to understand what instigates abnormal neuroplasticity in the auditory system, which may underpin tinnitus. The experimental chronology is conceptualised in Figure 2-1, indicating the experimental trajectory of animals in the study (Table 2-1).

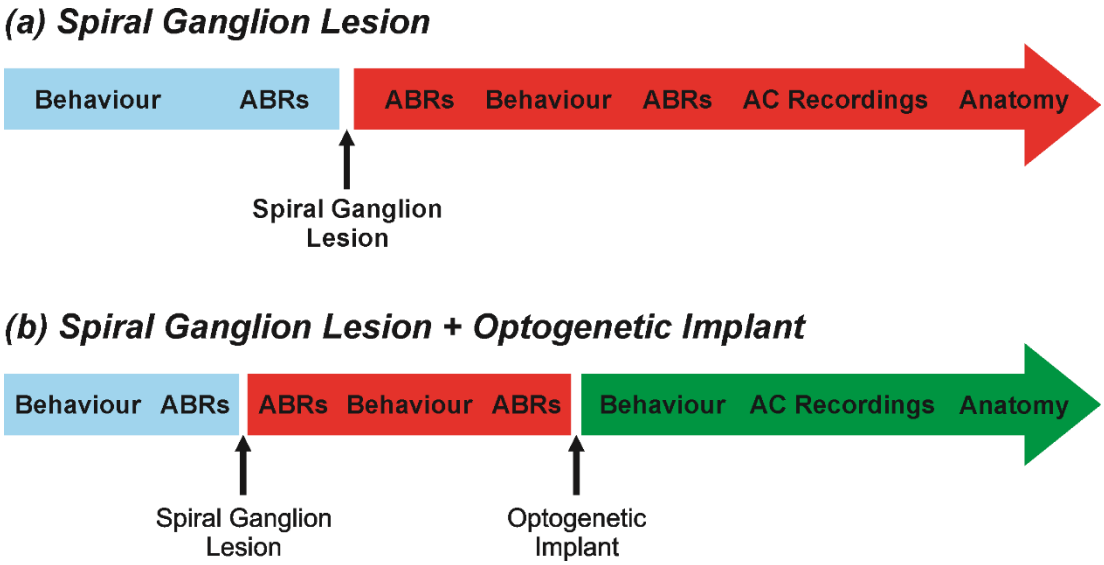

Figure 2-1: Experimental Design. Ferrets were subject to one of two chronologies for experimentation. In each case, animals underwent behavioural testing and measurement of auditory brainstem responses (ABRs) (in blue) prior to the SG lesion. Post-lesion (in red), animals were retested behaviourally, and were subject to ABR measurement at two time points. In some animals (*b*), bilateral cortical viral injection encoding Archaerhodopsin-T and optic fibre implantation was applied, and followed by further behavioural testing (in green). Animals underwent AC neurophysiology, and histological examination of the cochleae and the brain.

Ferret Number	Behaviour	Lesion	ABRs	Optogenetics	Neurophysiology	Histology
F1035	PRE	R	n/a	n/a	n/a	n/a
F1036	PRE/POST*	R	POST	n/a	YES (LESIONED)	YES
F1114	POST*	R	PRE/POST(A)	n/a	YES (LESIONED)	YES
F1201	POST*	R	PRE/POST(A)	n/a	YES (LESIONED)	YES
F1202	PRE/POST*	R	POST	n/a	NO	YES
F1226	PRE/POST	R	PRE/POST(A/C)	L/R	YES (LESIONED)	YES
F1227	PRE/POST	R	PRE/POST(A/C)	L/R	YES (LESIONED)	YES
F1228	PRE/POST	R	PRE/POST(A/C)	L/R	YES (LESIONED)	YES
F1316	n/a	n/a	n/a	n/a	YES (CONTROL)	YES
F1317	PRE/POST	R	PRE/POST(A/C)	L/R	tbp	tbp
F1318	PRE/POST	R	PRE/POST(A/C)	L/R	tbp	tbp
F1319	PRE/POST	R	PRE/POST(A/C)	L/R	tbp	tbp
F1414	n/a	n/a	n/a	n/a	YES (CONTROL)	YES
F1417	n/a	n/a	n/a	n/a	YES (CONTROL)	YES
F1208	n/a	n/a	n/a	n/a	YES (CONTROL)	YES
F1411	PRE/OPTO	n/a	n/a	L (CONTROL)	tbp	tbp
F1438	PRE/OPTO	n/a	YES	L/R	tbp	tbp

Table 2-1: Animals Involved in the Project. Animals in this project underwent evaluation using a number of measures of function. Behaviour PRE/POST: * = animals tested only on broadband noise (BBN) gap-in-noise detection (see below). ABRS: (A) = acute, (C) = chronic (see text). Optogenetics: L = left hemisphere, R = right hemisphere (see text). tbp = to be performed.

2.1 Gap-in-Noise Detection Behaviour

All experiments were conducted in sound-attenuated chambers, approved by local ethical review committees and, for ferret experiments, performed following ethical review by the Committee on Animal Care and Ethical Review of the University of Oxford and under licence from UK Home Office in accordance with the Animal (Scientific Procedures) Act (1986, amended in 2012).

2.1.1 Animals and welfare

Female adult pigmented ferrets (*Mustela putorius furo)* (age range: 5 – 36 months) were used in these experiments. Ferrets were housed in large communal pens, except during periods of behavioural testing. Herein, animals were motivated to perform the gap detection task by water access regulation, with each period of testing lasting ≤5 days, with two testing sessions/day. *Ad libitum* access to dry pelleted food was provided, whereas daily water requirements were obtained through correct performance of the task alongside supplementation (using a pellet/water mash) following completion of each day's testing (conducted morning and afternoon/evening). Animal body weights were monitored routinely and compared with baseline measurements obtained prior to starting each testing period, during which body weights typically fell by <5%. Between each testing period, animals were allowed ≥2 days with *ad libitum* access to water. Otoscopic examinations and tympanometry were performed periodically to assess the status of the outer/middle ear of each animal.

2.1.2 Testing apparatus and stimuli

Gap-detection behavioural testing was carried out in a circular arena (radius=70 cm) with a solid plastic floor and enclosed by a cylindrical mesh barrier, and located inside a double-walled testing chamber lined with acoustic foam (MelaTech; Hodgson & Hodgson Ltd., Melton Mowbray, UK) (Fig.2-2). Ferrets were monitored from an external room via a closed circuit monitor. Centred in the testing arena, a rectangular raised platform was present with a steel spout and an optical proximity sensor located at the head end (defined as 0°). To initiate a trial, ferrets were required to stand on the platform and nose-poke the central spout. Spout contact and the required animal orientation were ensured by coactivation of the centre spout sensor and an infrared beam sensor located at the platform rear corners.

Upon trial initiation, a sound was presented at the chamber's periphery, either from one of two loudspeakers, or a single loudspeaker (FRS 8; Visaton, Crewe, UK). Ferret responses were registered at two lateralized water spouts (at the arena periphery, at bearings of ±30° relative to centre), with correct responses rewarded by a fixed quantity of water. Following incorrect responses, only the first response was included for analysis, with ferrets required to reinitiate the trial ("correction trials", up to 20x). Stimulus presentation, response registration and water rewards were controlled using TDT System 3 hardware (Tucker-Davis Technologies, Alachua, FL, USA), with experimental contingencies controlled using custom-written scripts implemented in MATLAB (MathWorks, Natick, MA, USA).

Stimuli were generated *de novo* on each trial using TDT System 3 hardware. For each testing session, stimuli (all 2080 ms in duration) comprised either broadband

noise bursts (low-pass filtered up to 30 kHz; BBN) or one of three narrowband noise burst types (band-pass filtered with an octave-window logarithmically centred at 1 kHz, 4 kHz, or 16 kHz; NBN) and stopband roll-off ≈-52 dB/octave. For gap-containing stimuli, noise bursts contained silent gaps, while in no-gap stimuli, noise was continuous for the stimulus duration (see below). All stimuli were filtered using the inverse transfer function of the speaker to ensure a flattened frequency spectrum response, with overall level averaging 76±5 dB SPL from trial-to-trial, irrespective of stimulus type (Fig.2-3). These stimuli were designed to broadly sample the ferret's natural hearing spectrum, above threshold (Kelly et al., 1986).

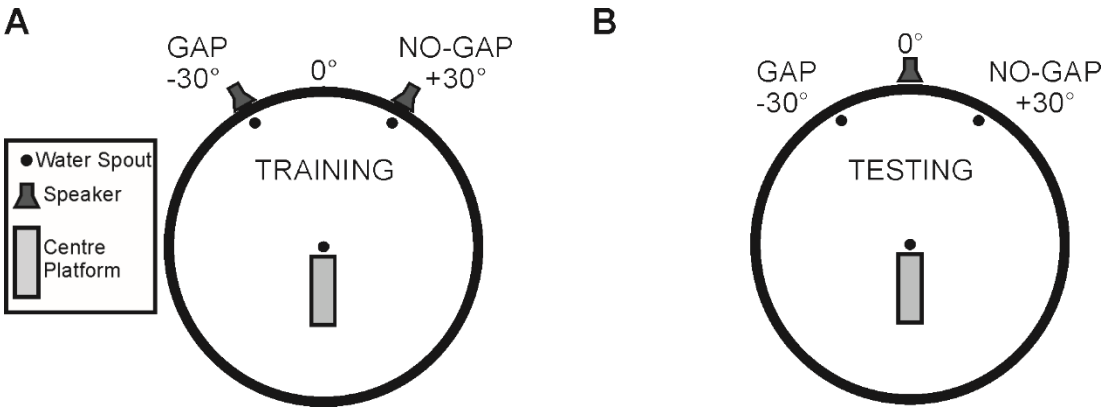

Figure 2-2: A) Ferrets were positively conditioned to report the presence of a silent gap-in-noise stimulus by nose-poking at one of two reward spouts at the periphery of a circular testing chamber. During the training phase, "gap" stimuli were presented from a loudspeaker above the spout at –30°, whereas "no-gap" stimuli were presented from a loudspeaker located at +30°. B) During the testing phase, once the stimulus types (gap vs. no-gap) were reliably paired with rewards at specific locations, all stimuli were presented from a loudspeaker at 0°, while responses were registered at water spouts positioned at ±30°.

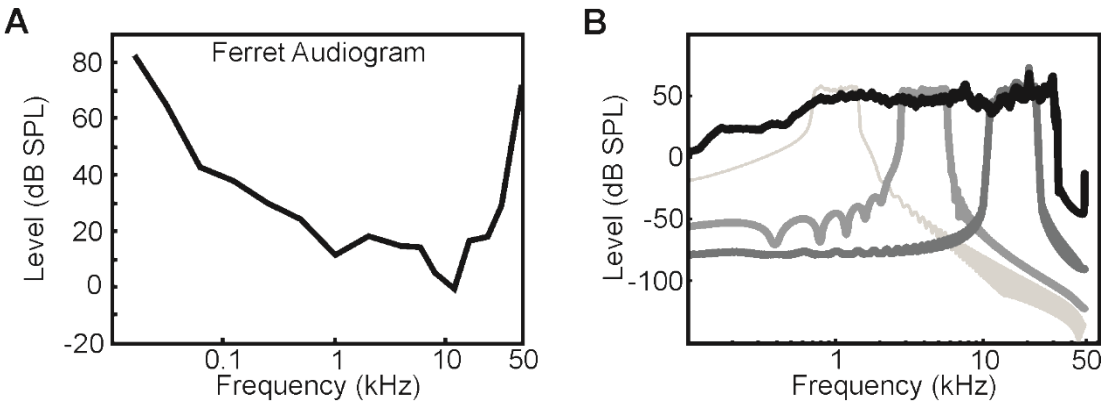

Figure 2-3: A) Mean behavioural audiogram of the pigmented ferret, obtained in response to pure tone stimuli of varying intensities. Modified from Kelly et al. (1986). B) Power spectra of the sound stimuli used in our experiments, comprising octave-bandpass narrowband noise (NBN) centred at 1 kHz (light grey), 4 kHz (mid-grey), or 16 kHz (dark grey), or flattened broadband noise (BBN) with a 30 kHz low-pass corner (black). By comparison with (A), these stimuli encompass much of the ferret's behavioural hearing range.

2.1.3 Behavioural training

During initial training, animals were familiarized with the testing arena and taught to approach the central spout facing 0°, for which they received a water reward; over time (and prior to beginning behavioural testing), this centre reward was reduced to a pseudorandomized probability of 0.05. Once trained, centre-spout approach was followed (at a delay slowly increased up to 500-1000 ms of maintained spout contact) by BBN stimulus presentation at one of two loudspeakers, each situated at ±30° bearing (Fig. 2-2). Stimuli presented from +30° were continuous noise bursts ("no-gap"); stimuli presented from -30° were noise bursts into which four silent gaps had been interleaved (gap duration 270 ms; 2 ms cosine ramp; "gap"). For gap stimuli, silent gaps were interleaved to be evenly spaced throughout the sound (which was 2080 ms in duration). Gap stimuli thus effectively comprised five distinct noise bursts, each of duration, in ms:

$$duration = \frac{2080 - 4(gap\ length)}{5}$$

Stimuli were pseudorandomly presented in a 1:1 ratio gap:no-gap.

Once a ferret's performance was consistently >90% correct, presentation of both stimulus types was switched to a single loudspeaker at 0° azimuth, with the duration of silent gaps in gap stimuli comprising 50 ms, 100 ms or 270 ms. Correct responses for gap and no-gap stimuli continued to be registered at water spouts situated at -30° and +30°, respectively, and rewarded with three drops of water (this remained consistent throughout behavioural testing).

2.1.4 Behavioural testing

Once task performance was consistently >90% correct for stimulus presentation at 0° azimuth, the tested set of gap lengths was expanded to include 3 ms, 5 ms, 10 ms, 20 ms, 50 ms, 100 ms, and 270 ms. Each trial's gap length was selected from this distribution and pseudorandomly varied from trial-to-trial. The gap:no-gap presentation ratio remained at 1:1, with gap/no-gap stimulus type also varied pseudorandomly, trial-to-trial. Testing was conducted until at least 1000 trials (over multiple sessions) were cumulatively collected for BBN. Afterwards, testing continued with each session's stimulus frequency content randomly chosen from the three NBN stimuli, until >1000 trials had been collected for each. On each trial, the animal's approach-to-target response time was registered as the time between stimulus onset and peripheral spout licking. Trials in which a centre spout reward was provided (5% of the trials) were not included for final analysis.

2.1.5 Head orienting responses

Due to the lateralized nature of the initial two-speaker training protocol and left-right response registration method, we measured ferrets' head orientation reactions to ensure that a latent sound-localization behaviour was not biasing the results. These measurements were obtained as described previously (Nodal et al., 2008). An infrared-sensitive camera was positioned above the central spout, to track the coordinates of a self-adhesive reflective strip, attached to the midline of the animal's head, at a rate of 60 frames per second, for the first second following stimulus onset. Thus, the angular extent of the animal's head orienting was calculated with respect to its initial head-bearing. A head-orienting response was defined as a period of >3

consecutive frames over which the animal's head moved in the same rotational direction, with initial head-orienting response time being defined as the time of the first frame of this response. The final head bearing was measured as the mean of the last three frames of the continuous head movement, or, if a head movement was not recorded, as the mean of the final three frames recorded prior to the animal moving from the platform. Trials were not analysed if the initial head bearing was more than 2σ from the population mean initial head bearing.

2.1.6 Human Psychophysics

We tested six young adult humans (four females, two males; mean age, 29 years) with audiograms collected prior to testing; subjects' thresholds were confirmed as having no impairments up to and including 16 kHz. Gap-in-noise detection performance was evaluated using spectrally-identical stimuli as described for the ferret experiments: BBN, and 1 kHz, 4 kHz, and 16 kHz NBN; all 76±5 dB SPL. Stimuli differed from those used for testing ferret gap detection in two ways: stimulus noise duration was 400 ms, and only a single gap was interleaved within the noise, such that each stimulus comprised two 200 ms noise bursts separated by a silent gap. Gap lengths were 2 ms, 5 ms, 10 ms and 20 ms during an initial training session; and 1 ms, 2 ms, 3 ms, 4 ms, and 10 ms during testing. Subjects were seated in a double-walled sound-attenuating chamber, with stimuli presented from a single loudspeaker (Audax TW025M0) located at 0° at eye level.

Responses were recorded via a graphical user interface using mouse clicks on labelled onscreen buttons for gap/no-gap responses. No feedback was provided during testing. Upon incorrect responses, correction trials were not provided, so as to

limit stimulus adaptation or learning. For each testing session (of which three were conducted for each stimulus type), data were collected in independent blocks of 100 trials, with stimulus frequency content pseudorandomised from block-to-block. Within each block of trials, gap/no-gap content and gap length were pseudorandomised as for ferret behavioural testing. All experimental contingencies were controlled by custom written scripts in MATLAB and implemented in TDT System 3 hardware. All trials were included for analysis.

2.1.7 Data Analyses

All ferret and human data were analysed using equivalent methodology in MATLAB, to ensure comparability between the two species. For gap detection responses, percent-gap functions (equivalent to percent correct functions, except with no-gap percent incorrect values included to anchor the function at gap length = 0 ms, i.e. no-gap) were calculated for each session. Sessions were excluded from analysis if <5 different gap lengths were tested <5 times within that session. Psychometric functions for percent-gap values were fitted using the MATLAB package psignifit (http://psignifit.sourceforge.net). For each psychometric function, percent-gap values were transformed into *d'* values according to Signal Detection Theory (SDT)(Macmillan and Creelman, 2005), a theoretical framework that has been previously validated in ferret operant behaviour (Alves-Pinto et al., 2012). *d'* values were obtained using the transform $d' = z(Hit) - z(FA)$, where *Hit* and *FA* are the hit and false alarm rates, i.e. the proportion of approach-to-target responses made correctly for gap stimuli and incorrectly for no-gap stimuli, respectively (Fig.2-9). Fit parameters were specified according to a right-weighted gumbel sigmoid fitted over

a linear transform of the stimulus intensity values ('mw0.1' core in the psignifit package). The function is as follows:

$$\Psi(x; m, w, \gamma, \lambda) = \gamma + (1 - \gamma - \lambda)$$

$$F(x; m, w)$$

where:

$$F(x; m, w) = \exp\left(-exp\left(-\frac{z(\delta) - z(1-\delta)}{w}(x - m) - z(0.5)\right)\right)$$

and:

$$z(\delta) = \log(-\log(\delta))$$

where x is the stimulus difficulty; m is the midpoint; w is the width of the interval over which $F(x;m, w)$ rises from δ to $1 - \delta$; λ is the lapse rate; and γ is the FA rate. In implementing the function in psignifit, both m and w were left unconstrained, while δ was fixed to the default value of 0.1. We used a beta distribution to estimate the prior FA rate, with beta distribution parameters a and β as $\alpha = FA + 1;\ \beta = CR + 1$, where FA and CR are the empirical FA rate and correct rejection (CR) rate for the evaluated response distribution, respectively. Estimates of prior lapse rate, also modelled as a beta distribution, were set using values previously recommended ($\alpha = 1;\ \beta = 12$) (Fründ et al., 2011; Buran et al., 2014).

Goodness-of-fit was determined for each session's psychometric function by bootstrapping the fit deviance to generate a reference distribution of 1000 sample sets. Fits exceeding the 95th percentile of the bootstrapped deviance population were

discarded from subsequent analysis, according to criteria recommended by Fründ et al. (2011).

From *d'*-transformed psychometric functions, we extracted various performance measures. Empirical threshold was defined as the fitted gap duration at which *d'*=1, which approximates a percent-gap rate of ~60%, given the mean population FA rate (mean = 0.23) recorded across all stimulus types (Fig.2-4). Psychometric function slope was calculated at threshold to determine the rate at which an animal's session performance approached asymptote performance. In addition, we calculated two measures of optimal performance: the lapse rate, being the observed proportion of incorrect responses obtained at the longest gap duration, and maximum sensitivity, being the *d'* value at each function's asymptote (Fig.2-4).

The distributions of approach-to-target and head-orienting response times in operantly-conditioned tasks of this kind are non-normal, and best-approximated using an ex-Gaussian function, which we fitted using the DISTRIB toolbox (V2.3; http://darwin.psy.ulaval.ca/~yves/distrib.html)(Lacouture and Cousineau, 2008; Leach et al., 2013). Confirmation of goodness-of-fit was made by comparing quantile-quantile (qq) plots generated from the fitted ex-Gaussian distribution, and from a Gaussian distribution whose mean and standard deviation matched those of the original dataset. In all cases, fit residuals were lower for ex-Gaussian quantiles compared with those from the Gaussian distribution. Statistical tests were performed on fitted parameters of each distribution: μ and σ (the mean and standard deviation

of the distribution's Gaussian component), and τ (the time constant of the distribution's exponential component).

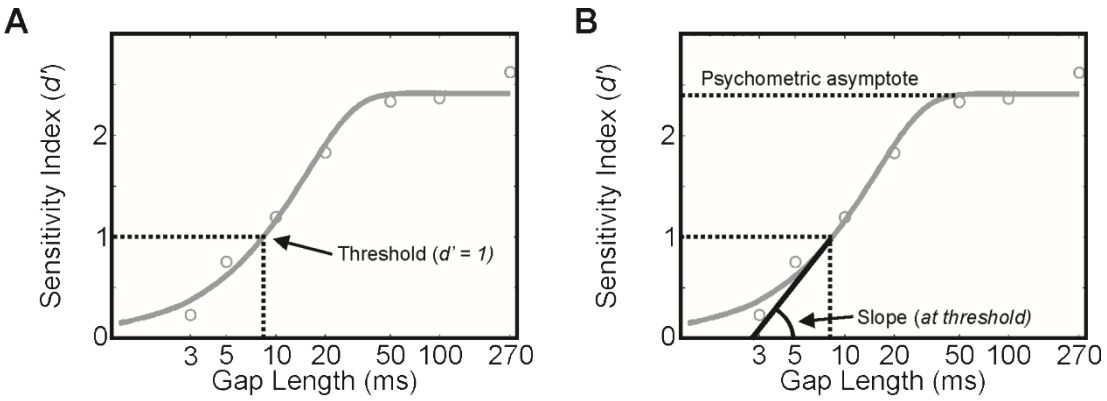

Figure 2-4: Psychometric Functions. A) Example performance of one ferret during a session of the gap-detection task for BBN. The percentages of correct responses for each gap length were used to construct psychometric functions, allowing estimation of the gap-detection threshold. Psychometric functions were transformed according to SDT into sensitivity (*d'*), using the fitted psychometric functions, including empirical FA rates, on a session-by-session basis. Threshold was defined as the estimated gap length corresponding to a sensitivity of $d' = 1$. B) The slope was the gradient of the psychometric curve at threshold sensitivity. The function's asymptote was used to compute the maximum sensitivity.

2.1.8 Statistical Analysis

Statistical tests were conducted using a generalized multi-level mixed effects model of the raw data, according to a Bernoulli distribution, in *R* (www.r-project.org), and in MATLAB. Mixed-effects modelling allowed us to establish the contribution of modulating fixed effects (e.g. stimulus type, gap duration) to any differences in the observed distributions, while controlling for small fluctuations in the distributions yielded by random effects (e.g. subject identity, testing session). Tests for significance of derived behavioural measures were performed in MATLAB using multi-level linear mixed effects models (lme), with subject identity and testing session included as nested random factors. Post-hoc tests were Tukey-corrected for multiple comparisons. Data are reported as mean ± standard error (SE).

In order to assess the significance of correlations between threshold and slope, a bootstrap procedure was employed. Here, the between-group correlation statistic (Spearman's ρ) was calculated (for threshold vs. slope across stimuli and subject). Pairs of data points were then resampled with replacement from each randomly shuffled set, and the correlation computed. This procedure was repeated 10000x to generate a reference distribution, from which the two-sided p-value of the actual statistic was computed.

2.2 Auditory Brainstem Responses (ABRs)

2.2.1 Recording Procedures

Animals underwent sedation with a mixture of Domitor (medetomidine hydrochloride, 0.022 mg/kg intramuscular, Pfizer) and Narketan-10 (ketamine hydrochloride, 0.05 mg/kg intramuscular, Vetoquinol), with repeat administration, if necessary, of an intramuscular bolus during recordings. Sterile subcutaneous monopolar needle electrodes (0.35 x 12 mm, MN3512P150, Spes Medica) were inserted bilaterally at the level of the mastoids behind the ipsilateral ear (active), medially at the vertex (reference), and above the scapula (ground) (Fig.2-5). Recordings were conducted until all stimuli had been presented or ferrets recovered spontaneously from sedation. Antisedan (atipamezole hydrochloride, 0.5mg/kg subcutaneously, Jansenn Animal Health) was administered to antagonise the effects of Domitor, and ferrets were returned to home cages. Recording sessions were conducted daily in blocks of ≤7 days.

Sounds were generated using TDT System 3 hardware and MATLAB. Sounds were presented monaurally to each ear in an anechoic room through earphone drivers (Panasonic RPHV297) mounted on otoscope speculae inserted into each ear canal. Earphones were closed-field calibrated using a 1/8 inch condenser microphone (Brüel and Kjær 4138), and inverse-filtered to flatten output between 100 Hz – 30 kHz.

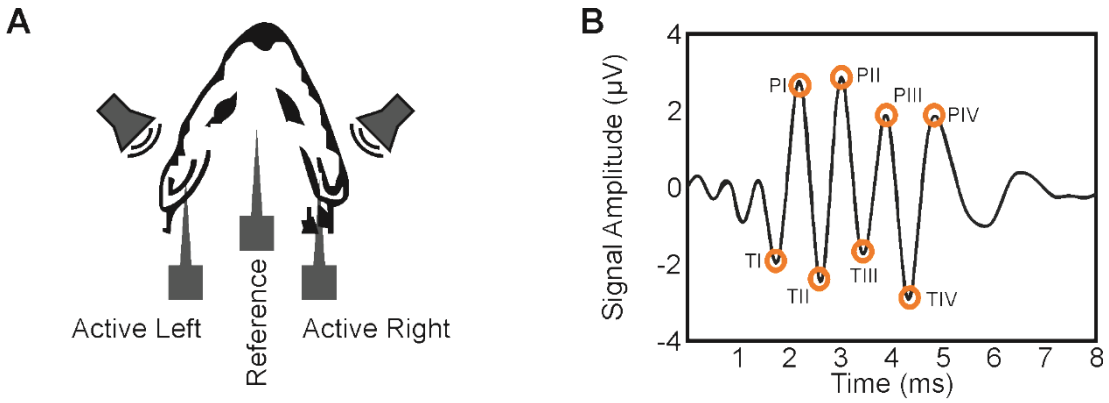

Figure 2-5: Auditory Brainstem Responses (ABRs). A) Recording Schematic. Following sedation, sharp electrodes (in grey) were inserted subcutaneously at the vertex (as reference) and bilaterally over the mastoids (as active). B) Example ferret ABR, which typically possesses four easily-identifiable waveform complexes (I – IV), each comprising a trough (T) and its following peak (P). Though possibly identifiable on this diagram, a fifth wave was unreliably detected, and so omitted from analysis. The trough-peak inversion of the ABR derives from the recording setup described in the main text. As such, each trough here corresponds to a peak in other publications, and vice-versa.

2.2.2 Acoustic Stimuli

ABRs were recorded bilaterally for three different stimulus types, in each case presented in blocks of 750 repetitions, in order of ascending level or high-pass corner frequency, as appropriate (see below). Stimuli were:

- rarefaction click trains (rectangular voltage pulse, 100 μsec duration, low-pass filtered at 30 kHz, ~20/sec, 40 - 90 or 100 dB SPL, 10 dB steps);
- narrow band-passed pink noise chirps (centre frequencies 1 kHz, 4 kHz, 8 kHz, 16 kHz; 100 μsec duration, half-octave high- and low-pass filtered, ~20/sec, 50- 90 dB SPL, 10dB steps);
- masked click trains modelled after Don et al. (2005) (clicks as above at 100 μsec duration, low-pass filtered at 30 kHz, ~20/sec, 80 dB SPL, with overlaid ipsilateral pink-noise acoustic mask, 80 dB SPL[1], initially high-pass filtered at 0.5 kHz, with increasing high-pass corners for each stimulus block, at 1 kHz, 2 kHz, 4 kHz, 8 kHz, 16 kHz, 24 kHz, and 50 kHz, i.e. unmasked click).

Stimulus presentation rate was not fixed at exactly 20/s due to variability in sweep buffering in TDT hardware, leading to sweep-to-sweep interstimulus interval variability (and thus preventing the extraction of any measure of the brainstem frequency following response).

[1] The level of the noise masker was optimised to minimise click signal for the broadest masker content; that is, for the 0.5 kHz high-pass masking condition, the lowest level of masker that reliably and completely masked an 80 dB SPL click was an 80 dB SPL pink noise masker.

2.2.3 Signal Processing

Recorded voltage signals were digitally sampled at 25 kHz. Data acquisition was performed using TDT System 3 hardware, and computers running BrainWare software (Tucker-Davis Technologies) and custom-written MATLAB scripts. Offline, digital signals were bandpass-filtered according to recommendations in Granzow et al. (2001) (finite impulse response (FIR) filter implemented in MATLAB using `dfiltdr`; 10 Hz to 1900 Hz, Hamming-windowed, 200 taps, 6 dB attenuation). We corrected for step response artefacts introduced during filtering by subtraction of the sweep mean baseline prior to filtering, followed by post-filtering time shift of -0.5*impulse response length, then addition of the sweep baseline value back to the sweep. The trace was then amplified up to 4000x to account for gain differences in the recording procedure.

To achieve optimal noise reduction during the averaging process, a sorted averaging approach based on cumulative noise power was applied (Mühler et al., 1999). The choice of noise threshold cannot be known in advance of the averaging procedure, meaning that any arbitrary cut-off that is applied may produce either unacceptably noisy or uninformative averages due to individual sweeps exceeding/falling short of a particular, arbitrarily chosen trace amplitude. Recording a very high number of sweeps can overcome this issue (e.g. 7920 – 15840 sweeps/stimulus in Gu et al. (2012)), since the signal-to-noise ratio (SNR) is enhanced proportional to the square root of the sweep number. However, due to time constraints that were primarily mediated by the sedation protocol, our recording procedure was limited to 750 sweeps/stimulus, precluding the use of weighted

averaging procedures optimised for high sweep numbers (Riedel et al., 2001; Gu et al., 2012). By contrast, sorted averaging approaches are effective for lower sweep numbers (<1000 sweeps), and do not require normalisation of sweep amplitudes (Rahne et al., 2008).

The double-iteration sorted averaging approach we used was conceptualised following Riedel et al. (2001) & Rahne et al. (2008). The SNR of each ABR sweep is very low (-20 to -30 dB). If we assume independence of the sources of signal (*S*) and noise (*N*), wherein signal is stable from sweep-to-sweep and noise is not, then each recorded sweep x_i at time t can be approximated as:

$$x_i(t) = S(t) + N_i(t) \approx N_i(t)$$

An estimate of the power P of each discrete sweep $x_i(t)$ of length T can be made as:

$$P(x_i) = \frac{1}{T}\sum_{t=1}^{T}\big(x_i(t)\big)^2$$

Using this estimate, all sweeps for a single stimulus block were sorted in order of increasing power $P\big(x_i(t)\big) \equiv P_i$. Thus, the noise value determined *a posteriori* as a threshold for inclusion in the final average waveform is computed by cumulatively averaging together sweeps (from low-to-high power) and minimising the power of the mean cumulative residual noise:

$$P_{cum}(J') = \frac{1}{J'(J'-1)}\sum_{j'=1}^{J'} P(N_{j'}) \approx \frac{1}{J'(J'-1)}\sum_{j'=1}^{J'} P_{j'}$$

where j' is an index of sorted sweeps, from least to most power.

An optimal number of sweeps is achieved such that the averaged waveform residual noise is minimised. Given the assumed non-stationarity of noise contributions to each sweep, there will be a J' such that a minimum is found after j' ordered sweeps, with further sweeps added leading to an increase in cumulative mean noise power beyond the increase in the denominator $J'(J'-1)$ caused by raising J' by 1. Therefore, the optimal number, J_s, of sweeps can be found using this approach, yielding a sorted average signal estimate:

$$s_s(t) = \frac{1}{J_s} \sum_{j'=1}^{J_s} x_{j'}(t)$$

Furthermore, we can enhance our estimate of the noise contribution to each sweep by subtracting this first-order signal estimate $s_s(t)$ from $x_{(t)}$:

$$x'_i(t) = S(t) + N_i(t) - s_s(t)$$

Since $x'_i(t)$ is a closer approximation of $N_i(t)$ than is $x_i(t)$, it follows that by repeating the sorted averaging procedure on this new set of corrected sweeps, a better signal estimate $s_{s'}(t)$ can be obtained. This iterative averaging procedure (Riedel et al., 2001) was conducted once (i.e. generating a first-order approximation of $S(t)$) due to computational constraints, though noting that additional iterated averaging-then-sorting would yield better estimates of $S(t)$.

2.2.4 Feature Extraction and Analysis

Automated feature detection of filtered waveforms, with visual verification and correction as necessary, was performed for each level*frequency stimulus combination by generating templates derived from grand average waveforms of all pre-lesion recording sessions across all animals. The boundaries of each time window coincided with peaks in the waveform, determined visually from the grand average waveform and by comparison with normative data (Piazza et al., 2014b), and being points of inflection in the waveform's first derivative. Each averaged ABR underwent automated feature detection prior to visual inspection to ensure features were not missed as a function of falling substantially outside the template boundaries.

The ferret ABR is typical of that observed in small mammals, possessing four easily-identifiable wave complexes within 8-10 ms after stimulus onset, reflecting activity in axon tracts containing the synchronised discharge of generator nuclei within the auditory brainstem (Melcher and Kiang, 1996; Melcher et al., 1996a, 1996b) (Fig.2-5). Troughs (I – IV, typical of the ferret ABR (Morey and Carlile, 1990; Moore, 1993; Piazza et al., 2014a, 2014b) were defined as local minima within specified time windows, and were equivalent to peaks described elsewhere due to inversion of the typical active-reference electrode locations. Thresholds were defined as the minimum stimulus intensity for reliable ABR detection.

To compute derived and stacked ABRs, Don et al.'s (2006) methodology was followed. After filtering (see above), an inferred ABR corresponding to an octave-band region of the cochlea can be obtained from masked-ABR waveforms by subtracting the waveform at masking high-pass corner frequency x from that directly

above x in our stimulus paradigm, yielding an ABR waveform logarithmically centred between the high-pass corner frequencies of the two stimuli. For example, an octave-band ABR putatively centred at 707 Hz can be obtained by subtracting the waveforms measured in response to masked click stimuli of HP = 500 Hz and HP = 1000 Hz, such that the centre frequency $f_c = \sqrt{500 \times 1000} \approx 707\ Hz$. On extracting these derived-ABRs, a stacked-ABR can be constructed – this technique examines the contribution of all regions of the cochlea contributing to the ABR, rather than predominantly high-frequency/basal regions of the cochlea, that dominate the click-ABR. The stacked-ABR was generated by temporally aligning the derived-ABR waveforms for each session such that the latencies of trough IV coincide, and then summing across these aligned derived-ABRs. Due to the robustness of waveform detection, alignment was performed to trough IV from the $\sqrt{24000 \times 50000} \approx 34.6\ kHz$ derived-ABR waveform. This temporal alignment procedure eliminates phase cancellation of lower frequency activity.

For all waveforms, latencies were measured as the time-to-trough from stimulus onset, with inter-wave latency differences obtained for waves II – IV in comparison with wave I from the same ABR complex; in those cases where wave I could not be detected, that waveform was excluded from analysis. We additionally derived the normalised interaural difference in the latency of wave IV between the ears of the same subject (IT4, equivalent to the IT5 measure in human patients) (Selters and Brackmann, 1977): in the absence of retrocochlear disease, the arrival time of ascending cochlear information should be symmetrical between the two ears, with

unilateral otoacoustic nerve disturbance inducing a conduction delay compared to the intact ear (Selters and Brackmann, 1977; Don et al., 2005).

Amplitudes were defined as the absolute difference between troughs of waves I – IV, and the subsequent peaks, yielding a measure of the signal strength of the contributory fibre bundles involved in wave generation, while amplitude ratios were calculated for waves II-IV normalised against the amplitude of session-matched wave I; as for interwave latencies, exclusion of a waveform complex would occur in the absence of detectable wave I. The total fibre population underlying the ABR was estimated by measuring the waveform root mean square (RMS) amplitude between 1 – 10 ms post-stimulus.

For each stimulus type, LMEs were constructed to statistically evaluate the effects of lesion status and stimulus parameters (level, frequency, etc.) on the observed measures of function obtained from ABR analysis, with correction for multiple comparisons using Tukey's method.

2.3 Lesion of the Spiral Ganglion

The procedure for partially lesioning the right spiral ganglion (SG) was adapted from a protocol described by Snyder and colleagues (Snyder et al., 2000). This was chosen to ensure hearing loss was restricted, predictably, to one ear only (compared with ototoxic or noise-trauma-mediated insults), and to mimic, in part, the kind of pathology observed following peripheral auditory damage, irrespective of the integrity of the cochlea and basilar membrane (which, in our case, were intended to remain undamaged).

2.3.1 Surgical Procedures

After sedation with a mixture of Domitor (medetomidine hydrochloride, 0.022mg/kg intramuscular, Pfizer) and Narketan-10 (ketamine hydrochloride, 0.05 mg/kg intramuscular, Vetoquinol), a tracheal cannula was inserted orally following glottis administration of lidocaine (5% w/w topically, Biorex), and gas anaesthesia induced with IsoFlo (isoflurane, 2% v/v in oxygen, Abbott). Antisedan (atipamezole hydrochloride, 0.5mg/kg subcutaneously, Jansenn Animal Health) was administered to antagonise the effects of Domitor once anaesthesia was stable with isoflurane.

A continuous infusion of normal saline with glucose (5% w/v) was provided through an intravenous cannula inserted into the radial vein. We administered Atrocare (atropine sulphate, 0.06mg/kg subcutaneous, AnimalCare) to minimise pulmonary secretions, Dopram (doxapram hydrochloride, 4mg/kg subcutaneously, Pfizer) to regulate cardiac rhythm and increase respiration rate, and Vetergesic (buprenorphine hydrochloride, 0.03mg/kg subcutaneous, Alstol Animal Health) and Metacam (meloxicam, 0.2mg/kg, subcutaneous, Boehringer Ingelheim) for

perioperative analgesia. The ferret's eyes were protected with Viscotears (carbomer, Novartis Pharmaceuticals). The electrocardiogram, respiration rate and end-tidal CO_2 were monitored, and body temperature maintained at ~38°C with a heated plate (covered by a blanket) and Bair Hugger warming device (3M).

After exposing the bulla on the right side of the ferret's skull, a bullotomy was performed to reveal the underlying cavernous bony convolutions, allowing access to the round window (Fig.2-6). SG was accessed directly by penetrating through the round window membrane and viewing the osseous spiral lamina. The bone overlying Rosenthal's canal was destroyed by manual curettage with a hypodermic needle, and the subjacent SG lesioned. Upon completing the lesion and stopping fluid effusion, the round window and overlying bulla were resealed using sterilised filter paper (Whatman) and BoneWax (Ethicon), with the overlying muscle and skin sutured. We provided postoperative analgesia with Vetergesic (as above) and Metacam (0.15mg/kg perorally), and Synulox (amoxicillin clavulanate, 30mg/kg subcutaneously, Pfizer) to minimise risk of bacterial infection. Animals were allowed at least 14 days to recover prior to reinitiating behavioural testing.

2.3.2 Histological Processing and Analysis

Verification of the site of SG lesion was performed by light-microscopic analysis of cochlear sections obtained *post-mortem*. Following pentobarbital overdose (Euthatal, 400mg/kg pentobarbital sodium intraperitoneally, Merial Animal Health), the animal was perfused transcardially with 200 ml of normal saline and 4% fresh paraformaldehyde in 0.1 M phosphate buffer (PB, pH = 7.2 – 7.4). The bulla was opened, and the cochleae extracted and incubated in decalcifying solution (5 mM

EDTA in 1% paraformaldehyde in 0.1M PB) for ≥6 weeks on a rotator at room temperature. Following removal of the bony shell of the cochlea, the cochlea was dehydrated in a graded ethanol series and embedded in resin. Serial sections (10 µm thick) tangential to the modiolus were cut and stained with Toluidine blue. SG cell counts were performed on five non-adjacent sections from the basal coils in each cochlea.

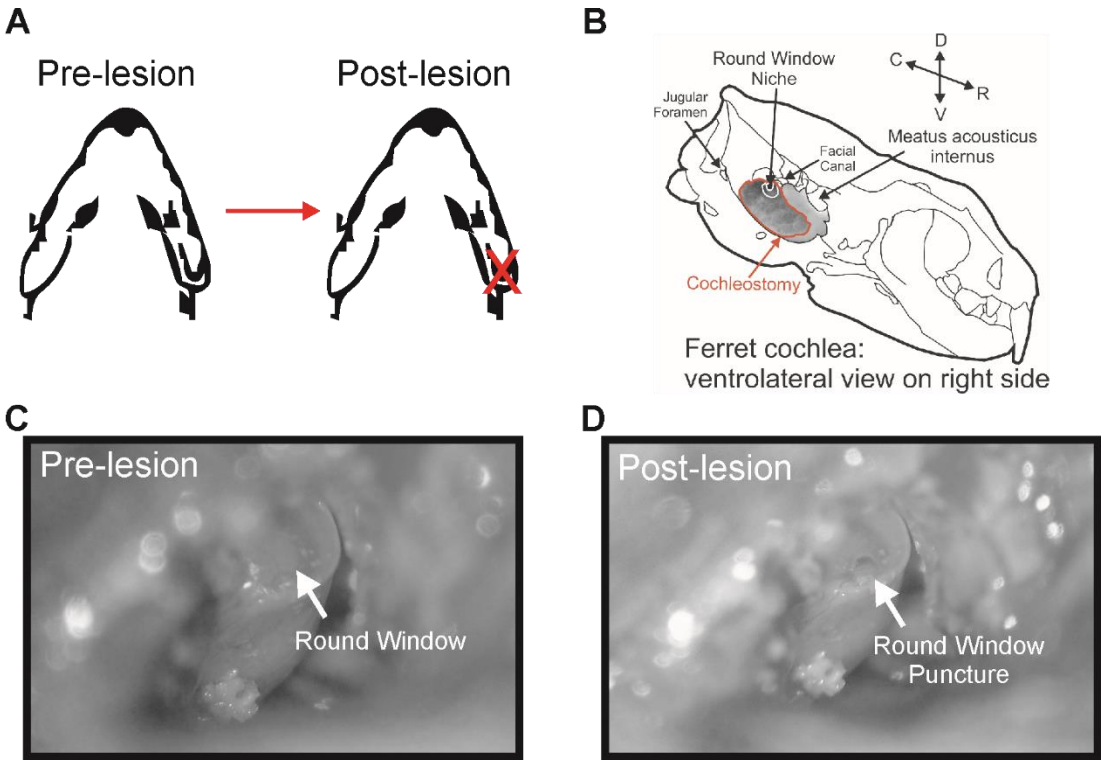

Figure 2-6: Lesion of the SG. A) Animals underwent selective lesion of the right SG, under general anaesthesia. B) Schematic of the ferret skull, following a large cochleostomy on the right. From the bony protrusions of the ferret skull at and near the bulla, we pinpointed a location for incision and subsequent drilling to expose the underlying bony convolutions of the inner ear and semi-circular canals. Note the proximity of the incision site to the facial canal, which ought to be avoided to minimise the risk of facial nerve injury. C) Photograph of the round window membrane, viewed through the bullotomy. The curve of the basal coil of the cochlea is obvious. D) The same round window following puncture, with the site of curettage apparent from the small hole in the round window membrane.

2.4 Optogenetic Implantation and Silencing of the Primary Auditory Cortex

2.4.1 Implantation Surgery

Preparation for surgery, sedation, anaesthesia, and perioperative care and monitoring were the same as previously mentioned for cochlear surgery (Section 2.3). Additionally, bi-hourly boluses of Augmentin (amoxicillin, 50mg/kg; clavulanic acid, 10 mg/kg intravenous; Pfizer) were administered peri-operatively to reduce the risk of infection.

The ferret was mounted in a stereotaxic frame, and after making incisions to expose the skull, the temporal muscles were retracted, and bilateral craniotomies and injection site-specific durotomies performed over the ACs at the middle ectosylvian gyri (MEG). At five sites in each A1/AAF, governed largely by cerebral vasculature, pressure injections were made of a viral vector encoding Archaerhodopsin-T (ArchT) (Han et al., 2011). Vector viral constructs were provided by E. Boyden (Massachusetts Institute of Technology), and manufactured by UNC VectorCore (Gene Therapy Centre, University of North Carolina, Chapel Hill), at typical viral titres of 10^{12} infectious units/ml. Within a serotype-8 adeno-associated viral plasmid (pAAV8), the ArchT opsin gene was fused without stop codons, in frame, ahead of green fluorescent protein (GFP) under the synthetic CAG promoter (pAAV8-CAG-ArchT-GFP) (Jun-ichi et al., 1989; Niwa et al., 1991) (Fig.2-7). Injections of pAAV8-CAG-ArchT-GFP were made with a microinjector (Nanoject II, Drummond Scientific) using a glass pipette with 15-30 μm tip internal diameter. Two injections of 41.4 nl each were made per injection site, at sub-pial depths of 1 mm and 500 μm. There was a delay of

at least 5 minutes between each injection to allow intracortical pressure to normalise, and to prevent reflux of injected boluses upon pipette removal. One control animal underwent an identical injection protocol, except that the injected plasmid contained no ArchT (pAAV8-CAG-GFP).

Following completion of injections, a single ceramic zirconia ferrule fibre-optic implant (multimode fibre, ⌀200 µm, 1.5 cm length with 0.5-1 mm exposed, numerical aperture = 0.22; Shanghai Laser and Optics Century Company) was lowered to the brain surface in each hemisphere, and centred between the injection sites as appropriate given the local vasculature. The fibre and surrounding craniotomy were sealed in place with silicone elastomer (Silastic, Dow Corning), and fixed with dental cement (C&B Superbond, Sun Medical). The optical implants were secured with a bone cement (Palacos, Zimmer Biomet) pedestal built around and between each fibre, with a threaded plastic cylinder and removable cap providing protection and access to the optic implant ferrule.

Before reinitiating behavioural testing, ferrets were allowed ≥6 weeks to recover and to enable maximal expression of ArchT protein in the membrane of transfected cortical cells.

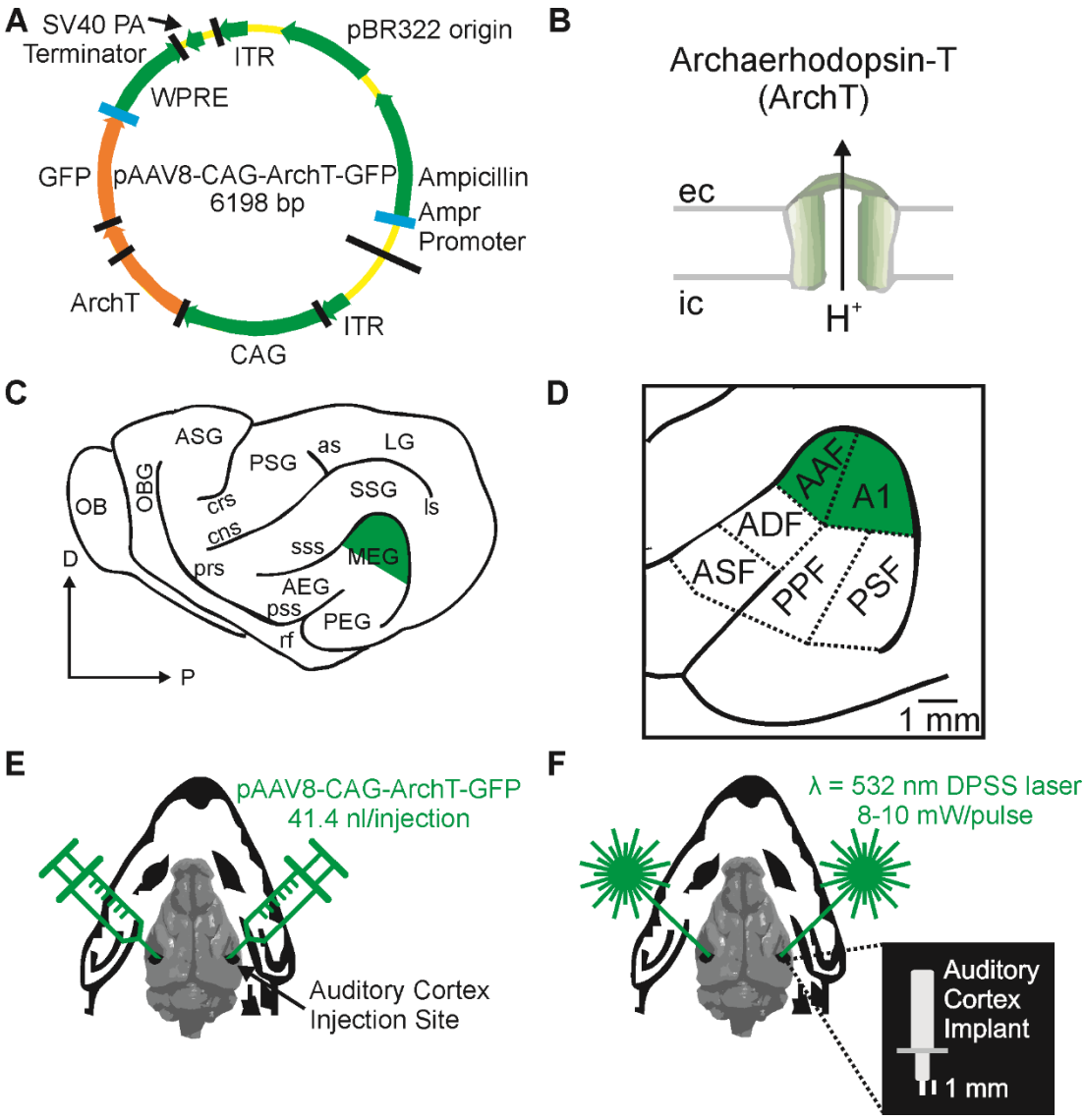

Figure 2-7: Overview of Optogenetics Methodologies. A) Schematic of optogenetic construct. The construct used was an adeno-associated viral plasmid, serotype-8 (pAAV8). Of note: the CAG promoter is a universal promoter facilitating high expression levels in all transfected cells; the ArchT locus, encoding opsin protein Archaerhodopsin-T, a light-activated membrane-bound outward proton pump; the GFP locus, encoding GFP for identification of transfected cells. B) ArchT activity. Cartoon shows the intracellular (ic) to extracellular (ec) H^+-pumping action of ArchT, upon light activation (Han et al., 2011). C) Schematic showing a lateral view of the ferret cerebral cortex. The injection sites throughout MEG are labelled in green. The ferret AC extends within the ectosylvian gyrus to encompass its anterior (AEG) and posterior (PEG) regions, and adjacent banks of the suprasylvian sulcus (sss). D = dorsal, P = posterior. D) Enlarged schematic of ferret AC, showing cortical fields. Injections were made throughout AAF/A1, together comprising primary AC. Modified from Bizley et al. (2015). For remaining terms, see list of abbreviations. E) Schematic showing injections bilaterally in AC. F) Following injections, fibre optic implants (see inset) were positioned above AC to allow laser (λ = 532 nm) illumination of injection sites.

2.4.2 Behavioural Testing

Following recovery, animals were reintroduced to behavioural testing without any optogenetic stimulation, to ensure behavioural consistency with pre-implant performance, prior to beginning testing during laser illumination. This period of behavioural testing was conducted while the ferret was attached to two flexible fibre optic tethers (multimodal fibres, ⌀ 200μm, 2 m length, numerical aperture = 0.22, Shanghai Laser and Optics Century Company) via ceramic ferrules connected to the implanted optical fibres (FC-type connection). The optic tethers were suspended from the ceiling of the behavioural testing chamber by a twin-path optical commutator (FRJ 2x2, Doric Lenses), to prevent cable twisting. The commutator was connected to two laser output devices (green light: λ = 532 nm, diode-pumped solid state (DPSS) laser, maximum power output = 260 mW, Shanghai Laser and Optics Century) located outside of the behavioural chamber, controlled via custom scripts written in MATLAB.

Once stable behavioural performance was achieved in the presence of the cables, animals underwent testing on gap-in-noise detection as described above. The testing procedure was repeated for each of three laser illumination configurations: left AC (contralesional), right AC (ipsilesional) and simultaneous bilateral. For each optical fibre configuration testing block, laser illumination was applied pseudorandomly 1:1 laser-ON:laser-OFF, i.e. 50% of trials (gap & no-gap) with illumination, 50% without. For each trial on which optogenetic suppression was applied, a single laser pulse was applied to the optic tethers, gated by a TTL-driven shutter. Illumination was initiated 100 ms prior to the sound onset, and maintained

for the sound's duration (2180 ms in total). Laser stimulation was applied at 8-10 mW, calibrated at the optic tether fibre tip.

Optogenetic behavioural data analysis was identical to that described above (subject to equivalent psychometric fitting parameters and evaluation of response time data). However, due to the low number of trials in each session for each gap-length*laser-state combination, session-by-session analysis was not conducted. That is, behavioural data were pooled across sessions, with an inclusion criterion of >30 trials/session. Due to the presence of the optical fibre implant and laser illumination, automated head-tracking data were not collected. The residual effects of laser illumination on behavioural performance were examined by constructing psychometric functions for each animal, based on the laser illumination state of each trial compared with the previous trial.

2.5 Neurophysiological Recordings of Auditory Cortex

Recordings made in ACs of lesioned ferrets (n = 6) and unlesioned controls (n = 3) were conducted under general anaesthesia, to eliminate any attentional aspects that might be related to the presence of the lesion impacting upon processing in the auditory cortex. Since tinnitus may occur exclusively during wakefulness (De Ridder et al., 2014), anaesthesia offers a way of removing phantom perceptual experience as a convoluting factor affecting neural responses.

2.5.1 Surgery

Preparation for surgery, sedation, and perioperative care and monitoring were the same as previously described for cochlear surgery. Anaesthesia was maintained with continuous intravenous infusion of Domitor and Narketan-10 in normal saline with glucose (5% w/v). Dexadreson (dexamethasone sodium phosphate, 0.5 mg/kg intramuscular, MSD Animal Health) was administered every 12 hours to reduce the risk of brain oedema.

The ferret was placed in a stereotaxic frame with blunt ear bars to secure the head, and the skull exposed. The temporal muscles were retracted, and a head-holder securely attached to the skull using dental cement (Super Bond C&B, Sun Medical), with the ears returned to their natural position. Bilateral craniotomies were performed over ACs at the position of MEG (Fig.2-8), and the surface of the brain protected with silicone oil (dimethyl siloxane). The animal was then moved into an anechoic chamber (Industrial Acoustics Co.).

2.5.2 Recording Procedure

Neural spiking activity was recorded using silicon multichannel probes (Neuronexus), with penetrations made using manual microdrives (Narishige) to sample broadly throughout A1, and occasionally in AAF (Fig. 2-8). At the site of each intended penetration (informed by vasculature and surface architecture), a small durotomy was made, with at least 15 minutes allowed between electrode insertion and the initiation of recordings, enabling cortical pressure to normalise. Electrode configuration was predominantly 4x8 (four shanks, each with eight active sites, 100 μm vertical spacing) (Neuronexus A4x8-5mm-100-200-177-A32) (Fig. 2-8). In some instances either 4x4 or 1x16 configurations were used. Recording locations were verified functionally by analysing, online and offline, frequency response areas of active units, which were used to estimate cortical field locations according to the tonotopic gradients that delineate them (Bizley et al., 2005); and anatomically, using reconstructions from photographic records and histological analyses made with Nissl-processed brain sections.

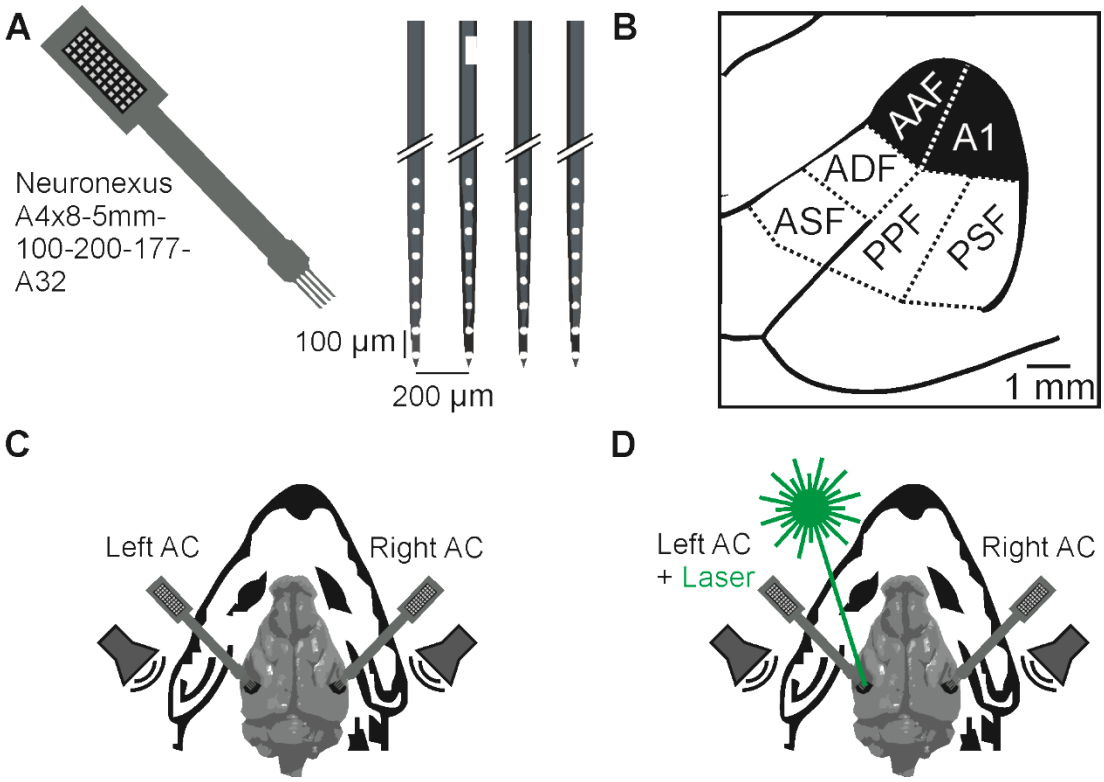

Figure 2-8: Neurophysiological Recording of Multiunit Activity in AC A) Schematic of extracellular silicon probes used for recordings. Most recordings employed 4x8 probes (Neuronexus), with 32 channels present as an array arranged evenly across four shanks, each 5 mm in length. The distance between active sites on each shank was 100 µm, while the distance between shanks was 200 µm. Active sites were 177 µm² in surface area. The reference site is visible as the white rectangle on the second shank from the left. Where different probe arrangements were used, the active site distance and surface area remained constant. B) Lateral view of the ferret AC. Recordings were primarily made in A1, and occasionally in AAF, according to local vascularisation. For remaining terms, see list of abbreviations. C) Recording setup. Under general anaesthesia, and following bilateral craniotomy, recordings were made in each AC. Acoustic stimulation was provided bilaterally from closed-field speakers. D) Optogenetic neurophysiology. In those animals that had undergone optogenetic implantation, recordings in AC were made following implant removal. Laser stimulation was applied directly to the cortical surface on the left.

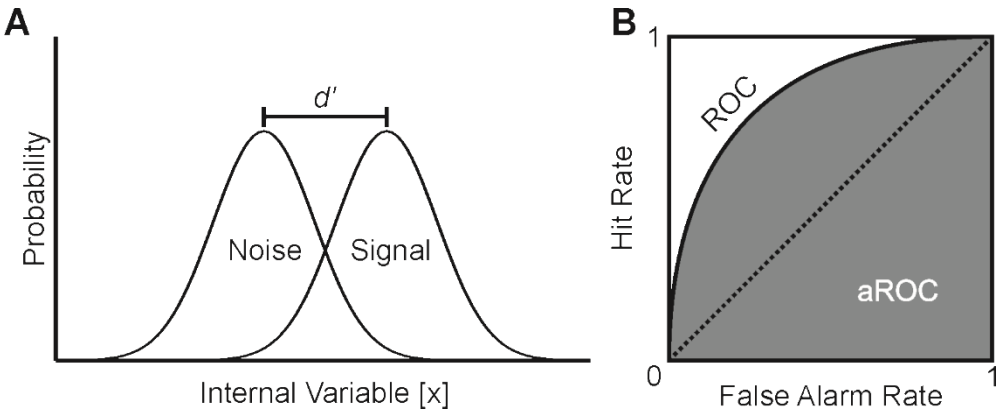

Figure 2-9 Overview of Signal Detection Theory (SDT). A) Under the standard model of SDT, stimulus information (e.g. gap length) is represented as some undefined, internal variable [x]. The probability distribution of [x], for each stimulus type, is Gaussian. For each stimulus presentation, the value of [x] can be mapped onto internal probability distributions that describe the likelihood of that value of [x] coming from a source categorised as signal or as noise. The linear distance between the midpoints of these two distributions defines the subject's capacity to discriminate signal trials from noise trials on the basis of [x], otherwise known as the index *d′*. In a related fashion, by placing a decision point, or criterion, between the two distributions, the rate of correct and incorrect responses can be defined: of interest are correct signal trials (Hit) and incorrect noise trials (False Alarm). B) By changing the position of the criterion along the abscissa, the relative Hit and False Alarm (FA) rates can be modified, with these values plotted as a so-called Receiver Operating Characteristic (ROC). For conditions where signal and noise are not discriminable, the Hit and FA rates are identical, and so the ROC curve is the unity line. As the signal and noise distributions become more separated, the ROC curve tends towards the upper left-hand corner of ROC space. The area under the ROC curve (aROC, in grey) is mathematically related to the value of *d′* illustrated in (A) (Macmillan and Creelman, 2005).

Voltage signals were filtered (300 Hz to 3 kHz), amplified up to 40000x, and digitized at 25 kHz using TDT System 3 processors. Neuronal spiking responses were isolated from digitized signal off-line. Spiking responses from a mixture of single units and small multiunit clusters (together referred to as "units"), and from A1 and AAF, were pooled to increase statistical power. Data were analysed in MATLAB.

2.5.3 Acoustic Stimuli

Sound stimuli were designed and generated in MATLAB, and were presented through earphone drivers (Panasonic RPHV297) mounted on otoscope speculae inserted into each ear canal close to the tympanic membrane. The earphones were closed-field calibrated using a 1/8 inch condenser microphone (Brüel and Kjær 4138), and inverse-filtered to flatten output between 100 Hz – 30 kHz. During each penetration, stimuli were presented sequentially, with fifteen pseudorandomised sweeps recorded of each stimulus component combination (level, frequency, etc.):

- Broadband noise bursts (400 ms duration, 50 – 90 dB SPL; 600 ms interstimulus interval (ISI); or 2080 ms duration, 50 – 90 dB SPL; 920 ms ISI)
- Silence (3000 ms sweep duration) to estimate spontaneous firing rates (SFR).
- Pure sine-wave tones (100 ms duration, 5 ms cosine-ramped; 400 ms ISI; 40-90 dB SPL, 10 dB steps; 500 Hz – 30 kHz, 0.16 octave steps).
- Gap-in-noise stimuli: Broadband noise bursts (low-pass filtered up to 30 kHz; BBN) or one of three narrowband noise burst types (band-pass filtered with an octave-window logarithmically centred at 1 kHz, 4 kHz, or 16 kHz; NBN) and stopband roll-off ≈-52 dB/octave.

In case F1036, gap-in-noise stimuli comprised two 200-msec noise bursts bounding a gap 0-100 msec in duration, producing a stimulus of 400-500 msec duration, 5 msec cosine ramped; 600-500 msec ISI; 71dB SPL.

In other animals, gap-in-noise stimuli comprised a 2080 ms noise, interleaved with 4 gaps of duration 1-, 2-, 3-, 5-, 10-, 20-, 50-, 100-, or 270 ms, or 0 ms (i.e. no gap); >3000 msec inter-stimulus interval; 71dB SPL) was used instead.

For those animals that had undergone optogenetic implantation, laser illumination was conducted during electrophysiological recordings in response to the gap-in-noise stimuli above. The protocol was identical to that used during behavioural testing; i.e. laser illumination was pseudorandomised to 50% of sweeps, with laser onset 100 ms prior to acoustic stimulation, and lasting the duration of the sound (2180 ms in total). Laser illumination was applied only to the left AC, while recordings were made concurrently in both hemispheres. At each penetration, the optical fibre was repositioned to be directly adjacent to the site of the silicon probe penetration.

2.5.4 Data Analysis

For all analyses, unit responses were thresholded for inclusion using a 1-way ANOVA evaluating firing rates in 50 ms windows after stimulus onset ("onset") and after stimulus offset ("offset"), and equivalent windows in the ISI period. A significant response ($p < 0.05$) to any component of the stimulus grid led to a unit being included for analysis.

Frequency Response Areas (FRAs) to tonal stimuli were constructed by summing activity during each stimulus response window across all sweeps for each frequency-level combination. A nine-point running Hamming window was applied to smooth the resulting spike matrix (Bizley et al., 2005). From this smoothed matrix, a tuning curve was derived by establishing a criterion for responsiveness, defined as the mean spontaneous rate plus 20% of the peak firing rate (Sutter and Schreiner, 1991; Bizley et al., 2005). All FRAs were visually inspected to ensure congruency between the spike matrixes and derived tuning curves. From this tuning curve, the characteristic frequency (CF) was defined as the frequency at which a significant response was generated for the lowest sound level within the tuning curve; the best frequency (BF) was defined as the frequency*level combination to which the unit generated the largest response. For both CF and BF, where more than one stimulus generated the same response magnitude, the logarithmically-weighted mean was derived. Rate-level functions (RLFs) were computed as the change in firing rate at each unit's BF across all tested levels; to enable comparison across units, responses were normalised by computing the *z*-scored tone-evoked firing rate relative to the spontaneous rate (Marlin et al., 2015):

$$z = \frac{(\mu_{evoked} - \mu_{spontaneous})}{\sigma_{spontaneous}}$$

where μ and σ represent the mean and standard deviation of the firing rate, respectively. Response bandwidths (BW) were computed as CF divided by the frequency range at +10 dB (Q10) and +30 dB (Q30).

Neural synchrony was evaluated by computing cross-correlation histograms (CCHs) for clusters in response to broadband noise. For each cluster pair, the number of spike coincidences during stimulus presentation ("driven") and silence ("spontaneous") was counted, for time lags of -50 to +50 ms (1 ms bins). The CCHs were normalised bin-by-bin by the expectancy of chance correlation, *E* (Brosch and Schreiner, 1999):

$$E = \frac{N_a \cdot N_b}{N}$$

where N_a and N_b are the number of spikes in clusters *a* and *b*, and *N* is the number of bins in the recording. The shift predictor was also calculated to estimate the stimulus coordination artefact for driven trains (Perkel et al., 1967), and subtracted from driven CCHs to generate residual CCHs. Correlation strength was defined as the maximum correlation for each normalised CCH.

For gap-in-noise analysis, peri-stimulus time histograms (PSTHs) were derived for each gap length and pooled across hemispheres (5 ms bins). While approaches vary elsewhere as to the optimal means by which to evaluate gap detection sensitivity (e.g. Allen et al., 2003; Yin et al., 2008; Recanzone et al., 2011; Berger et al., 2014), we wished to utilise a measure of neural responsivity that was not reliant upon visual inspection of individual PSTHs, nor was restricted to post-gap onset responses. Thus, we employed a receiver operating characteristic (ROC) analysis, which provides a criterion-free method for estimating gap/no-gap discriminability, and has previously been employed to explore neural sensitivity in response to auditory stimuli (Skottun et al., 2001; Lemus et al., 2009; Alves-Pinto et

al., 2010; Bizley et al., 2013). The area under the ROC curve (aROC) is mathematically related to the sensitivity index *d'* of an ideal observer performing a two-alternative forced-choice task (Macmillan and Creelman, 2005), with perfect performance yielding aROC = 0 or 1, and chance performance yielding aROC = 0.5 (i.e. the major diagonal) (Fig. 2-9). While not identical to our behavioural paradigm, the use of SDT allows for some degree of comparison between neurometric and psychometric performance.

For each gap length, aROC was calculated for the distribution of spiking responses after each gap across sweeps, compared to equivalent windows in the no-gap stimulus. The ROC curve was generated from a 100-point criterion vector ranging from the minimum to the maximum of the recorded no-gap responses. For each of these criteria, a corresponding FA and hit rate were derived from the no-gap and gap spike distributions, respectively. aROC was then calculated using `trapz` in MATLAB, and normalised such that all aROC values were between 0.5 and 1 (since a discriminability of 0.1 is equivalent to 0.9 in aROC space, and so on).

To test for aROC significance, a bootstrap procedure was employed (Bizley et al., 2013): spike trains were pooled and then resampled, with replacement, to generate two new distributions, from which the aROC was computed. This approach was repeated 1000 times to yield an empirical estimate of the aROC distribution expected under the null hypothesis; the distribution was centred at 0.5, and reflected about 0.5 as necessary. An aROC value was significant if it exceeded the 95th percentile of this bootstrapped distribution. Finally, neurometric curves were plotted for each unit

yielding significant aROC values, and for each penetration, hemisphere and the brain as a whole, in which the maximum aROC value from each group's constituent components (units, penetrations and hemispheres, respectively) was used to generate the neurometric function. Neurometric curves were fitted using psignifit as for psychometric functions, except that FA rate and lapse rate priors were left unspecified. A neurometric gap detection threshold was chosen as aROC = 0.6915, equivalent to d' = 1 for a 2AFC task (Macmillan and Creelman, 2005; Walker et al., 2009).

Mutual information (MI) was computed to determine the reduction in uncertainty provided by MU responses for gap vs. no-gap stimuli , since we also aimed to employ a model-free estimate of neurometric gap detection that was not constrained to spike-rate coding, an approach used previously in ferret electrophysiology (Walker et al., 2011). MI is measured in bits, with the reduction in uncertainty about the presence of gap length *X* provided by MU response *R* indicated by the magnitude of the MI value, computed as:

$$MI(X;R) = \sum_{x \in X} \sum_{r \in R} p(x,r) \log_2 \left(\frac{p(x,r)}{p(x)p(r)} \right)$$

MI calculations were performed using the Information Breakdown Toolbox (Magri et al., 2009). MI was computed for spikes across sweeps binned using a 20 ms sliding window, sliding at half the window width to evaluate how response discriminability changes as a function of integration time. De-biasing of MI estimates was performed in the Information Breakdown Toolbox using the method of Panzeri

and Treves (1996), although different bias estimation algorithms are highly similar for ferret neurophysiological data (Walker et al., 2011).

Statistical analyses of group differences for different stimuli were performed using a bootstrap approach similar to those described above for correlation tests and aROC evaluation. Briefly, the difference between groups was computed using an appropriate statistic (for example: difference of means, *t*-statistic, *F*-statistic, rank-sum statistic, or χ^2-statistic) using an appropriate test in-built into MATLAB. Then, the data were pooled and resampled, with replacement, to generate new distributions for which the same statistic was obtained. This procedure was repeated ≥1000x to yield a bootstrapped reference distribution that would be expected under the null hypothesis, from which significance was estimated as ≥95th percentile. The pseudorandom number generator in MATLAB was seeded identically for each test, to enable reproduction of *p* values. Post-hoc tests were Tukey-corrected for multiple comparisons.

2.6 Brain Anatomy

Following these longitudinal studies (Fig 2-1), every ferret was transcardially perfused following anaesthetic overdose and the cochleae and brains were extracted for further analysis. Cochleae were processed and analysed in the Furness Laboratory, University of Keele, using methods described above; ferret brains were processed and analysed in Oxford.

2.6.1 Perfusion

Following pentobarbital overdose (Euthatal, 200mg/ml pentobarbital sodium intraperitoneal, Merial Animal Health), preceded by sedation with Domitor (medetomidine hydrochloride, 0.022 mg/kg intramuscular, Pfizer), blood vessels were intracardially washed with 200 ml of normal saline, followed by fixation with 4% paraformaldehyde in 0.1M PB (pH=7.4).

2.6.2 Histological processing

Brains were extracted from the skull, post-fixated in the same fixative for ≥12 hours and embedded in a 30% sucrose PB solution for cryoprotection. Sections were cut on a freezing microtome at 45 μm thickness and collected serially. For two ferrets (F1036, F1114), sections were cut in the pseudo-parasagittal plane parallel to the suprasylvian sulcus (sss, Fig.2-7C) and stained to visualise Nissl substance with cresyl violet (0.5% w/v). Otherwise, sections were cut in the coronal plane and collected in five sets of parallel serial sections, with sections in one set undergoing Nissl staining. A second set of sections were used to visualise neurons and ArchT via GFP fluorescence using immunostaining with two different fluorophores. Rabbit polyclonal anti-GFP (AbCam) and mouse anti-neuronal nuclei protein (NeuN, Millipore) were used as

primary antibodies (72 hours at 5 ℃, dilution 1:500) and anti-rabbit conjugated to Alexa Fluor®488 for GFP detection and anti-mouse conjugated to Alexa Fluor®568 for NeuN detection were used as secondary antibodies in the same sections (Molecular Probes Inc., dilution 1:200). Sections were mounted and coverslipped with Vectashield mounting medium containing DAPI (Vector Labs.).

The third set of sections underwent staining to reveal NADPH-diaphorase activity by incubation at 37°C in 1.2 mM β-NADPH (tetrasodium salt; Sigma-Aldrich), 0.1 mM nitroblue tetrazolium (Sigma) and 0.8% (w/v) Triton X-100 in phosphate buffer saline (PBS, pH8.0) while the fourth and fifth set of sections were used for nNOS and Egr1/Arc immunocytochemistry following Coote and Rees (2008) and Korb et al. (2013), respectively. After endogenous peroxidase activity was blocked, sections were first incubated in 0.1 M PB saline (PBS) with 5% normal horse serum to reduce non-specific binding of antibodies, followed by 72 hours incubation in primary antibodies (anti-nNOS mouse monoclonal antibody, clone 3G6B10, Fisher Scientific; anti-Arc mouse monoclonal antibody, cell line 48B2, Synaptic Systems GmbH. Both at dilution 1:500, 5°C). Two hours incubation in biotinylated secondary antibody (horse anti-mouse, 1:200, Vector Labs) preceded 90 minutes incubation with avidin-biotin complex (ABC Vectastain Elite, Vector Labs) and 3, 3'-diaminobenzidine tetrahydrochloride reaction (0.4 mM DAB and 9.14 mM H_2O_2 in 0.1 M PB). Negative and positive controls were performed by incubating some sections without the primary antibodies and by combining sections from controls and experimental cases in the same immunoreaction, respectively.

2.6.3 Analysis and quantification

Brain sections were analysed using optical and fluorescence microscopy (Leica DMR microscope) and a confocal microscope (LSM 710, Carl Zeiss Microimaging). The peak excitation and emission wavelengths of the fluorophores used are, respectively: 402 and 421 nm for DAPI, 488 and 525 nm for GFP and Alexa Fluor®488, and 568 and 603 nm for Alexa Fluor®568.

Neurolucida and StereoInvestigator software (MicroBright Field) were used for histological pictures and reconstructions and stereological estimations.

Chapter 3

Auditory Gap-in-Noise Detection Behaviour in Ferrets and Humans

3.1 Introduction

Ethologically-relevant auditory stimuli are complex, with the auditory system displaying sensitivity to information represented not only by the frequency content of sound, but also the temporal structure of sounds such as human speech and animal vocalizations (Lisker and Abramson, 1964; Kuhl and Miller, 1978; Sinnott and Adams, 1987; Viemeister, 2014). Gap-in-noise stimuli may be considered an experimental analogue of more complex acoustic features such as voice-onset time and phonemic separation (Eggermont, 1999; Frisina, 2001; Phillips et al., 2002; Tomita et al., 2004). As a simplified representation of these temporal variations in stimulus content, behavioural gap-detection paradigms have facilitated the interrogation of auditory

temporal processing, and the characterisation of the effects of degraded listening conditions associated, for example, with ageing and hearing loss, on human temporal processing (Barsz et al., 2002; Busby & Clark, 1999; Gośdon-Salant & Fitzgibbons, 1993; Harris et al., 2010; Schneider & Hamstra, 1999; Schneider et al., 1994; Snell & Frisina, 2000; Walton, 2010).

Across different species, changes in gap-detection thresholds have been reported following central or peripheral auditory insults, with recent interest in the possible utility of gap-detection measures to indicate the presence of tinnitus-like auditory perceptual abnormalities (Turner et al., 2006, 2012). Although the neural mechanisms underlying maladaptive changes in temporal processing remain to be elucidated, behavioural testing may nevertheless allow for these mechanisms to be classified and understood (Gold and Bajo, 2014). The characterisation of relevant animal models may thus improve our understanding of both the neurobiological basis for these changes in perception, and how the temporal structure of sounds is represented in the impaired human auditory system.

As a model experimental species, the ferret has demonstrated remarkable utility in investigating acoustically-driven behaviours, and for interrogating the underlying brain structures and physiological processes. Ferrets vocalise (Nodal and King, 2014) and hear in a frequency range overlapping that of humans (Kelly et al., 1986), and have been used extensively to behaviourally investigate spatial hearing (Keating et al., 2014; King et al., 2007; Nodal et al., 2008; Tolnai et al., 2014), pitch processing (Walker et al., 2009; Yin et al., 2010), and auditory scene analysis (Ma et

al., 2010; Alves-Pinto et al., 2012). The ferret's well-described AC fields (Bizley et al., 2005; Kelly et al., 1986; Nelken et al., 2004; Wallace & Harper, 1997; Wallace et al., 1997) and sub-cortical connectivity (Bajo et al., 2007, 2010a) have made this species well-suited for investigation of the neural circuitry responsible for adaptation to altered peripheral inputs (Bajo et al., 2010a; Bizley et al., 2007; Hartley et al., 2010; Irving et al., 2011; Isaiah et al., 2014; Keating et al., 2013; Nodal et al., 2010, 2012).

Using a combination of operant- and reflex-based paradigms, behavioural gap-detection thresholds and response parameters have been well-described in other experimental animals (Dooling et al., 1978; Giraudi et al., 1980; Okanoya and Dooling, 1990; Ison et al., 1991; Wagner et al., 2003; Hamann et al., 2004; Turner et al., 2006; Radziwon et al., 2009; Dehmel et al., 2012; Chen et al., 2013; Lobarinas et al., 2013; Salloum et al., 2014; Höbel, 2014). Gap-detection psychophysical experiments have also been conducted in normal-hearing humans (Plomp, 1964; Penner, 1977; Buunen and van Valkenburg, 1979; Shailer and Moore, 1983, 1985; Snell et al., 1994; Phillips et al., 1997; Formby et al., 1998; Snell and Hu, 1999; Oxenham, 2000; Phillips and Hall, 2000; Allen et al., 2002; Samelli and Schochat, 2008; Horwitz et al., 2011). By contrast, little is known about gap-in-sound perception in ferrets, apart from one study comprising two comprehensively-tested animals with heterogeneous performance (Kelly et al., 1996).

In this chapter, we sought to establish gap-detection behavioural parameters in the ferret using an operant conditioning paradigm, and to measure detection thresholds and related behavioural parameters (including approach-to-target and

head-orienting dynamics) in response to spectrally varied stimuli presented in the free-field. To verify the use of the ferret as a suitable model of human auditory processing, we also tested a cohort of human listeners on a similar psychophysical task.

3.2 Results

3.2.1 Behavioural Performance

Gap-detection sensitivity was measured by the gap length at which the psychometric function for each session reached threshold, defined as $d' = 1$. This sensitivity level was chosen to simplify comparison with other non-human behavioural paradigms (Macmillan and Creelman, 2005). The mean false alarm (FA) rate across all tested animals for the broadband stimulus was 0.23; therefore to achieve a $d' = 1$, an equivalent hit rate of 0.61 was required. These parameters correspond to an equivalent corrected performance (*[Hit Rate – FA Rate] / [1 – FA Rate]*) of 0.5, which has previously been used for threshold estimation (Kelly et al., 1996). Detection thresholds remained fairly constant session-to-session, ruling out any effect of learning beyond the initial training phase.

Ferrets (n = 9) displayed significant inter-individual differences in performance irrespective of testing conditions (linear mixed effects model (lme), $F_{(8, 390)} = 15.82$; $p < 0.001$). When testing for stimulus spectrum-dependent differences in gap-detection threshold, there emerged a significant main effect of stimulus type on threshold (lme, $F_{(3, 390)} = 13.21$; $p < 0.001$) (Fig.3-1). Post-hoc comparisons of stimulus type indicated that animals were more sensitive to gaps presented in BBN (threshold (ms) = 11.93±1.26) or 16 kHz NBN (threshold (ms) = 16.40±1.73), relative to 1 kHz (threshold (ms) = 24.56±2.00) or 4 kHz NBN (threshold (ms) = 21.83±1.66). To verify our session-by-session analysis protocol, we reanalysed our data as all trials pooled across testing sessions. Again, a significant main effect of stimulus type was observed (lme, $F_{(3, 21)} = 3.63$; $p = 0.02$), with frequency group thresholds (ms, mean ± SE) of: 1

kHz NBN = 29.3±10.4; 4 kHz NBN = 20.0±3.4; 16 kHz NBN = 15.7±3.1; BBN = 10.4±2.7. These estimates are each within error limits provided in our session-by-session analysis.

We explored whether differential sensitivity to gap length with stimulus types could derive from individual variations in performance, owing to the significant ferret*stimulus type interaction (lme, $F_{(8, 24)} = 10.07; p < 0.001$). To do this, we restricted our analysis to include only those data from each animal's three best sessions (Fig.3-1), likely to reduce the within-subject variability, as indicated previously (Buran et al., 2014). From this analysis, a significant main effect of stimulus remained (lme, $F_{(3, 72)} = 4.09; p = 0.018$) (Fig.3-1), whereas a main effect of ferret was not observed ($F_{(8, 72)} = 0.97; p = 0.48$). Post-hoc comparisons revealed significant differences in performance between all stimuli ($p < 0.05$, *Tukey-corrected*), except between 4 kHz and 16 kHz (threshold (ms), mean ± SE: 1 kHz NBN = 18.19±2.56; 4 kHz NBN = 11.03±1.98; 16 kHz NBN = 8.31±1.17; BBN = 4.22±0.89).

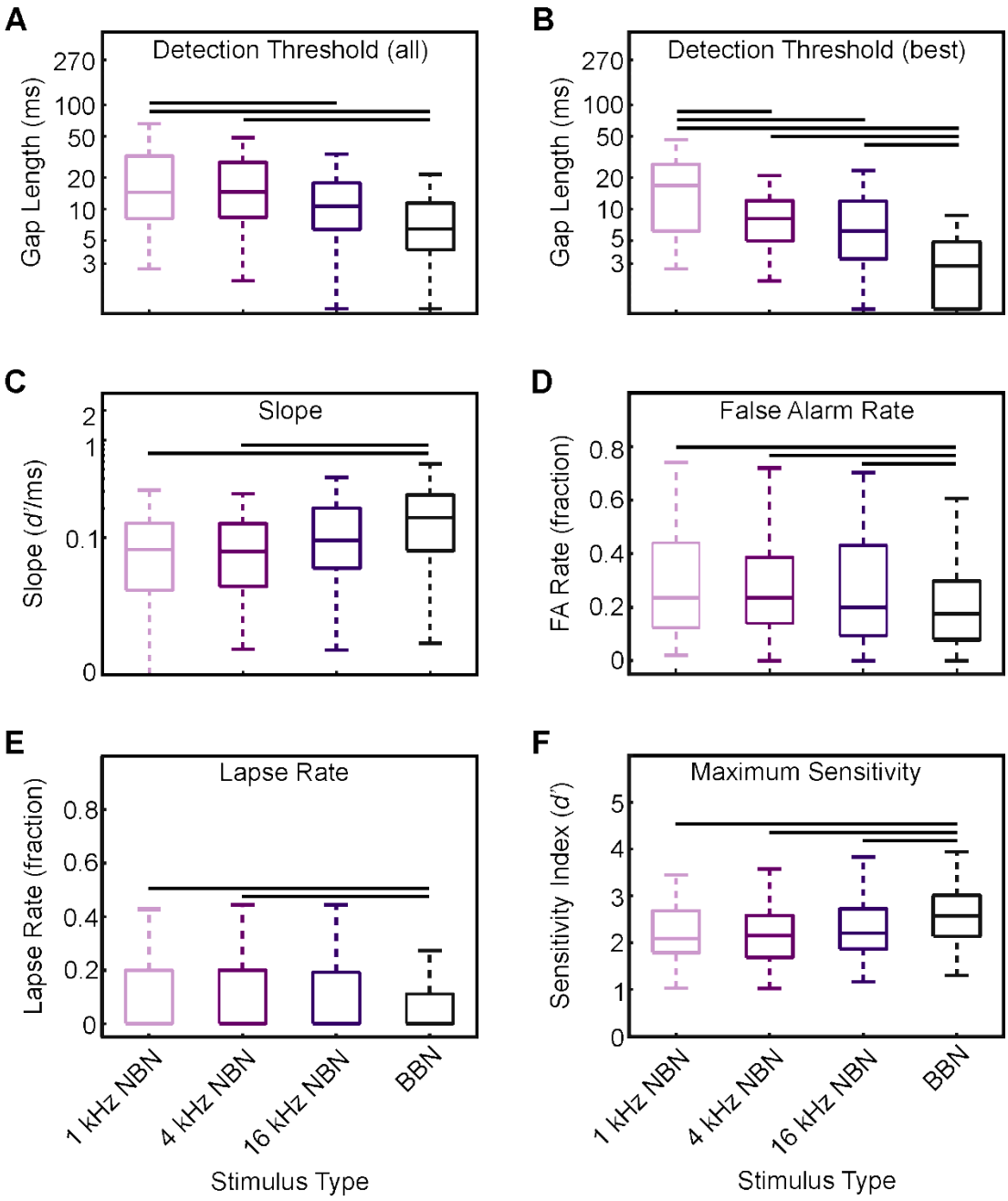

Figure 3-1: Ferret Psychometrics. Data plotted comprise all sessions across all subjects, where box plots indicate medians and interquartile ranges in each condition, with whiskers illustrating maxima and minima. Box outline colours correspond to stimulus frequency: pink = 1 kHz NBN; light purple = 4 kHz NBN; dark purple = 16 kHz NBN; black = BBN. Horizontal bars indicate significant pairwise post-hoc difference at $p<0.05$, corrected for multiple comparisons. A) Gap-detection threshold measured as gap length at sensitivity of d' = 1, across stimulus types. B) Gap-detection thresholds calculated from each animal's three best sessions. C) Psychometric function slope at threshold. D) FA rates, equivalent to proportion of incorrect trials for no-gap stimuli. E) Lapse rates, equivalent to proportion of incorrect trials for stimuli with gap length = 270 ms. F) Maximum sensitivity, measured at the asymptote of each session's psychometric function.

This result suggests that each animal was operating within a similar behavioural range in their respective best sessions, though gives no insight into the variability in subject performance. To evaluate the degree to which ferrets differed in their session-to-session performance, we calculated the standard deviation of thresholds collected on each session for each subject, for each stimulus type. This provides an estimate of the variability from session-to-session of ferret performance. For each stimulus, these data were (mean ± SEM): 1 kHz NBN = 14.6±4.6; 4 kHz NBN = 13.3±3.4; 16 kHz NBN = 10.8±3.1; BBN = 10.1±4.2, with no significant differences found (Kruskal-Wallis, $\chi^2 = 3.24$, $df = 3, 35$; $p = 0.36$). Given the significant ferret*stimulus interaction, this indicates that all animals are performing within a similar range across stimulus types, though individual animals perform better or worse in general.

To investigate whether stimulus type affected the degree to which ferrets were sensitive to changes in gap length, we measured the slopes of psychometric functions at threshold (Fig.3-1). An inverse relationship was found between gap length and slope at threshold, with a stimulus-dependent main effect observed (lme, $F_{(3, 390)} = 4.59$; $p = 0.004$) (Fig.3-1). Significantly steeper psychometric functions – indicating that smaller differences in gap length could be better discriminated – were recorded for BBN than for 1 kHz and 4 kHz narrowband noise (slope (d'/ms), mean ± SE : 1 kHz NBN = 0.10±0.04; 4 kHz NBN = 0.13±0.03; 16 kHz NBN = 0.14±0.04; BBN = 0.25±0.03).

To quantify the relationship between threshold and slope, we calculated the correlation between threshold vs. slope across all sessions. We found a strong negative correlation between gap-detection threshold and slope (Spearman's rank

correlation, $\rho = -0.86$, $p < 0.0001$) (Fig.3-2). Thus, where thresholds are low, ferrets display greater sensitivity to small stimulus increments.

We computed three additional measures of the ferret's operant performance: first, we calculated the FA rate (the proportion of no-gap trials for which animals reported the presence of a gap-in-noise), which in Signal Detection Theory (SDT) depends on the subject's internal decision criterion and varies with the set of stimulus conditions (Fig.2-9). A significant main effect of stimulus type emerged for FA rates (lme, $F_{(3, 390)} = 6.52$; $p < 0.001$), mainly explained by significantly lower FA rates of BBN compared with NBN stimuli (FA rate (fraction), mean ± SE: 1 kHz NBN = 0.28±0.02; 4 kHz NBN = 0.29±0.01; 16 kHz NBN = 0.28±0.01; BBN = 0.23±0.01). The significant correlation between slope at threshold and FA rate (Spearman's rank correlation, $\rho = -0.51$, $p < 0.0001$) (Fig.3-2) indicates that shifts towards higher FA responses are associated with a reduction in ferrets' capacities to detect small changes in gap length at empirical threshold.

To investigate influences upon the ferret's decision-making process, two parameters were calculated to describe the upper end of the psychometric function: lapse rate (the proportion of incorrect responses for gap width of 270 ms), and behavioural sensitivity at asymptote (Fig.2-4). Each measure describes the maximal expected performance of an individual animal for each stimulus type – for example, high lapse rates for easy stimuli could indicate a general lack of attention. For both parameters, a main effect of stimulus type was significant (lme: lapse rate: $F_{(3, 390)} = 9.35$; $p < 0.001$; max. sensitivity: $F_{(3, 390)} = 18.78$; $p < 0.001$) (Fig.3-1), suggesting that

performance was indeed influenced by one or more of these factors in a stimulus-dependent fashion.

There were significant differences between lapse rates for BBN vs. 1 kHz and 4 kHz NBN (lapse rate (fraction), mean ± SE: 1 kHz NBN = 0.13±0.02; 4 kHz NBN = 0.12±0.01; 16 kHz NBN = 0.09±0.01; BBN = 0.05±0.01) (Fig.3-1), although the absence of significant lapse rate vs. performance correlations (Fig.3-2) suggests that the processes responsible for governing performance at threshold are not necessarily associated with performance for easily discriminable stimuli. Post-hoc tests of asymptotic sensitivity values indicated that animals were more sensitive to BBN than to any NBNs (max. sensitivity (*d'*), mean ± SE: 1 kHz NBN = 2.07±0.08; 4 kHz NBN = 2.12±0.06; 16 kHz NBN = 2.28±0.07; BBN = 2.61±0.05) (Fig.3-1). Each of these measures represents a combination of the lower hit rates and higher FA rates obtained with NBN vs. BBN.

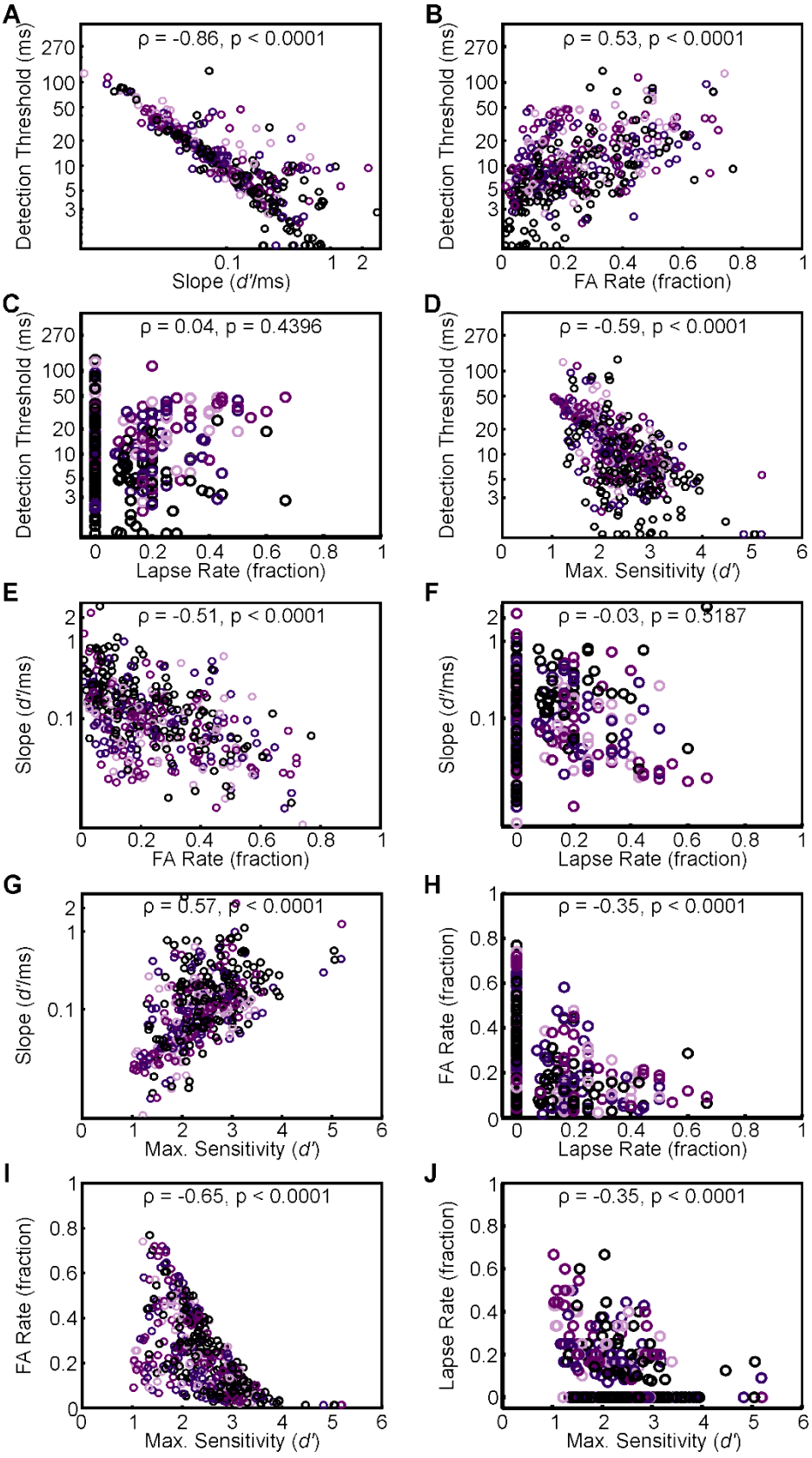
A
ρ = -0.86, p < 0.0001
Detection Threshold (ms)
Slope (d'/ms)
B
ρ = 0.53, p < 0.0001
Detection Threshold (ms)
FA Rate (fraction)
C
ρ = 0.04, p = 0.4396
Detection Threshold (ms)
Lapse Rate (fraction)
D
ρ = -0.59, p < 0.0001
Detection Threshold (ms)
Max. Sensitivity (d')
E
ρ = -0.51, p < 0.0001
Slope (d'/ms)
FA Rate (fraction)
F
ρ = -0.03, p = 0.5187
Slope (d'/ms)
Lapse Rate (fraction)
G
ρ = 0.57, p < 0.0001
Slope (d'/ms)
Max. Sensitivity (d')
H
ρ = -0.35, p < 0.0001
FA Rate (fraction)
Lapse Rate (fraction)
I
ρ = -0.65, p < 0.0001
FA Rate (fraction)
Max. Sensitivity (d')
J
ρ = -0.35, p < 0.0001
Lapse Rate (fraction)
Max. Sensitivity (d')

Figure 3-2 (previous page): Gap-detection measures outlined in Fig.3-1, plotted as session-by-session scatter plots for each measure: gap-detection threshold at $d' = 1$; slope; FA rate; lapse rate; and maximum sensitivity. In each plot, circle colours correspond to stimulus frequency: pink = 1 kHz NBN; light purple = 4 kHz NBN; dark purple = 16 kHz NBN; black = BBN. ρ is Spearman's correlation coefficient, and p is the empirical *p-value*.

We can thus conclude that the ferret's gap-detection performance is significantly affected by the frequency of stimulus used as a noise carrier in the operant task. Ferrets displayed better behavioural performance and sensitivity to silent gaps interleaved within BBN relative to NBN stimuli, with the greatest differences seen for low- and mid-frequency-centred NBN.

3.2.2 Behavioural Response Times

Previously, ferret operant response times – the time between stimulus onset and response registration – have been measured, and found to be correlated with task difficulty and with changes in auditory cortex physiology (Bajo et al., 2010b; Leach et al., 2013; Nodal et al., 2008, 2010). Indeed, responses times may provide a measure of the effects of attention in behavioural paradigms (Saltzman and Garner, 1948; Buck, 1966; Luce and Green, 1972; Salthouse and Hedden, 2002; Buran et al., 2014).

Response time distributions were highly non-normal and were well-fitted using an Ex-Gaussian function (e.g. Fig.3-3A). Statistics were performed on the mean of the Gaussian component of the fitted curve (μ), representing the shorter-latency component of the response time distribution. For each NBN (Figs.3-3, 3-4, 3-5) and BBN (Fig.3-6) stimuli, plotting the post-stimulus response time histogram in comparison with the fitted Ex-Gaussian function indicates the non-normality of the distribution. Comparison of the μ component of each function with the mean of the Gaussian function fitted to the same distribution clearly indicates the disparity between the two, and thus the appropriateness of the ex-Gaussian to evaluate across-subject response time distributions. From these figures, we wondered whether there may be task contingency effects on ferrets' response times: for example, responses

made to the right spout appearing to be faster in general, regardless of stimulus. Additionally, BBN response times were sharply peaked, suggesting greater response stereotypy than for NBN stimuli – this may be due to the increased certainty with which animals generated their responses for BBN, particularly towards the right spout (i.e. incorrect gap, and correct no-gap). To explore these possibilities, we fitted Ex-Gaussian functions to each animal's response time distributions and conducted mixed effects modelling to determine the effects of these trial contingencies, and stimulus frequency.

Stimulus type significantly affected response times (lme $F_{(3, 15)} = 15.24$; $p < 0.001$). due to significantly longer μ values for BBN compared with NBN conditions (μ (s), mean ± SE: 1 kHz NBN = 1.85±0.43; 4 kHz NBN = 1.83±0.42; 16 kHz NBN = 1.76±0.42; BBN = 1.97±0.39)(Fig.3-7). We examined the effects of the location of response spouts and the differences in correct vs. incorrect response locations for gap vs. no-gap stimuli on response times. When we investigated the effect of the direction the animals made their response (±30°), irrespective of stimulus spectrum, and collapsing across gap/no-gap stimulus type, we found a significant main effect on response time μ ($F_{(1, 38)} = 6.78$; $p = 0.013$), with shorter μ values for the spout at +30° for all conditions (μ (s), mean ± SE: left = 1.90±0.40; right = 1.81±0.36) (Fig.3-7).

Given that rightward responses correspond to incorrect responses on gap trials and to correct responses on no-gap trials (Fig.3-1), a similar main effect was found when factoring in stimulus type (gap/no-gap) and response outcome (correct vs. incorrect), such that incorrect gap responses were significantly faster than correct gap-stimulus responses ($F_{(1, 38)} = 9.60$; $p = 0.004$; μ (s), mean ± SE: correct = 1.91±0.40;

incorrect = 1.80±0.38) (Fig.3-7). Interestingly, such effects were not seen for no-gap stimuli ($F_{(1, 38)} = 1.12$; $p = 0.30$; μ (s), mean ± SE: correct = 1.84±0.36; incorrect = 1.88±0.46) (Fig.3-7), suggesting that ferrets exhibited a stereotyped behaviour directed towards the rightward no-gap response spout, with FAs made faster than misses.

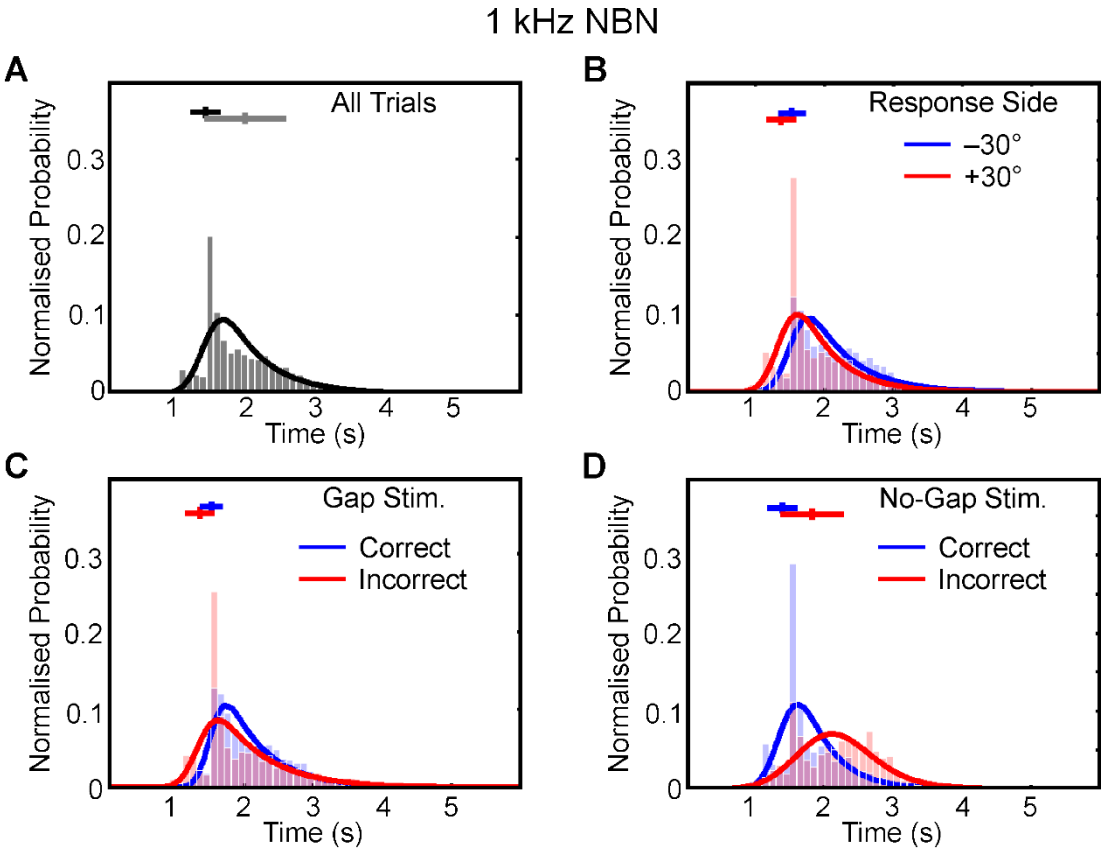

Figure 3-3: Ferret Gap-Detection Response Times. A) Normalized histogram of response times for all trials performed by all animals in response to 1 kHz NBN. Values were binned at 100 ms, and indicate the time between stimulus onset and a nose-poke response being made at the periphery (at either reward spout). An ex-Gaussian distribution (black) was used to model these data in MATLAB using the DISTRIB toolbox. Markers with horizontal bars indicate mean ± standard deviation (grey) of the data, and $\mu \pm \sigma$ (black) values of the ex-Gaussian distribution. B) Normalised histograms with fitted ex-Gaussians for all trials, sorted according to the location of the final approach-to-target response (blue = left; red = right). Markers with horizontal bars indicate $\mu \pm \sigma$ values of the fitted distribution in corresponding colours. C) Normalised histograms with fitted ex-Gaussians for all trials in response to gap stimuli, sorted according to whether the final approach-to-target response was correct (blue) or incorrect (red). D) Normalised histograms with fitted ex-Gaussians for all trials in response to no-gap stimuli, sorted according to whether the final approach-to-target response was correct (blue) or incorrect (red).

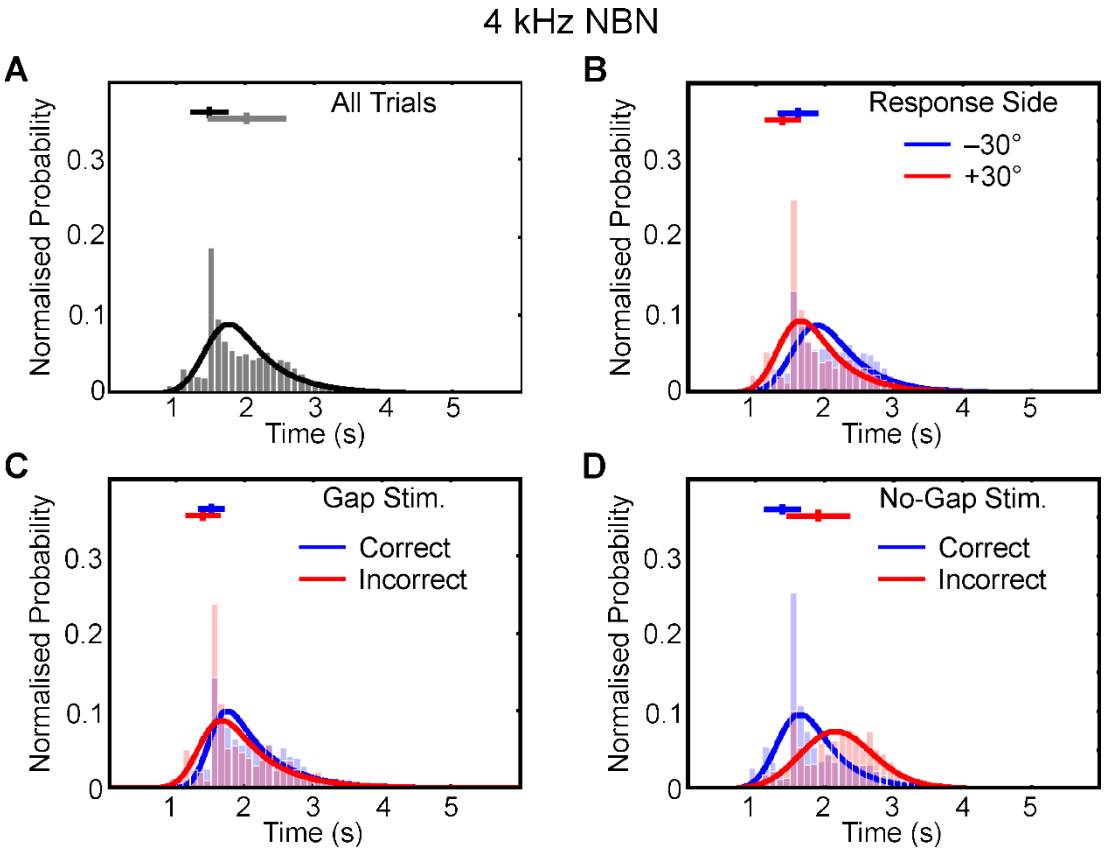

Figure 3-4: As for Fig.3-3, in response to 4 kHz NBN.

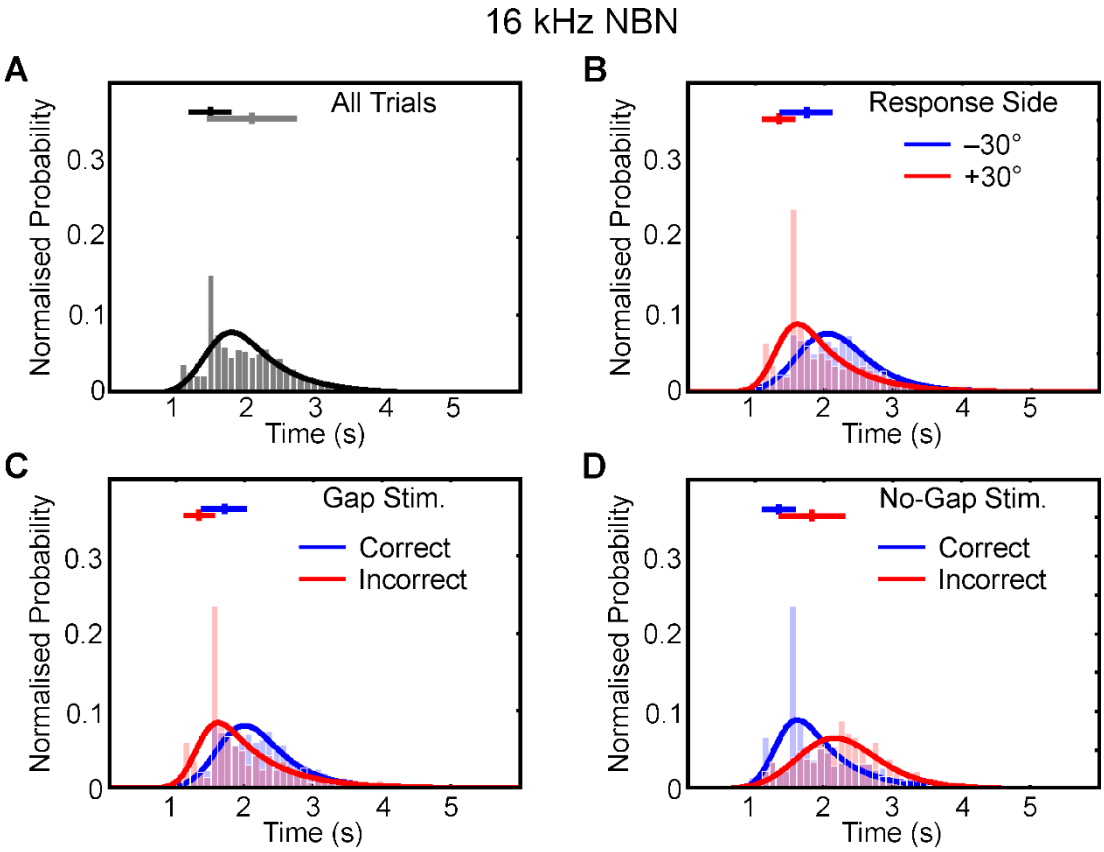

Figure 3-5: As for Fig.3-3, in response to 16 kHz NBN.

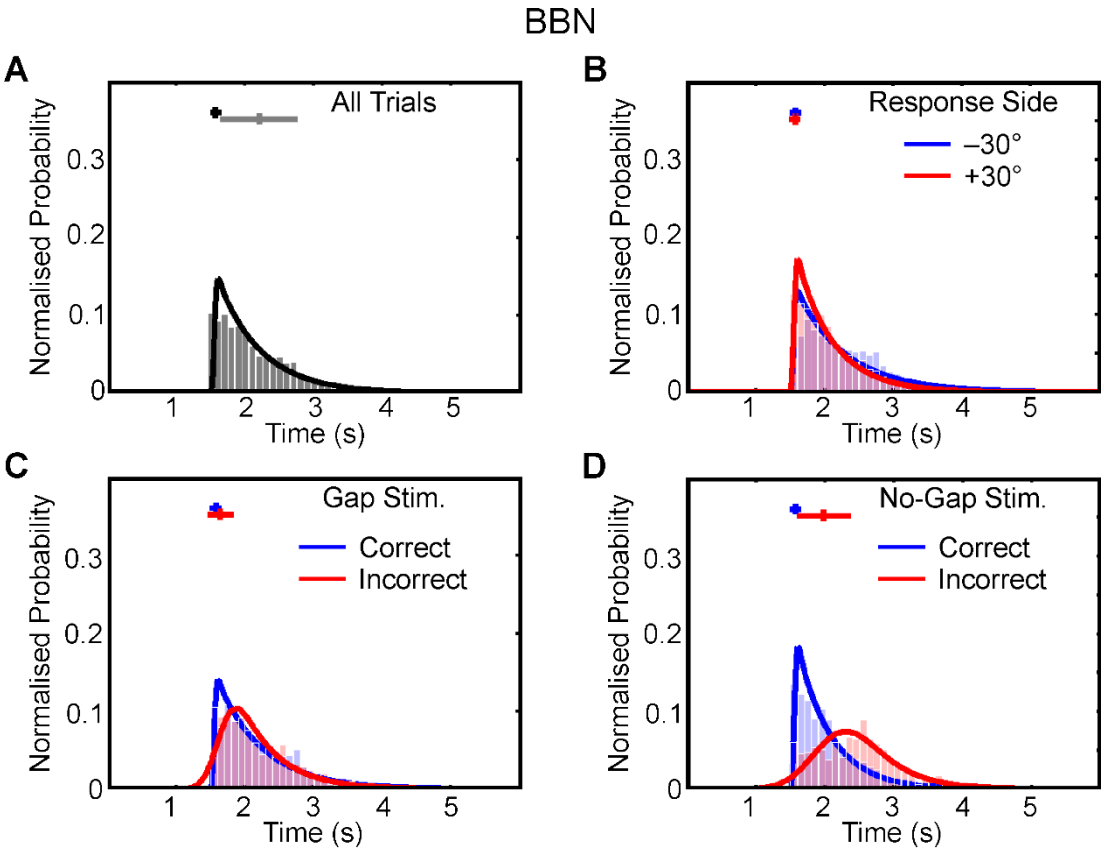

Figure 3-6: As for Fig.3-3, in response to BBN.

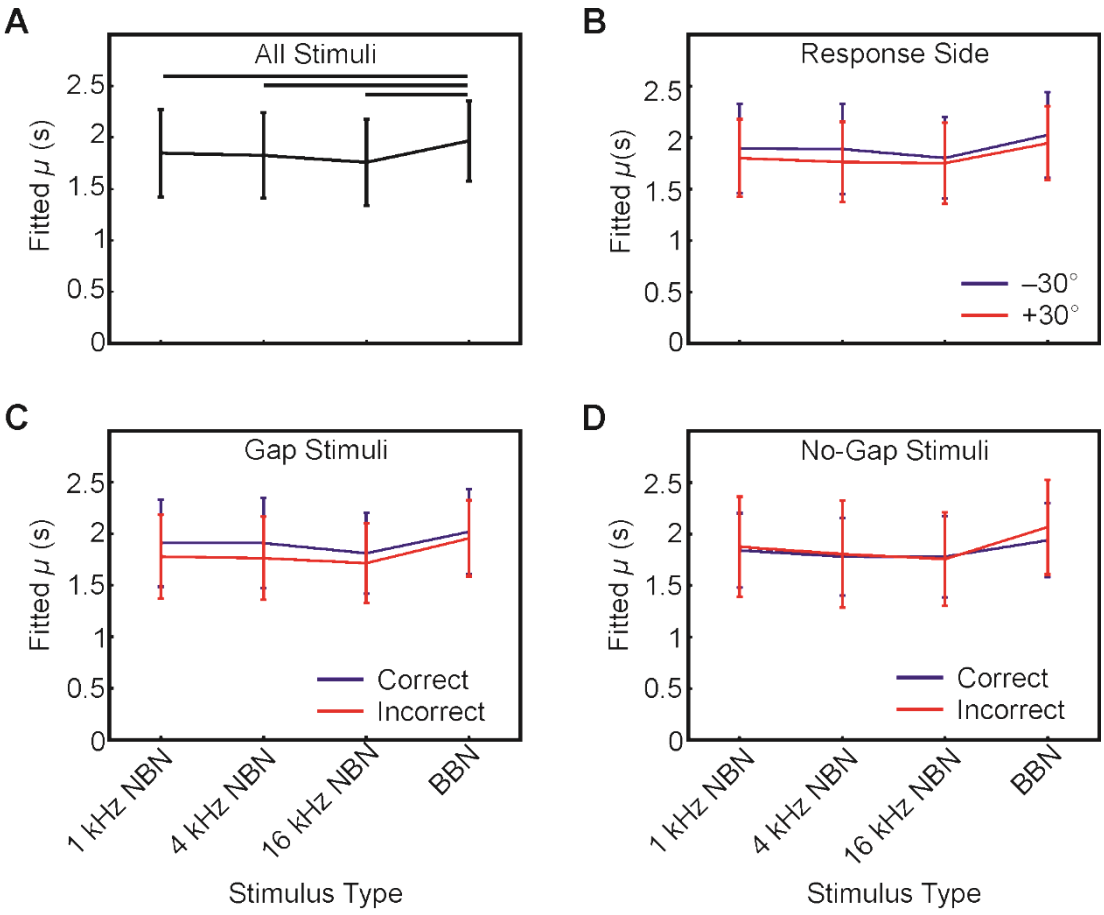

Figure 3-7: Summary of Ferret Gap-Detection Response Times. A) μ as a function of stimulus type for all trials collected from all animals; line plots indicate mean ± SE across all data in each case. Horizontal bars indicate significant pairwise post-hoc difference at $p<0.05$, corrected for multiple comparisons. B) μ values subdivided according to whether the approach-to-target response made to the left/–30° reward spout (blue) or the right/+30° reward spout (red). Between-group differences significant, $p = 0.013$. C) μ values from gap stimuli trials, subdivided into correct (blue) and incorrect (red) responses. Between-group differences significant at $p = 0.004$. D) μ values from no-gap stimuli trials, subdivided into correct (blue) and incorrect (red) responses. Between-group differences not significant, $p = 0.30$.

3.2.3 Head-orienting Behaviour

Since there is a demonstrated relationship between approach-to-target sound localization behaviour accuracy and head-orienting response accuracy in ferrets (Nodal et al., 2008; Leach et al., 2013), we thus sought to determine the extent to which this head-orienting behaviour was influenced by stimulus lateralization used to bind gap/no-gap identity to specific response spouts during the training phase, and if this may have biased the results described above (Fig.2-2).

From the example plots of head-tracking angular displacement over time (Fig.3-8), recordings of head-orienting behaviour clearly yielded a stereotyped angular displacement over time towards the right regardless of left-right response location, or the correct/incorrect outcome of the trial for either gap or no-gap stimuli. Notably, the pattern of head orienting behaviour for no-gap stimuli was inverted, with larger displacements to the right on correct trials. However, when initial and final bearing angles were evaluated, no significant effects of stimulus type were seen (lme: initial head bearing: $F_{(3, 10689)} = 0.137$; $p = 0.934$; final head bearing: $F_{(3, 10689)} = 0.03$; $p = 0.993$) (Fig.3-9). Even when head bearing angles were sorted according to the above-described decision criteria (by response location or response correctness), no significant main effect was observed (Fig.3-9). This is despite the systematic differences between conditions seen particularly for final head bearing angles – the lack of significant difference in these instances is likely due to the large, non-systematic variance in bearing angles exhibited from trial-to-trial within individuals. Therefore, the lateralized operant response training phase did not affect the orienting responses when a single loudspeaker was used. Consequently, final head bearing cannot be used to predict which reward location the ferrets approached. However,

the non-significant bias towards the right, which may simply indicate a preference for leaving the platform from this side of the centre spout, could partially explain why approach-to-target responses to the right were quicker, since the head-orienting response presumably comprises the initial component of the approach-to-target response.

Analysis of the head-orienting response latencies to stimuli located at 0° azimuth can provide insight into the decision/detection process, since these times were also informative in spatial hearing tasks involving ferrets (Nodal et al., 2008). Head-orienting response latencies were also well-fitted using ex-Gaussian distributions. We measured latencies both for the initial head movement (initial; this may be regarded as the reaction time) and at the time when either the head movement terminated or the animal left the central platform (final). Initial head bearing latencies were not significantly affected by stimulus type (lme: $F_{(3, 15)} = 0.41$; $p = 0.75$; μ (ms), mean ± SE: 1 kHz NBN = 196.79±255.16; 4 kHz NBN = 189.20±285.96; 16 kHz NBN = 189.13±302.48; BBN = 206.79±328.91) (Fig.3-10). However, a marginally significant effect on μ was found for no-gap stimuli when these responses were subdivided according to trial correct/incorrect outcome ($F_{(1, 38)} = 4.41$; $p = 0.042$) (Fig 3-10). This result suggests that animals displayed a characteristic rightwards response bias that facilitated earlier, correct responses for no-gap stimuli, as hypothesized above. Contrastingly, final response latency μ was significantly greater for broadband stimuli than for 4 kHz or 16 kHz NBN (lme: $F_{(3, 15)} = 6.50$; $p = 0.005$; fitted μ (ms), mean ± SE: 1 kHz NBN = 588.66±205.65; 4 kHz NBN = 542.44±180.00; 16 kHz NBN = 527.30±178.36; BBN = 628.28±181.45) (Fig 3-10), but no differences were found for no-gap stimuli between correct and incorrect responses (lme: $F_{(1, 38)} = 3.76$; $p = 0.060$)

(Fig.3-10). There was no significant effect of response correctness for gap stimuli for either the initial or the final head-orienting response times.

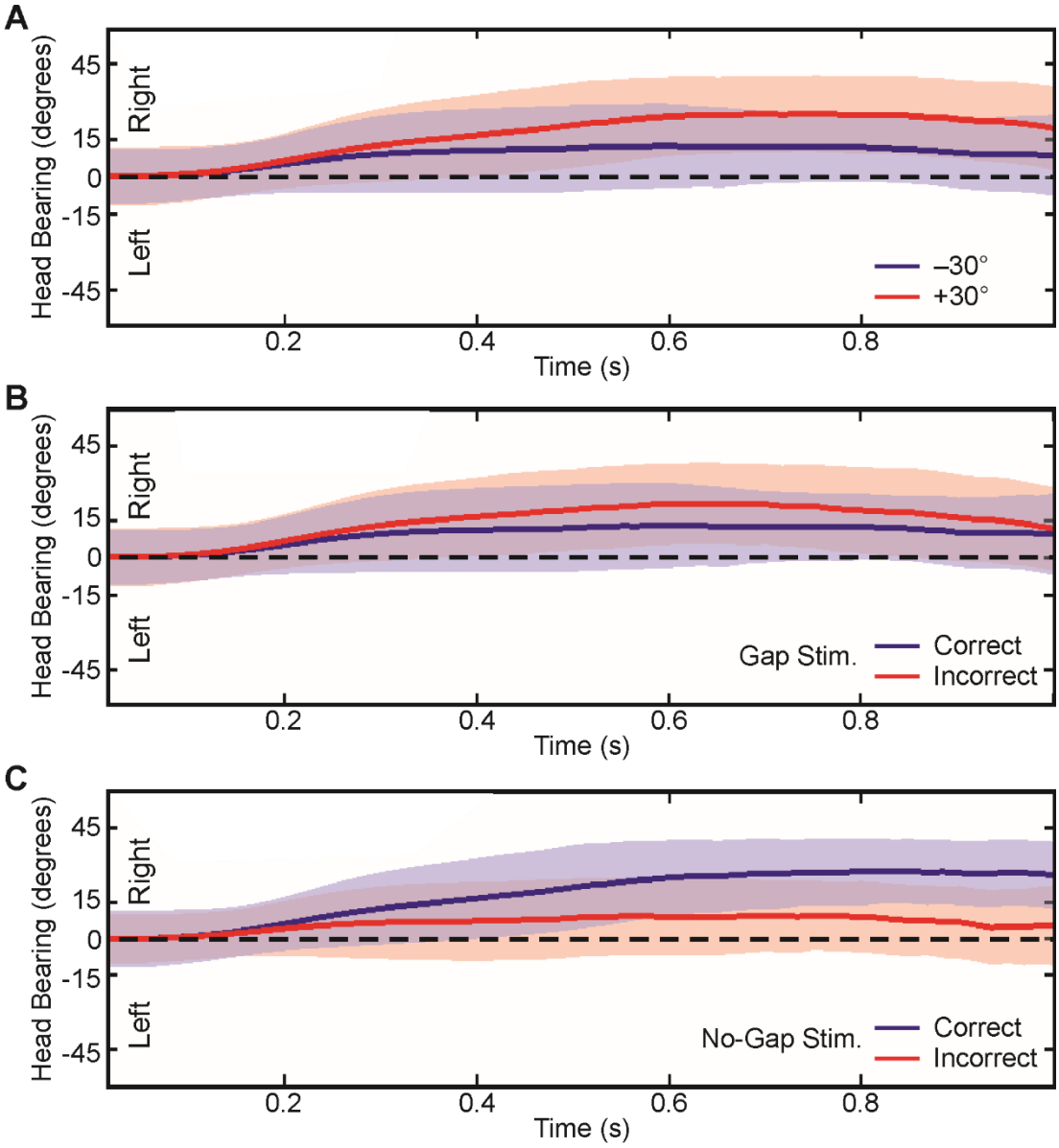

Figure 3-8: Ferret Head-Orienting Response Traces. Example horizontal head angle trajectories from all animals as a function of time during BBN presentation for all gap lengths. Traces are mean (thick line) ± SE (shadow). Ordinate values are positive for rightward bearing. A) Responses made following either gap or no-gap stimulus presentation, to the left (blue) or right (red) reward spout. B) Responses made following gap stimulus presentation, to the correct (blue) or incorrect (red) reward spout. C) Responses made following no-gap stimulus presentation, to the correct (blue) or incorrect (red) reward spout.

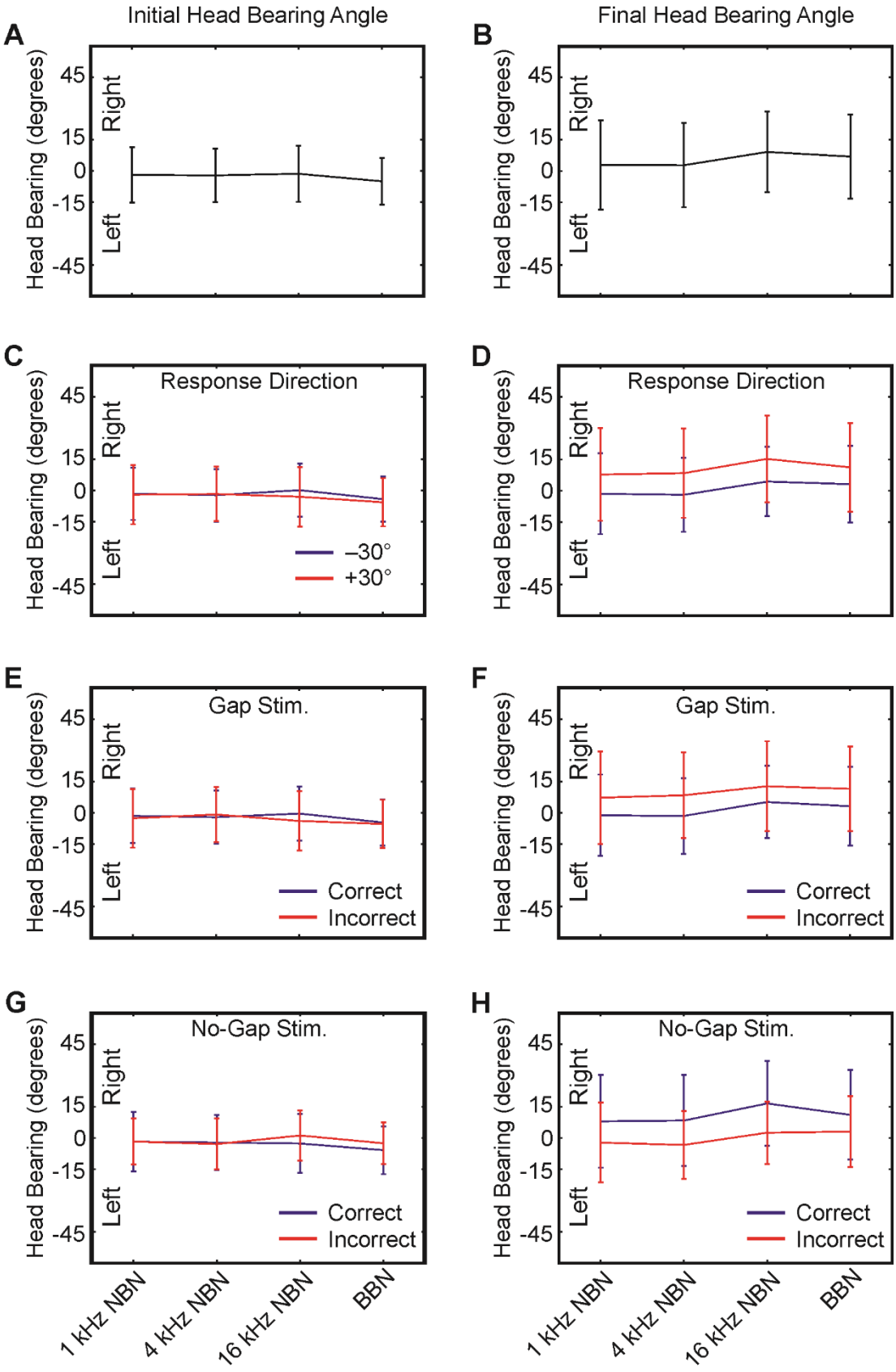
A
Initial Head Bearing Angle
B
Final Head Bearing Angle
Head Bearing (degrees)
45
15
0
-15
-45
Right
Left
C
Response Direction
D
Response Direction
–30°
+30°
E
Gap Stim.
F
Gap Stim.
Correct
Incorrect
G
No-Gap Stim.
H
No-Gap Stim.
1 kHz NBN
4 kHz NBN
16 kHz NBN
BBN

Figure 3-9 (previous page): Summary of Ferret Head-Orienting Bearing Data. Head bearing angles for all animals as a function of time during each stimulus presentation for all gap lengths. Initial head bearing angle (left column) represents the head bearing in the first three frames following trial initiation. Final head bearing angle (right column) represents the head bearing after 1 second or once headstrip signal had been lost (whichever came first). Ordinate values are positive for rightward bearing. A, B) Head bearing angles for all trials in response to all stimuli. C, D) Head bearing angles following either gap or no-gap stimulus presentation, for responses made to the left (blue) or right (red) reward spout. E, F) Head bearing angles following gap stimulus presentation, for responses made to the correct (blue) or incorrect (red) reward spout. G, H) Head bearing angles following no-gap stimulus presentation, for responses made to the correct (blue) or incorrect (red) reward spout.

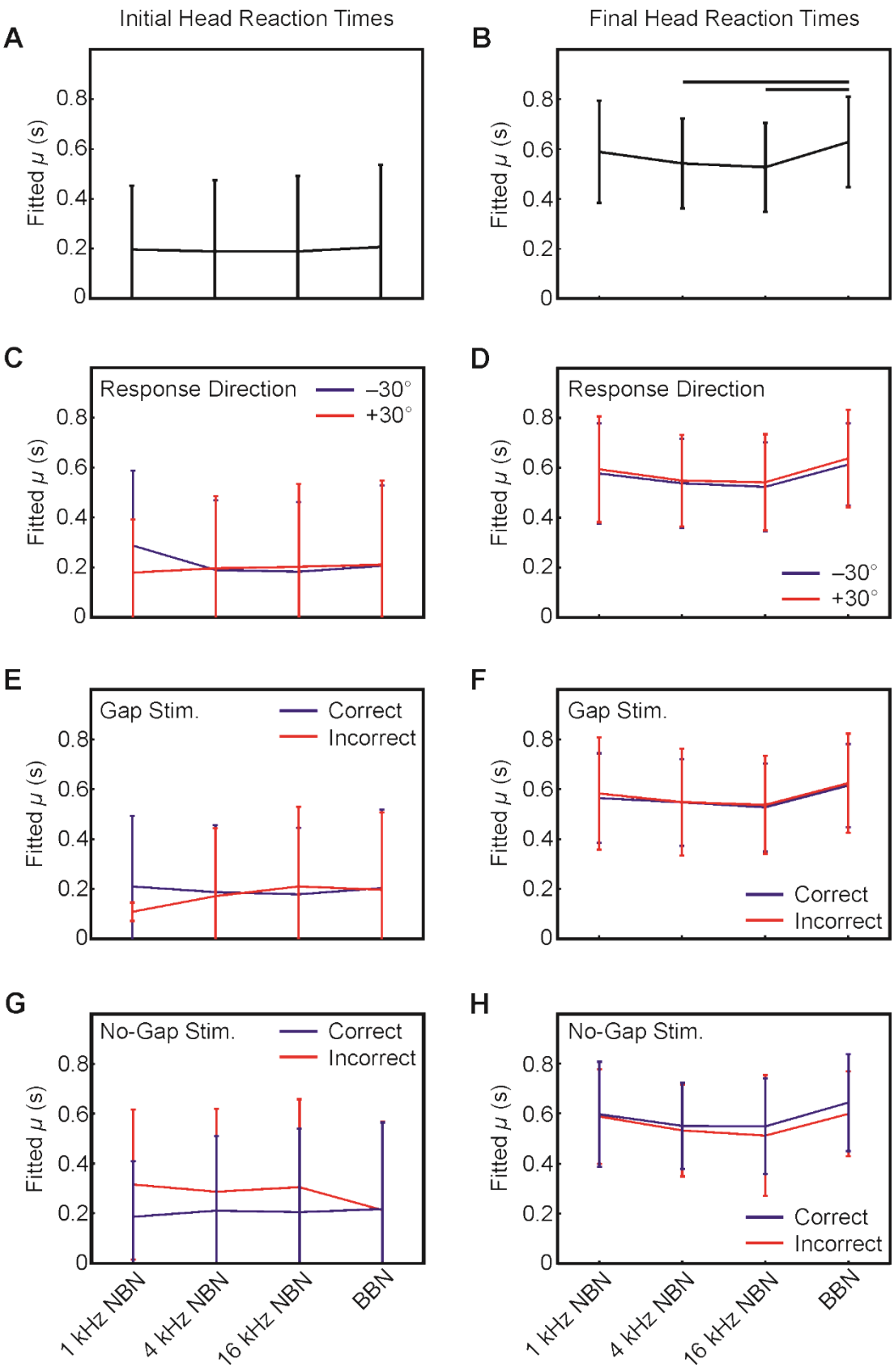
A
Initial Head Reaction Times
B
Final Head Reaction Times
Fitted μ (s)
0
0.2
0.4
0.6
0.8
C
Response Direction
−30°
+30°
D
Response Direction
−30°
+30°
E
Gap Stim.
Correct
Incorrect
F
Gap Stim.
Correct
Incorrect
G
No-Gap Stim.
Correct
Incorrect
H
No-Gap Stim.
Correct
Incorrect
1 kHz NBN
4 kHz NBN
16 kHz NBN
BBN

Figure 3-10: Summary of Ferret Head-Orienting Latency Data. Head-orienting latencies for all animals as a function of time during each stimulus presentation for all gap lengths. Initial head-orienting latency (left column) represents the time following stimulus onset during which a consistent unidirectional head-orienting response was observed. Final head-orienting latency (right column) represents the time at which the head-orienting response is terminated (either as the animal leaving the central platform, or after 1 second, whichever comes first). A, B) μ (in seconds) for head-orienting latency as a function of stimulus type. Line plots indicate reaction time (RT) mean ± SE in each case. Horizontal bars indicate significant pairwise post-hoc difference at $p<0.05$, corrected for multiple comparisons. C, D) μ following either gap or no-gap stimulus presentation, for responses made to the left (blue) or right (red) reward spout. E, F) μ for head-orienting latencies for gap trials, subdivided into correct (blue) and incorrect (red) responses. G, H) μ for head-orienting latencies for no-gap trials, subdivided into correct (blue) and incorrect (red) responses. Initial latency no-gap correct vs. incorrect between-group main effect significant at $p = 0.042$.

3.2.4 Human Psychophysics

To evaluate the utility of the ferret as a reliable and accurate model of human auditory processing, we tested young adult human subjects (n = 6) on a gap-detection task using identical spectral filters to generate sound stimuli. Although response times were not measured, correct/incorrect response type data underwent identical analyses to those conducted for the animal behavioural results to facilitate comparison of psychometric function features (Fig.3-11). Thresholds for gap-in-noise resolution were mostly <10 ms (gap length at $d' = 1$ (ms), mean ± SE: 1 kHz NBN = 5.21±2.78; 4 kHz NBN = 1.76±1.00; 16 kHz NBN = 1.72±1.13; BBN = 2.15±1.58). As in our ferret cohort, human subjects displayed a significant main effect of stimulus type on detection threshold at $d' = 1$ (lme: $F_{(3, 45)} = 15.79$; $p < 0.001$) (Fig.3-11). This derived from a significant difference between 1 kHz NBN detection thresholds and those recorded for all other stimuli.

Although there was no main effect of slope (Fig.3-11), we found a moderate but significant inverse correlation between detection threshold and slope for our human subjects (Spearman's rank correlation, $\rho = -0.45$, $p = 0.0007$), in line with the relationship between threshold and incremental sensitivity seen in ferrets. For each of FA rate and asymptote sensitivity, we did not find a significant main effect of stimulus type (Fig.3-11). Lapse rates for all stimuli were exceptionally low (Fig.3-11), with no lapses made at all for the BBN, 4 kHz and 16 kHz NBN conditions, indicating the highly attentive state of our subjects.

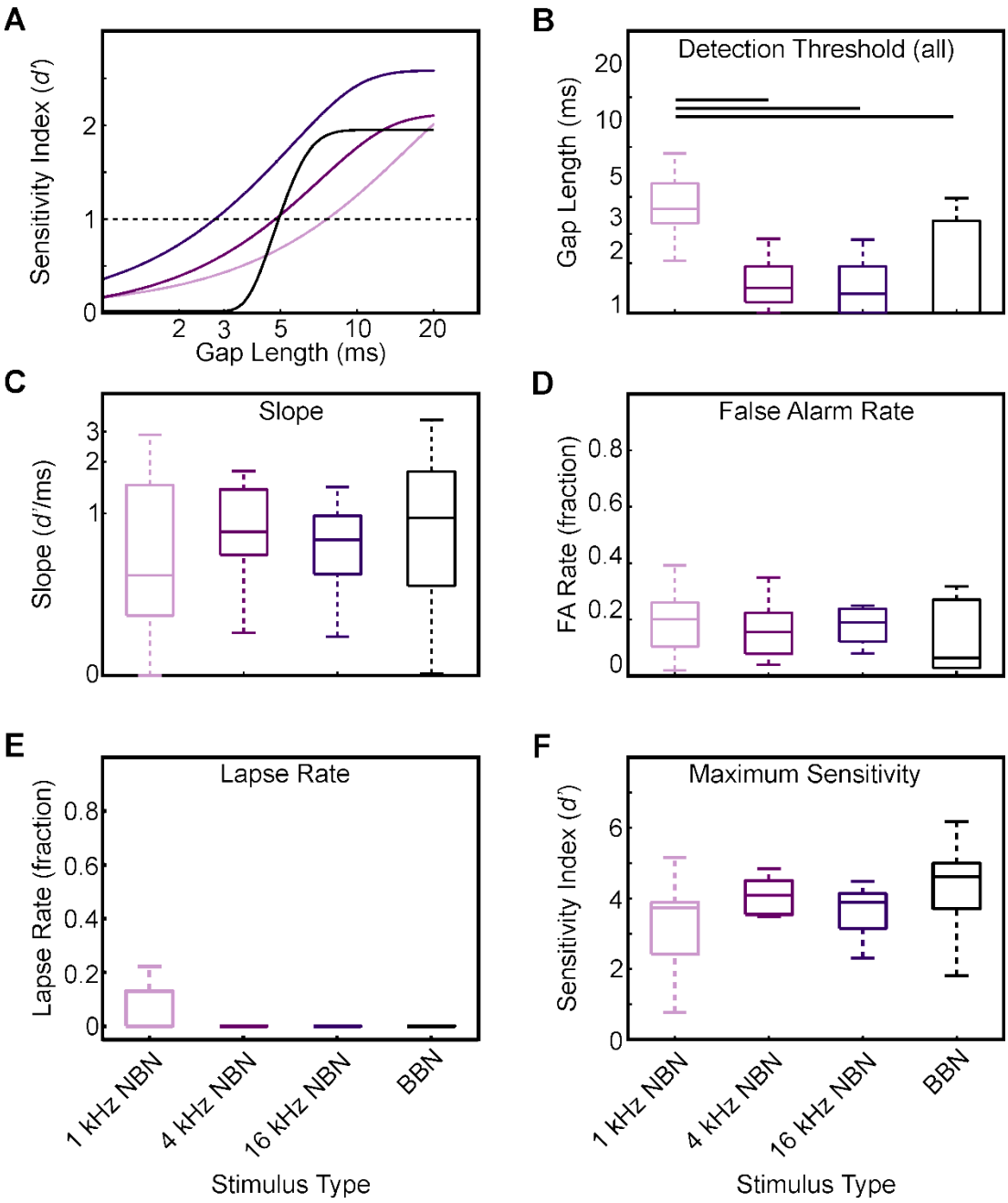

Figure 3-11: Human Gap-Detection Behaviour. A) Example psychometric functions for one subject plotted as sensitivity (*d'*) for each stimulus type. Trace colours correspond to stimulus frequency: pink = 1 kHz NBN; light purple = 4 kHz NBN; dark purple = 16 kHz NBN; black = BBN. For visualisation of parameters extracted from psychometric functions, refer to Fig 2-4) Gap-detection thresholds. Box plots indicate medians and interquartile ranges in each case, with whiskers illustrating maxima and minima. Horizontal bars indicate significant pairwise post-hoc difference at $p<0.05$, corrected for multiple comparisons. C) Psychometric function slopes at threshold. D) FA rates. E) Lapse rates. Note that no lapses were made by any subject for the 4 kHz NBN, 16 kHz NBN, and BBN conditions. F) Maximum sensitivity at psychometric function asymptote.

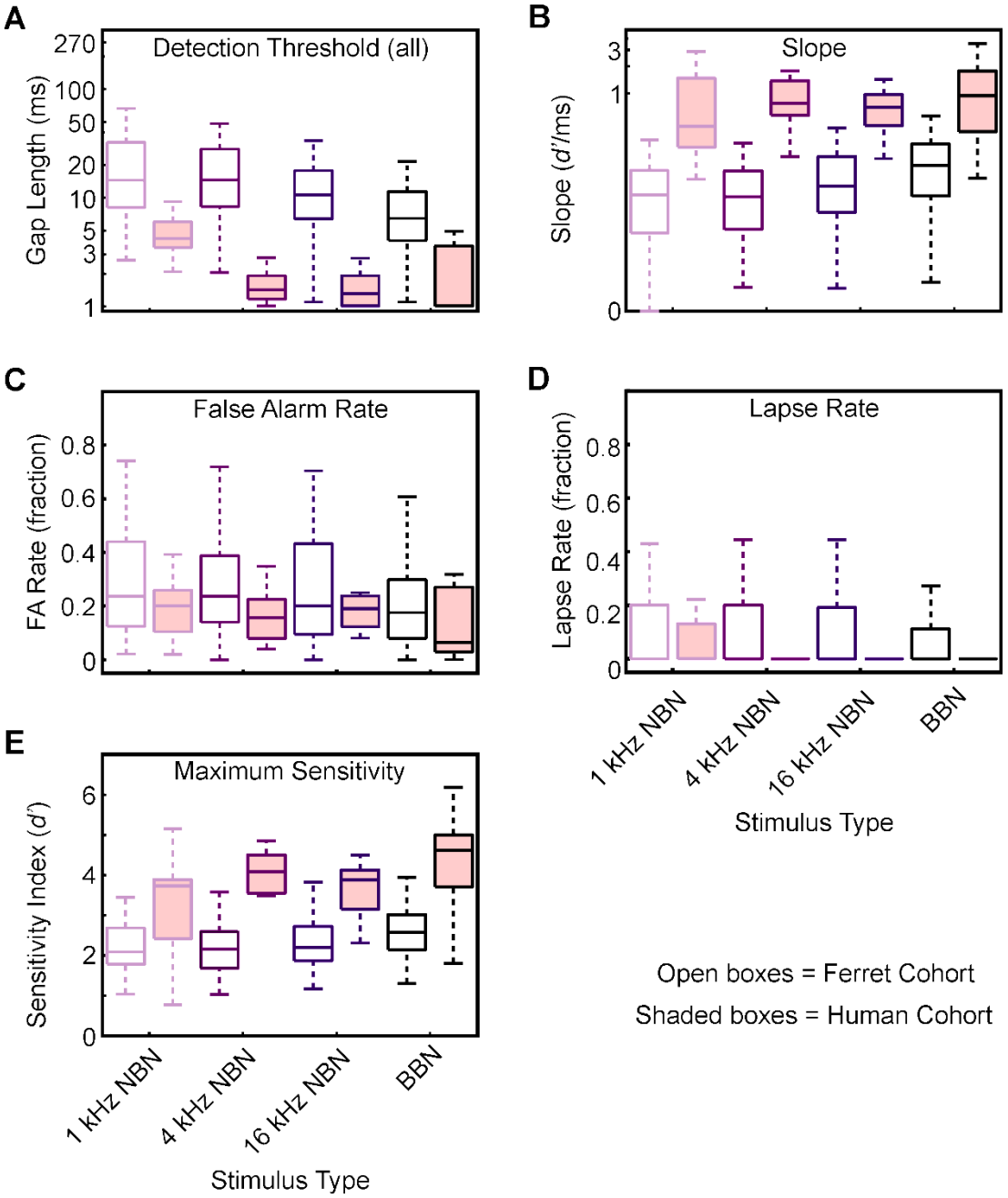

Figure 3-12: Comparison of Ferret and Human Gap-Detection Data. For each panel, open boxes represent ferret cohort data, while the shaded boxes represent human cohort data. Box plots indicate medians and interquartile ranges in each case, with whiskers illustrating maxima and minima. Box edge colours correspond to stimulus frequency: pink = 1 kHz NBN; light purple = 4 kHz NBN; dark purple = 16 kHz NBN; black = BBN. Statistical tests evaluated differences between ferret and human cohorts, controlling for stimulus type, subject identity, and subject species. A) Gap-detection thresholds. Between-group differences significant at $p = 0.007$. B) Psychometric function slopes at threshold. Between-group differences significant at $p < 0.001$. C) False Alarm rates. D) Lapse rates. E) Maximum sensitivity at psychometric function asymptote. Between-group differences significant at $p < 0.001$.

By deriving identical parameters from the gap-detection behaviour of ferrets and humans, we could compare their performance directly (Fig.3-12). We found a significant difference between ferrets and humans in threshold at $d' = 1$ (lme: $F_{(1, 438)} = 9.27$; $p = 0.007$) (Fig.3-12). This difference in sensitivity may reflect a broader range of threshold values from session-to-session for ferrets compared with humans. We quantified this variability by calculating the standard deviation of thresholds across sessions for each subject. While within-individual variability was not affected by stimulus type (Kruskal-Wallis: ferrets, $\chi^2 = 3.24$, $df = 3, 35$, $p = 0.36$; humans, $\chi^2 = 2.49$, $df = 3, 15$, $p = 0.48$), a large difference emerged between ferrets (mean standard deviation across sessions = 12.21 ms) and humans (mean standard deviation across sessions = 0.95 ms). There was also a highly significant main effect of species on slope at threshold (lme: $F_{(1, 438)} = 54.55$; $p < 0.001$) (Fig.3-12). These results suggest that, at threshold performance, humans are capable of consistently discriminating smaller gap lengths, and finer differences in gap length, than are ferrets. There was no difference in FA rate between species (lme: $F_{(1, 438)} = 2.22$; $p = 0.16$) (Fig.3-12), and the effects on sensitivity did not appear to result from differences of attention in our animal cohort (relative to the human group), since the subject species did not affect lapse rates (lme: $F_{(1, 438)} = 3.36$; $p = 0.08$) (Fig.3-12). We did, however, find that humans showed significantly greater asymptote sensitivity than ferrets (lme: $F_{(1, 438)} = 61.39$; $p < 0.001$) (Fig.3-12). Notably, there was no significant interaction between stimulus type and species for any of the parameters investigated (lme: gap-detection threshold, $F_{(3, 398)} = 0.85$, $p = 0.47$; slope, $F_{(3, 398)} = 1.49$, $p = 0.22$; FA rate, $F_{(3, 398)} = 0.37$, $p = 0.78$; lapse rate, $F_{(3, 398)} = 0.21$, $p = 0.87$; asymptote sensitivity, $F_{(3, 398)} = 1.03$, $p = 0.38$).

Consequently, we can conclude that ferret gap-detection behaviour resembles that exhibited by human listeners, but with diminished sensitivity.

3.3 Discussion

By testing gap-detection using BBN and different NBN stimuli, our results demonstrate that, as in humans, ferret temporal processing depends on stimulus spectral content, with worse performance observed when low frequency sounds were used. In the only previous report of gap-detection in ferrets, Kelly et al. (1996) tested two animals on a battery of stimuli akin to those used here, with one ferret displaying a frequency-dependent enhancement for bandpassed noise stimuli centred at frequencies above 8 kHz, whereas the other animal yielded consistent thresholds across all tested frequencies. Nevertheless, the mean thresholds reported in our study were similar to those reported by Kelly et al. (1996), despite their study not finding clear evidence for stimulus frequency affecting detection sensitivity.

Our ferret cohort displayed mean thresholds ≥11.9 ms when BBN stimuli were used, with thresholds increasing in a frequency-dependent fashion during NBN testing. Previously reported gap-detection thresholds obtained using operant testing in smaller mammals range from 1.6 ms in mice (Radziwon et al., 2009) and rats (Syka et al., 2002), 2.1 ms in gerbils (Wagner et al., 2003), to 3 ms in chinchillas (Giraudi et al., 1980). Our data place ferrets at the upper end of the scale of gap-detection in small mammals. The origin of this difference between ferrets and other animals tested is unclear, although detection thresholds were occasionally as low as 3 ms in single sessions, suggesting that ferrets are capable of detecting gaps to a degree comparable with other small mammals.

Notably, as indicated in Fig.3-1, the reported "threshold" data in fact place only an upper bound on performance, with actual psychophysical thresholds liable

to be lower. Syka et al. (2002) reported that gap-detection thresholds in rats were much lower at 70 dB SPL for broadband and low-frequency narrowband noise than when the stimulus level approached an audiometric threshold, where gap-detection thresholds were as high as 10.6 ms and 31.3 ms for broadband and low-frequency noise, respectively. While not investigated in this chapter, an effect of overall level on gap-detection has been reported in ferrets (Kelly et al., 1996) and widely explored in humans (e.g. Plomp, 1964; Penner, 1977; Fitzgibbons, 1983; Shailer and Moore, 1983). However, the upper detection limits for rats are remarkably in line with those obtained for our ferrets (BBN: 11.9; 1 kHz NBN: 24.6 ms), for gaps-in-noise well above audiometric threshold, and similarly that the lower detection limits obtained in each ferret's best sessions (Fig.3-1) were much closer to those described in other species.

One possibility is that ferrets were performing sub-optimally in our behavioural setup, yielding detection sensitivity values at the upper limit of a strategy that will reliably yield reward. This may have developed as a function of the positive conditioning paradigm utilized, wherein punishment of poor performance was avoided in favour of rewarding correct performance. A previous study of operant detection behaviour indicated that ferrets can modify their decision criteria on a trial-by-trial basis to optimize the reward probability, conditional upon the outcome of the previous trial (Alves-Pinto et al., 2012).

The FA rate is notably associated with the decision process, and while high in our study, was consistent with this species (Alves-Pinto et al., 2012). This may reflect a species-related idiosyncrasy of operant decision-making, since a similar conditioning paradigm in European starlings (*Sturnus vulgaris*) yielded FA rates

approaching 0.04 (Klump and Maier, 1989), and better psychometric asymptote sensitivies were seen in other species utilizing operant measures of gap-detection thresholds (Wagner et al., 2003; Radziwon et al., 2009). However, direct comparison is problematic, since those studies used high FA rates as an exclusion criterion for session analysis. Nevertheless, that a proportion of ferrets in our study displayed detection thresholds within approximately the same range as those previously reported in other species likely indicates a conserved central mechanism for encoding features of gap-in-noise stimuli in a behaviourally salient fashion.

Effective gap-detection is established to be contingent upon the normal operation of AC circuitry (Ison et al., 1991; Kelly et al., 1996; Threlkeld et al., 2008; Weible et al., 2014), and the integrity of the cochlea (Giraudi-Perry et al., 1982; Gold et al., 2013; Rybalko & Syka, 2005; Salvi & Arehole, 1985; Yin et al., 2008). Indeed, Klump and Maier (1989) have postulated that temporal processing underpinning perceptual gap-detection may be determined by the time constants of the cochlear filters in a frequency-dependent manner. Recordings from ferret auditory nerve have indicated the presence of an unexpectedly low proportion of fibres tuned to very low-frequency sounds, despite functionally appropriate behavioural and collicular/cortical thresholds within this range (Sumner and Palmer, 2012). Nevertheless, further data from that study imply that the ferret is peripherally more similar to the chinchilla or guinea pig than the cat (Sumner and Palmer, 2012), with which comparisons are often drawn (Kelly et al., 1986a; Phillips et al., 1988). It is interesting, therefore, that detection thresholds should be as high as they are in ferrets, particularly since the width of their auditory filters would provide shorter integration time constants, and thus ought to yield the physiological basis necessary

to detect shorter gaps-in-noise. A recent neurophysiological study of guinea pig IC found mean neural gap-detection thresholds for single units to be 10.95 ms in response to broadband noise (Berger et al., 2014). This figure is remarkably close to our behaviourally measured thresholds (though greater than previously reported neurometric gap thresholds measured using evoked potentials in guinea-pig IC and AC (Yin et al., 2008)). As we shall see in Chapter 5, neural gap-detection thresholds in ferrets are higher than those observed behaviourally, but display the same frequency/performance relationship.

The well-documented reduction in gap-detection performance with age in both humans and other species (Barsz et al., 2002; Walton et al., 2002; Allen et al., 2003; Hamann et al., 2004; Reed et al., 2009; Recanzone et al., 2011) may correlate with the progressive loss of high-frequency sensitivity (Gold and Bajo, 2014). We would predict, on the basis of the ferret's peripheral physiology and central encoding of sound frequency (Bizley et al., 2005; Kelly, et al., 1986; Kelly & Judge, 1994), that this species might be particularly susceptible to age-related impairments in the detection of temporally complex sounds. To date, ageing studies in ferrets are lacking. Since the induction of peripheral lesions in this species results in central processing deficits throughout the auditory system that are typical of those seen in other species (Gold & Bajo, 2014; McAlpine et al., 1997; Moore et al., 1997), ferrets are likely to be well-suited for evaluating the effects on temporal processing of induced or acquired auditory processing deficits. Indeed, we show in the next chapter that partially deafened ferrets are prone to developing gap-detection deficits.

As in ferrets and our human subjects, previous studies of gap-detection in humans was found to depend on sound frequency content (Fitzgibbons, 1983, 1984; Shailer and Moore, 1983), and the thresholds reported here are in line with previously published data, which showed that thresholds and asymptotic performance were both superior for broadband versus low-frequency bandpassed noise. Previous authors have reported that the lowest thresholds in humans are seen for broadband noise (Plomp, 1964; Penner, 1977) or for sounds containing high-frequency components >5 kHz (Fitzgibbons, 1983, 1984), as long as the stimulus was presented above a critical level of ~50 dB SPL (a factor not affecting our own data, which were collected at sound levels > 70 dB SPL). While not testing for level effects here, we might expect to find concordant results.

Although our data do not conform with the suggestion from Eddins and colleagues (1992) that gap-detection performance does not change as a function of frequency in the low-to-mid range of the human audiogram, they nevertheless support the proposal of enhanced acuity as a function of stimulus bandwidth (with improved performance observed for wider-band stimuli), possibly deriving from integration of temporal information across processing channels (Shailer and Moore, 1983, 1987). Data obtained in other animal species (e.g. Ison et al., 2005; Radziwon et al., 2009) have revealed a similar stimulus dependence, as do our own results in ferrets, which also showed that stimulus frequency content affected our subjects' sensitivity to the size of incremental changes in gap length at threshold (Fig.3-12). From our data, it is interesting that the same pattern of descriptive statistics was seen in both ferrets and humans across the range of stimuli tested, despite clear differences in their respective overall gap-detection sensitivity.

Ferrets also show much higher thresholds than humans on a two-alternative forced choice task, in which they were trained to label artificial vowels as high or low in pitch (Walker et al., 2009), with similar parallels between the effects of stimulus type on performance in the two species to what we observed here. Although this difference in sensitivity may reflect the complexity of the task used, one factor that is liable to have affected estimates of threshold performance is the session-to-session variability observed within each species. In the present study, we quantified this variability by calculating the standard deviation of thresholds across sessions for each animal and human subject, and in each case there was no effect of stimulus on within-individual variability. However, there was a large difference between ferrets (mean = 12.21 ms) and humans (mean = 0.95 ms). This would suggest that ferrets are an order of magnitude more variable in their between-session performance than humans, a factor possibly influenced by motivation. Additional explanations may include task design (e.g. feedback provided only to ferrets, not human subjects) and difficulty (a factor that could be altered by implementing a method of limits in the future, rather than constant stimuli as used here). There may also be fundamental interspecies differences in peripheral encoding of temporally complex acoustic stimuli as a function of differing cochlear physiology (Elliott et al., 1960) or cochlear nonlinear dynamics, which might influence gap-in-noise detection (Reed et al., 2009; Horwitz et al., 2011). This latter hypothesis seems unlikely, since the ferret displays basilar membrane compressive growth at a rate comparable with other mammalian species, including guinea pigs and non-human primates (Sumner and Palmer, 2012).

Our key finding that both ferrets and humans display a comparable main effect of frequency content on psychometric performance supports not only the utility

of our paradigm for gap-detection testing, but also the ferret as a model species for investigating the neurobiology of temporal processing in a human-relevant manner. While the ferret's detection thresholds are likely to be higher than those in humans, and certainly are worse than those reported in other experimental mammals, as a model species the ferret possesses a number of advantages that make it suitable for continued exploration of the substrates for temporal coding. In the first case, operant conditioning as a paradigm, while influenced by attentional and motivational factors (Heffner and Heffner, 2014), provides insight into cortical processes that are critical to task performance (Kelly et al., 1996). This is in contrast to startle-based paradigms, which are predominantly mediated by subcortical networks (Yeomans and Frankland, 1995).

In addition to the ferret being one of the most widely used models for the exploration of spatial hearing (King et al., 2007), in which the accurate integration of temporally precise cues is important to the localization of a sound source (Keating et al., 2014, 2015), the appropriateness of this species for auditory research in general is enhanced by the opportunity to simultaneously investigate, over extended periods of time and within single animals, the activity of populations of neurons during behavioural tasks (Bizley et al., 2013), and the consequences of selective inhibition (Bajo et al., 2013) or ablation (Bajo et al., 2010b) of specific neural populations.

In summary, results show that ferrets perform well in operantly-trained gap-detection, with detection thresholds that are comparable to those previously described in this species, as well as other smaller mammals trained on similar tasks. This work sets the stage for subsequent experiments, to be described in the next two

chapters, which examine how those capabilities are affected by selective hearing loss, which may or may not induce a tinnitus-like percept.

Chapter 4

Behavioural and Physiological Effects of Lesioning the Ferret Spiral Ganglion – A Possible Model of Tinnitus?

4.1 Introduction

Hearing loss is the most common sensory impairment affecting humans, with rates of impairment in adults – by some estimates approaching ~40% (Agrawal et al., 2008; Nondahl et al., 2010, 2011) – suggesting that the quality of life of many people will be substantially diminished, especially among the elderly. Problematically for sufferers of presbyacusis is a handful of recent studies suggesting that it be may causally involved in age-related cognitive decline (Wayne and Johnsrude, 2015). Although controversial, such studies indicate the challenge posed by hearing loss, particularly given the dearth of treatments available for curtailing it wholesale (Müller and Barr-Gillespie, 2015).

Recent work in animal models of hearing loss has started to uncover physiological and anatomical disturbances that develop following deafferentation (see Chapter 1; Gold and Bajo, 2014). Though broad in scope and variable according to experimental preparation, the changes that occur have begun to crystallise into a putative post-insult syndrome. As elaborated earlier in this thesis, peripheral trauma mediates deafferentation/damage of the spiral ganglion (SG). This damage, in turn, manifests as excitatory/inhibitory imbalance of circuits throughout the central auditory system, leading to disruptions in the neural representation of sounds. Hearing loss, rather than simply raising thresholds, likely instigates neuroplastic changes in brain architecture that may fundamentally impair the capacity for sufferers to functionally adapt.

Features of this maladaptive neuroplasticity have become associated with the development of chronic subjective tinnitus, with signs recognised in human tinnitus patients also shared by subsets of animals with experimentally-induced hearing impairment (e.g. Schaette and McAlpine, 2011; Dehmel et al., 2012; Gu et al., 2012; Coomber et al., 2014). Since the seminal review from Eggermont and Roberts in 2004 that revitalised interest in tinnitus as a model of (abnormal) neural plasticity (Eggermont and Roberts, 2004), insight into the underlying mechanisms responsible for tinnitus, and how these differ from those neurophysiological and anatomical changes that are observed in the context of hearing loss in general, remains obscure (Baguley et al., 2013; Langguth et al., 2013). Consequently, none of the Cochrane reviews on tinnitus therapy found any treatment to be more effective than "equivocal" (Martinez-Devesa et al., 2010; Phillips and McFerran, 2010; Hoekstra et

al., 2011; Meng et al., 2011; Baldo et al., 2012; Bennett et al., 2012; Hobson et al., 2012; Hilton et al., 2013; Hoare et al., 2014).

To address this issue in both hearing loss and tinnitus, we must develop and investigate animal models that recapitulate key features of each disease. Specifically, there should be consistency in the instantiation of hearing loss, but variability in the emergence of perceptual abnormalities, such that the two might be disentangled. One promising avenue is the disturbance to auditory temporal processing described following hearing loss (DeFilippo and Snell, 1986; Fitzgibbons and Gordon-Salant, 1987; He et al., 1999; Horwitz et al., 2011; Moore et al., 2012), and which may be specifically related to, or affected by, tinnitus (Fournier and Hébert, 2013; Mehdizade Gilani et al., 2013; Moon et al., 2015).

Recent approaches to address this perceptual change have characterised the physiological correlates of gap-mediated prepulse inhibition of the acoustic startle reflex, a paradigm that has revealed behavioural correlates of abnormal post-insult plasticity (Engineer et al., 2011; Middleton et al., 2011; Ahlf et al., 2012; Llano et al., 2012; Koehler and Shore, 2013; Coomber et al., 2015; Sametsky et al., 2015). However, this behaviour may be mediated through subcortical circuits (potentially under corticofugal influence (Weible et al., 2014b)), whereas tinnitus critically involves cortical structures in human sufferers (Ridder and Vanneste, 2014; Elgoyhen et al., 2015). Animal models therefore ought to leverage a behavioural paradigm that requires cortical involvement, and that is sensitive to perceptual changes following hearing loss, of which tinnitus may be one.

In this chapter, we aimed to develop, in the ferret, a model of hearing loss that replicates aspects of peripheral auditory trauma observed in cases of acquired hearing loss, and determine whether any physiological markers were associated not only with the hearing loss itself, but also any behavioural changes that emerge. As outlined above and in Chapter 1, SG appears to be eminently susceptible to damage after a host of different kinds of insults: thus it was here that we induced a selective, unilateral auditory deafferentation. From Chapter 3, we have developed a robust behavioural paradigm that evaluates auditory temporal processing in the ferret, and from which we have shown that ferrets possess temporal processing capabilities with similar frequency sensitivity to humans. We are therefore well-positioned to explore changes to auditory-driven behaviour induced by hearing loss in a potentially clinically relevant fashion. By coupling these detailed behavioural observations to longitudinal evaluation of auditory brainstem function (by way of auditory brainstem response (ABR) measurements), multiunit neurophysiological recordings in auditory cortex (AC), and anatomical evaluation of central auditory structures, this chapter seeks to examine the constellation of changes that are effected by deafferentation, and if these might be indicative of an underlying tinnitus-like condition in ferrets.

4.2 Results

Our results concern the multifaceted investigation of how the adult ferret responds to a putatively selective lesion of the SG of the right cochlea. This lesion was made to ensure that complete hearing loss was not produced, and thus any behavioural effects were independent of audibility issues; to determine the possibility of lateralised physiological effects of an asymmetrical sensory deafferentation; and to preserve the contralateral ear as a source of inputs to control for changes following deafferentation. Since each animal (Table 2-1) underwent a longitudinal, in-depth study using behavioural, physiological, and anatomical techniques, this section comprises four main components, explaining the findings from different methodologies used to investigate the effects of the SG lesion: gap-in-noise detection behaviour; ABRs; AC neurophysiological recordings; and *post-mortem* histological characterisation at SG cell level and in brain tissue (Fig 2-1).

4.2.1 Perceptual Temporal Processing Shifts: Gap-in-Noise Detection Behaviour

Gap-in-noise detection was used to evaluate changes in auditory temporal processing that may have developed following SG lesion, using identical parameters to those in Chapter 3. In each testing session, trial-by-trial percent-gap values were collected, alongside trial response times. Response times were analysed according to response contingency, and pre/post-lesion statistics were extracted from ex-Gaussian fits. Head-tracking data were omitted due to the lack of variability of either head orienting bearings or reaction times found in Chapter 3.

Each animal was compared with its own pre-lesion behavioural data under identical conditions to determine the statistical effects of the lesion. Psychometric measures were the same as those in Chapter 3, namely threshold performance (gap length at $d' = 1$), slope at threshold, FA rate, lapse rate, and asymptote performance. Performance was determined as a function of the overall psychometric function extracted for each stimulus type across testing sessions (from all pooled trials), due to many sessions in which animals performed <70 trials. In each case, performance deficits could be described as significant shifts in the psychometric function. Such shifts could be horizontal, determined statistically by comparing the empirically-derived 95% confidence intervals (CIs) at the curves' respective thresholds; or vertical, evaluated using a Friedman Test on d' values at each gap length.

Summary of findings

The behavioural effects of SG lesion in our cohort appear to separate into two identifiable strands. First, a commonality in the pattern of response times developed, with all ferrets displaying shortened response times across measured conditions. By contrast, the psychometric functions of each animal displayed a spectrum of performance changes. Specifically, some animals displayed clear, largely frequency-specific impairments in gaps-detection, while others displayed distinct post-lesion improvements in performance: nevertheless, the change in response times, and the relationship between response times and decision biases, were similar.

In quantifying the similarity in response time changes following SG lesion, a statistical analysis was conducted of each animal's response time distribution

median, μ, and τ. A general trend towards lower response times developed for all stimuli: while this trend failed to reach significance for μ (lme: $F_{(1, 15)} = 2.92; p = 0.15$) (Fig.4-1), the distribution medians and τ statistics were significantly reduced (lme: median: $F_{(1, 15)} = 13.46; p = 0.014;$ τ: $F_{(1, 15)} = 11.33; p = 0.020$). This pattern was recapitulated for each of the behavioural response contingencies detailed in Chapter 3, indicating universally shortened response times following SG lesion.

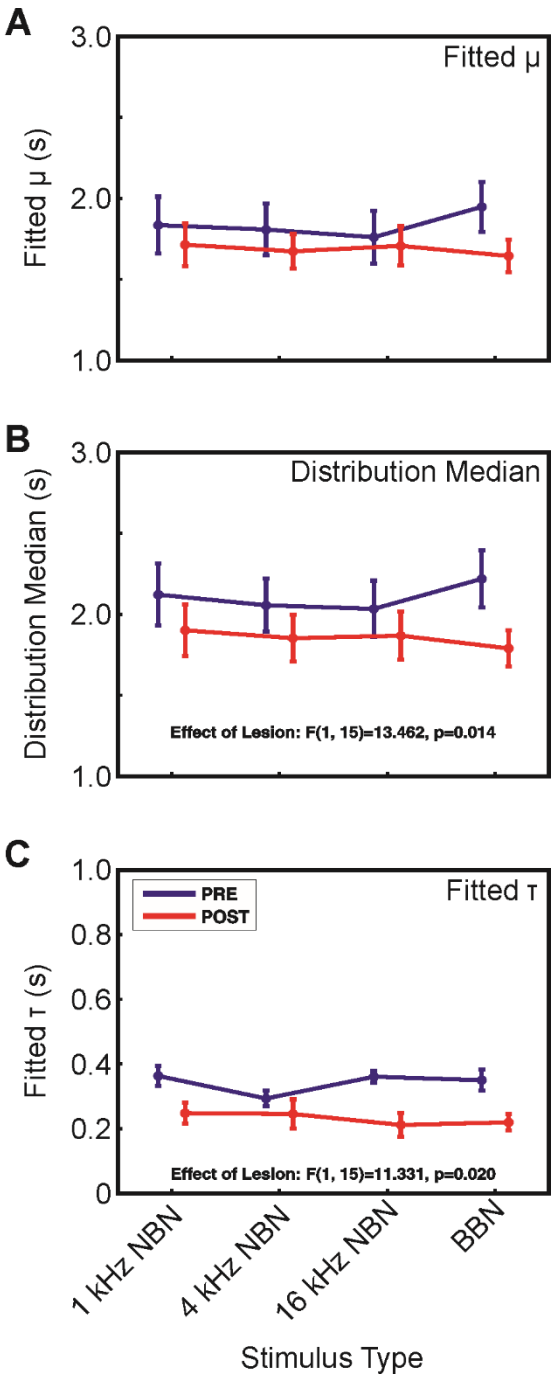

Figure 4-1: Approach-to-Target Response Time Statistics. Pre-lesion = blue; post-lesion = red. Axes indicate measure of interest (seconds) vs. stimulus type (1-, 4-, or 16 kHz NBN, & BBN). Data shown as mean ± standard error. A) Ex-Gaussian fitted μ. B) Empirical median. Main effect of lesion: $F_{(1, 15)} = 13.462$, $p = 0.014$. C) Ex-Gaussian fitted τ. Main effect of lesion: $F_{(1, 15)} = 11.331$, $p = 0.02$.

Conversely, the psychometric effects of the SG lesion appeared to be heterogeneous within our tested cohort. Impairments or improvements were found to develop after SG lesion, at different stimulus frequencies when compared with each animal's respective performance from pre-lesion control testing. Thus, it seemed inappropriate to compile all data into a large statistical model with the aim of capturing these effects, simply due to the between-individual variability.

Ferret F1227

Of our tested cohort, F1227 displayed the greatest behavioural deficits following SG lesion. By examining the pooled psychometric data (Fig.4-2), substantial downwards shifts in psychometric functions were observed across stimulus types. χ^2 statistics were significant for 1 kHz and BBN stimuli, and approached significance for 4 kHz and 16 kHz NBN (Friedman Test, $\chi^2 = 3.57$, $p = 0.059$ in these latter cases). These changes manifested as non-specific, significant post-lesion changes in asymptote sensitivity and FA rate. Significant rightward psychometric shifts were observed for 1 kHz, 4 kHz and BBN, indicating a lesion-mediated impairment in temporal processing sensitivity. Together, these data suggest that SG lesion produced substantial impairments in low—to-mid frequency gap detection, affecting performance for BBN.

Ferret F1228

We found no significant differences in the psychometric functions following the introduction of SG lesion for F1228. However, a trend emerged among 1 kHz NBN, 4 kHz NBN and BBN sessions, with post-lesion reductions in d' for easily detectable gaps, compared to pre-lesion values (Fig.4-3). This yielded significant reductions in

post-lesion maximum *d'* for these stimuli, and by accompanying elevations in FA rates (data not shown). Although there was a corresponding improvement in performance at 16 kHz, only a reduction in lapse rate was significant, indicating an attentional improvement.

Ferret F1317

F1317 displayed both behavioural impairment and improvement following SG lesion. We found a selective elevation in threshold sensitivity for 16 kHz NBN (Fig.4-4), with a significant rightwards shift in the post-lesion psychometric function. This selective high-frequency impairment is a predicted sequela of the intended basal focus of the SG lesion. Although 1 kHz NBN and BBN displayed increases in asymptotic *d'*, only BBN was significant. Behaviour at 1 kHz NBN displayed a small but significant reduction in detection threshold, though this was not conserved across all sessions.

Ferret F1226

F1226 displayed a mild post-lesion deficit that was stimulus-selective, possibly related to the basal (high-frequency) region of SG that was lesioned. From Fig.4-5, post-lesion performance was significantly impaired for 16 kHz NBN ($\chi^2 = 7.00$, $p = 0.008$). A trend emerged towards a rightwards shift in the post-lesion psychometric functions for 1 kHz and 4 kHz NBN. Importantly, the BBN psychometric function remained stable after SG lesion. Accordingly, there were trends in the derived measures that correlate with changes described above, although none reached significance. This included an upward trend in the median 16 kHz threshold, with

an associated downward trend in the slope for 4 kHz and 16 kHz, indicating a reduction in temporal sensitivity for these sound ranges.

Ferret F1318

This animal represents one of the two ferrets that showed significant behavioural improvements. Almost paradoxically, large and significant improvements in detection threshold were seen for both 16 kHz NBN and BBN trials (Fig.4-6), with BBN displaying significant increases in *d'* values across all tested gap lengths. These observations contradict predictions based on the intended lesion location. The absence of any improvements at 1 kHz or 4 kHz is interesting, since this might preclude some kind of procedural improvement as an explanatory factor. Alternatively, in the context of the substantial hearing loss suffered by this animal (see *ABRs*, below), this selective lack of improvement may be a consequence of an interaction between a generalised central compensation process and some selective low-to-mid frequency impairment in the wake of the lesion.

Ferret F1319

F1319 displayed large behavioural changes after SG lesion, though unexpectedly they were all compensatory. A generalised, high-frequency-to-broadband improvement in sensitivity was observed across trials (Fig.4-7), with asymptotic increases occurring for 1 kHz and BBN, and a non-significant trend at 4 kHz NBN. Notably, significant improvements in most/all stimuli were seen for threshold, slope, and asymptotic *d'*, alongside significant post-lesion reductions in FA rates, suggesting general shifts in the animal's internal decision biases in a presumably optimising fashion.

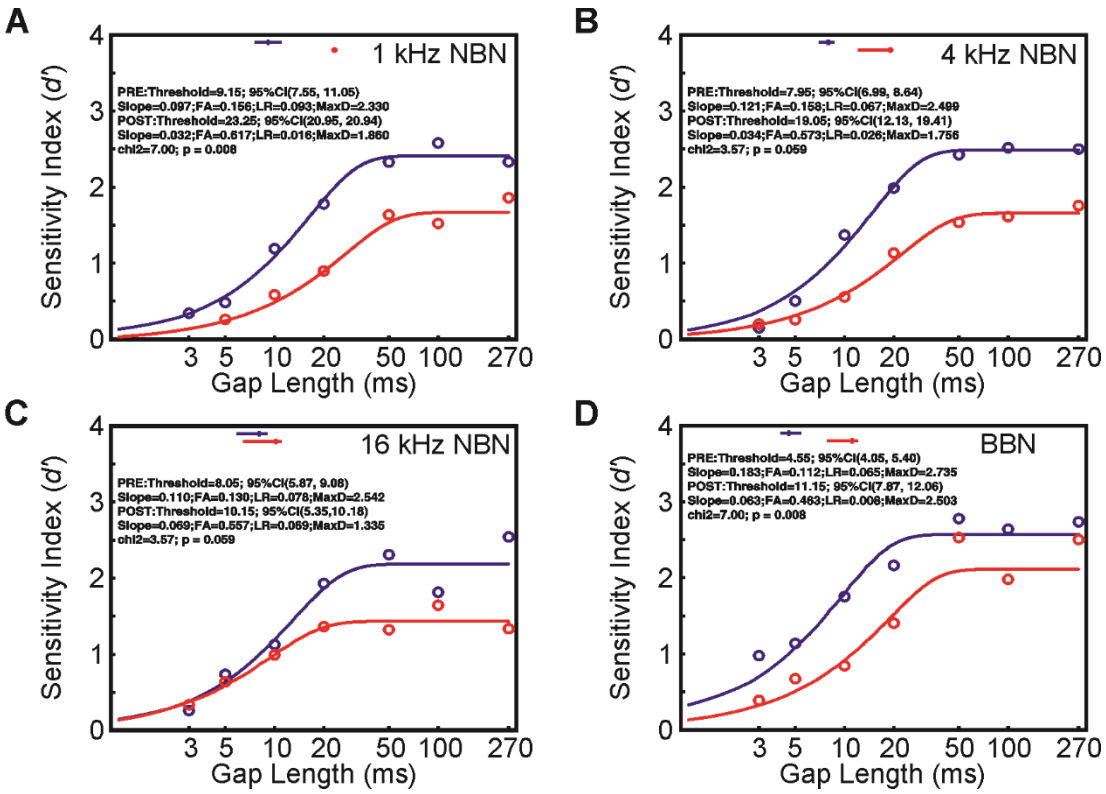

Figure 4-2 Psychometric functions, F1227. Pre-lesion = blue; post-lesion = red. Psychometric functions were fitted as right-weighted gumbel sigmoids to data pooled across sessions. Axes indicate *d'* plotted as a function of gap length. Dots and horizontal bars at the top of each panel indicate the fitted threshold and 95% confidence intervals (CIs) on the fit at threshold, respectively. Text describes numerical values, pre- and post-lesion, for threshold, 95% CIs, curve slope at threshold (slope), empirical FA rate (FA), empirical lapse rate (LR), and maximum fitted *d'* value (MaxD). χ^2 and *p* values are given for pre- vs. post-lesion Friedman test. A) 1 kHz NBN. B) 4 kHz NBN. C) 16 kHz NBN. D) BBN.

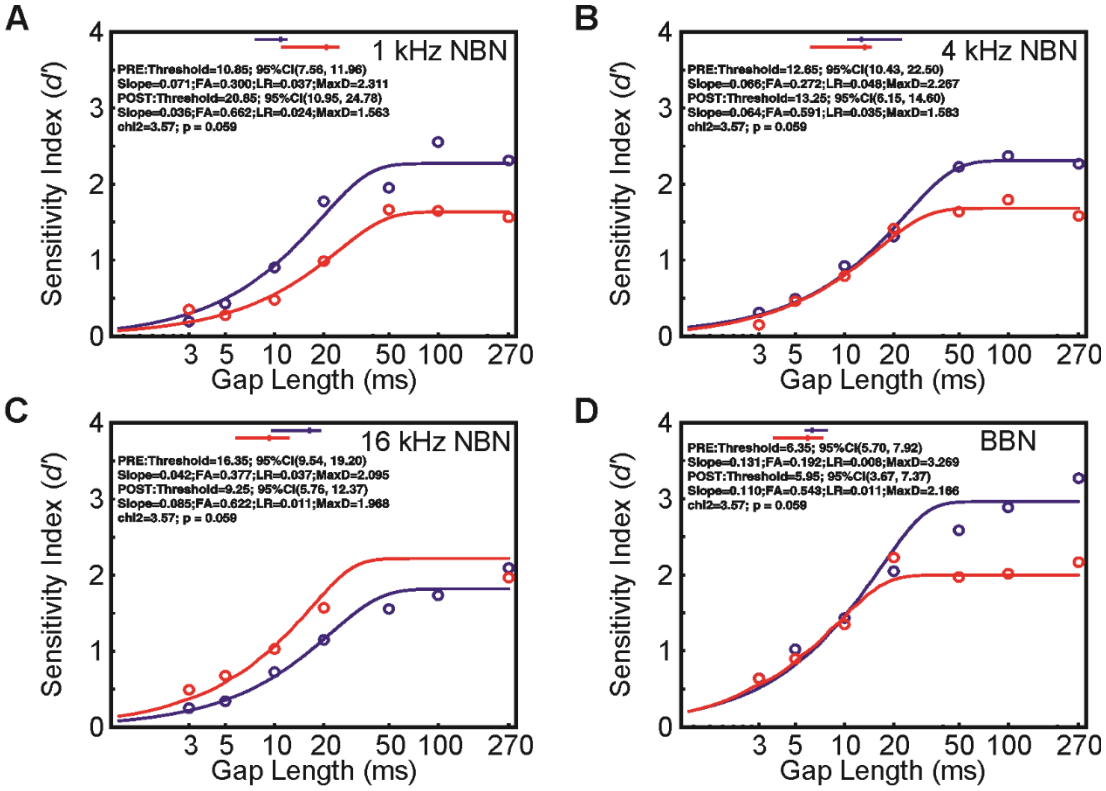

Figure 4-3 Psychometric functions, F1228. See description for Fig 4-2.

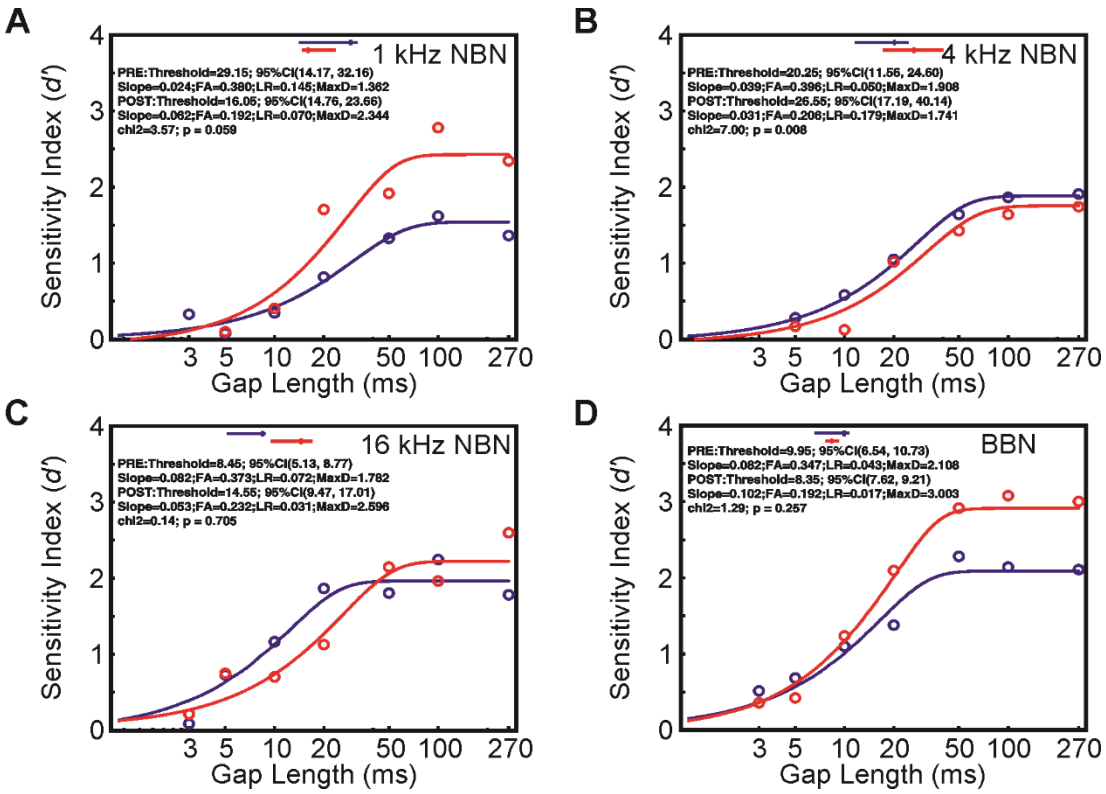

Figure 4-4: Psychometric functions, F1317. See description for Fig 4-2.

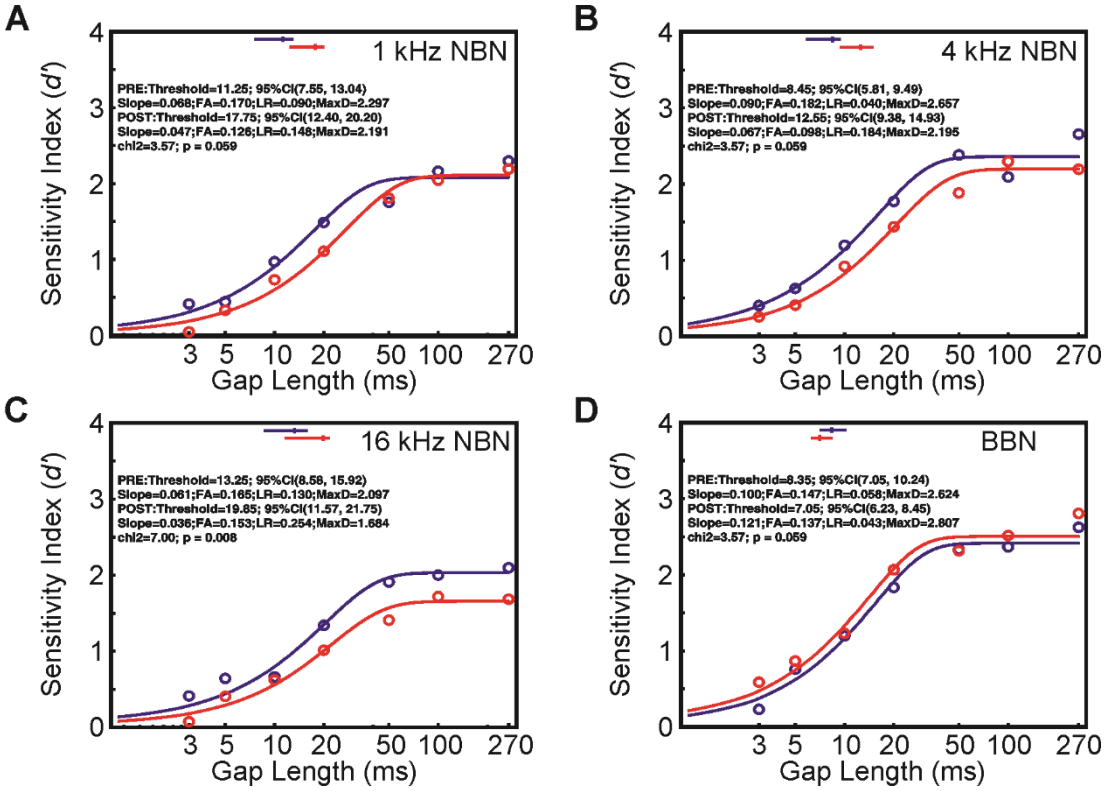

Figure 4-5: Psychometric functions, F1226. See description for Fig 4-2.

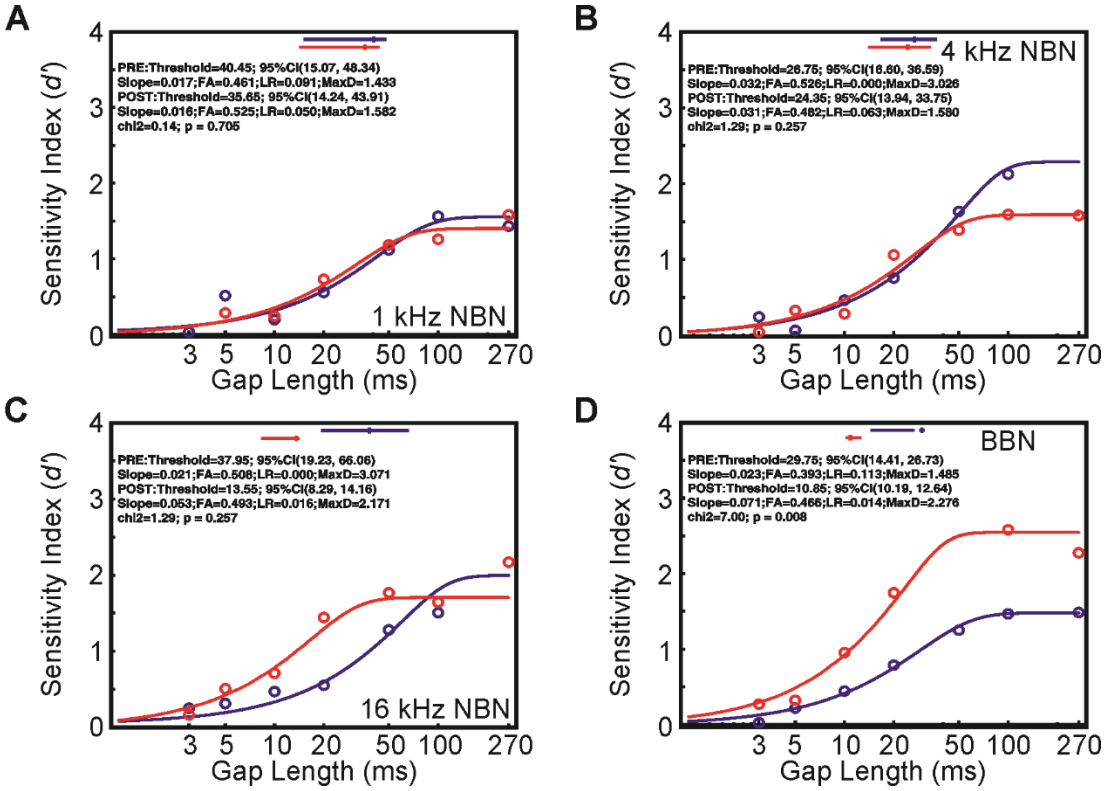

Figure 4-6: Psychometric functions, F1318. See description for Fig 4-2.

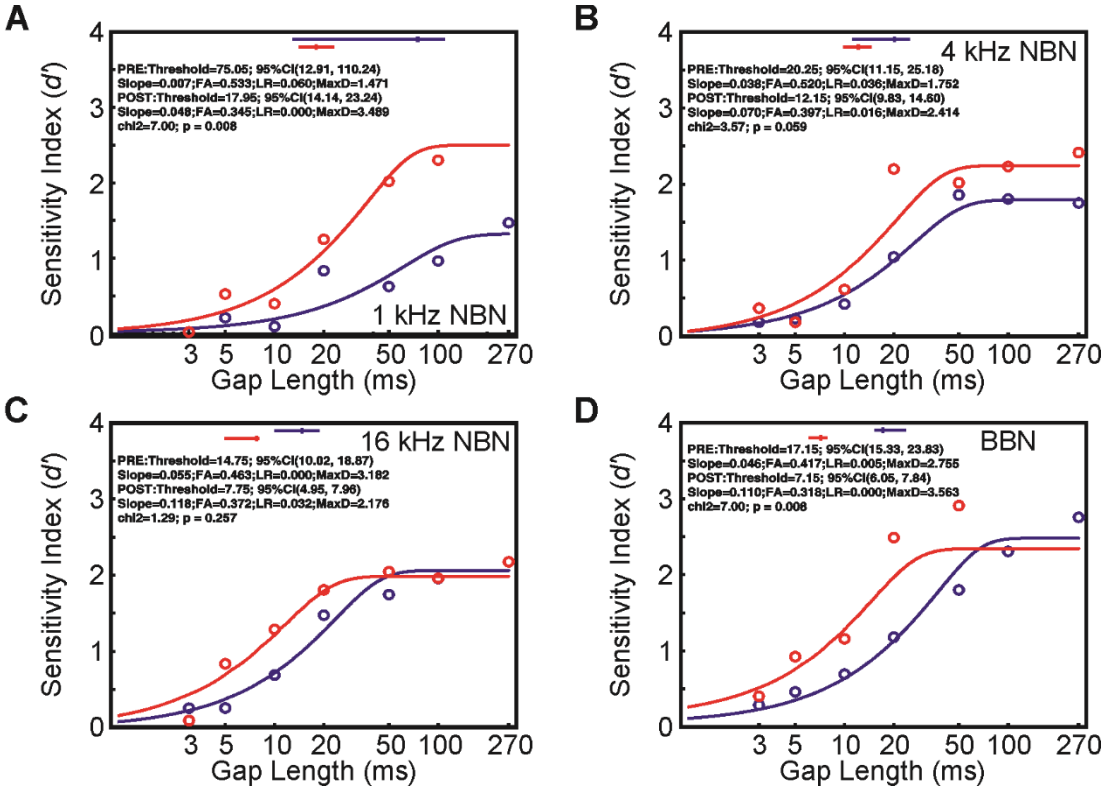

Figure 4-7: Psychometric functions, F1319. See description for Fig 4-2.

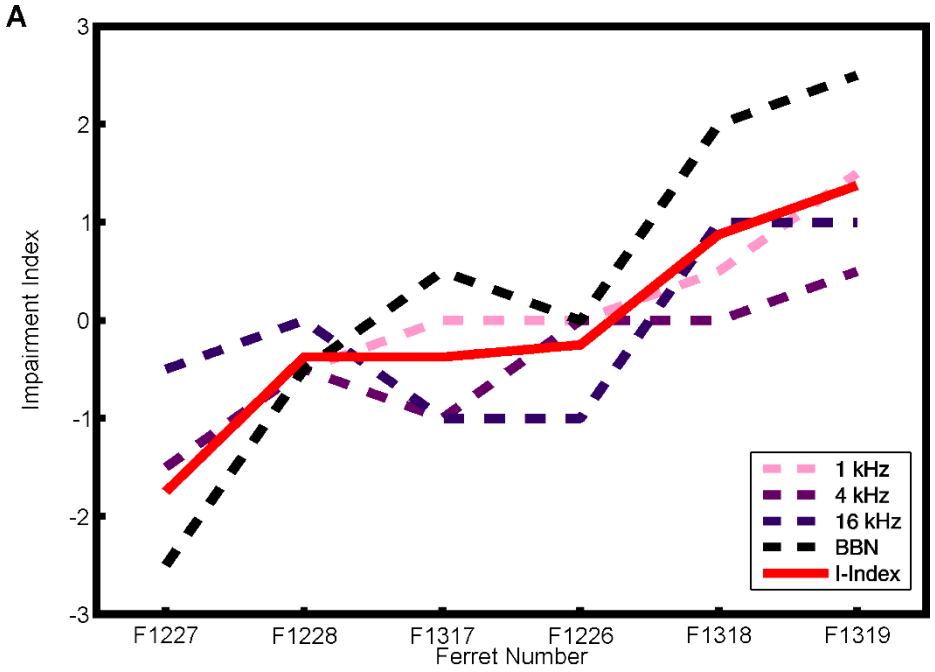

Figure 4-8: Behavioural Impairment/Improvement Index (I-Index). For each animal, the I-Index per stimulus was quantified pointwise as the magnitude and direction of behavioural changes in the pre-lesion vs. post-lesion conditions. Negative values indicate a worsening of performance in the post-lesion condition, compared with pre-lesion values. The overall I-Index (in red) was calculated as the average across all four stimulus types (pink: 1 kHz NBN; light purple: 4 kHz NBN; dark purple: 16 kHz NBN; black: BBN). Axes indicate I-Index scores, plotted for each animal.

Impairment/Improvement Index

We derived a metric to capture the post-lesion behavioural spectrum observed across our cohort, and as a means of categorising data of other modalities (i.e. ABRs, neurophysiological recordings, and histological data) where similar heterogeneity (or possibly lack thereof) developed. Since the focus of the investigation was driven by characterising the objective correlates of a perceptual phenomenon/pathology, this behaviourally-driven categorisation approach seemed most useful.

The metric derived was termed an Impairment/Improvement Index (I-Index), and was designed to quantify, in a normalised manner, any post-lesion behavioural changes, animal-by-animal. For each stimulus, behavioural changes were scored as follows: ±1 for a significant vertical shift in the psychometric function; ±1 for a significant horizontal shift in the psychometric function; ±0.5 for a significant change in the asymptotic d' across sessions. Stimulus-type scores were then averaged to provide an index centred at 0, indicating the directionality of the animal's behavioural changes, where positive indices imply an improvement, and negative indices an impairment, with maximum possible scores of ±2.5 in either direction. The trends described in the sections above emerge clearly when tabulated according to each individual's I-Index (Fig 4-8).

When ranked according to I-Index, ferrets fell into three distinct categories: one ferret with a large negative I-Index (F1227), where performance impairments were observed on three of the four stimulus frequencies, and a mild impairment developed for 16 kHz; three ferrets with small, negative I-Indices (F1226, F1228, F1317), indicating either minor performance reductions across a range of stimuli

(F1228), or substantial impairment in one stimulus type (F1226, F1317); and ferrets with a positive I-Index, showing universal or near-universal improvements in performance (F1318, F1319). For clarity where grouping is appropriate, we will refer to animals as falling into two groups: either impaired or not-impaired, as appropriate.

4.2.2 Lesion-Mediated Changes in Auditory Brainstem Responses (ABRs)

We sought to use the ferret ABR to verify the presence and determine the extent of damage caused by the SG lesion; and to explore the possible emergence of changes in auditory brainstem physiology that might be correlated with, and possibly predictive of, the behavioural changes described above. ABRs were collected from each of the above animals (n = 6) prior to and following SG lesion: post-lesion recordings were made soon after lesion surgery (<10 days after surgery, termed the "acute" period), and following post-lesion behavioural testing (>3 months post-surgery; "chronic" period).

From pilot data (n = 4), we observed a non-trivial amount of variability from session-to-session, deriving from ferret identity and small differences between recording sessions (e.g. electrode placement relative to the mastoid, depth of sedation). To control for these sources of variability, data were collected over multiple days, rather than relying upon single recording sessions, while variations introduced by ferret identity were accounted for by including this as a random factor during statistical analysis. Within-subject control data were supplied post-lesion by collecting ABRs in response to stimulation of the left (unlesioned) ear

during all recording sessions. It was thus hoped that any unrelated differences would occur in common for both ears, and so could be discounted.

ABRs have been collected as a convenient means of determining hearing thresholds in animal subjects without the requirement of training on behavioural audiometric tasks. In our hands, however, reliable ABR detection below 40-50 dB SPL was often not possible, with sweep fidelity occasionally affected by extrinsic noise of unknown origin, impacting the capacity to reliably identify all components of the ABR waveform, particularly at low stimulus amplitudes.

Stacked-ABRs as Indicators of Cochlear Disruption

We focussed our analysis upon the stacked-ABR aligned to trough IV, as this was the most reliably evoked and detected wave from session-to-session, and is the method previously applied by Don and colleagues in their evaluation of acoustic nerve defects (Don et al., 2005). The stacked-ABR wave IV amplitude for the lesioned ear was significantly diminished in size compared with pre-lesion control data in each animal (lme: lesion main effect: $F_{(2, 58)} = 11.168$, $p < 0.001$) (Fig 4-9). This amplitude reduction was greater in the acute period, and despite some recovery over time, stacked-ABR wave IV amplitude remained significantly depressed in the chronic period (*post-hoc*: pre-lesion vs. acute, chronic: $p < 0.05$ in each case). There were no significant long-term deficits for the control ear (lme: lesion main effect: $F_{(1, 52)} = 0.585$, $p = 0.448$), confirming the sensitivity of the stacked-ABR to lesion-related auditory disruptions.

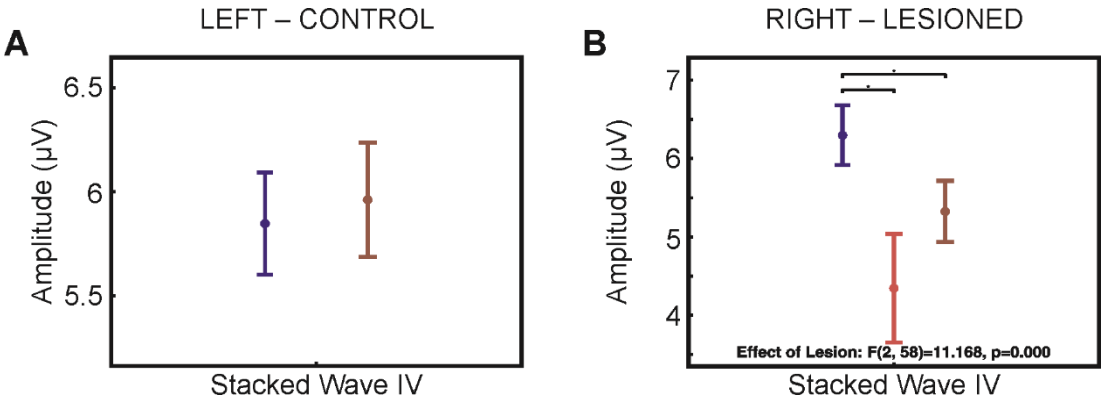

Figure 4-9: Stacked ABR Wave IV amplitudes. Pre-lesion = blue; acute period = red; chronic period = brown. Presence of text indicates significant main effect of lesion/recording period, giving main-effect F-statistic and *p*-value for lme model. A) Left (control) ear. B) Right (lesioned ear). Bars indicate *post hoc* $p < 0.05$.

Click-ABRs: Wholesale Lesion-Induced Changes in Brainstem Function

Typically, information from click-evoked ABRs (click-ABRs) is derived from the latencies and amplitudes of waves I – IV, with the origins of any changes derived from localising disruptions to synchronous auditory nucleus discharge. Additionally, the ABR RMS amplitude has been used as a proxy for the overall efficacy of auditory brainstem function (Ahlf et al., 2012; Hickox and Liberman, 2014). These measures were examined for changes related to the SG lesion.

Substantial click-ABR latency shifts emerged with right–ear stimulation after the SG lesion (Fig.4-10). Changes developed over time at the presumptive level of the auditory nerve, with significant Wave I latency increases observed in the chronic period (lme: $F_{(2, 687)} = 54.32$, $p < 0.001$). This pattern of increased latencies persisted throughout the brainstem, whereas significant short-term latency elevations were seen in Waves III – IV (lme: III: $F_{(2, 688)} = 82.08$, $p < 0.001$; IV: $F_{(2, 690)} = 74.13$, $p < 0.001$). From the between-wave latency differences of Waves II, III and IV with Wave I, the occurrence of further processing changes – alongside those directly imposed by acoustic nerve trauma – can be revealed. For latency ratios III:I and IV:I, changes were seen both acutely and chronically, and were highly significant (lme: III: $F_{(2, 685)} = 28.74$; IV: $F_{(2, 690)} = 42.84$; $p < 0.001$ in each case).

The reliability of click-ABR latencies was questioned on the basis of control (left-ear) data (Fig.4-10). Across all waves, significant left-ear latency differences were observed (lme: I: $F_{(2, 645)} = 116.49$, $p < 0.001$; II: $F_{(2.645)} = 120.09$, $p < 0.001$; III: $F_{(2, 645)} = 88.68$, $p < 0.001$; IV: $F_{(2, 645)} = 117.69$, $p < 0.001$). At each wave, a distinct pattern was seen wherein acute latencies were reduced, and chronic latencies elevated,

compared with pre-lesion matched controls. Due to these differences, emerging early (from Wave I) on the left-ear click ABR (where no imposed damage is liable to be present), it is unclear if click-ABR latency, in our hands, is a useful indicator of peripheral trauma or its sequelae.

We therefore examined a measure of auditory dysfunction previously used to detect otoacoustic tumours: the interaural Wave IV delay (IT4; equivalent to wave V in human subjects), for which positive values indicate that the latency of responses to stimulation of the lesioned ear is greater than that of the control (unlesioned) ear (Bauch et al., 1996). As a normalised measure, IT4 shows little-to-no deviance from 0 in subjects with normal hearing (Selters and Brackmann, 1977). In our ferrets, pre-lesion values were centred at 0, irrespective of sound intensity (Fig.4-11). By contrast, there were significant post-lesion (acute & chronic) increases that exceeded +0.2 ms in some instances (lme: $F_{(2, 557)} = 61.21; p < 0.001$). It therefore appears that click-ABR latencies, compared bilaterally, may enable detection of retrocochlear damage in experimental animals.

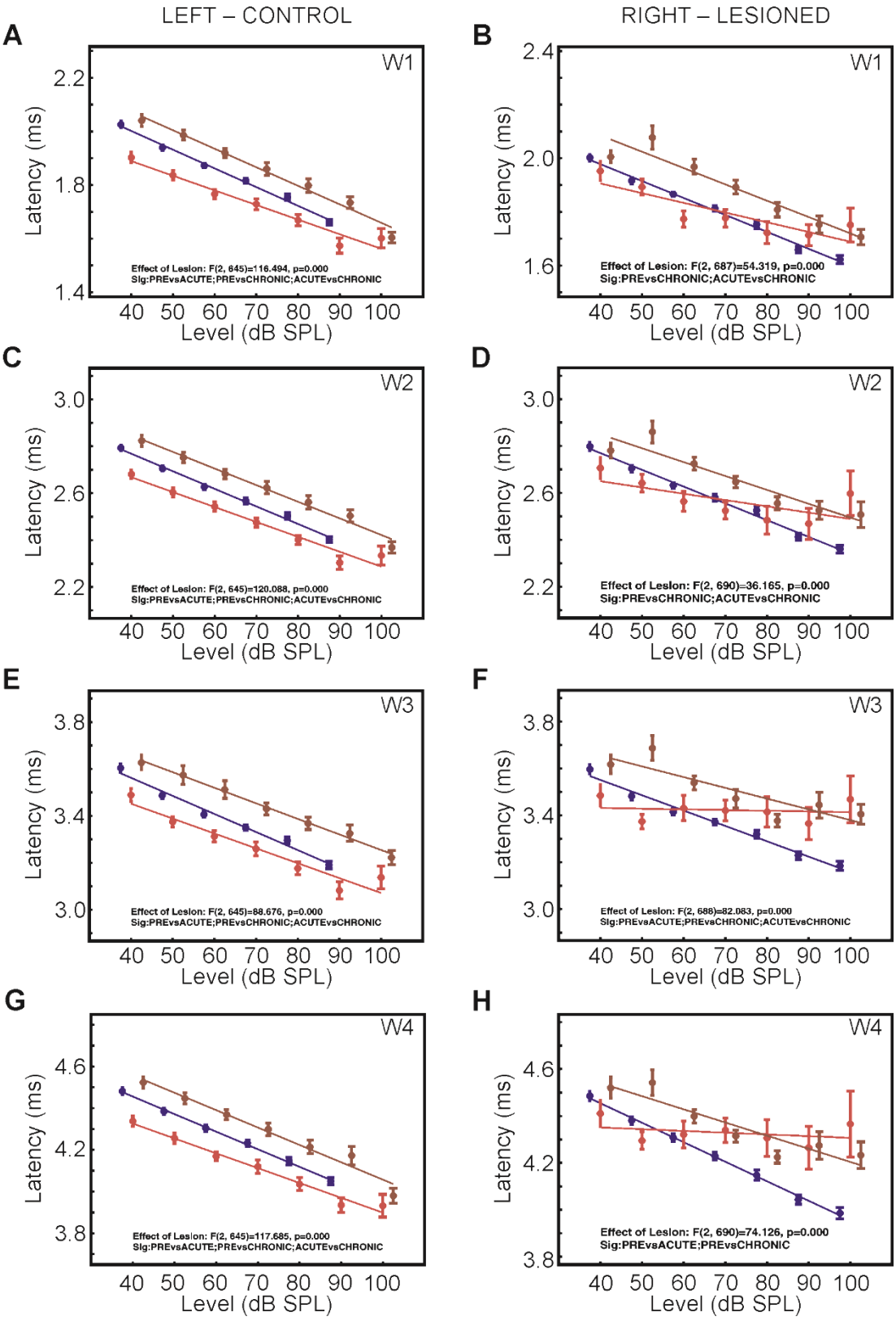

Figure 4-10: Click-ABR latencies. Latency calculated as time between stimulus onset and local minimum of trough associated with each of Waves I – IV. Axes indicate waveform latency

(milliseconds) vs. click level (dB SPL). Left column = left (control) ear; right column = right (lesioned) ear. Rows 1 – 4 indicate waves I – IV (W1 – W4) of ABR waveform complex.

For all ABR figures: Pre-lesion = blue; acute post-lesion period = red; chronic post-lesion period = brown. Presence of text indicates significant main effect of lesion/recording period, giving F-statistic and *p*-value for lme statistical model; "Sig:…" indicates *post hoc* comparisons between recording periods that were significant at $a = 0.05$.

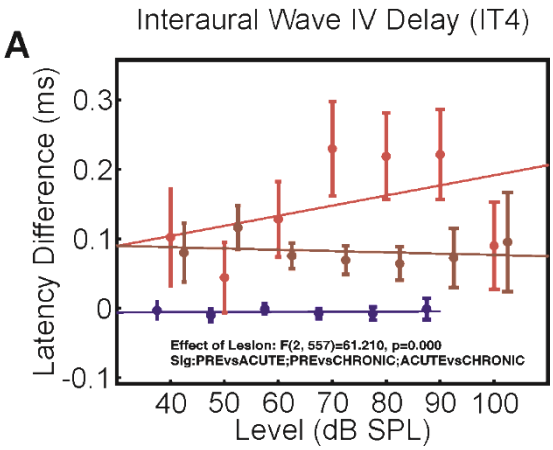

Figure 4-11: Click-ABR interaural Wave IV delay (IT4). IT4 calculated as difference between latency of Wave IV in the right (lesioned) and left ears; positive values indicate longer relative latency in the right ear. Axes indicate wave IV interaural latency delay (milliseconds) vs. click level (dB SPL).

Changes to click-ABR amplitudes appeared better related to lesion-related trauma. Throughout the ipsilesional ABR waveform, reductions in wave amplitudes were seen acutely post-lesion, persisting into the chronic period, and becoming larger with higher sound intensities, as typified in the Wave I response (lme: $F_{(2, 687)} = 90.94; p < 0.001$) (Fig.4-12). Larger differences between pre- and post-lesion data at higher sound intensities suggests an impairment in ANF recruitment following SG lesion. Although this pattern appears to be inherited along the auditory pathway, between-wave ratios (comparing Waves II, III and IV with Wave I) suggest the occurrence of adaptive processes in response to the partial deafferentation. In particular, acute enhancement of the II:I amplitude ratio (lme: $F_{(2, 674)} = 35.65; p < 0.001$) developed, and was seen also in the acute III:I and IV:I amplitude ratios, though not chronically.

Importantly, control ear click-ABR amplitudes conformed to the expected pattern of lesion-related changes (Fig.4-12). Neither Waves I or II showed any evidence of lesion-related amplitude changes, albeit with a marginally significant difference between the acute and chronic data of Wave I (lme: $F_{(2, 645)} = 3.23; p = 0.04$). The generators of Waves III and IV represent input from both ears (Wada and Starr, 1983; Melcher et al., 1996)), and so may be subject to plasticity in response to contralateral deafferentation. Accordingly, post-lesion reductions were present in Waves III and IV amplitudes. This amplitude reduction failed to reach significance in the Wave IV chronic period, consistent with the suggested adaptation to the unilateral deafferentation.

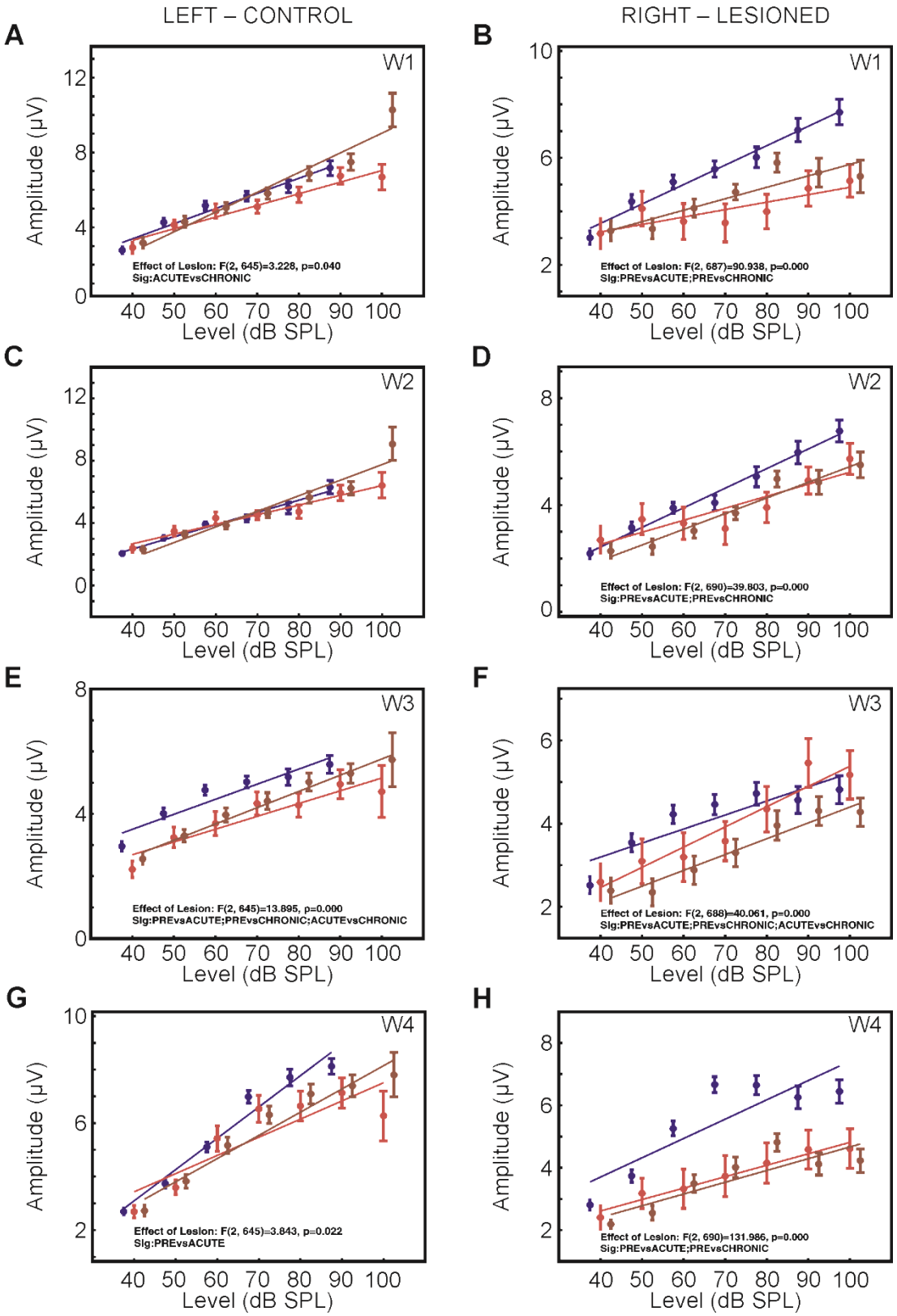

Figure 4-12: Click ABR amplitudes. Amplitude calculated as trough-to-peak distance, in μV, for each of Waves I – IV. Axes indicate waveform amplitude (μV) vs. click level (dB SPL). Left column = left

(control) ear; right column = right (lesioned) ear. Rows 1 – 4 = waves I – IV (W1 – W4) of ABR waveform complex.

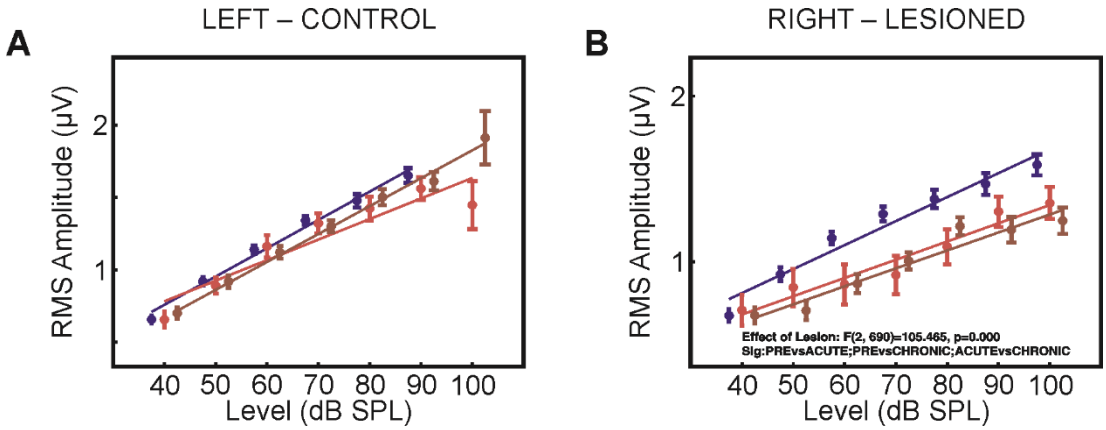

Figure 4-13: Click ABR root mean square (RMS) amplitude. Calculated as the RMS of the ABR between 1 – 10 ms after stimulus onset. Axes indicate waveform RMS amplitude (µV) vs. click level (dB SPL). A) Left (control) ear. B) Right (lesioned) ear.

In line with observations described for stacked-ABRs, a large and long-lasting reduction in the post-lesion click-ABR RMS was observed in the lesioned ear (lme: $F_{(2, 690)} = 105.47; p < 0.001$) (Fig.4-13). This effect was absent from left-ear click ABRs (lme: $F_{(2, 645)} = 0.791; p = 0.454$), where all acute data were available, as distinct from the stacked-ABR dataset. Thus, the click-ABR RMS provides another simple tool for evaluating the presence of a peripheral trauma affecting cochlear afferent activity. In our hands, bilateral recordings were necessary to ensure the efficacy of the recording technique, and to avoid systematic disruptions to the ABR signal that are independent of hearing loss.

Narrowband ABRs

A set of octave-bandwidth NB stimuli was tested with centre frequencies that would putatively span much of the basilar membrane's tonotopy (1, 4, 8 and 16 kHz). NB-ABR waveforms evoked in response to low-intensity NB stimuli could often not be reliably identified, particularly for low-to-mid frequency sounds. Nevertheless, a number of interesting observations emerged that were largely in line with those already described for click- and stacked-ABR measurements.

First, the expected increase in ipsilateral latencies was seen in the chronic period (vs. pre-lesion and acute) for NB-ABRs centred at 4, 8 and 16 kHz, developing at Wave I and persisting in each case through to Wave IV; no significant latency shifts developed for any waveforms evoked in response to 1 kHz stimuli. As with click ABR data, systematic latency shifts were observed in the contralesional ear across all frequencies, largely manifesting as significant reductions in the acute period, and increases in the chronic period.

Second, inspection of NB-ABR amplitudes was unhelpful for identifying the putative site and/or extent of the SG lesion. Although large reductions occurred in NB-ABR amplitudes for Waves I–IV, these were observed for all stimuli ipsilesionally, and so only indicated *that* a disruption of cochlear afferent signalling had taken place, rather than *where*. Similarly, RMS magnitudes were depressed across all NB-ABRs in the acute and chronic periods ipsilesionally. NB-ABRs from the control ear were not as predicted, either. For example, significant acute reductions in amplitude were seen at Wave I in response to 4 kHz ($F_{(2, 390)} = 4.60$; $p = 0.01$) and 8 kHz ($F_{(2, 443)} = 3.42$; $p = 0.03$). Thus, the unreliability of NB-ABR identification, in combination with systematic epoch effects upon recording fidelity, means these measurements have limited utility in the ferret, especially under the conditions imposed by our model.

4.2.3 Cortical Neurophysiology: Lesion-Mediated Changes in Brain Activity

By employing bilateral neurophysiological recordings in ferret ACs under general anaesthesia, we sought to determine whether the types of neural changes previously reported as being "tinnitus-like" in AC were present in our model; and, if so, whether there existed any hemispheric asymmetry related to the unilateral nature of the SG lesion. To evaluate these possibilities, we measured spontaneous activity in the absence of acoustic stimulation; evoked responses to pure tone stimuli; and responses to bandpassed noise stimuli, modelled after those used during behavioural testing. These data were collected in Lesioned animals (n = 6) (L) in which behavioural impairment was either present (Impaired, I) or absent (Not-

Impaired, NI), and a cohort of behaviourally-naïve, non-lesioned Controls (n = 3) (C).

Tone-evoked Responses Indicate Evoked Cortical Hyperactivity

The SG lesion produced no large-scale, long-term tonotopic remapping, in contrast with descriptions from previous lesion models (e.g. Robertson and Irvine, 1989; Rajan et al., 1993). Unit frequency response areas (FRAs) were found in each subject that spanned the range of stimulus frequencies (0.5-30 kHz, 1/6 octave steps, 40-90 dB SPL, 10 dB steps, 100 ms duration), and by combining responses across animals composite FRA maps for each hemisphere were constructed (Fig.4-14). As discussed below, the composition of FRA maps depends on where in AC neural responses are sampled, although we aimed to ensure consistency across experiments.

Upon examining FRA maps for Controls, even without hearing loss interhemispheric mapping differences can occur, determined by evaluating the proportion of units significantly responding to each tone frequency (Fig.4-15). Specifically, right AC units pooled across Controls displayed a significantly greater representation of frequencies <4 kHz when compared with units from left AC (rank-sum, $p < 0.001$). By contrast, Lesioned animals displayed no significant hemisphere tonotopic asymmetry (rank-sum, $p = 0.16$), despite the trend towards lower frequency tuning in right AC. Comparison of the left and right AC maps obtained from the Control and Lesion cohorts yielded no significant differences within the respective comparisons (rank-sum: Left: $p = 0.193$; Right: $p = 0.221$).

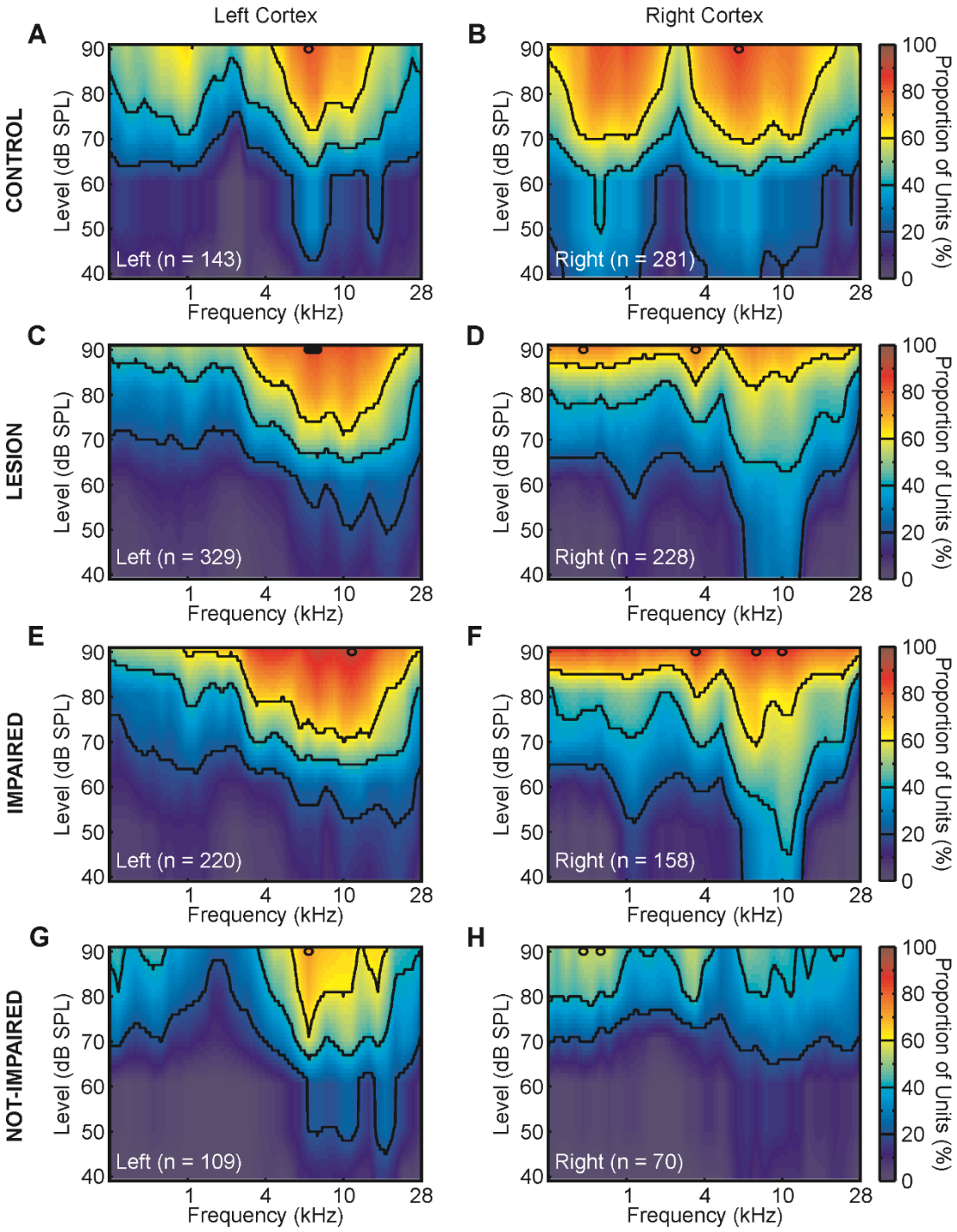

Figure 4-14: Average Frequency Response Area (FRA) Maps, Pooled Within Cohorts. In each panel, axes indicate level (dB SPL) vs. frequency (kHz) of tone stimulus; FRA heatmap indicates proportion of neurons that responded at each tone frequency*level combination, with black outlines describing borders between 20%, 40%, and 60% of neurons responding. Black circle/s indicate frequency*level combination at which the most cells responded. White text indicates the hemisphere and number of cells recorded within that hemisphere, for each group. Left column = left AC; right column = right AC. A, B) Unlesioned controls. C, D) Lesioned animals. E, F) Impaired animals. G, H) Not-Impaired animals.

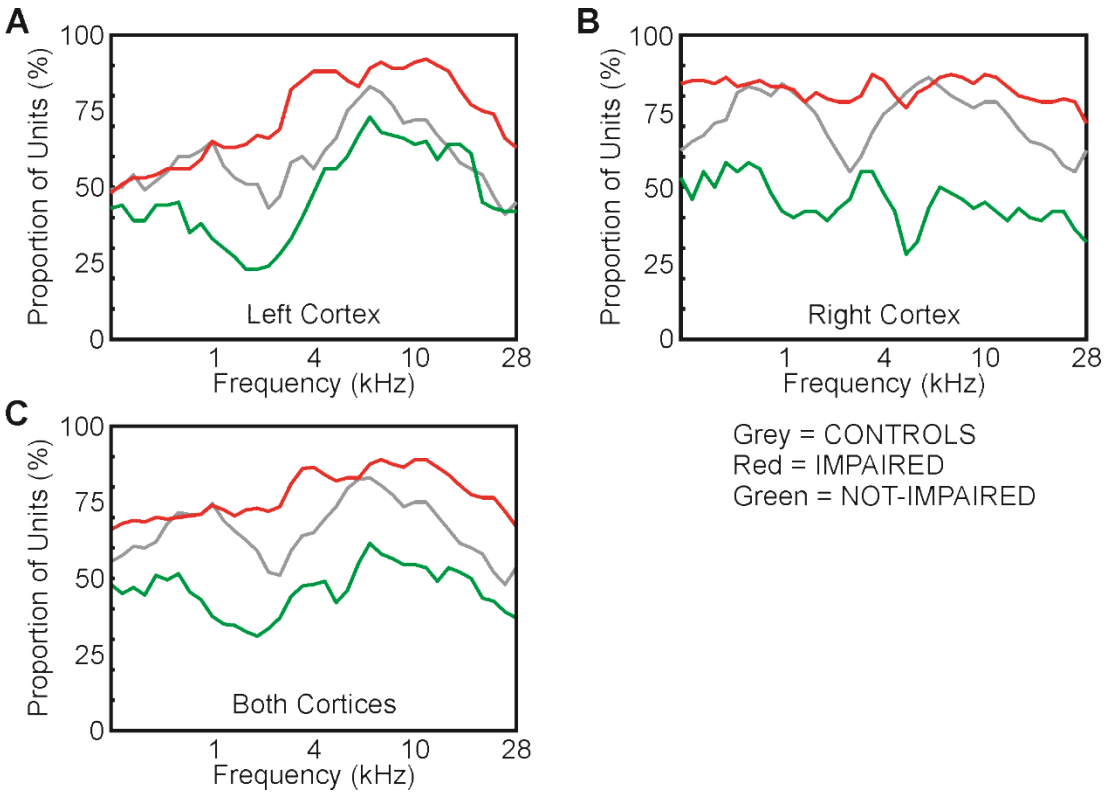

Figure 4-15: FRA Map Proportions. Grey = Unlesioned Controls; Red = Impaired animals; Green = Not-Impaired animals. In each panel, lines indicate the proportion of units (%) significantly responding at each tone frequency, irrespective of level. A) Left AC. B) Right AC. C) Pooled data across both left and right ACs.

Subdivision of the Lesion group into Impaired and Not-Impaired *did* reveal cortical map differences between groups, though not of the kind previously associated with selective hearing loss. In both left and right ACs, the proportion of units responding at any particular frequency was significantly lower in the Not-Impaired group, and significantly greater in the Impaired group, compared with Controls (Kruskal-Wallis, $\chi^2 = 77.99$; $p < 0.0001$; all *post-hoc* comparisons significant at $a = 0.05$) (Fig 4-15). This proportionally-different frequency representation between cohorts suggests the existence of bandwidth effects in the FRAs. Surprisingly, the FRA widths of tuned Lesion units were significantly narrower than those obtained from Control animals, at 10 dB above threshold (Median Q10: C = 1.8; L = 2.3. rank sum: $p = 0.001$) (Fig.4-16). Although units from both Impaired and Not-Impaired ferrets had a median Q10 that was greater than Controls (Median Q10: I = 2.2; NI = 2.6), pairwise comparisons indicated a significant difference between Control and Impaired groups only (Kruskal-Wallis: $\chi^2 = 10.20$; $p = 0.006$; *post-hoc* $p < 0.05$). The absence of significant differences in the Not-Impaired group likely derives from wider interquartile ranges for these data. Notably, at 30 dB above the lowest response level, tuning bandwidths were equivalent for all three groups (Median Q30: C = 0.4; I = 0.5; NI = 0.5. Kruskal-Wallis: $\chi^2 = 3.69$; $p = 0.158$).

Since certain evoked neural response properties to pure tones (response proportions and Q10 values) are affected in the presence of a deafferentation that is associated with behavioural impairment, we next asked whether evoked response magnitudes were also modified, or whether the subtle changes in FRA mapping/bandwidth developed without changes to the number of spikes generated per stimulus. Rate-level functions (RLFs) were constructed at each tuned unit's best

frequency (BF), with responses normalised as z-scores to enable between-unit comparisons. We examined two features of RLFs: the maximum z-score of each unit (irrespective of the sound intensity at which this occurred), and the slope of the linear fit made to each RLF. Despite the SG lesion lateralisation, no effect of recording hemisphere was seen in any group, and so data were pooled across left and right ACs. We found a significant increase in the maximum z-score of units from Lesioned ferrets when compared with Controls, with no post-hoc differences observed between Impaired and Not-Impaired units (Median max. z-score: C = 8.8; I = 11.1; NI = 11.0. Kruskal-Wallis: $\chi^2 = 59.91; p < 0.0001$) (Fig.4-17). Control units also had significantly shallower RLFs compared with both Impaired and Not-Impaired groups, between which no difference was found (Median RLF slope (z-score/dB): C = 0.1; I = 0.2; NI = 0.2. Kruskal-Wallis $\chi^2 = 80.35; p < 0.0001$).

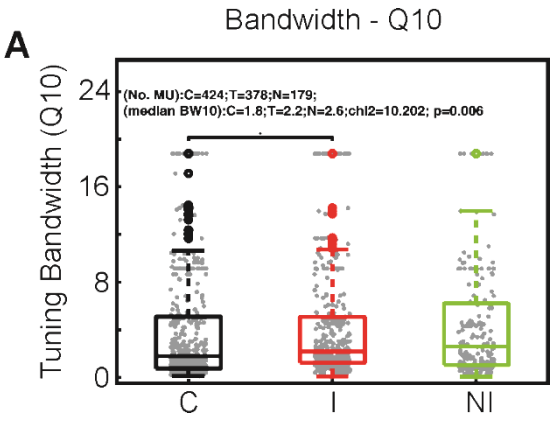

Figure 4-16: Multiunit FRA Tuning Bandwidth at 10 dB Above Threshold (Q10). For each FRA, the Q10 was calculated as the FRA width, in kHz, at 10 dB above threshold, divided by the frequency at threshold. Axis indicates Q10 vs. animal group: C (black) = Unlesioned Controls; I (red) = Impaired animals; NI (green) = Not-Impaired animals. Boxes indicate median ± interquartile range, whiskers indicate extremes, outliers represented as coloured circles. Grey dots indicate individual units. Black bar indicates significant between-group comparison, for *post hoc a = 0.05.*

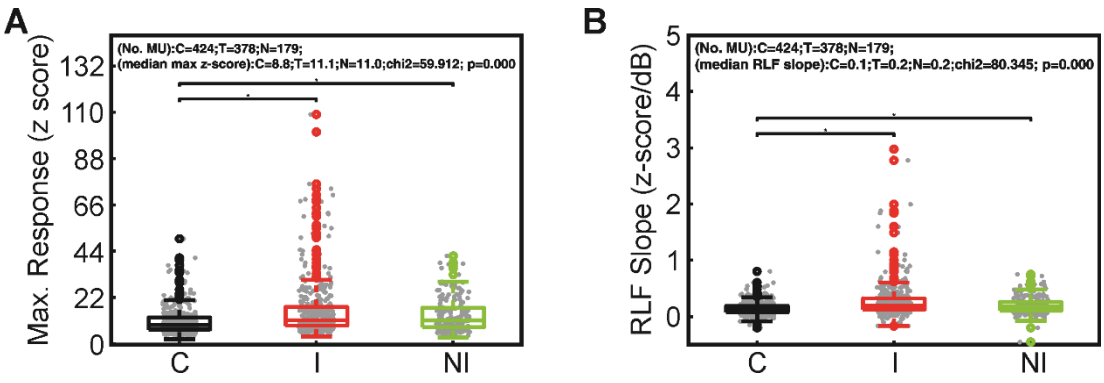

Figure 4-17: Pure Tone Rate-Level Functions (RLFs). For each unit, RLF was calculated at BF, and normalised by SFR to generate z-score values (see text). Axes indicate measure of interest vs. animal group: C (black) = Unlesioned Controls; I (red) = Impaired animals; NI (green) = Not-Impaired animals. Boxes indicate median ± interquartile range, whiskers indicate extremes, outliers represented as coloured circles. Grey dots indicate individual units. Black bars indicate significant between-group comparison, for *post hoc a = 0.05.* A) RLF maximum response, i.e. z-score at BF. B) RLF slope, measured as slope of linear fit to RLF values.

Thus, the SG lesion induced a significant enhancement of the activity of AC units in response to acoustic stimulation, implying the development of hyper-responsivity described in previous studies as tinnitus-like physiology (Qiu et al., 2000; Engineer et al., 2011): the enhancement of both maximum response magnitude and RLF slope is indicative of a central gain increase. Importantly, the z-score describes the driven rate normalised by the spontaneous rate of each unit, rather than evoked spiking activity alone. As such, elevated z-scores may indicate an underlying increase in the driven spike rate, a reduction in the spontaneous rate, or a combination of the two. Therefore, we next explored whether spiking activity changed in the absence of acoustic stimulation.

Baseline Hyperactivity in the Wake of SG Lesion

Spontaneous firing rates (SFRs) were estimated from activity observed over a >30 second period of silence, after stable pure tone responses had been verified. SFRs were then computed for those units that displayed a significant response to pure tone and/or bandpassed gap-in-noise stimuli. We adopted this approach to ensure that only acoustically responsive units were analysed, since activity on channels that were not acoustically driven may have been artefactual.

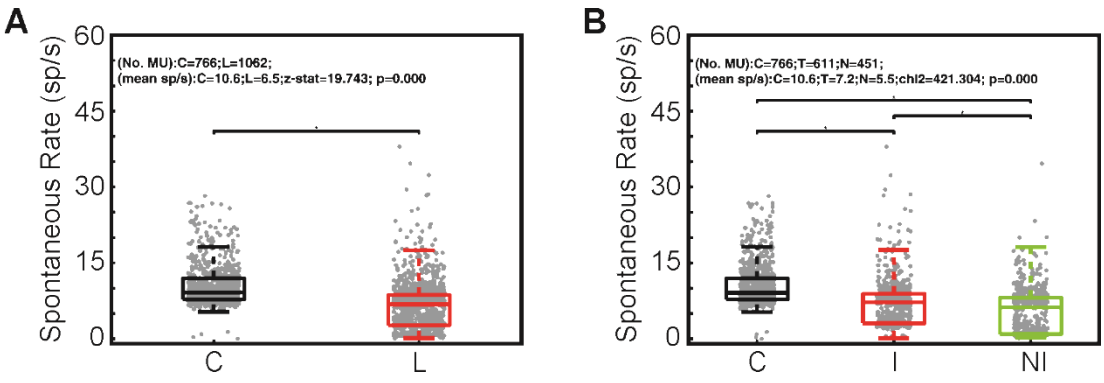

Figure 4-18: Spontaneous Firing Rates (SFRs) of AC Units. Axes indicates SFR (in spikes/second) vs. animal group: C (black) = Controls; L (red, in (A)) = Lesioned; I (red, in (B)) = Impaired; NI (green) = Not-Impaired. Boxes indicate median ± interquartile range, whiskers indicate extremes, outliers represented as coloured circles. Grey dots indicate individual units. Black bars indicate significant between-group comparison, for *post hoc* $a = 0.05$. A) Controls vs. Lesioned animals. B) Controls vs. Impaired vs. Not-Impaired animals.

Units from Lesioned ferrets did not display hemispheric asymmetry in SFRs (tuned units, rank-sum $p = 0.439$), as was also the case in Controls (rank-sum: tuned: $p = 0.4$; untuned: $p = 0.448$). However, we found a marked reduction in Lesion SFRs overall, decreasing by almost 40% (Mean SFR (spikes/second): C = 10.6; L = 6.5. rank-sum: $p < 0.0001$) (Fig.4-18). When behavioural status was considered, SFRs of Not-Impaired units were significantly lower than those from Impaired animals, both being less than Controls (Mean SFR (spikes/second): C = 10.6; I = 7.2; NI = 5.5. Kruskal-Wallis: $\chi^2 = 421.30$, $p < 0.0001$) (Fig.4-18). Therefore, the SG lesion appears to reduce the afferent drive to AC, but animals with a behavioural impairment showed a significant basal hyperactivity within this context of diminished afferent input when compared with similarly deafferented, but behaviourally unimpaired, ferrets.

SG Lesion Amplifies Driven Neural Synchrony

Alongside indications of neural hyperactivity and AC functional reorganisation, post-traumatic shifts in the neural synchrony profile of driven and spontaneous responses have been correlated with the administration of known tinnitus inducer salicylate (Yang et al., 2007), and with acoustic trauma leading to tinnitus-like behavioural indications (Engineer et al., 2011). To evaluate the spiking synchrony among our cohort, the pairwise cross-correlation coefficient (r) was calculated for acoustically-responsive units within the same ensembles. By extracting the peak of the cross-correlation histogram (CCH) for spontaneous activity and driven responses, as well as the residual CCH using the shift-predictor (SP) correction (Perkel et al., 1967), estimates could be made of how the underlying input commonality of the analysed units changed as a result of peripheral deafferentation

(Brosch and Schreiner, 1999; Noreña and Eggermont, 2003; Seki and Eggermont, 2003).

Estimates of correlation strength within the Control cohort, for both the driven (median $r = 0.151$) and spontaneous (median $r = 0.057$) conditions, were similar to previous data from cat AC (Brosch and Schreiner, 1999). Contrasting with previously reported effects of hearing loss, however, the SG lesion induced significant *reductions* in r for acoustic stimulation (median r: L = 0.100. rank-sum: $p < 0.0001$ vs Control) and spontaneous activity (median r: L = 0.049. rank-sum: $p < 0.0001$ vs Control) (Fig.4-19). By contrast, the Lesion residual r was significantly greater than Controls (median r: C = -0.305; L = -0.053. rank-sum: $p < 0.0001$) (Fig.4-19E), although each displayed negative CCHs overall. This suggests an abnormally high artefactual correlation strength, possibly due to the mixed single/multiunit nature of the data, and the absence of cluster-cutting algorithms applied to separate single unit responses on individual and/or multiple electrodes.

Regarding spontaneous synchrony, Impaired units displayed a significant reduction in comparison with Controls, whereas Not-Impaired units showed a neural synchrony enhancement (median r: I = 0.046; NI = 0.070. Kruskal-Wallis: $\chi^2 = 83.84$, $p < 0.0001$; all post-hoc comparisons significant at $a = 0.05$) (Fig.4-19). The diminished synchrony in Impaired animals compared with their Not-Impaired counterparts was also seen for driven CCHs (median r: I = 0.093; NI = 0.123. Kruskal-Wallis: $\chi^2 = 117.85$, $p < 0.0001$; C vs I and NI vs I *post-hoc* pairwise comparisons significant at $a = 0.05$). As above, SP-corrected residual r values displayed significant differences between all groups (median r: I = -0.066; NI = -

0.011. Kruskal-Wallis: $\chi^2 = 781.92$, $p < 0.0001$; all post-hoc pairwise comparisons significant at $a = 0.05$).

Overall, the SG lesion appeared to reduce spontaneous neural synchrony in general, although we did find evidence of SP-corrected driven hypersynchrony, as in previous accounts (Noreña et al., 2003; Seki and Eggermont, 2003), particularly among Not-Impaired units. Indeed, both Impaired and Not-Impaired units had enhanced neural synchrony vs. Controls, but Impaired animals displayed spontaneous desynchronization, whereas Not-Impaired animals exhibited spontaneous hypersynchrony. Exposure to partial hearing loss appears to affect the input-output relationships within neural ensembles, both in the resting state and in response to acoustic stimulation. To determine how this putative neuroplastic effect may impact upon the spiking representation of behaviourally relevant stimuli, we next examined the neural encoding of gap-in-noise stimuli.

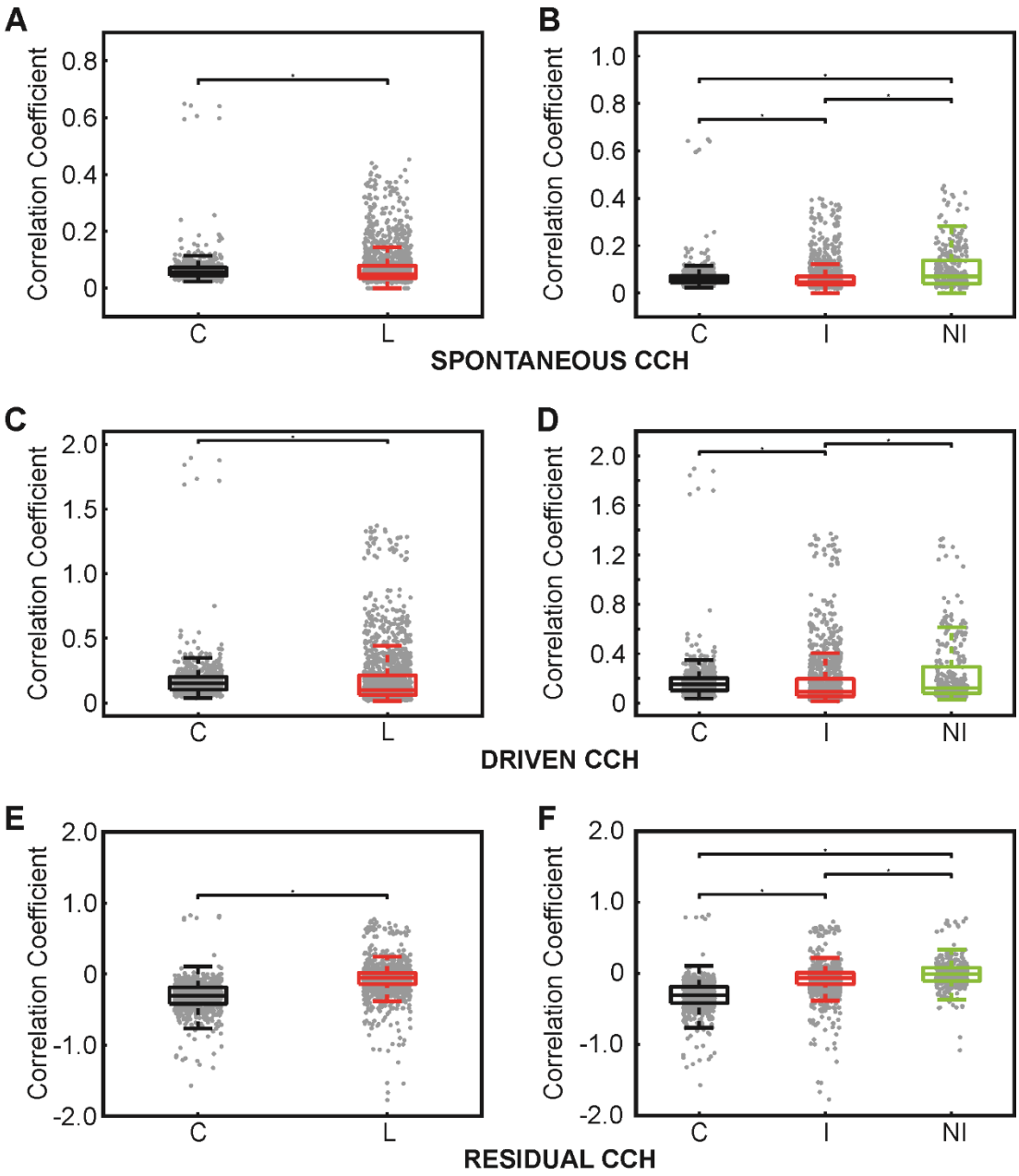

Figure 4-19: Normalised Cross-Correlation Histograms (CCH) of AC Units. Axes indicate Correlation Coefficient *r* vs. animal group: C (black) = Unlesioned Controls; L (red, in left column) = Lesioned animals; I (red, in right column) = Impaired animals; NI (green) = Not-Impaired animals. Boxes indicate median ± interquartile range, whiskers indicate extremes. Grey dots indicate individual units. Black bars indicate significant between-group comparison, for *post hoc* $\alpha = 0.05$. A, B) CCH during silence (Spontaneous CCH). C, D) CCH during BBN stimulation (Driven CCH). E, F) CCH during BBN stimulation, corrected by SP (Residual CCH).

Gap-in-Noise Neurometric Thresholds Are Unchanged by SG Lesion

To evaluate the gap-detection capabilities of units from the different experimental cohorts, we measured neural responses to stimuli that were spectrally identical to those used during behaviour: broadband (BBN) and narrow-bandpassed noise (NBN) stimuli (octave bandwidths, centred at 1, 4, and 16 kHz), containing silent gaps ranging from 1 – 270 ms.

On exploring responses of individual units from different ferrets, a set of response types emerged that typified the encoding of gap-in-noise stimuli, irrespective of stimulus frequency or bandwidth (Fig.4-20). Following an initial onset peak in the peri-stimulus time histogram (PSTH), the presence of a gap was predominantly marked by a robust onset PSTH peak at the start of the post-gap noise burst, with spiking quickly falling to spontaneous levels. Occasionally, units displayed tonic spiking elevation throughout acoustic stimulation, diminishing towards SFR during the silent gaps. Some units displayed a robust peak in the PSTH at the noise burst *offset*, effectively marking the gap onset. Therefore, although the acoustic onset PSTH peak represents a useful correlate for neural gap detection, it is not isolated in this respect. These data indicate that a more objective approach, with less stringent response categorisation than simply "onset-responsive", is needed to identify reliable gap-detection responses.

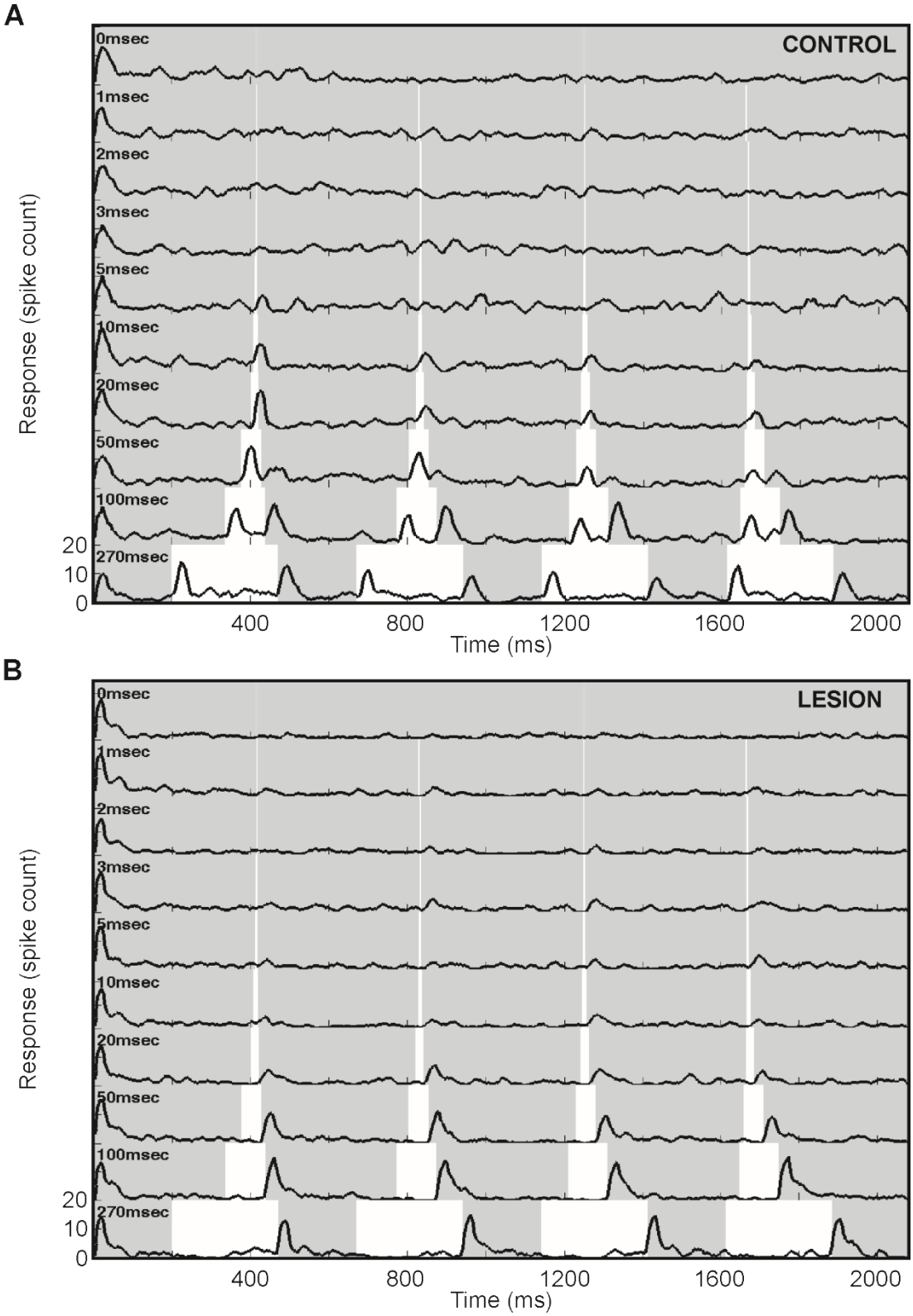

Figure 4-20: Gap-in-Noise PSTHs. PSTHs for example neurons from a Control (A) and a Lesioned (B) animal, in response to gap-in-noise stimuli. Axes indicate neural response (spikes count per bin) vs. time following stimulus onset (milliseconds). Black traces indicate spike count across sweeps,

organised by gap length, and smoothed with a moving 5-bin average. Grey background indicates the presence of noise, with white gaps indicating silent gaps-in-noise.

To determine which components of the PSTH were informative, we performed a mutual information (MI) analysis of unit spiking responses. Using this approach demonstrated that the most informative epochs within the PSTH occurred after the end of each silent gap (Fig.4-21). Elevations, albeit small, in MI were sustained over the course of the noise bursts, and after their offset. On these grounds, we therefore sought to employ an analysis of spiking responses over the course of the stimulus presentation, rather than for ad-hoc epochs.

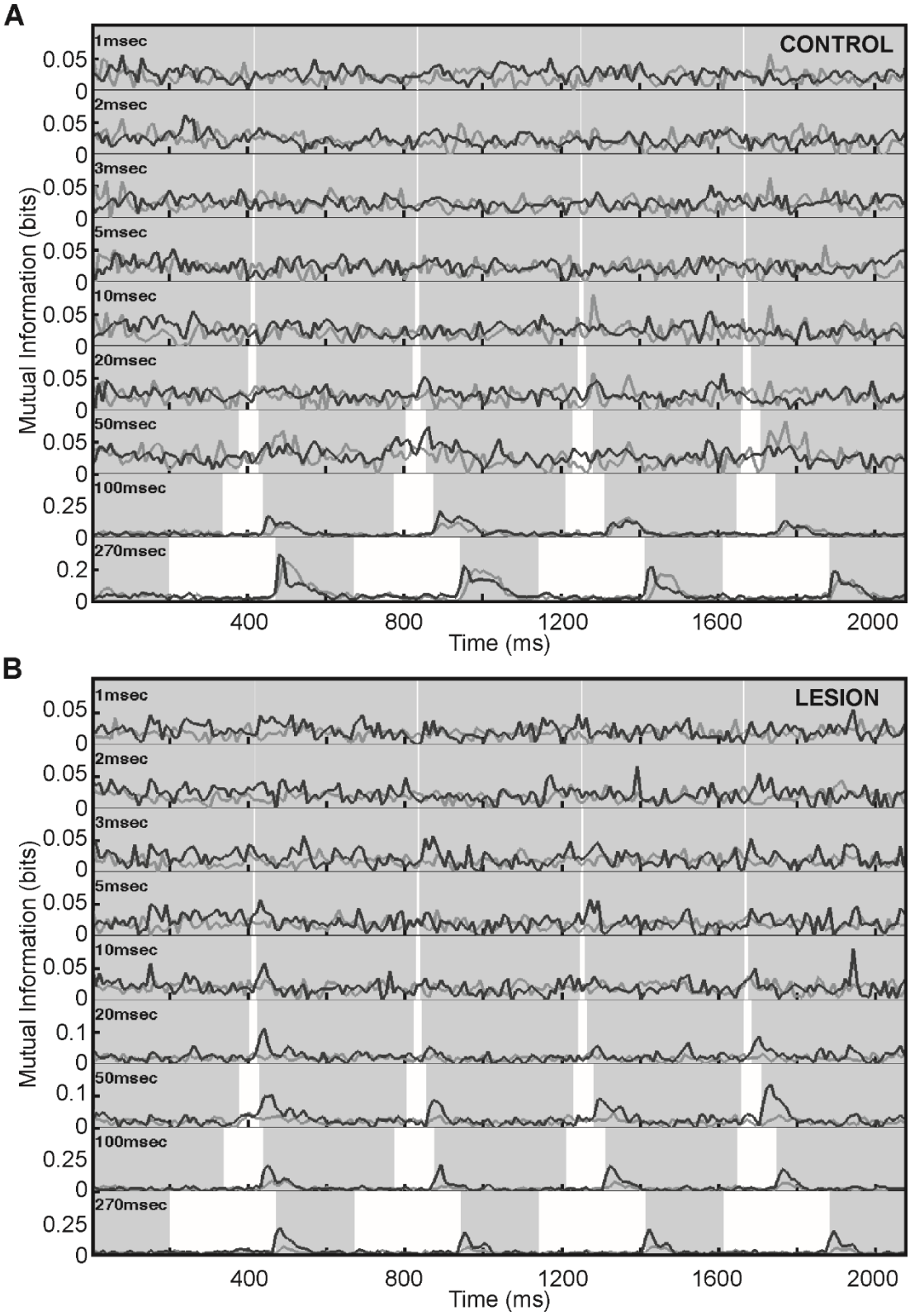

Figure 4-21: Gap-in-Noise Mutual Information (MI) traces. Pooled MI traces for responsive neurons from a Control (A) and a Lesioned (B) animal, in response to gap-in-noise stimuli. Binned MI traces calculated using a 20 ms sliding window (see Chapter 2). Axes indicate gap-in-noise MI (bits) vs.

time following sound onset (milliseconds). Line traces indicate average MI across sweeps, organised by gap length; dark grey = right AC, light grey = left AC. Grey background indicates the presence of noise, with white gaps indicating silent gaps-in-noise.

We decided to leverage a Signal Detection Theory (SDT)-based calculation of neurometric gap-detection capabilities (Petkov et al., 2007; Recanzone et al., 2011; Bizley et al., 2013), akin to that used for our behavioural analysis (Fig 2-9). Irrespective of cohort (Control, Lesioned, Impaired or Not-Impaired), neurometric data were similar, with no units approaching behavioural detection thresholds (Fig.4-22). Where supra-threshold neurometric performance was observed (*auROC* >*0.6915*; see Chapter 2), this was usually in the context of significant *auROC* values for gap lengths >10-20 ms, peaking at *auROC* >*0.9*. Counterintuitively, the best detection sensitivity (*auROC* = *0.6915* at gap length = 21.05 ms) was seen in response to BBN in a Lesioned ferret with substantial behavioural impairment (F1227) (Fig.4-22). The next-closest performance was observed in a Control ferret at a gap length ~15 ms longer. Hemispheric differences in neurometric gap-detection did not clearly emerge within animals. Our data therefore do not support the emergence of central gap-detection deficits following SG lesion, despite the otherwise restructured cortical physiology discussed above.

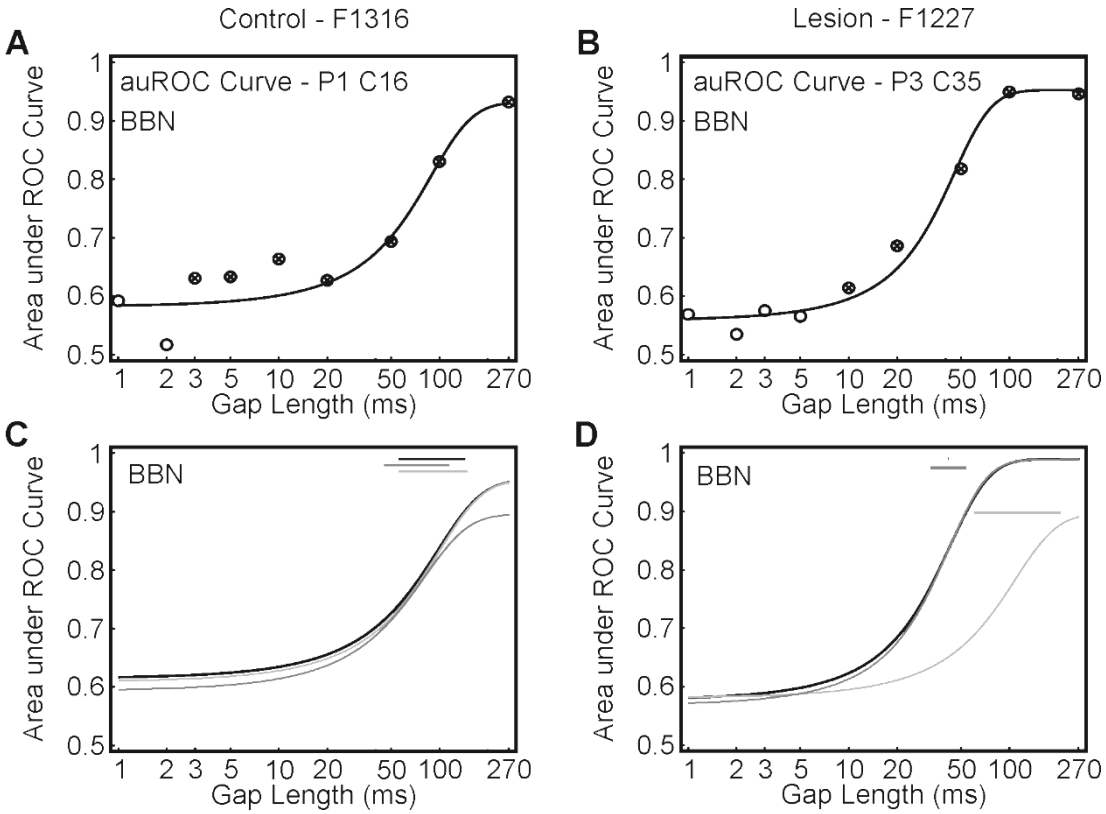

Figure 4-22: Gap-in-Noise Receiver Operating Characteristic (ROC) Analysis. Example ROC analyses for neurons from a Control animal (A, C) and a Lesioned animal (B, D). Axes indicate area under the ROC curve (*auROC*) vs. gap-in-noise length (milliseconds). A, B) Example *auROC* neurometric functions for two neurons in response to BBN. *auROC* values at each gap length are indicated by open circles, with significant *auROC* values indicated by filled circles. Curves were fitted using psignifit (see text). C, D) Population neurometric gap-in-noise curves for these animals. Black = entire recorded unit population, pooled across ACs; dark grey = right AC population; light grey = left AC. Horizontal bars indicate 95% CIs on fits at threshold (*auROC = 69.15*).

4.2.4 Anatomical Changes in the Deafferented Central Auditory System

Spiral Ganglion Cell Density Counts

To quantify the effect of the SG lesion on the density of SG cells (SGCs), toluidine blue-based staining of cochlear sections from lesioned animals (n = 6) was conducted. In each animal, stereological counts of SGC density were made of the lesioned (right) and control (left) cochleae.

As illustrated by the sections in Fig.4-23 (A, B), both obtained from the same animal (F1036), the SG lesion produced a substantial reduction in the density of SGC body staining. SGC soma counts were obtained from multiple sections obtained from the basal coils of each animal's cochleae. Cohort statistical analysis revealed a significant reduction in SGC density in lesioned ears compared with control ears (median SGC density (cells/mm^2: Left = 2051; Right = 1492. lme: $F_{(1, 48)} = 10.93$, $p = 0.021$) (Fig.4-23), accounting for random variation between ferrets (lme: $F_{(5, 48)} = 0.92$, $p = 0.53$). We found a significant interaction between the lesion-related reduction in SGC densities and the ferret identities (lesion*ferret, lme: $F_{(5, 48)} = 12.02$, $p < 0.0001$). This effect is seemingly driven by the variable decrement in SGC densities within animals (12.6 – 41.1% without ABR threshold shift; 81.1% for the one animal with threshold shift), from section-to-section. Nevertheless, all ferrets displayed clear reductions in the ipsilesional basal SGC population density.

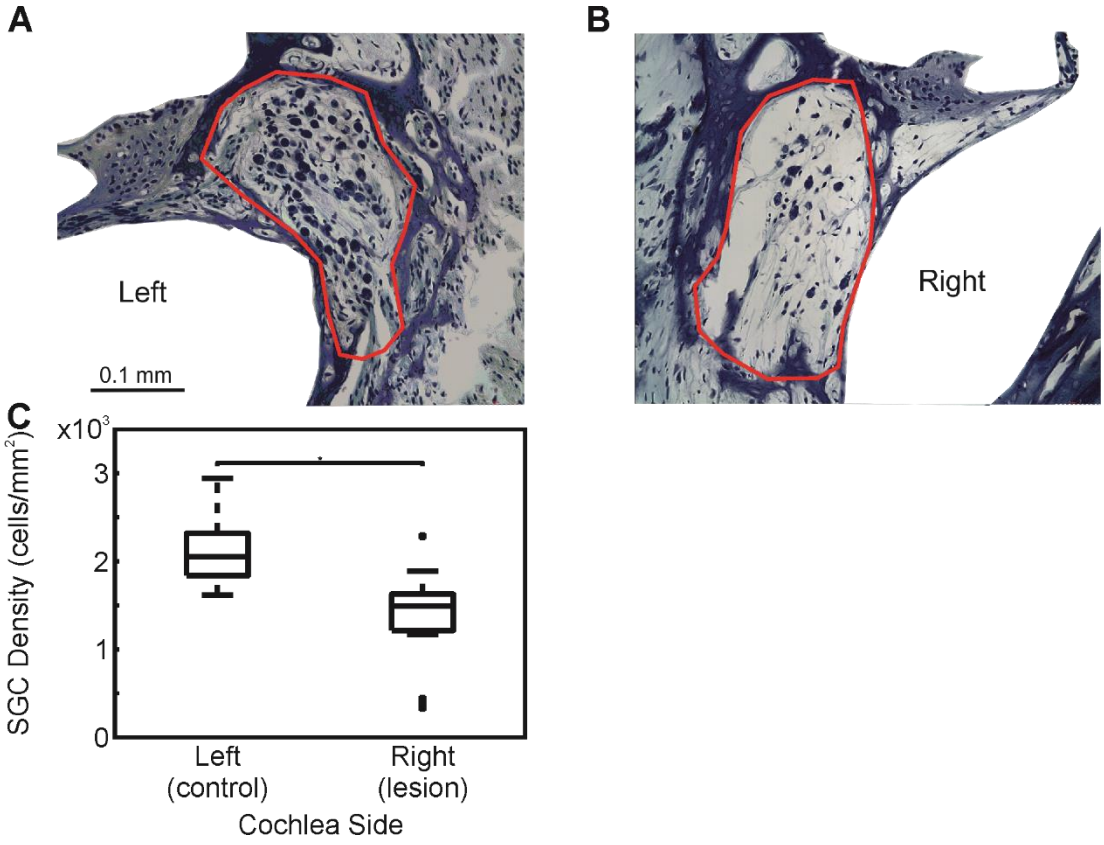

Figure 4-23: SG Histological Analysis. A, B) Toluidine blue-stained sections from the basal coils of the left (unlesioned, A) and right (lesioned, B) cochleae from the same animal (F1036). Red outline indicates region quantified. SGC somas identifiable within red outline as darkened puncta. C) SGC quantification (n = 6 animals), comparing SG cell density (cells/mm²) for left vs. right cochleae. Boxes indicate median ± interquartile range, whiskers indicate extremes, dots indicate outliers. Horizontal line indicates $p < 0.05$.

No morphological changes were found in central auditory structures after SG lesion

Brain sections from animals with SG lesion (n= 6) were examined and compared with normal controls (n=3). Using Nissl staining, no changes in appearance or neuronal morphology were found at the level of auditory brainstem (including cochlear nuclei, superior olivary complex, and lateral lemniscus nuclei), auditory midbrain (inferior colliculus (IC) and superior colliculus (SC)), auditory thalamus (medial geniculate body (MGB), all divisions) and AC in the Ectosylvian Gyrus (EG) (Fig.4-24). Even within individuals, no differences were observed between structures on the right (ipsilesional) and the left (contralesional) sides of the brain (Fig.4-24, I-L). However, no morphometric analysis was performed, due to the differences in the plane in which the sections were cut (pseudo-parasagittal or coronal plane), or differences in the procedures performed in the tissue (see chapter 2).

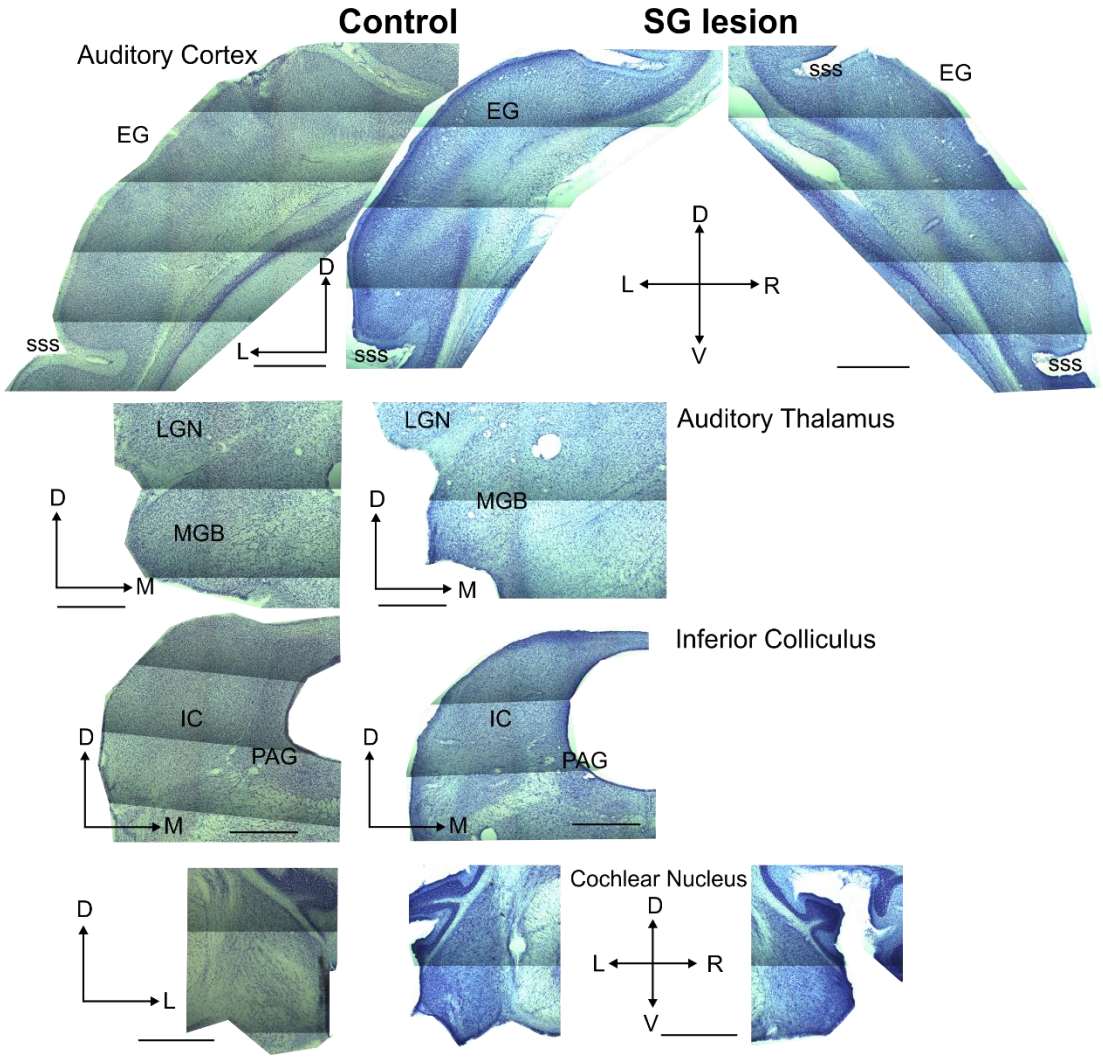

Figure 4-24: Central auditory system morphology. Unilateral, partial SG lesion in the right ear does not change the normal appearance of the central auditory system. Low-magnification Nissl-stained pictures taken from coronal sections at different levels of the auditory pathway in a control case (left) and in a SG lesion case (F1202). Right and left ACs and cochlear nuclei in the lesioned animal are shown for comparison. For remaining terms, see list of abbreviations. Scale bars = 1mm. D, dorsal; V, ventral; M, medial; L, lateral; L, R = left/right.

Nitric Oxide Synthase (NOS) activity was upregulated by the peripheral lesion

The distribution of NOS was explored using an antibody against neuronal NOS (nNOS) (see Chapter 2). While specific, the quality of staining for anti-nNOS in ferret brain tissue was poor. Thus, we employed staining with reduced nicotinamide adenine dinucleotide phosphate diaphorase (NADPHd), which represents the presence of all isoforms of NOS in general rather than nNOS only (Coote and Rees, 2008; Coomber et al., 2014, 2015; Gray et al., 2014). Using NADPHd, better staining was achieved that allowed the identification of different neuronal types and morphologies (Controls, n = 2; Lesioned, n = 5) (Fig.4-25).

We observed NADPHd staining mainly in striatum, particularly in the Islands of Calleja of ventral striatum; in hippocampus; in basal forebrain, including the nucleus basalis; in the paraventricular zone surrounding the 3rd ventricle; in subthalamic nucleus; in cortex (mainly infragranular layers); in fibres medial and ventral to MGB; dorsal to the substantia nigra; in deep layers of SC and tegmental areas in midbrain, including the ventral and lateral periventricular zone; in paralemniscal areas and within the IC, particularly its dorsal cortex and lateral nucleus (Fig.4-25, 4-26, 4-27).

NOS activity was observed to be especially strong in IC (mainly dorsomedial compartment), and infragranular layers of AC (Fig.4-26). Therefore, we sought to determine if NADPHd up- or down-regulation correlated with SG lesion, by comparing the staining between Lesion cases and Controls, and within Lesion cases, between right (ipsilesional) and left (contralesional) sides of the brain (Fig.4-26E). When we examined $NADPHd^{+}$ neurons at the level of AC, the SG lesion was

associated with a significant enhancement in NADPHd+ cell density (main effect of lesion, lme: $F_{(1, 80)} = 40.23$, $p = 0.0079$). No NADPHd hemispheric asymmetry was observed, either as a main effect, or within the interactions between ferret*side, or lesion*side, indicating not only that NADPHd staining was similar between contralesional and ipsilesional cortices (or left and right in controls), but that NOS expression is unlikely to be linked to the behavioural phenotype of lesioned animals. All animals (lesioned and control) displayed significantly greater NADPHd+ density in infragranular AC (main effect of cortical layer, lme: $F_{(1, 80)} = 77.73$, $p = 0.0031$), with a larger increase in infragranular NADPHd+ density in lesioned animals (lesion*layer interaction, lme: $F_{(1, 80)} = 29.27$, $p = 0.0124$).

NADPHd+ neurons were more abundant in infragranular, corticofugal layers (layers V and VI) of AC. The morphology of NADPHd+ stained cells ranged from medium-to-large-sized pyramidal neurons in layers III and V, typically with triangular cell bodies. In these neurons, the proximal first- and second-order dendrites were stained, whereas the apical dendrites outside the somatic layer were not (Fig.4-26). In layer VI, stained cells possessed more bipolar or stellate morphologies, with dendrites oriented parallel to the layer, occasionally extending deep in the white matter. Additionally, small interneurons of various morphologies were stained across cortical layers.

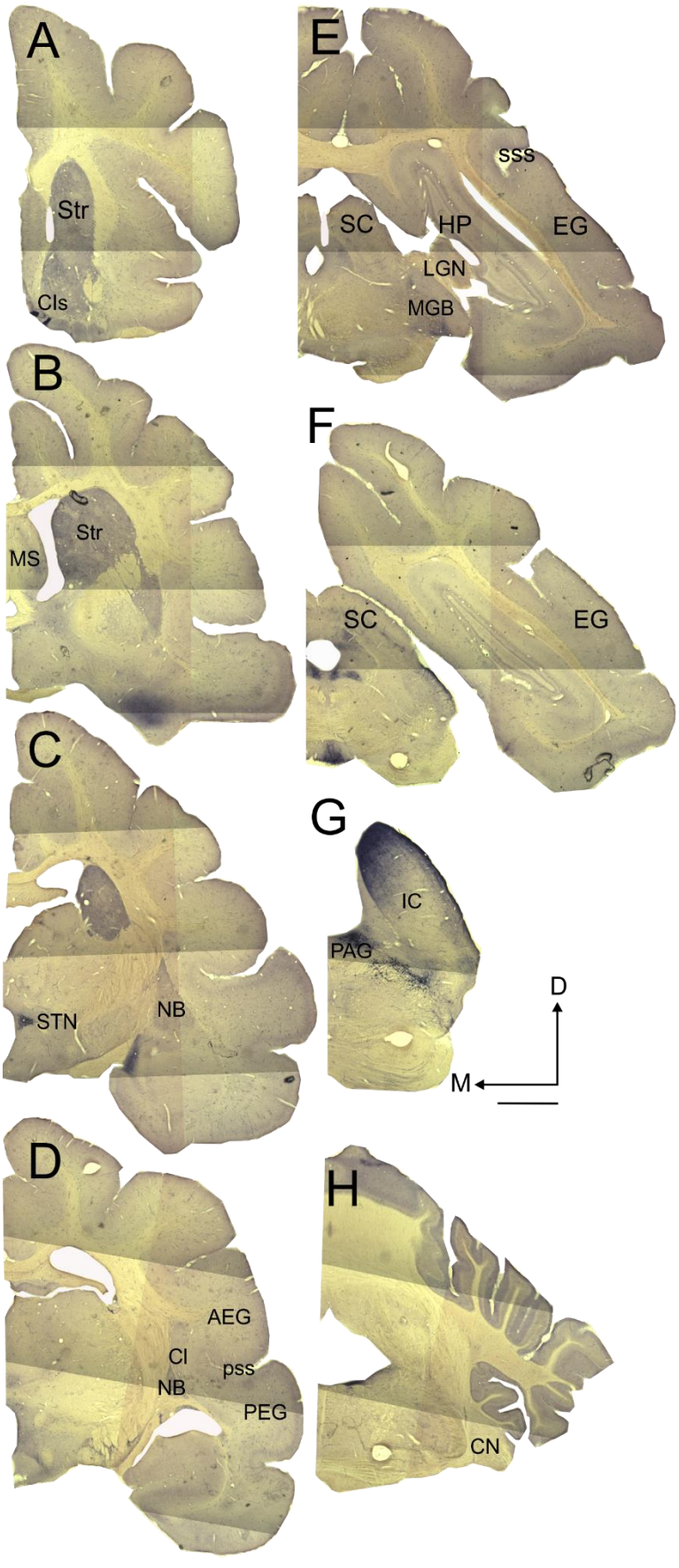
A
Str
Cls
B
MS
Str
C
STN
NB
D
AEG
Cl
pss
NB
PEG
E
sss
SC
HP
EG
LGN
MGB
F
SC
EG
G
IC
PAG
D
M
H
CN

Figure 4-25 (previous page): NOS Activity in the SG-Lesioned Ferret Brain, Visualised by NADPHd Staining. Pictures in the coronal plane, taken from the right side showing NADPHd in: the striatum (A-C), including the Calleja islands (A), the basal forebrain (B-D), subthalamic nucleus (C), auditory thalamus (H), auditory cortex (H, F), acetyl cholinesterase$^+$ groups 5 and 6 in the tegmentum (F-G), inferior colliculus (G) and cerebellum (H). For abbrevations, see page…. Scale bar = 1mm. D, dorsal; M, medial.

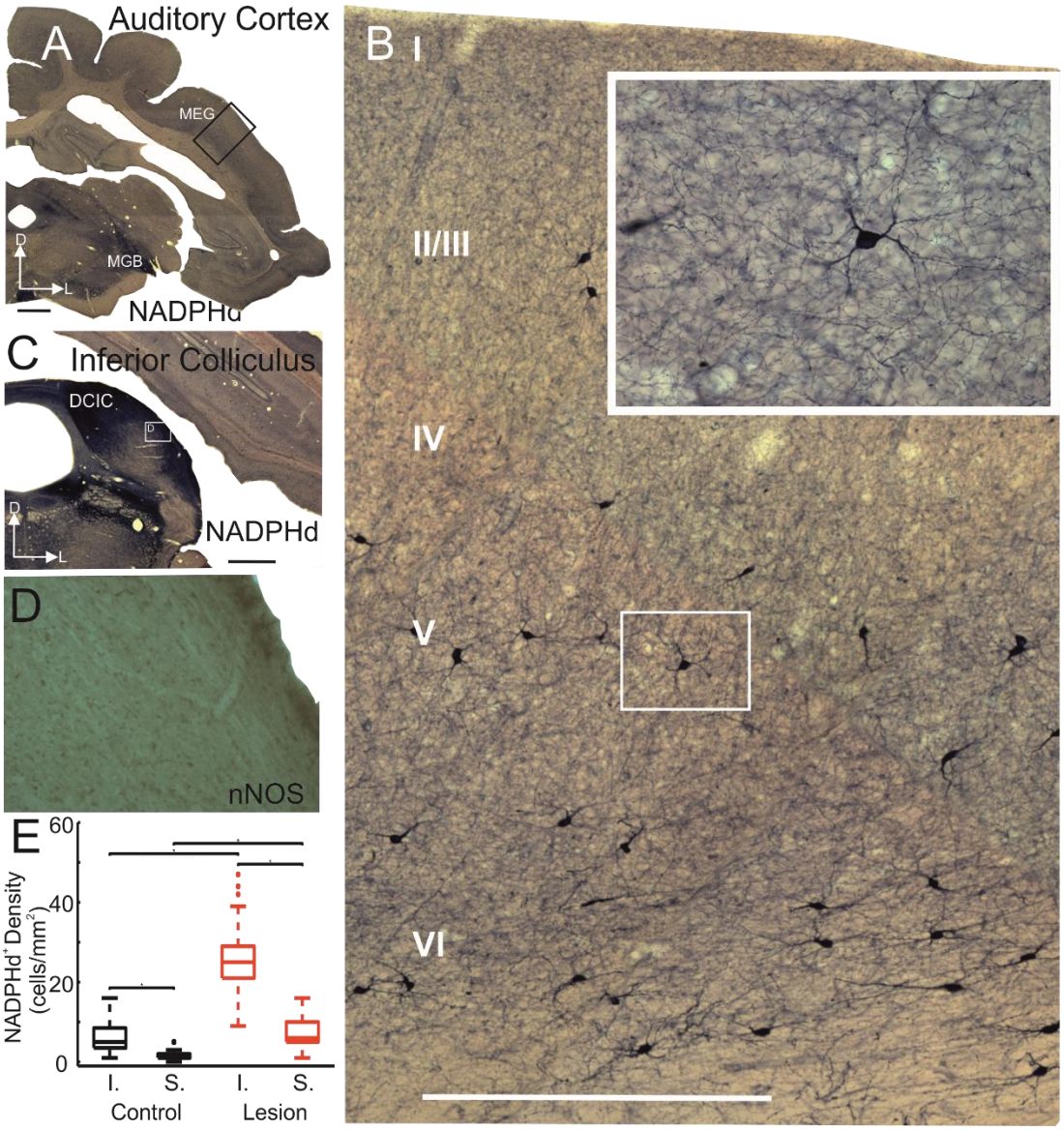

Figure 4-26: NOS Activity in SG-Lesioned Ferret AC (A, B) and IC (C, D) Observed by NADPHd Staining (A-C) and nNOS Immunoreaction (D) (case F1201). A) Cellular labelling was found in infragranular AC (B, marked by box in A and detail at higher magnification showing staining in different cortical layers). C) Dense labelling is present in the IC. D) nNOS activity is also visualised using a nNOS-specific antibody, but with lower resolution than NADPHd staining. E) Quantification of NADPHd⁺ labelling density (cells/mm²) in AC of control (n = 2, black) and lesioned (n = 5, red) animals, subdivided into infragranular (I) and supragranular (S) layers of cortex. Boxes indicate median ± interquartile range, whiskers indicate extremes, dots indicate outliers. Bars indicate significant between-group differences, for *post hoc* $a = 0.05$. D, dorsal; L, lateral; I to VI, cortical layers; calibration bars are 1 mm in (B) and 0.5 mm in (A, C), and 0.1 mm in (D).

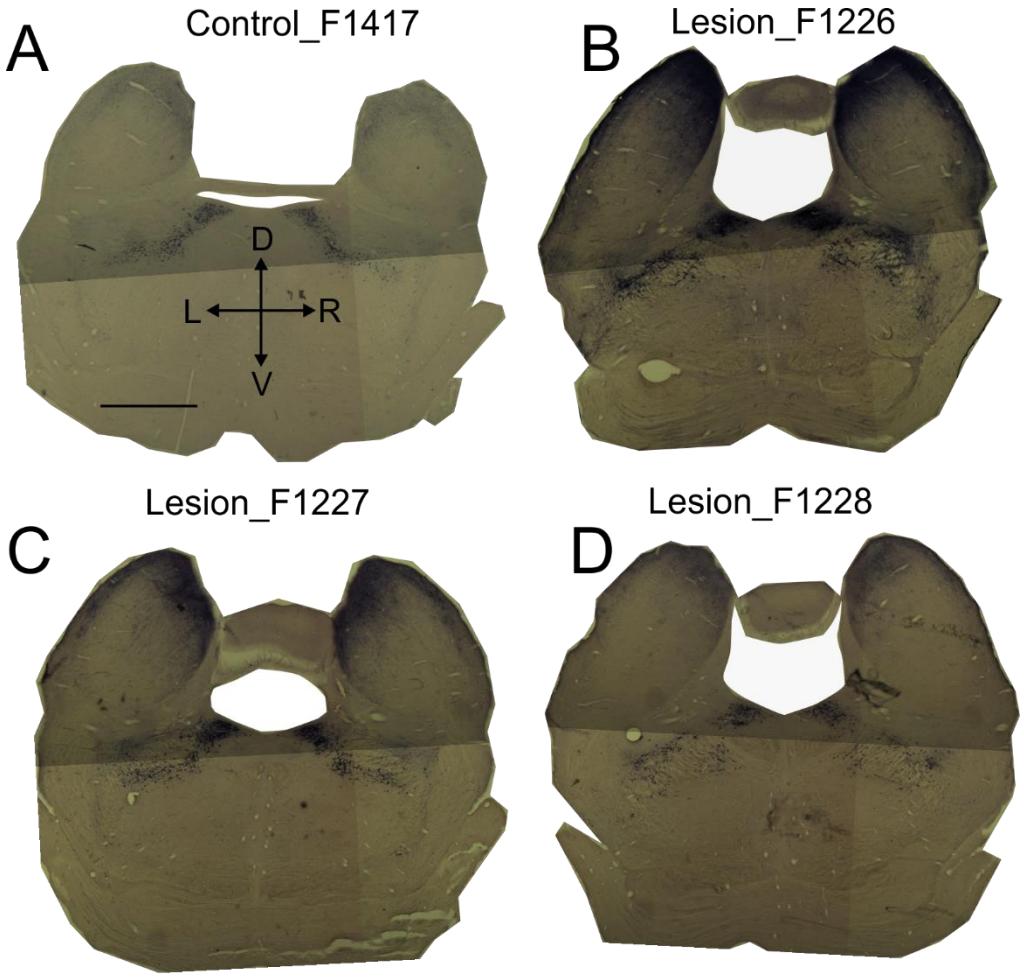

Figure 4-27: NADPHd Activity in IC. Pictures taken at the level of the IC in a control case (F1417) and three SG lesion animals (F1226, F1227 & F1228). Scale bar = 1mm. D, dorsal; V, ventral; L, left; R, right.

Changes in Arg3.1/Arc expression reveal cortical plasticity

Arg3.1/Arc is an immediate-early gene related to homeostatic cortical synaptic plasticity (Shepherd et al., 2006; Bramham et al., 2010; Gao et al., 2010; Béïque et al., 2011), whose expression in AC has been associated with hearing loss and tinnitus (Tan et al., 2007; Knipper et al., 2013; Rüttiger et al., 2013; Singer et al., 2013). We examined Arg3.1/Arc in AC using a specific antibody, to determine whether changes in Agr3.1/Arc expression were associated with SG lesion and/or behavioural changes.

Arg3.1/Arc was differentially expressed in AC of lesioned animals (Lesioned, n = 3). While no lateralisation was observed (main effect of side, lme: $F_{(1, 24)} = 7.18$, $p = 0.116$), there was a significant subject*side interaction (lme $F_{(2, 24)} = 29.33$, $p < 0.0001$). In particular, two animals (F1226, F1227) displayed significantly greater Arg3.1/Arc density in the contralesional (left) AC ($p < 0.01$, significant after Bonferroni correction) (Fig.4-29). Arg3.1/Arc$^+$-labelled cells were always pyramidal neurons from layers III and V that were typically localised in clusters of high immunoreactivity (Fig 4-29). Contrary to the more diffuse pattern of NADPHd$^+$ staining, Arg3.1/Arc$^+$-labelled cells were stained only in the soma and initial apical dendrite; no other cell morphology or type was positively labelled.

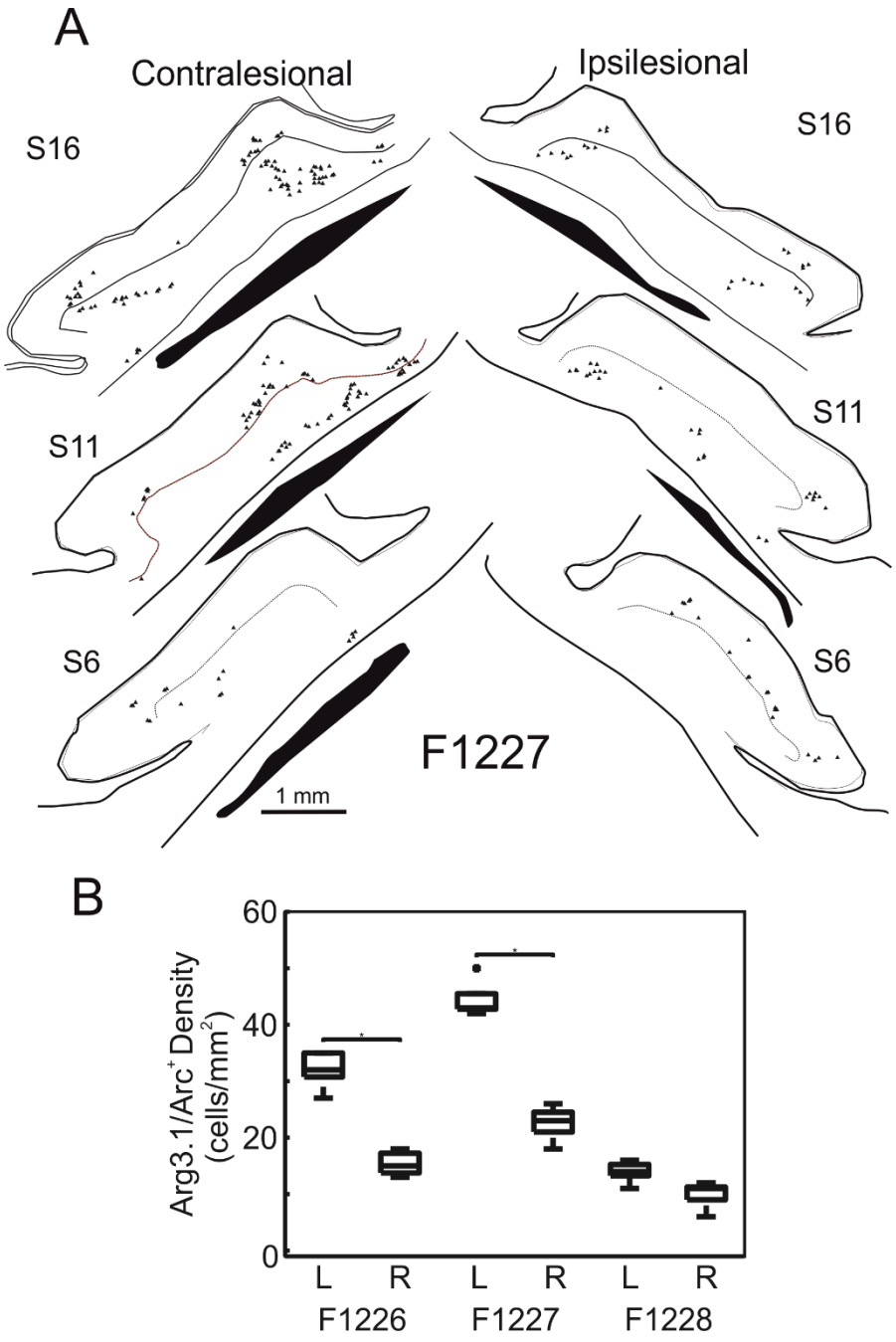

Figure 4-28: Arg3.1/Arc in AC of Lesioned Ferrets. A) Distribution of Arg3.1/Arc in AC of ferret F1227. Sections arranged rostral to caudal. B) Quantification of Arg3.1/Arc⁺ labelling density (cells/mm²) in AC of lesioned animals (F1226, F1227, F1228), comparing between left (L) and right (R) AC of each animal. Boxes indicate median ± interquartile range, whiskers indicate extremes, dots indicate outliers. Horizontal bars indicate significant between-group comparison, for *post-hoc* $a = 0.05$.

4.3 Discussion

In this chapter, we have attempted to understand how unilateral, partial hearing loss manifests throughout the ferret auditory system, and how these changes might relate to auditory perception. By measuring changes in gap-in-noise detection behaviour, we found that a selective SG lesion produced heterogeneous effects in behaviourally-expressed auditory temporal processing. These behavioural changes – both impairments and improvements – occurred following SG lesion in different animals, suggesting that temporal processing was affected. Concurrently, by recording ABRs at two time periods following deafferentation, long-lasting changes in auditory physiology were found, beginning at the auditory nerve, and manifesting throughout auditory brainstem structures. Multiunit recordings obtained from lesioned ferrets also established the presence of long-lasting changes to auditory function within AC, affecting the basal activity of cortical circuits, though without substantially affecting the tonotopic representation of sound frequency, or the neural encoding of gap-in-noise sounds. Histological analysis confirmed that the SG lesion induced a significant reduction in SGC density of the right ear, compared with control sections obtained from each animal's left cochlea. Additionally, neurochemical changes in NADPHd and Arg3.1/Arc expression in AC were associated with hearing loss and behavioural changes, respectively. These data together indicate that the types of changes that emerge following auditory deafferentation are complex and nuanced, differentially affecting sound perception in a manner that could be considered tinnitus-like or -related.

4.3.1 What is Indicated by Changes in Gap-in-Noise Detection Behaviour?

Although an animal's perceptual state cannot be directly probed, from our behavioural results it is possible that our impaired animals experienced something that could be described as "tinnitus-like". At the time of our study's inception, gap-detection paradigms had gained traction for tinnitus screening in animal models, mainly in rodents and other small mammals (e.g. Heffner and Harrington, 2002; Turner et al., 2006, 2012; Dehmel et al., 2012; Berger et al., 2013). In contrast, there existed no objective measures of tinnitus in human patients, with studies exclusively relying upon self-reporting rather than objective psychometric evaluation. Recently, however, this has been challenged, with reports emerging that evaluated gap-in-noise detection, and other measures of auditory perception, in human tinnitus patients. Although some data have indicated the absence of specific gap-detection impairments in humans (Campolo et al., 2013; An et al., 2014), other studies have confirmed that gap-detection measures can reveal temporal processing changes, if frequency-nonspecific (Fournier and Hébert, 2013; Mehdizade Gilani et al., 2013), alongside other auditory temporal processing deficits that have been identified (Moon et al., 2015). Thus, temporal detection impairments in our own subjects could indicate development of tinnitus-like percepts, akin to non-specific defects observed in humans.

That performance impairments developed in many subjects as a result of the peripheral deafferentation accords with previously-described animal models of acoustic trauma-induced hearing loss (Giraudi-Perry et al., 1982; Salvi and Arehole, 1985; Rybalko and Syka, 2005). From these studies, the magnitude of gap-detection threshold impairments was predominantly correlated with signal detectability,

measured as audiometric threshold elevations. Although partial section of the auditory nerve does not induce shifts in audiometric functions (Neff, 1947; Schuknecht and Woellner, 1953, 1955), damage to the outer hair cell (OHC) population does (Ryan and Dallos, 1975; Hawkins et al., 1976; Ryan et al., 1979; Lobarinas et al., 2013). Extended monitoring of noise-exposed animals has revealed physiological threshold recovery, even after extensive cochlear damage due to earlier exposure to traumatic noise (Kujawa and Liberman, 2006, 2009; Lin et al., 2011), with similar findings in audiometrically normal, aged humans (Viana et al., 2015). While the performance impairments displayed in our ferrets may represent an exclusively peripheral threshold elevation, the fact that we saw heterogeneous effects of SG lesion, rather than homogeneous behavioural impairment, speaks for an underlying central modulation, rather than simply audiological detection issues. Moreover, hearing threshold shifts are unlikely to explain the behavioural changes we have observed, since comparison of ABRs pre- and post-lesion largely revealed no threshold elevations in post-lesion data (although one animal, F1318, did show substantial ipsilesional ABR threshold elevations, it was behaviourally improved, rather than impaired).

Since our experimental model involved a targeted reduction in SGC density (Fig 4-24), our findings may be comparable to the effects of presbyacusis, rather than traumatic hearing loss. Aged humans display temporal processing deficits that manifest as gap-detection impairments (He et al., 1999; Schneider and Hamstra, 1999; Snell and Hu, 1999; Harris et al., 2010), as do aged animals (Suta et al., 2011; Llano et al., 2012). Presbyacusis affects the cochlea in a stereotyped, multifactorial manner (Schuknecht, 1964; Schuknecht and Gacek, 1993; Ohlemiller, 2004), with one

form – neural presbyacusis – producing atrophy and/or apoptosis of the afferent SG cell fibres. Although neural presbyacusis is often accompanied by sensory or metabolic deficits, largely affecting the OHCs and stria vascularis, respectively, these pathologies may occur in isolation, whereas SG damage is the most common symptom seen in presbyacusis. Presbyacusis is a comorbidity of tinnitus (Langguth et al., 2013), yet little work has been done to establish the relationship between cochlear pathology over time and the patient's perceptual or behavioural status. Therefore, where impairments were seen in our behavioural model, they may approximate the kinds of temporal processing changes that might be instantiated in tinnitus, with or without presbyacusis.

Despite the intended uniformity of the deafferentation, the temporal processing effects we described were heterogeneous. The lesion itself produced a somewhat consistent reduction in SGC density, ranging from 12 – 41% in the basal coil of the right cochlea, and this modest variation was not obviously correlated with the degree/direction of behavioural changes. Theoretically, the specific site of hearing loss might have differed enough between subjects to affect which hearing frequencies were ultimately impaired. Alternatively, the diverse arrangement of fibres within SG may mean that disparate effects on auditory processing were almost unavoidable when inducing a nonspecific mechanical lesion of the kind described here. In this context, it is noteworthy that off-channel gap-detection deficits in regions of normal pure tone thresholds have previously been observed in human hearing loss patients (Leigh-Paffenroth and Elangovan, 2011), as well as physiologically in animals (Yin et al., 2008).

It also appears that some undefined post-deafferentation adaptive mechanism may be at play among some ferrets, given that at least three animals in this study presented *improvements* in performance following the SG lesion. Although a parsimonious explanation may suggest a regression to the mean, there was no correlation between performance before and after the lesion across animals, implying that animals were not simply improving where they had been undertrained, or diminishing where they had previously been exceptional. Instead, some kind of training-related perceptual enhancement may have emerged in some subjects, as described in aged rats trained on an operant auditory temporal processing task (de Villers-Sidani et al., 2010), and possibly manifesting as adaptive remapping of cortical auditory regions in response to changes in auditory inputs (Fritz et al., 2003; Reed et al., 2011; Ahlf et al., 2012; Kilgard, 2012). Therefore, we examined what underlying physiological changes might explain these behavioural shifts, particularly in those cases where adaptive improvements in performance were found.

4.3.2 Behavioural Correlates in the Ferret ABRs

We reanalysed our behavioural and ABR results together by constructing analyses of covariance (ANCOVAs), examining the main effect of measurement period for click-ABRs at 90 dB SPL (at which all animals yielded supra-threshold responses), and stacked-ABRs. The I-Index was included as a covariate, with interaction terms examined for changes in the relationship between the lesion status and the I-Index.

Inclusion of the I-Index into the stacked-ABR statistical model did not reveal any systematic relationship between the stacked-ABR Wave IV amplitude and each

animal's behavioural impairment, for either ear. More interestingly, upon taking a similar approach with click-ABR latency data, the I-Index explained a significant proportion of the variance of the click-ABR latencies across all waves (Fig.4-30). There was no significant interaction between the lesion status and I-Index, for any click-ABR wave: that is, the correlation between latency and I-Index seen in the post-lesion periods was also observed in the pre-lesion click-ABR data, even for Wave I of the ABR. The correlation between I-Index and ABR Wave I latency was significant in the pre-lesion (Spearman's $\rho = 0.714$, $p < 0.001$) and chronic (Spearman's $\rho = 0.376$, $p = 0.017$) periods, indicating that longer latencies at Wave I were associated with post-lesion behavioural improvement, and shorter latencies with post-lesion behavioural impairment (Fig.4-30). This effect was also found in the left ear (pre-lesion: Spearman's $\rho = 0.765$, $p < 0.001$; chronic: Spearman's $\rho = 0.563$, $p = 0.001$).

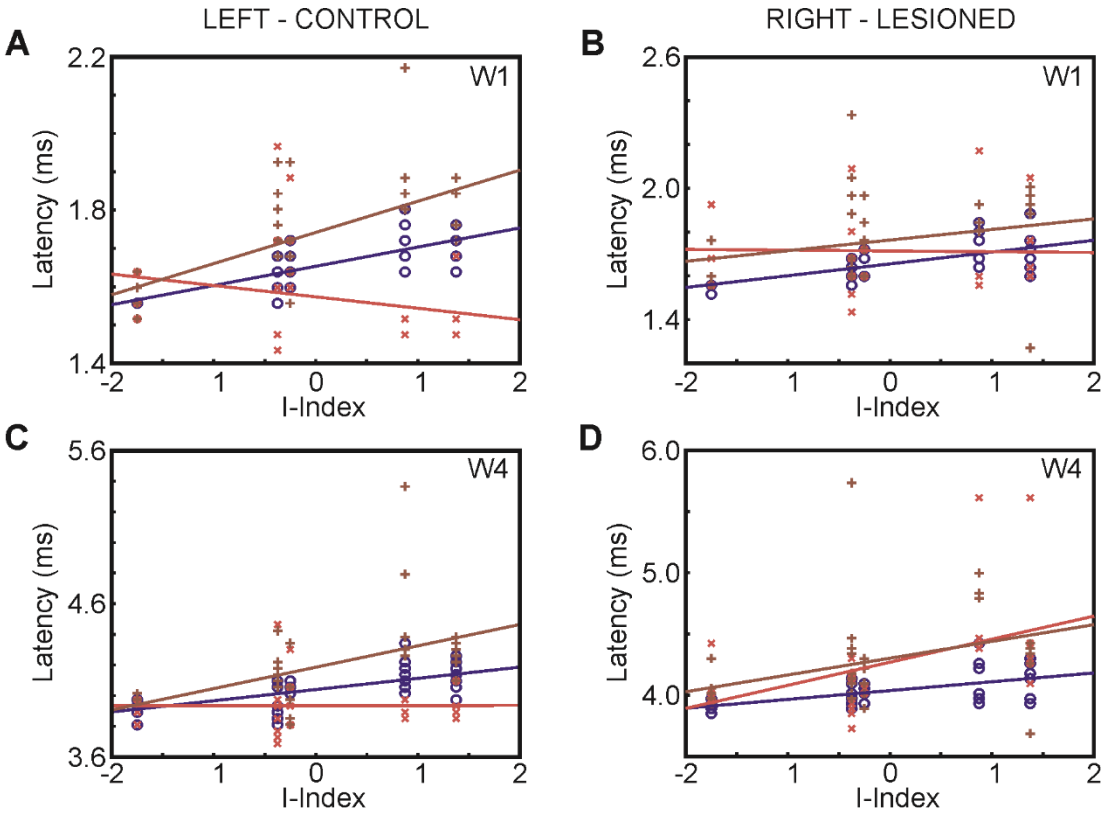

Figure 4-29: Correlation Analysis between Click-ABR Latencies and Behavioural I-Index. Pre-lesion = blue (circles); acute period = red (crosses); chronic period = brown (pluses). Left column = left (control) ear; right column = right (lesioned) ear. Axes indicate latency of click-ABRs at 90 dB SPL (milliseconds) vs. behavioural I-Index. Lines are linear best fits through data. A, B) Wave I. C, D) Wave IV.

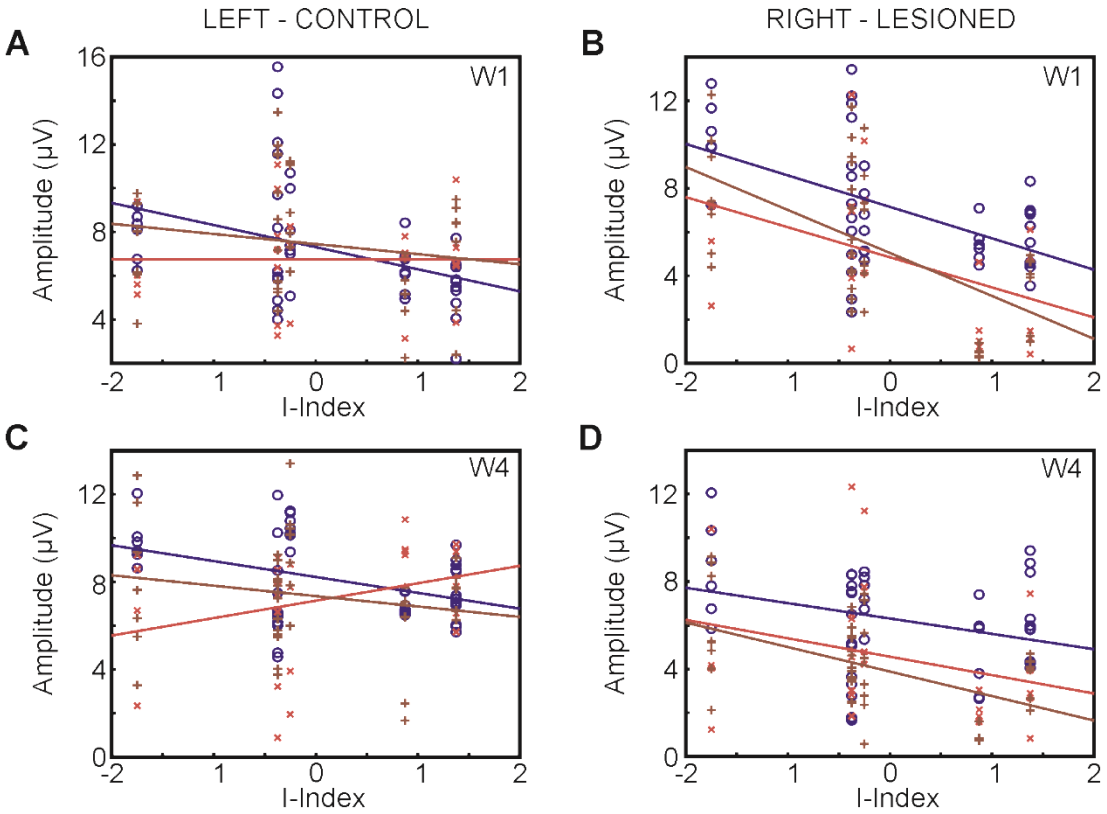

Figure 4-30: Correlation Analysis Between Click-ABR Amplitudes and Behavioural I-Index. Pre-lesion = blue (circles); acute period = red (crosses); chronic period = brown (pluses). Left column = left (control) ear; right column = right (lesioned) ear. Axes indicate amplitude of click-ABRs at 90 dB SPL (µV) vs. behavioural I-Index. Lines are linear best fits through data. A, B) Wave I. C, D) Wave IV.

Regarding click-ABR amplitudes, again the I-Index main effect was significant (ANCOVA: $F_{(1, 101)} = 41.46$; $p < 0.001$), without a lesion*I-Index interaction (Fig.4-31). There was a significant *inverse* correlation between lesioned ear Wave I amplitude and I-Index across animals, both pre- and post-lesion (Pre-lesion: Spearman's $\rho = -0.498$, $p = 0.001$; Acute: Spearman's $\rho = -0.431$, $p = 0.036$; Chronic: Spearman's $\rho = -0.577$, $p < 0.001$), and for contralesional Wave I amplitudes (Fig.4-31) (Pre-lesion: *Spearman's* $\rho = -0.449$, $p = 0.002$). By contrast, contralesional Wave II chronic period amplitudes were significantly correlated with the I-Index across animals, possibly indicative of a selective degradation process affecting the VCN. However, these predictive effects were not inherited at higher centres, with Waves III/IV displaying no significant relationship with behaviour.

In summary, not only do our ABR measurements concur with previous reports of tinnitus-like physiology in animals, but the pre-lesion click-ABR correlations with behavioural changes suggest that some underlying differences between ferrets may predispose them to differentially adapting/maladapting to peripheral trauma. This hypothesis is not to suggest that neuroplastic remodelling of brainstem circuitry does not occur: amplitude shifts indicated a reactive disinhibition within the VCN, the site of Wave II generation (Melcher et al., 1996), according with observations from human tinnitus patients (Gu et al., 2012). These changes were absent from Wave IV chronically, implying that plastic renormalisation of signal amplitude may occur in the auditory midbrain in the context of peripheral deafferentation. This development was missing in lower auditory centres involved in ABR generation, and is akin to the selective Wave V adaptation described by Schaette and McAlpine (2011). Since significant correlations

emerged between cochlear function (from ABR Wave I) and behaviourally-evident auditory temporal processing, certain animals (and perhaps, therefore, certain people) may react differentially to a similar peripheral insult, suggestive of an endogenous predisposition to insult-induced tinnitus.

Herein, the manner in which our behavioural data were systematically related to the ABR recordings may be informative. On the normal ABR, louder sounds evoke shorter latency and larger amplitude responses. Therefore, it appears that within an apparently homogeneous cohort of ferrets, those animals that displayed behavioural impairments were encoding sounds, *at the level of the cochlea*, as if they were louder, compared with unimpaired animals. The origin of these low-level physiological differences is unclear, even with previous work examining the ABR correlates of tinnitus-like symptoms.

A handful of animal studies have described a relationship between late-wave ABR features and noise-exposed animals' behavioural changes (Ahlf et al., 2012; Dehmel et al., 2012; Coomber et al., 2014). Only Ahlf and colleagues found pre-trauma ABRs to be predictive of later-developing tinnitus-like behaviours. The changes they described were, however, opposite to what we observed, with unaffected animals in their study displaying *higher* basal ABR RMS amplitudes, compared with tinnitus-like animals. Importantly, that study examined the effects of noise trauma (an OHC-damaging insult) on reflex-based gap-detection, which may be mediated entirely through midbrain circuitry (Yeomans and Frankland, 1995; Eggermont, 2013), and so is dissimilar to our operant paradigm. In other studies, ABR latency shifts were deemed to be markers of tinnitus-related brainstem activity

(Dehmel et al., 2012; Coomber et al., 2014). Although we observed latency effects, changes also occurred in contralesional ABRs across all frequencies, with significant latency reductions acutely, and increases chronically. These effects manifested from Wave I, and persisted to Wave IV across all NB-ABRs. Although IT4 increases were correlated with shifts in ipsilesional latencies, emerging as significant in the acute and chronic periods for 4, 8 and 16 kHz, the generalised and systematic shifts in contralesional ABR latencies – unrelated to the lesion or stimulus type – are a cause for concern in the future interpretation of ABR latencies.

There remains the indication of excitatory/inhibitory dysregulation, which may be differentially expressed in "tinnitus" animals, representing a point of future exploration. Post-traumatic disturbances to brainstem inhibitory function have been well-described following hearing loss (for reviews, see Caspary et al., 2008; Ouda and Syka, 2012; Gold and Bajo, 2014). Such inhibitory changes might impact cochlear function directly through disruption of the efferent olivocochlear system, which is impaired following peripheral trauma (Bledsoe et al., 2009). Indeed, following the development of hearing loss-induced abnormal activity in the IC (Mulders and Robertson, 2009, 2011), targeted electrical and chemical stimulations of the olivocochlear bundle produced a reduction in midbrain hyperactivity, a potential correlate of tinnitus-like perceptual changes (Mulders et al., 2010). Therefore, functional differences in the olivocochlear system, via the efferent olivocochlear bundle, may at baseline manifest as differences in cochlear activity, in turn being expressed in the ABR, and putatively in temporal processing-dependent behavioural changes.

An alternative hypothesis concerns the nature of sound encoding within the SG itself, and how this may be affected following partial deafferentation. In mammals, auditory nerve fibre (ANF) SFRs display a well-conserved bimodal distribution, with units showing low (< ~20 spikes/second) or high (> ~20 spikes/second) SFRs, and high or low response thresholds, respectively (Kiang et al., 1975; Evans and Palmer, 1980; Tsuji and Liberman, 1997; Taberner and Liberman, 2005; Sumner and Palmer, 2012). Notable in the ferret is the lower incidence of low-SFR fibres, compared with other species (Sumner and Palmer, 2012). While possibly idiosyncratic to ferrets, there may also be inter-individual variability, such that some animals possess a greater proportion of high-SFR units at baseline. In such animals, sounds substantially above threshold would produce a relatively larger synchronised afferent discharge (owing to a larger high-threshold ANF population), manifesting as elevated amplitudes and reduced latencies of ABRs from both ears: this diverse pattern is exactly what we observed in our unlesioned ferrets.

A problem with this hypothesis is the effect of trauma itself: whereas we did not see any breakdown in the ABR/I-Index correlation post-lesion, low-SFR ANFs are described as more susceptible to trauma (Schmiedt et al., 1996; Ohlemiller, 2004; Furman et al., 2013). Were this the case following the SG lesion described here, this susceptibility may have mediated a more selective, long-term degradation of low-SFR ANFs. This appears not to have occurred, since the net amplitude of Wave I, and its RMS, were not changed between the acute and chronic epochs (Figs.4-12, 4-13). Nevertheless, there exist morphological and structural differences between low-SFR vs. high-SFR fibres, at least in the cat and guinea-pig (Liberman, 1982, 1991,

1993; Tsuji and Liberman, 1997). Thus, the relative fibre-type distribution in the ferret could, theoretically, be described anatomically on the basis of fibre termination locus and morphological features, providing a way to evaluate our intriguing hypothesis.

4.3.3 Neurophysiological Markers of Lesion-Related Central Mal/Adaptation

Given our ABR data, and their relationship to the heterogeneous behavioural results reported, the question remains as to whether these effects manifest in AC. Our results, though atypical, agree with signs associated with hearing loss-related plasticity and tinnitus-like behaviour. Canonically, large hearing losses induce (tonotopic) map reorganisation (Robertson and Irvine, 1989; Calford et al., 1993; Rajan et al., 1993), elevations in spontaneous spiking activity (Noreña and Eggermont, 2003; Seki and Eggermont, 2003; Hughes et al., 2010; Juarez-Salinas et al., 2010), increases in the synchrony of neural spike discharge, both spontaneously and in response to sound stimulation (Noreña and Eggermont, 2003, 2006; Engineer et al., 2011), and other indicators of abnormal hyperactivity, such as modifications to cortical inhibition or rate-level functions (Rajan, 2001; Noreña et al., 2003; Engineer et al., 2011).

We found no substantial tonotopic reorganisation: remarkably few effects were observed, despite considerable precedent for modified frequency representations in IC following a similar experimental deafferentation (Snyder et al., 2000, 2008; Snyder and Sinex, 2002), which might have been expected to be inherited by AC tonotopy. A parsimonious explanation for this relates to incomplete mapping of the cortical surface during our recordings. Although our approach was highly dependent on local cerebral vasculature, we endeavoured to sample widely across

the cortical surface in each experiment, in order to minimise this sort of location bias. Despite the emergence of greater proportional tonotopic representation among units recorded from Lesioned animals, compared with Controls, we did not find the more typical overrepresentation of *specific* sound frequencies. Rather, these effects may be derived from differences in tuning widths, with changes in the Q10 profile of lesioned units possibly affecting the proportion of frequency space represented by each cell. However, no such changes were seen for Q30, suggesting that supra-threshold tuning was largely unaffected.

Importantly, a number of previous studies have demonstrated the non-canonical nature of this "typical" post-deafferentation remapping. Over time courses ranging from weeks-to-months, recordings from A1 have indicated that tonotopy may either return to its previous pattern of frequency representation, over a similar time course as ABR threshold normalisation (Ahlf et al., 2012), or for the contralesional cortex to fall into register with the unaffected ipsilesional map, leading to apparently normal tonotopy (Cheung et al., 2009). This tonotopy adaptation may even occur within a few hours: while monitoring BF response thresholds in the contralesional AC of a unilaterally-cochleotomised ferret, a gradual decline in response thresholds to acoustic stimulation of the unlesioned ear was described, suggesting an adaptive reweighting to favour conserved inputs (Moore et al., 1997). Therefore, some form of long-term adaptation may well have emerged, since we recorded from AC in animals >12 months post-lesion. Since changes to cortical mapping do not impair performance on appropriately-designed behavioural tasks (Yang et al., 2009; Takahashi et al., 2011; Kilgard, 2012), the interpretation of our results is unclear. Certainly the relationship between tinnitus

and tonotopic remapping remains controversial (Mühlnickel et al., 1998; Langers et al., 2012), suggesting that it is not necessarily a useful indicator of tinnitus-like perceptual changes.

We found that SG lesion substantially affects the activity of AC neurons, both in terms of their sound-evoked responses (Fig 4-17) and SFRs (Fig 4-18). There is little precedent for this latter effect, with the literature typically describing SFR hyper-, rather than hypo-, activity (see Chapter 1). However, when studies did report SFRs, each utilised either acoustic trauma, or ototoxic drug administration, which both damage cochlear hair cells directly, with only secondary effects at the SG. Hair cell ribbon synapses can induce excitotoxicity following over-activation (Puel et al., 1998), suggesting that post-traumatic hyperactivity could be initially derived from the cochlea (Mulders and Robertson, 2009), and only later becomes centralised in brainstem and midbrain structures (Mulders and Robertson, 2011; Vogler et al., 2011). Data on SFRs are scarce in lesion-type studies: one study in ferrets described hyperactivity in the ipsilateral IC >3 months after cochlear removal, thought to be due to diminished inhibitory drive from the lesioned ear, although SFRs in general remained low (<5 spikes/second) (McAlpine et al., 1997). It therefore seems parsimonious to conclude that damage to SGCs produces a general reduction in central SFRs through a proportional loss of feedforward basal drive (irrespective of central excitatory/inhibitory effects), particularly since mean SFRs of ferret ANFs can vary by up to 100 spikes/second (Sumner and Palmer, 2012).

Our behavioural analysis may provide a degree of clarification. Specifically, compared with units recorded from Not-Impaired animals, units recorded from behaviourally-Impaired ferrets displayed higher SFRs and diminished spontaneous neural synchrony (possibly due to the diminished SFR spike density) (Fig.4-19). Conversely, Impaired and Not-Impaired units showed enhanced tone-evoked responses compared with Controls (Fig.4-17), and significant residual hypersynchrony. Given that our estimates of driven activity are normalised by the SFR of each unit, evoked hyperactivity may be epiphenomenal, deriving from the diminished SFRs in Lesioned cases. Nevertheless, the steeper RLF slopes and evoked hypersynchrony suggest the development of a gain change (whether adaptive or maladaptive) in the representation of acoustic stimuli (akin to wave IV ABR changes discussed above), within the context of a global hypo-activity.

That no differences were seen in peak z-scores of Impaired vs Not-Impaired units, despite the latter group's lower SFRs and higher neural synchrony, may correspond to putative "tinnitus" vs. "non-tinnitus" units of noise-exposed guinea pigs (Ahlf et al., 2012). These divergent effects may derive from differences in AC inhibition, wherein peripheral deafferentation induces excitatory/inhibitory homeostatic rebalancing (Chrostowski et al., 2011; Yang et al., 2011, 2012). The original site of this different inhibitory modulation is unclear, since AC may have inherited these effects from elsewhere in the disrupted auditory system, as may be the case in the IC (Manzoor et al., 2013; Robertson et al., 2013).

The normalcy of neurometric gap-detection thresholds following deafferentation is puzzling, particularly in the context of the behavioural changes

described. Despite the stringent criteria applied to quantify unit detection thresholds, they may vary according to the analytic approach used. However, ROC analysis has revealed auditory neural responses that correspond with psychometric performance (Skottun et al., 2001; Lemus et al., 2009; Recanzone et al., 2011; Bizley et al., 2013), implying that it is a robust framework for determining neural correlates of behaviour. Moreover, the thresholds we reported across all animals, while high (~20 – 50 ms), are within the normal physiological range for gap-detection in cat A1/AAF (Eggermont, 1999). Though these data set an upper limit on the gap-coding capabilities of AC, we can be reasonably confident in our estimates of the gap-detection capabilities of ferret AC, particularly since the relationship between detection threshold and stimulus type varied similarly in both neurometric and psychometric data (with low-to-mid frequency NBNs yielding higher thresholds, in our hands, than high frequency NBN or BBN).

Furthermore, the results of previous studies examining neurometric gap-detection following hearing loss have been heterogeneous. Hearing loss does not immediately impair gap-detection, since cortical cells retain coding capabilities following wholesale cochlear removal (Kirby and Middlebrooks, 2010). A recent study of noise-exposed guinea pigs found that in those animals with behaviourally-evident temporal processing deficits, detection thresholds for gaps in broadband noise carriers were significantly elevated, but not when gaps were placed within tonal or narrowband stimuli (Berger et al., 2014). These data might imply an impairment in cross-channel information integration, rather than a frequency-specific temporal processing deficit, as observed in AC following noise trauma (Yin et al., 2008). Heterogeneous neurometric gap-detection during presbyacusis has

been found in mice (Walton et al., 1998) and non-human primates (Recanzone et al., 2011), wherein detection thresholds remained unperturbed overall, but the proportion of units that responded at "threshold" was diminished. However, given the limited data available in the literature, and their heterogeneous nature, the temporal processing changes we and others have observed manifesting behaviourally might be localised to regions other than AC (or other lemniscal auditory structures). While necessary for effective gap detection performance (Ison et al., 1991; Kelly et al., 1996; Threlkeld et al., 2008; Weible et al., 2014b), AC may not be the critical locus for the instantiation of post-deafferentation perceptual changes. This does not rule out the possibility of AC acting as a necessary relay for perceptually-salient temporal information affecting behavioural performance (Bajo et al., 2010b; Bajo and King, 2012; Weible et al., 2014a).

One system in humans that is important to the instantiation of tinnitus, and particularly the degree of tinnitus-related suffering, is the limbic system. Structures including the parahippocampus, amygdala and other non-auditory regions have been broadly implicated in tinnitus-related connectivity and functional differences (e.g. Wallhäusser-Franke et al., 2003; Leaver et al., 2011; Langguth et al., 2013; Sedley et al., 2015). Interestingly, overlap exists between tinnitus-related limbic involvement and that which accompanies phantom limb syndrome, another deafferentation-based perceptual abnormality in which suffering (as phantom limb pain) is associated with non-sensory telencephalic modulation (Rauschecker et al., 2015). Since our project has not considered these structures, it remains unclear what, if any, role the limbic system might play in animal models of hearing loss and tinnitus-like symptoms.

Overall, the physiological changes reported here broadly agree with those reported in previous models of hearing loss/tinnitus. However, given the particular kind of deafferentation we have investigated, the above-described shifts in neural excitability and response properties occur within the context of a substantial hypo-activity, leading to overt changes that are unique from those typically observed following noise-induced trauma. That there was a relationship between cortical processing changes and the perceptual shifts seen during gap-detection behaviour is indicative of a key role for higher sensory circuits in the response to peripheral deafferentation. Nonetheless, the details remain to be discovered of where the underlying adaptive/maladaptive neuroplasticity occurs, although AC represents an excellent candidate for exploration.

4.3.4 Neurochemical Markers of Plasticity: Discrimination between Hearing Loss and Tinnitus?

We undertook an exploration of the neurochemical changes underlying hearing-loss related plasticity, via two molecules related to synaptic function: NOS (by NADPHd staining) (Hardingham et al., 2013), and Arg3.1/Arc (Bramham et al., 2010; Korb et al., 2013). NOS displays high expression density throughout the central auditory system, except layer I of AC, and with distinctly greater infragranular density (Druga and Syka, 1993), as we also observed. Additionally, IC displays high NOS activity (Coote and Rees, 2008), with elevated NOS density in the IC of aged rats (Sanchez-Zuriaga et al., 2007; Huh et al., 2008). Our observations of augmented NADPHd in dorsal cortex and lateral nucleus of the IC agrees with brainstem-localised NOS upregulation after noise overexposure (Coomber et al., 2014; Berger and Coomber, 2015). This occurs particularly in VCN, which has been correlated

with central gain in tinnitus (Vogler et al., 2011, 2014; Coomber et al., 2015), while increases in the medial superior olive have been correlated with ageing and presbyacusis (Gray et al., 2014). Enhanced NADPHd/NOS$^+$ density also develops in the aged AC of small mammals (Huh et al., 1997, 1998, 2008; Ouda et al., 2003; Sanchez-Zuriaga et al., 2007) and humans (Unger and Lange, 1992), suggesting a role for NOS-mediated signalling in presbyacusis-mediated functional changes.

Contrasting with the asymmetric NOS expression in the tinnitus-like CN (Coomber et al., 2014, 2015), we found no evidence for cortical asymmetry, aligning with our neurophysiological data. Thus, hearing loss-related plasticity, while lateralised in lower auditory centres, may induce generalised neurochemical/neurophysiological changes more rostrally. It may be that AC NADPHd$^+$ density is predominantly related to hearing loss specifically, rather than any perceptual changes, given that no differences in staining emerged among our behaviourally diverse lesioned cohort. Interestingly, enhanced NO in aged rat AC is associated with suppression of neuronal excitability (Lee et al., 2008): since we observed diminished SFRs in both Impaired and Not-Impaired animals, a similar process may be at play in our experimental model, common amongst deafferented AC cells, though particularly within infragranular neurons.

Furthermore, Arg3.1/Arc appeared to be upregulated in the context of specific behavioural impairment, though in contrast to NADPHd density, Arg3.1/Arc *did* appear lateralised to contralesional AC, akin to nNOS expression in the ipsilesional VCN (Coomber et al., 2014). The magnitude of Arg3.1/Arc density increases appeared to be correlated with behavioural phenotype, although the

number of animals in this sample is too few for sufficiently well-powered statistical analysis of this relationship. Importantly, Knipper and colleagues have reported that, as in our preparation, Arg3.1/Arc upregulation is associated with acoustic trauma-induced hearing loss that leaves ribbon synapses intact (Rüttiger et al., 2013; Singer et al., 2013). In their hands, however, a strong *decline* in Arg3.1/Arc density, particularly in layers II/III, was associated with tinnitus-like behaviour. Nevertheless, the laminar pattern and relative density of Arg3.1/Arc expression in our samples resembles that reported following injection of gerbils with salicylate, a known tinnitus inducer (Mahlke and Wallhäusser-Franke, 2004). Mechanistically, Arg3.1/Arc is an effector of homeostatic plasticity, acting through glutamatergic postsynaptic receptor modulation (Béïque et al., 2011; Jakkamsetti et al., 2013), again suggesting that complex excitatory/inhibitory processes are in play following deafferentation.

On these grounds, we have reason to believe that AC may be important in mediating the behavioural/perceptual changes following SG lesion. In the following chapter, we therefore will explore what happens to behaviour and neurophysiology when we selectively suppress activity in the post-lesion AC.

Chapter 5

Optogenetic Silencing of the Ferret Auditory Cortex

5.1 Introduction

A wealth of evidence indicates that the auditory cortex (AC) undergoes neuroplastic remodelling in the wake of sensory impairment, such as that experienced during hearing loss (see Chapters 1 & 4; Gold and Bajo, 2014). The types of changes are broad, ranging from low-level changes in the activity levels of individual AC neurons – both spontaneous and sound-evoked – to more complex receptive field shifts, analogous to other sensory systems (Buonomano and Merzenich, 1998). The post-deafferentation changes described in AC could be partially inherited from lower auditory structures, which also display modified response characteristics (Kaltenbach, 2011; Koehler and Shore, 2013). Nevertheless, early observations of low-threshold response profiles in AC (Robertson and Irvine, 1989; Rajan et al., 1993; Kamke et al., 2005), as distinct from subcortical nuclei (Rajan and Irvine, 1998; Irvine

et al., 2003; Izquierdo et al., 2008), suggest that AC sustains a distinct configuration of hearing loss-related plasticity.

Neuroimaging studies have implicated abnormal AC activity, and likely post-impairment plasticity, in the development and maintenance of tinnitus (De Ridder and Vanneste, 2014; Elgoyhen et al., 2015). The manner and magnitude of these changes are subtle, and their manifestations in AC functional architecture remains disputed (Langers et al., 2012). By analogy with phantom pain, preservation of the cortex's functional organisation may actually be important for the emergence of abnormal sensation (Makin et al., 2013). Further similarity includes the substantial involvement of non-sensory – especially limbic – areas in the conscious gating and possible enhancement of sensory-derived neural activity (Leaver et al., 2011; Elgoyhen et al., 2015; Rauschecker et al., 2015). Thus, in addition to primary sensory cortical regions, a functional and anatomical network of higher, non-sensory brain regions could be fundamental to phantom percept generation. In this case, AC likely acts as a lynchpin in the emergence of tinnitus (De Ridder et al., 2015), and is probably the focus of abnormal tinnitus-related activity following some kind of hearing loss.

Since adaptive/maladaptive plasticity in AC may influence perception, what remains unclear is whether some *causal* role for AC may exist in generating abnormal perception itself; or whether, in the long term, deafferentation-mediated perceptual changes become instantiated beyond sensory cortex, in a more distributed fashion (as in the IC, for example (Mulders and Robertson, 2011; Robertson et al., 2013)). Efforts in human patients to disrupt AC activity to discover its causal involvement in

tinnitus-related plasticity have met with some success. Invasive (Smit et al., 2015) and non-invasive (Residual Inhibition; Roberts, 2007) therapeutic experiments have suggested that by targeting AC specifically, the conscious percept of tinnitus itself can be modified. However, to conclude that AC is indeed subject to post-traumatic plasticity, this region must be selectively targeted in a model system wherein the expected outcomes of the type of treatment can be hypothesised.

The experimental system developed over the previous two chapters allowed us to explore this possibility: in a cohort of ferrets, behavioural heterogeneity has been correlated with physiological effects throughout the central auditory system – in particular, with functional changes in AC. Simultaneously, the emergence of optogenetic tools has afforded the kind of spatiotemporal specificity necessary to dissect out the role of anatomically well-defined circuits in generating certain behaviours (Hausser, 2014; Grosenick et al., 2015). Notably, high-resolution AC suppression employing Archaerhodopsin (Chow et al., 2010; Han et al., 2011) has been used to disrupt AC circuitry in a behaviourally-relevant manner (Bajo et al., 2013; Znamenskiy and Zador, 2013).

We hypothesised that, by optogenetically suppressing AC in ferrets that had received a partial SG lesion, we could modulate expression of gap-detection behaviour that itself was affected by the deafferentation due to reactive plasticity in AC, a region necessary for near-threshold gap-detection behaviour (Kelly et al., 1996; Threlkeld et al., 2008; Weible et al., 2014b). Although the possible lateralisation of abnormal AC plasticity remains controversial, we postulated that contralesional

suppression, specifically, would produce behavioural modifications, since many animal studies have described contralesional physiological changes following an auditory insult. Our cohort comprised some animals that appeared to have adapted to the hearing loss, and some that had failed to do so. Thus, we suspected that the outcomes of optogenetic AC suppression would differ, depending on each animal's post-deafferentation behavioural phenotype. Finally, we sought to understand the neurophysiological underpinnings of any behavioural changes observed, by recording multiunit activity in ferret AC during laser illumination.

5.2 Results

Here, we present results describing the effects of suppressing neural activity in ferret AC. An adeno-associated virus (AAV)-based optogenetic construct was used, containing the gene encoding the outward proton pump ArchT (Fig 2-7). Multiple small injections of the construct were made bilaterally in the ACs of each ferret (two injections per penetration site, at depths of 0.5 and 1 mm), enabling the laser-mediated optogenetic suppression of either or both ACs. These ferrets (n = 6, see Table 2-1) displayed a mixture of behavioural effects resulting from the SG lesion. Using uni-/bi-lateral laser illumination during behaviour, we sought to explore the possible hemispheric lateralisation of deafferentation-related plasticity, and determine the behavioural consequences of suppressing any abnormal AC activity.

This section comprises three components: first, the effects of pseudorandomised laser illumination during gap-detection behaviour, unilaterally (both ipsilesional/right and contralesional/left) and bilaterally; second, AC neurophysiological recordings in the presence/absence of contralesional laser illumination; and anatomical examination of injected brains to verify the presence and extent of viral gene product expression (elucidated using green fluorescent protein (GFP) expression by the AAV construct).

5.2.1 Gap-in-Noise Detection Behaviour

Animals underwent behavioural testing in response to the four spectrally different noise types (1 kHz, 4 kHz, and 16 kHz narrowband noise, NBN; and broadband noise, BBN), tested in blocks as outlined in Chapter 3. A key difference during task performance in this chapter is the laser illumination, which was designed to mediate

steady-state suppression during acoustic stimulation. Laser illumination was applied pseudorandomly from trial-to-trial, yielding an approximately 50/50 laser/no-laser ratio. The site of illumination was block-varied, with contralesional-only (left AC) illumination evaluated first in all animals, across all stimuli, followed by ipsilesional-only illumination, and finally bilateral illumination. On the basis of this task design, therefore, behavioural results will be described for each such condition in order of treatment application.

Our approach to laser silencing was hypothesis-driven: that the site of lesion-derived plasticity was within primary AC (comprising A1 and AAF), based on observations of lesion-related activity within AC from multiunit recordings obtained there (see Chapter 4). How each AC (ipsilesional vs. contralesional) contributed to this abnormal SG lesion-related activity, and what effects bilateral AC suppression might have, were unknown. Moreover, the acoustic stimulus frequency-specificity of laser illumination was not known, and so the Impairment Index (I-Index)[1] of each animal at each stimulus was analysed.

Contralesional Suppression Affects Temporal Detection Performance

We and others have suggested the involvement of contralesional AC in deafferentation-based neuroplasticity (Robertson and Irvine, 1989; McAlpine et al., 1997; Engineer et al., 2011). We therefore sought to suppress contralesional AC activity in SG-lesioned animals with heterogeneous behavioural I-Indices, to

[1] As described in Chapter 4, the I-Index is a behavioural scoring metric to describe significant changes in behaviour following SG lesion. The magnitude and sign of the I-Index value for each stimulus type are determined by the degree of significant differences between the pre- and post-lesion conditions, and whether these changes represented improvements or impairments in performance, where impairments lead to an I-Index <0.

determine if some underlying, possibly asymmetric neuroplastic process may have been responsible.

No clear association was found between approach-to-target response times and laser illumination. In each animal's response time distribution medians, and the fitted μ and τ statistics of the descriptive ex-Gaussian fits, we found no effect of laser illumination on ferrets' abilities to perform the task efficiently (Fig.5-1).

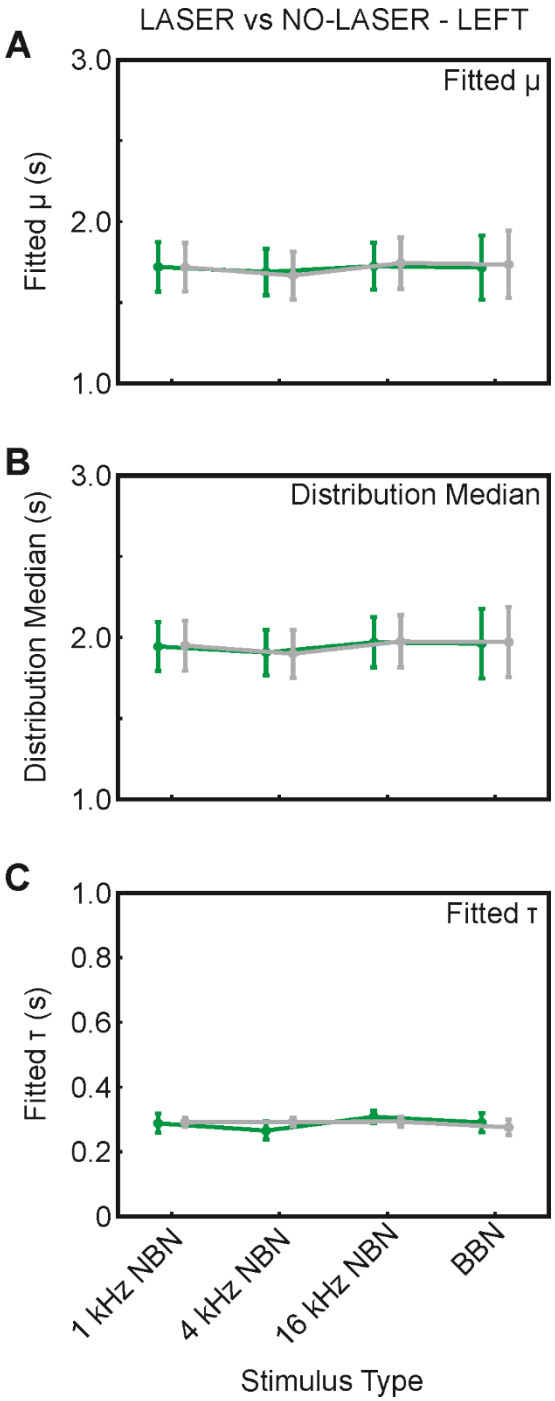

Figure 5-1: LEFT Unilateral Laser Illumination, Approach-to-Target Response Time Statistics. In each panel, laser-ON = green; laser-OFF = grey. Axes indicate measure of interest (seconds) vs. stimulus type (1-, 4-, or 16 kHz NBN, & BBN). Data shown as mean ± standard error. A) Ex-Gaussian fitted μ. B) Empirical median. C) Ex-Gaussian fitted τ.

Laser illumination did produce heterogeneous effects in each ferret's psychometric functions (Figs.5-2 to 5-7). For animals that displayed post-lesion behavioural impairments (I-Index < 0), a general trend emerged whereby laser illumination often induced no changes to behaviour. For example, F1226 (Fig.5-2) displayed no significant changes when compared with the laser-OFF condition, although performance appeared to be marginally improved for low-to-mid frequency NBN. Surprisingly, in certain animals optogenetic suppression yielded behavioural *improvements* for specific sound stimuli, compared with respective laser-OFF conditions. In those animals where laser-mediated improvements – significant ($p < 0.05$) or trending towards significant ($p < 0.1$) – were seen, they tended to coincide with those respective stimuli in which each animal had displayed post-lesion behavioural impairments; for example, F1227 displayed marked improvements for 1 kHz and 4 kHz, but no changes to BBN performance (Fig.5-3; cf. Fig.4-2).

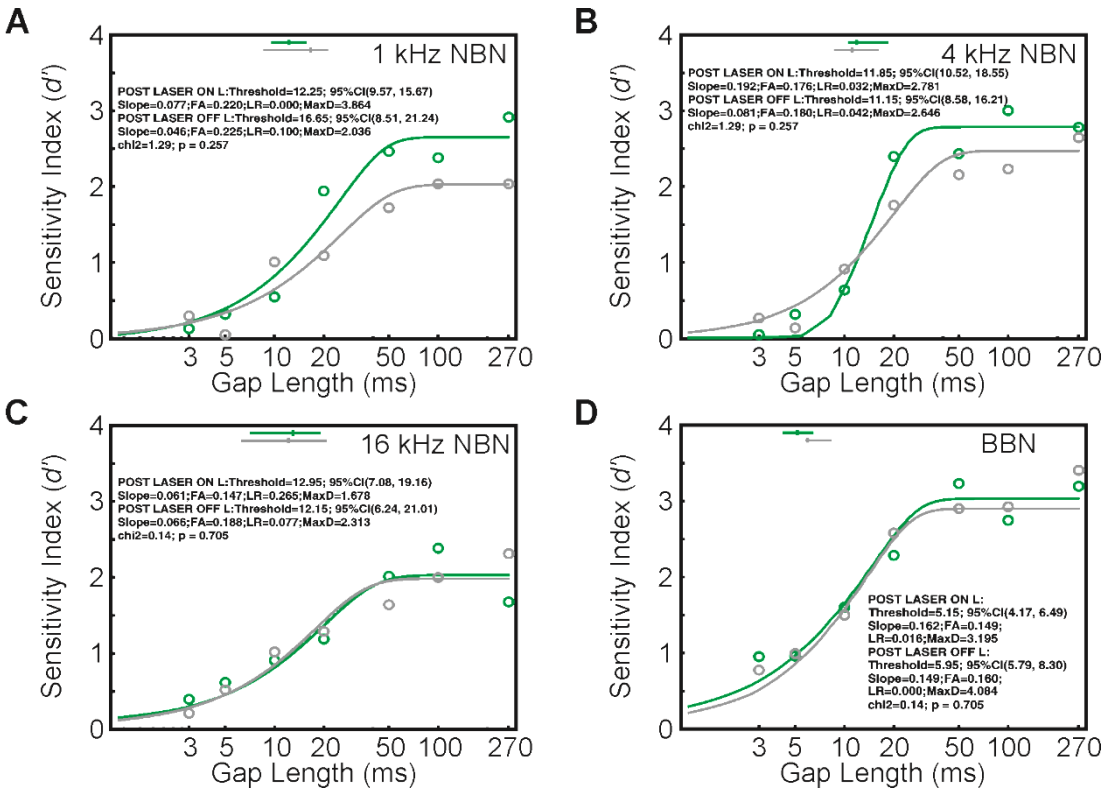

Figure 5-2: LEFT Unilateral Laser Illumination, Psychometric Functions, F1226. Laser-ON = green; laser-OFF = grey. Psychometric functions were fitted as right-weighted gumbel sigmoids to data pooled across sessions. Axes indicate *d'* plotted against gap length. Dots and horizontal bars at the top of each panel indicate the fitted threshold and 95% confidence intervals (CIs) on the fit at threshold, respectively. Text describes numerical values, laser-ON and laser-OFF, for threshold, 95% CIs, curve slope at threshold (slope), empirical FA rate (FA), empirical lapse rate (LR), and maximum fitted *d'* value (MaxD). χ^2 and *p* values are given for LEFT laser-ON vs. laser-OFF, Friedman test. A) 1 kHz NBN. B) 4 kHz NBN. C) 16 kHz NBN. D) BBN.

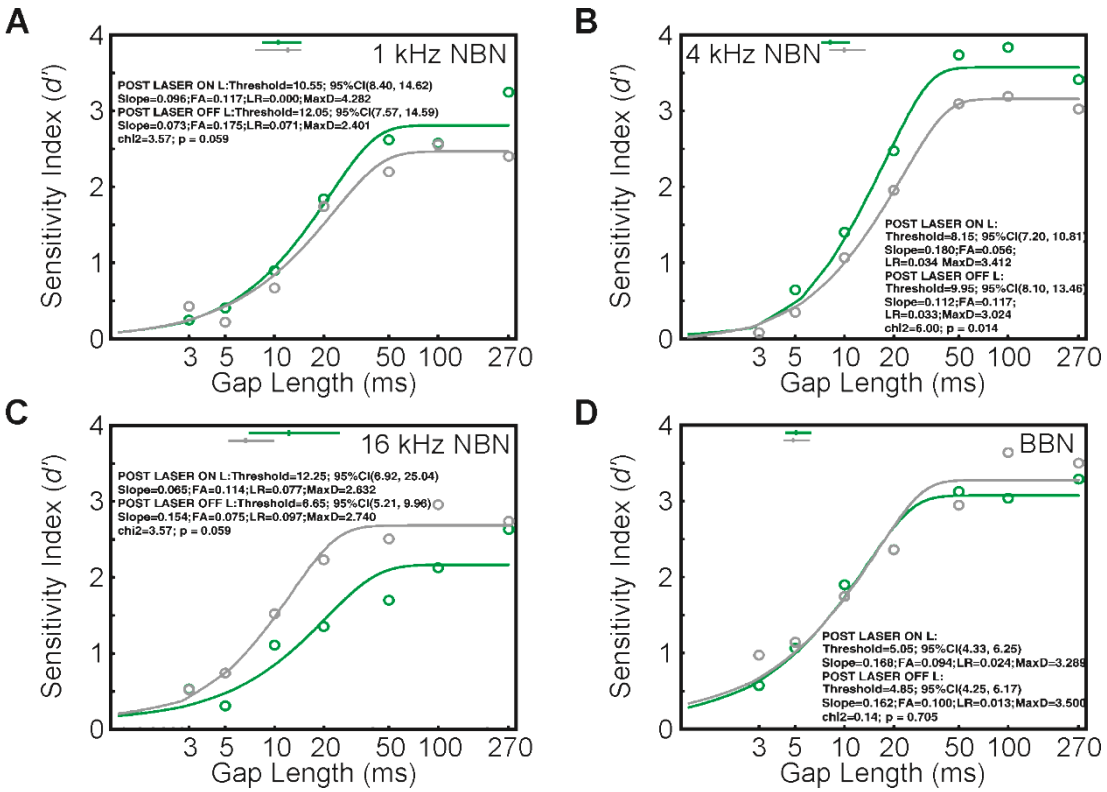

Figure 5-3: LEFT Unilateral Laser Illumination, Psychometric Functions, F1227. See description for Fig.5-2.

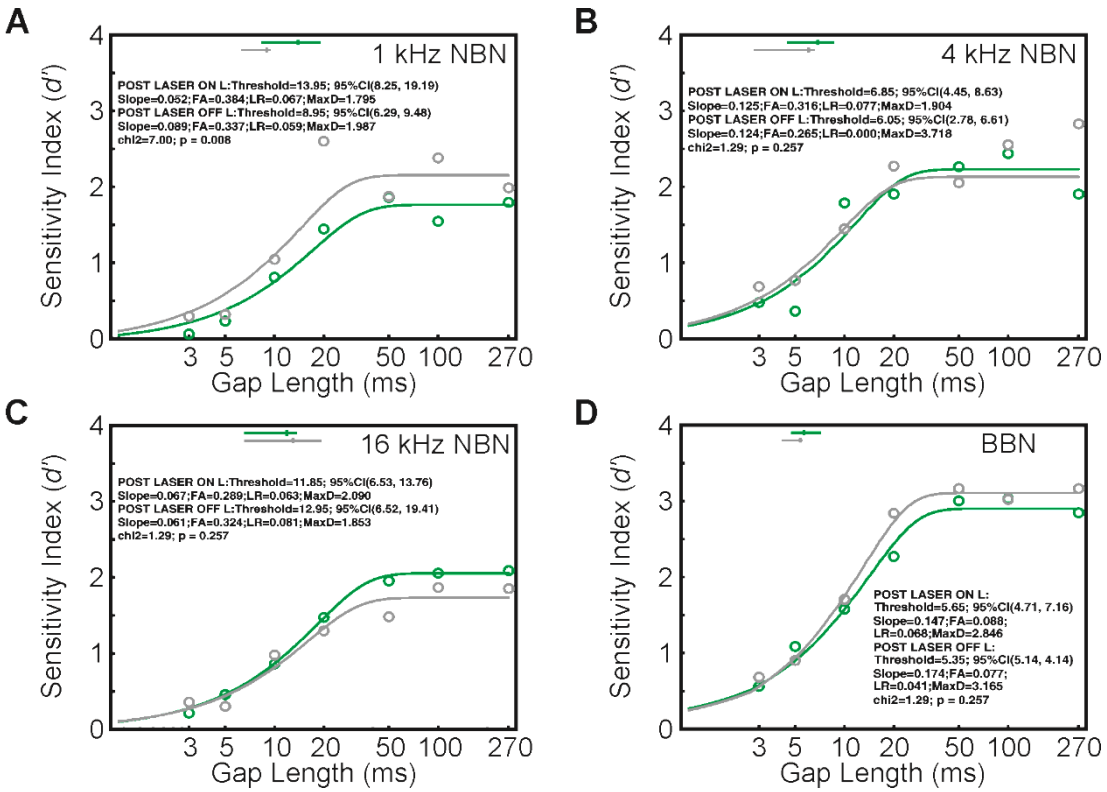

Figure 5-4: LEFT Unilateral Laser Illumination, Psychometric Functions, F1228. See description for Fig.5-2.

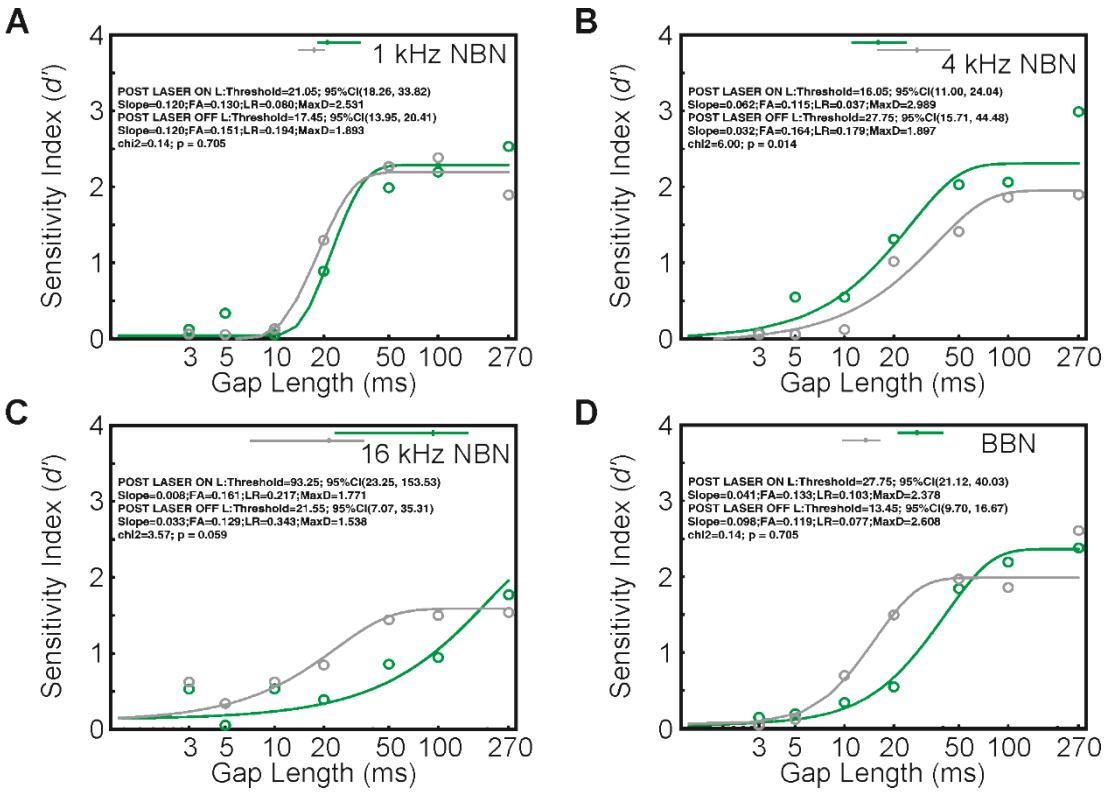

Figure 5-5: LEFT Unilateral Laser Illumination, Psychometric Functions, F1317. See description for Fig.5-2.

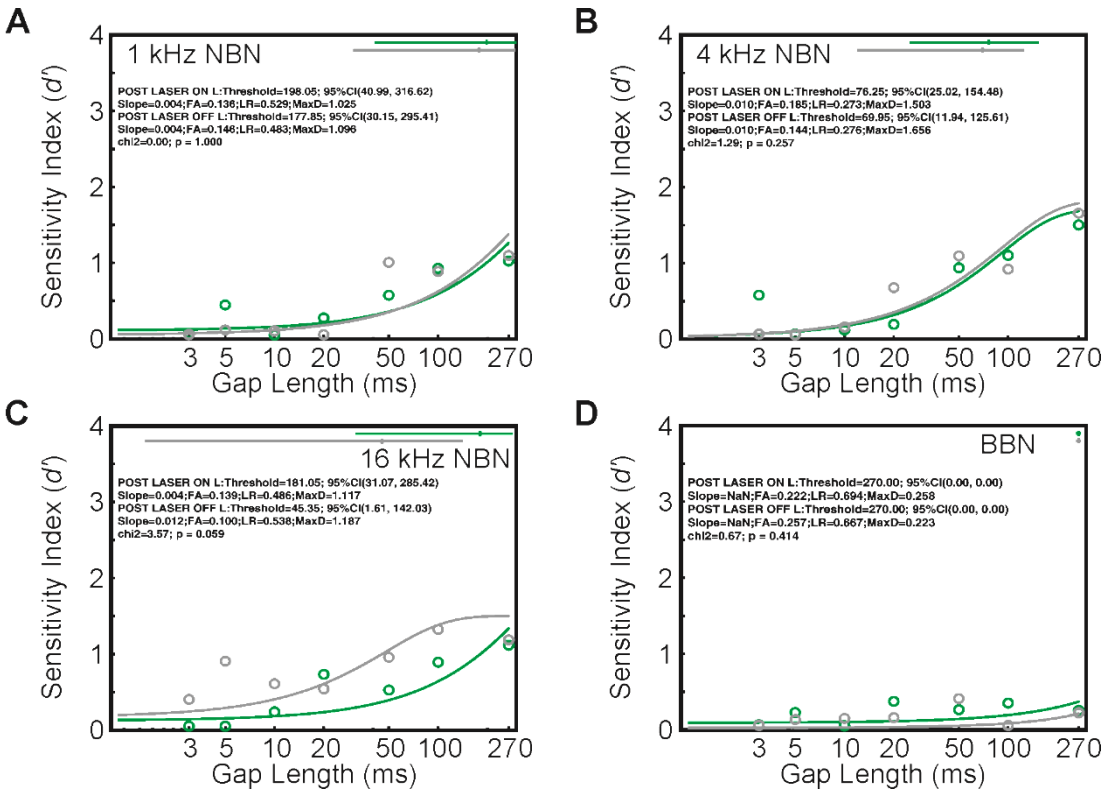

Figure 5-6: LEFT Unilateral Laser Illumination, Psychometric Functions, F1318. See description for Fig.5-2.

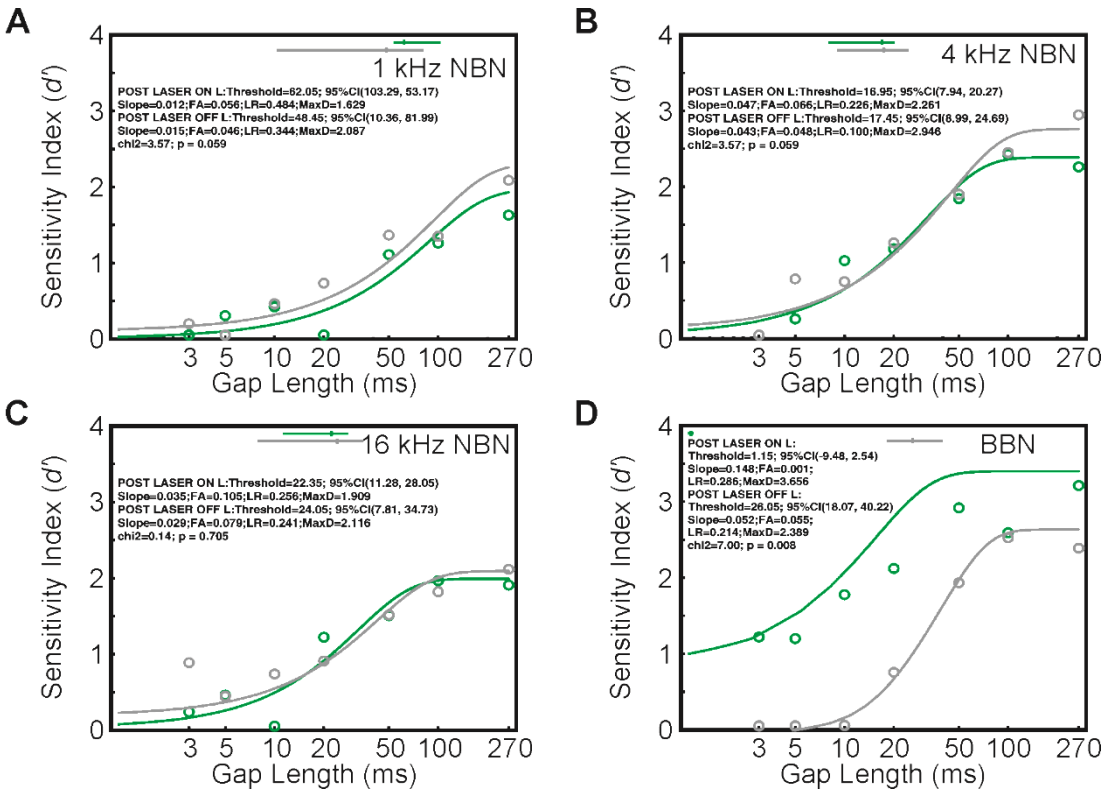

Figure 5-7: LEFT Unilateral Laser Illumination, Psychometric Functions, F1319. See description for Fig.5-2.

For unimpaired (I-Index >0) ferrets, laser illumination also selectively modulated task performance. For one ferret in which large post-lesion improvements emerged (F1319), contralesional laser illumination mildly impaired gap-detection performance for 1 kHz and 4 kHz NBN stimuli: two stimuli for which post-lesion improvements were seen. While no such changes occurred at 16 kHz NBN, the laser illumination also significantly improved performance for BBN (Fig.5-7), for which large post-lesion improvements also were seen. These data would suggest that contralesional laser illumination does not yield wholesale detriments or improvements to performance, functioning instead in a frequency-specific manner. This is important when considering F1318, in which performance across all stimuli collapsed (Fig.5-6). The occasional absence of above-threshold performance in F1318, combined with considerably elevated ipsilesional click-ABR thresholds (>80-90 dB SPL), indicate the development of substantial long-term temporal processing deficits.

For all laser-ON vs. laser-OFF behavioural data, we applied a scoring paradigm similar to the I-Index (Fig.5-8). By comparing the Laser Index against the I-Index across all animals, at each stimulus frequency, we found a trend towards a negative correlation between laser-mediated improvement and I-Index (Fig.5-8) (*Spearman's* $\rho = -0.38$; $p = 0.096$). This means that contralesional suppression appears to selectively *improve* performance where post-lesion behaviour was *impaired*, and vice-versa. Therefore, contralesional optogenetic suppression may be capable of normalising SG lesion-induced perceptual plasticity, maladaptive or otherwise.

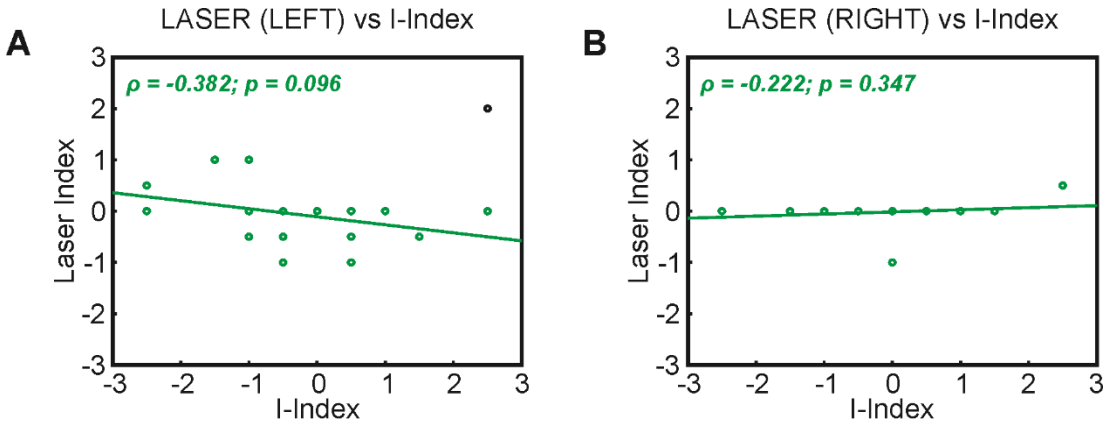

Figure 5-8: Laser Effect vs. Behavioural Impairment Index. Laser Effect Score was calculated as for the I-Index. Negative values indicate a worsening of performance in the laser-ON vs. laser-OFF condition. Axes indicate Laser Effect vs. I-Index scores, with each circle indicating one stimulus type for one animal; lines indicate linear best fits through data, with text indicating Spearman's rho (ρ) and p-value. A) LEFT laser illumination effect. Trend line (ρ = -0.382, p = 0.096) does not include outlier in black (>2σ). B) RIGHT laser illumination effect.

To determine whether similar effects to Residual Inhibition (RI) (Roberts, 2007; Roberts et al., 2008) could be modelled, laser-OFF trials were reanalysed according to each preceding trial's laser illumination state, being either preceded by laser illumination ("ONOFF"), or not ("OFFOFF"). If laser illumination mediates some form of long-lasting disruption of abnormal neural activity, associated changes in performance would emerge for ONOFF trials, compared with OFFOFF trials in which no such suppression was present.

Remarkably, this effect, which we term Residual Suppression (RS), was present in some ferrets. A mild behavioural enhancement of ONOFF vs OFFOFF trials was observed generally for F1227 (Fig.5-9), while the magnitude of behavioural effects was substantially increased in F1317 (Fig.5-10). Across the ferret cohort, the between-condition differences at each stimulus frequency were of similar magnitude when ONOFF vs. OFFOFF comparisons were made, as with laser-ON vs. laser-OFF comparisons. Specifically, the sign of behavioural changes induced by RS, when observed, was similar to the difference mediated by within-trial laser illumination. The negative correlation between I-Index and RS Index was not significant (*Spearman's* $\rho = -0.22$; $p = 0.351$) (Fig.5-11); nevertheless, the select emergence of RS may represent an experimental correlate for RI.

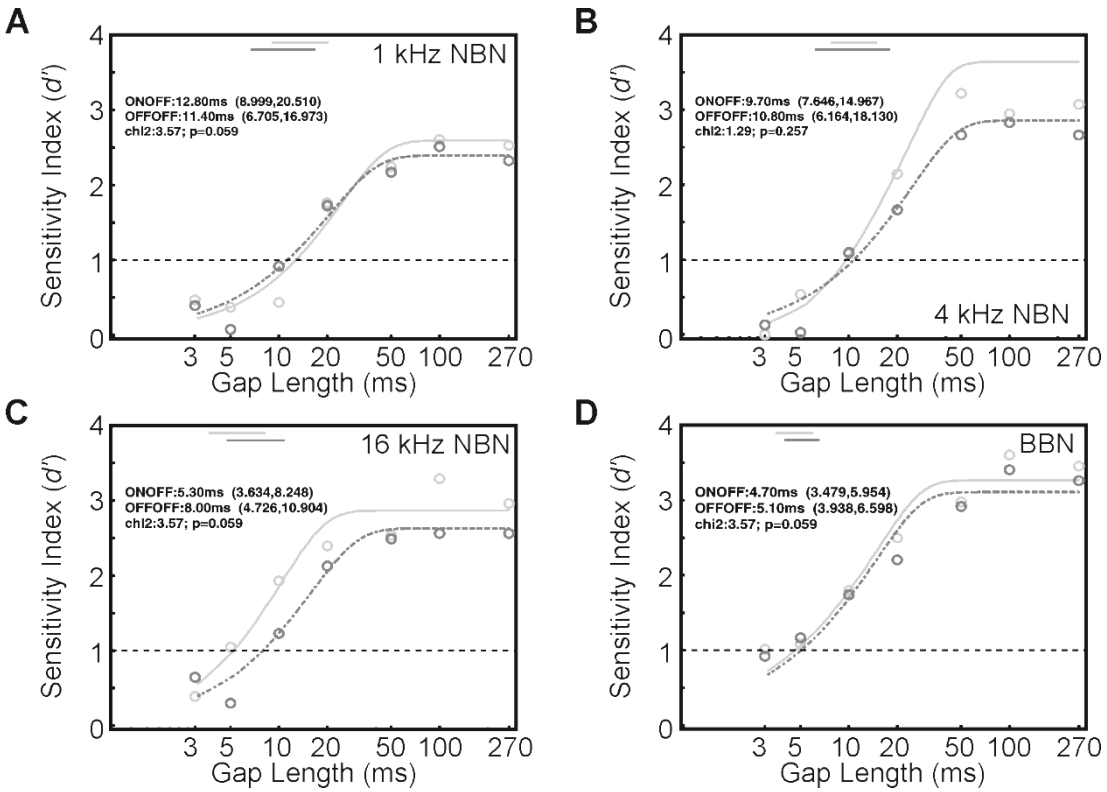

Figure 5-9: LEFT Unilateral Residual Suppression (RS), Psychometric Functions, F1227. ON-OFF (RS) = light grey, continuous line; OFF-OFF (no RS) = dark grey, broken line. Psychometric functions were fitted as right-weighted gumbel sigmoids to data pooled across sessions. Axes indicate *d'* plotted against gap length. Dots and horizontal bars at the top of each panel indicate the fitted threshold and 95% confidence intervals (CIs) on the fit at threshold, respectively. Text describes numerical values, ON-OFF and OFF-OFF, for threshold and 95% CIs. χ^2 and *p* values are given for ON-OFF vs. OFF-OFF Friedman test. A) 1 kHz NBN. B) 4 kHz NBN. C) 16 kHz NBN. D) BBN.

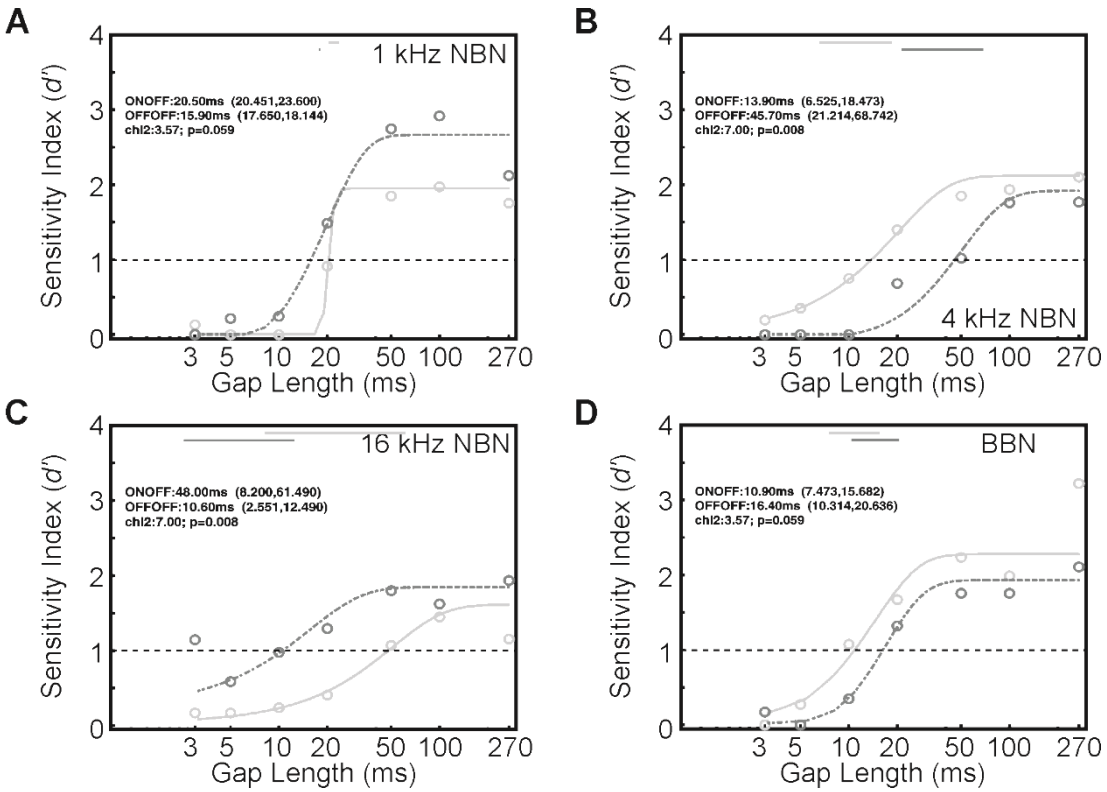

Figure 5-10: LEFT Unilateral Residual Suppression (RS), Psychometric Functions, F1317. See description for Fig.5-9.

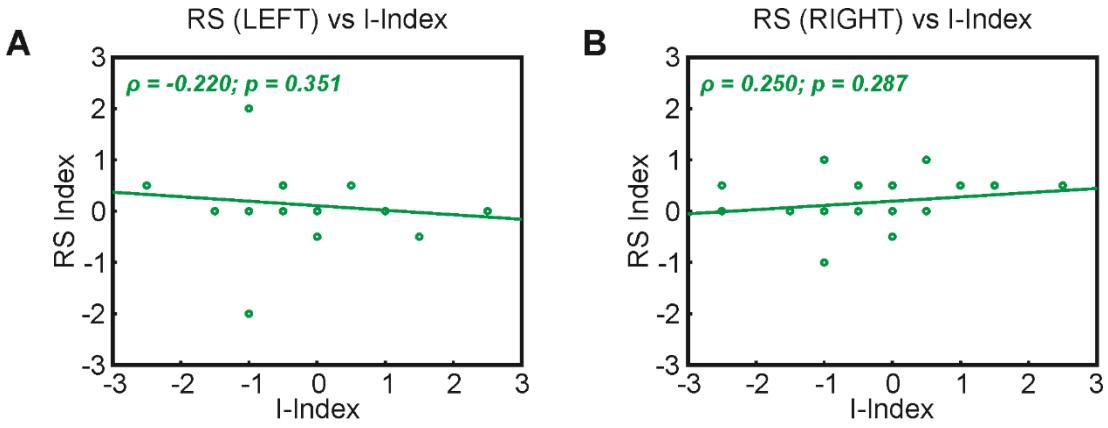

Figure 5-11: Residual Suppression (RS) Index vs. Behavioural Impairment Index. RS Effect Index was calculated as for the Laser Effect and I-Indices. Negative values indicate a worsening of performance in the ON-OFF vs. OFF-OFF condition. Axes indicate RS Index vs. I-Index scores, with each circle indicating one stimulus type for one animal; lines indicate linear best fits through data, with text indicating Spearman's rho (ρ) and p-value. A) LEFT laser RS effect. B) RIGHT laser RS effect.

Ipsilesional Suppression is Ineffective in Modulating Detection Behaviour

Unilateral laser illumination was applied to right AC in a second testing block. This served to determine the presence, if any, of maladaptive/adaptive plasticity in the ipsilesional cortex.

These results contrasted with contralesional laser illumination, with little-to-no effect of ipsilesional laser illumination found across the entire cohort. Response times were largely identical to those observed during contralesional suppression (Fig.5-12). Psychophysically, changes to behavioural performance were scarce, with F1317 displaying the only significant change: an impairment at 1 kHz, for which contralesional illumination elicited no effect, and SG lesion induced no behavioural changes. The ipsilesional Laser Effect Index and I-Index were not correlated (*Spearman's* $\rho = 0.22$; $p = 0.347$) (Fig.5-8).

Bilateral Suppression Does Not Affect Gap Detection Performance

Finally, a subset of implanted ferrets (n = 5) underwent behavioural testing during bilateral laser illumination, using identical illumination conditions as in the two unilateral testing blocks. Remarkably, bilateral laser illumination did not yield any effects whatsoever on approach-to-target response times, nor on gap-detection performance, with no ferrets displaying differences between the laser-ON and laser-OFF conditions.

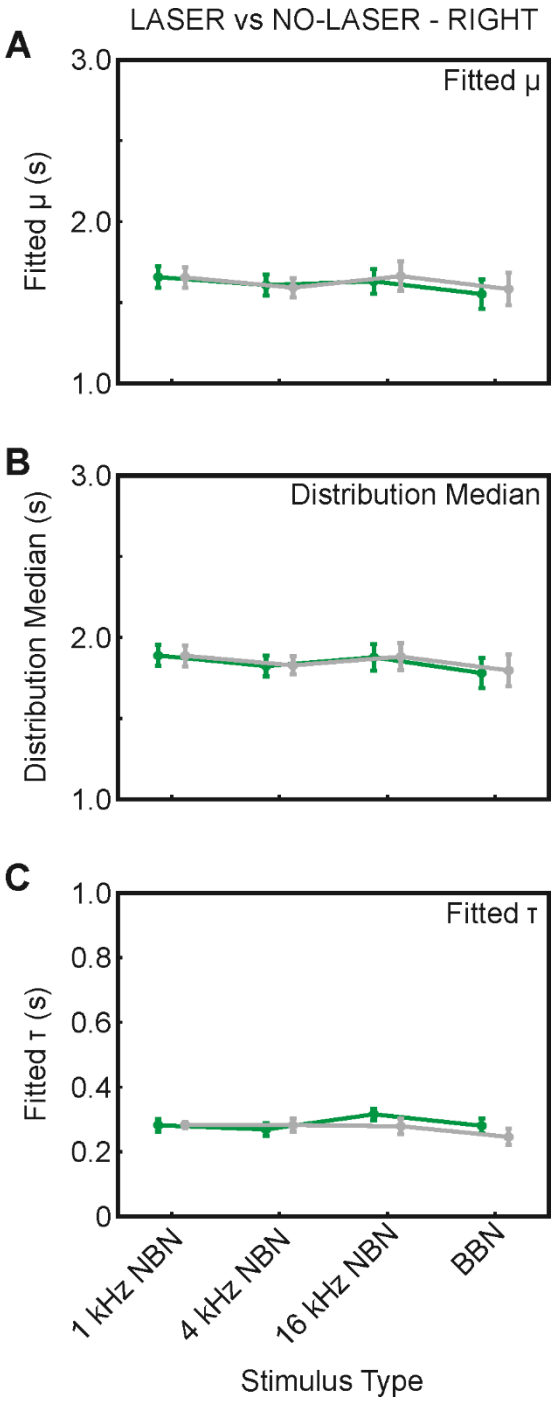

Figure 5-12: RIGHT unilateral laser illumination approach-to-target response time statistics. See description for Fig. 5-1.

In summary, selected effects on gap-detection behaviour could be observed in a frequency- and subject-dependent manner, according to the AC exposed to laser illumination. The largest effects were observed during laser illumination of the contralesional AC. The outcome of this presumed suppression generally appeared to be a renormalisation of deafferentation-mediated behavioural shifts, putatively achieved by modifying or disrupting contralesional AC processing. Thus, we next undertook AC recordings while simultaneously applying laser illumination.

5.2.2 Contralesional Cortical Suppression Affects Gap-in-Noise Processing

Under the same preparations as in Chapter 4, we examined the efficacy of our optogenetic transfection, by simultaneously applying laser illumination to the contralesional AC surface during acoustic stimulation. This illumination protocol was designed to approximate that used during contralesional behavioural suppression, with pseudorandom laser illumination from sweep-to-sweep (see Chapter 2).

First, we examined the peri-stimulus time histograms (PSTHs) of units that were both acoustically responsive to gap-in-noise stimuli (>2σ from spontaneous activity), and showed significant changes to their response magnitudes during laser illumination ($p < 0.05$, paired t-test, laser-ON vs. laser-OFF mean spike rates). A number of initial observations were of effect of laser illumination, on the basis of contralesional unit activity. As exemplified in Fig.5-13, during optogenetic suppression, units systematically retained onset spiking to the sound. Whereas the latency-to-peak activity was unperturbed by the laser, the onset magnitude was often diminished. Spiking activity was generally suppressed by laser illumination, particularly during tonic spiking following onset response to noise bursts, and also

following the (simultaneous) offset of the laser and acoustic stimuli. Therefore, while laser-mediated neuronal spiking suppression was not complete, laser illumination did yield uniform reductions in spiking in response to gap-in-noise sounds.

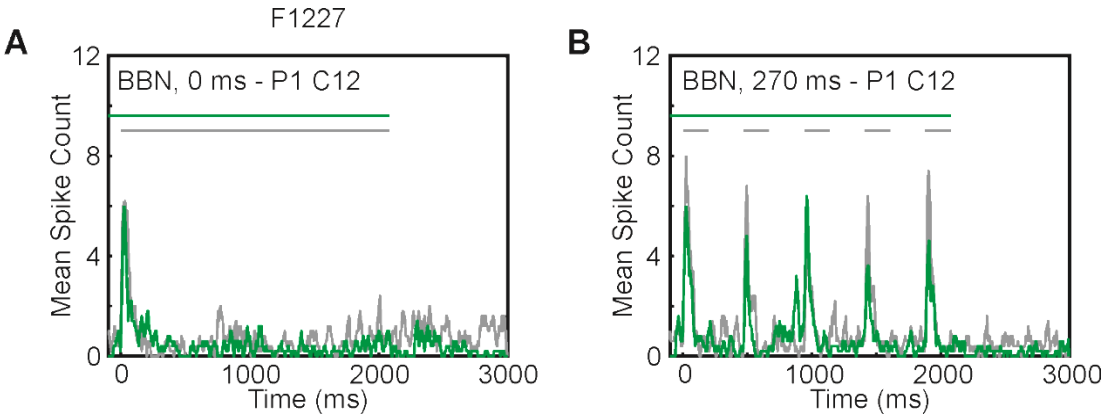

Figure 5-13: LEFT Laser Illumination, Gap-in-Noise PSTHs. Example PSTHs for a left hemisphere neuron from one animal (F1227), in response to gap-in-noise sounds. Axes indicate neural response (spikes count per bin) vs. time following stimulus onset (milliseconds). Traces indicate spike count across sweeps, smoothed with moving 5-bin average; green = laser-ON; grey = laser-OFF. Green horizontal bar indicates laser illumination. Grey horizontal bars indicate acoustic stimulation (BBN). A) Gap length = 0 ms (i.e. continuous BBN). B) Gap length = 270 ms.

To quantify the effects on spike rates of contralesional laser illumination, we compared unit responses with and without laser illumination. We evaluated the z-scored response for three epochs: during the acoustic stimulus initial onset period (at t = 5 – 55 ms in Fig.5-13); during the acoustic steady state period (throughout the duration of the gap-in-noise acoustic stimulus, excluding onset; t = 56 – 2080 ms); and during the last 100 ms of the sweep, ~800 ms after laser/acoustic offset.

In contralesional AC, laser illumination produced an initially mixed positive/negative effect among the affected unit population, with ~2/3 of units displaying an overall significant reduction in firing rate at sound onset (mean z-score, *p-value* as significantly different from 0: Positive: 0.21, p = 0.02; Negative: -0.25, p = 0.01) (Fig.5-14). During acoustic stimulation, the proportion and magnitude of this suppression response was much greater, with 96% of responsive units displaying a negative z-score (Negative: -1.18, p = 0.04) (Fig.5-14). This suppression effect was sustained by 95% of units into the recovery phase, well after stimulation offset (Negative: -0.60; p = 0.02) (Fig.5-14). Laser illumination of contralesional AC also affected ipsilesional AC spiking activity, although here equal proportions of units showing positive and negative firing rate changes across epochs (Fig.5-14); during no epoch did the magnitude of these ipsilesional effects match those seen in contralesional AC.

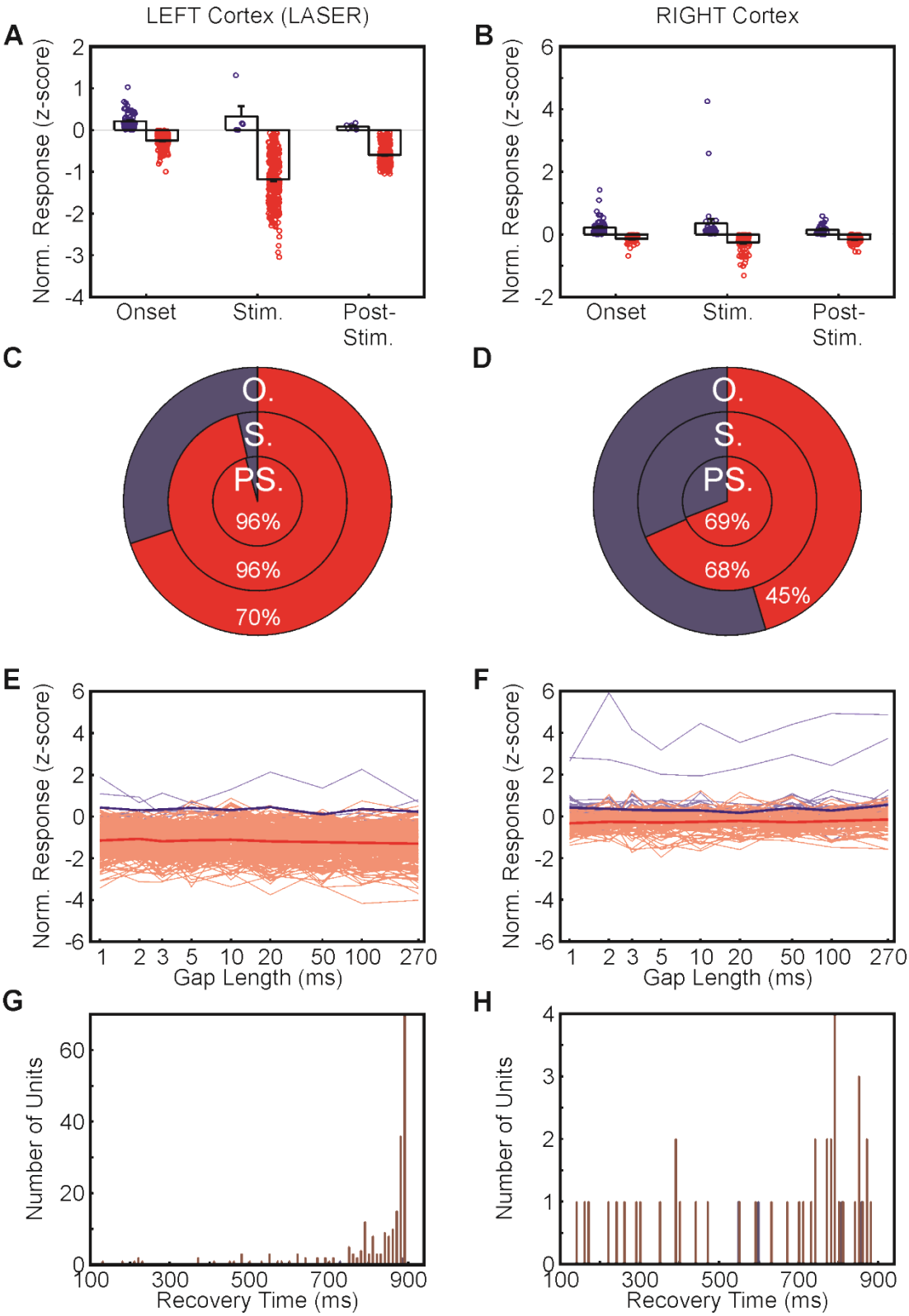

Figure 5-14: LEFT Laser Illumination, Gap-in-Noise Z-Scores. In each panel, red = units suppressed by laser illumination; blue = units enhanced by laser illumination. Left column = left AC units (ipsilateral to laser illumination); right column = right cortical units (contralateral to laser

illumination). A, B) Bar plots indicating mean (± standard error) z-scored response for enhanced and suppressed units. Responses measured at sound onset (Onset, O.), throughout sound duration (Stim., S.), and following the offset of laser illumination and sound (Post-Stim., PS.). C, D) Pie charts indicating proportional effect of laser illumination at each epoch. Numerical values indicate proportion of units displaying laser-mediated suppression in that epoch, compared with laser-OFF sweeps. E, F) Z-scores as a function of gap length during Stim. epoch. Thin traces indicate individual units; bold traces indicate mean across units. G, H) Spike rate recovery time histogram, calculated as time required following laser/sound offset for each unit to return to baseline firing rate (see text).

We also measured z-scored responses as a function of gap length: in both cortices, and for all laser-affected units, no systematic relationship was found between the firing rate change mediated by laser illumination and the silent gap length (Fig.5-14). This suggests that the activity of transfected units was systematically modulated by the laser, irrespective of the details of the sound presented.

Interestingly, the time required to recover to baseline spiking rates following laser illumination was particularly long. In contralesional AC, the vast majority of units reached laser-OFF levels of spiking >700 ms after laser offset, with some units remaining suppressed at the sweep's conclusion (Fig.5-14); notably, the inter-sweep interval exceeded 3-4 seconds, allowing additional time for recovery. This rightward skew in the recovery time distribution was also observed in ipsilesional AC, although to a lesser degree.

Overall, laser illumination mediated a predominantly suppressive effect on steady-state spiking of ipsilateral units, while preserving the capacity for these units to generate robust responses to acoustic onset cues. We hypothesised that this might lead to an improved signal-to-noise ratio (SNR) among contralesional cells, possibly facilitating neurometric gap-detection. We therefore repeated the ROC analysis described in Chapter 4, comparing detection thresholds under laser-ON and laser-OFF conditions (Fig.5-15) for unit groups from left (laser illuminated) and right cortices. Surprisingly, on evaluating detection performance of units that surpassed *auROC >0.6915* in left AC, laser illumination produced a significant reduction (i.e. *improvement*) in ROC gap-detection thresholds (rank-sum, $p = 0.0025$) (Fig.5-15). The

slope of the relationship between the two conditions was significantly less than 1 ($p < 0.05$, from slope 95% confidence intervals). Thus, laser-mediated suppression improved the temporal processing efficacy of contralesional cortical units, particularly for contralesional AC units that were initially less good at reliably encoding gaps-in-noise. By contrast, this same suppression paradigm induced a milder, though significant, increase (i.e. *impairment*) in detection thresholds of units in the right AC (rank-sum, $p = 0.0334$).

Together, these outcomes suggest that targeted optogenetic suppression of contralesional AC mediates an enhancement of SNR in the neural spike rate-based representation of temporally-modulated acoustic stimuli. These effects may, in part, account for the selective behavioural outcomes of contralesional laser illumination described above.

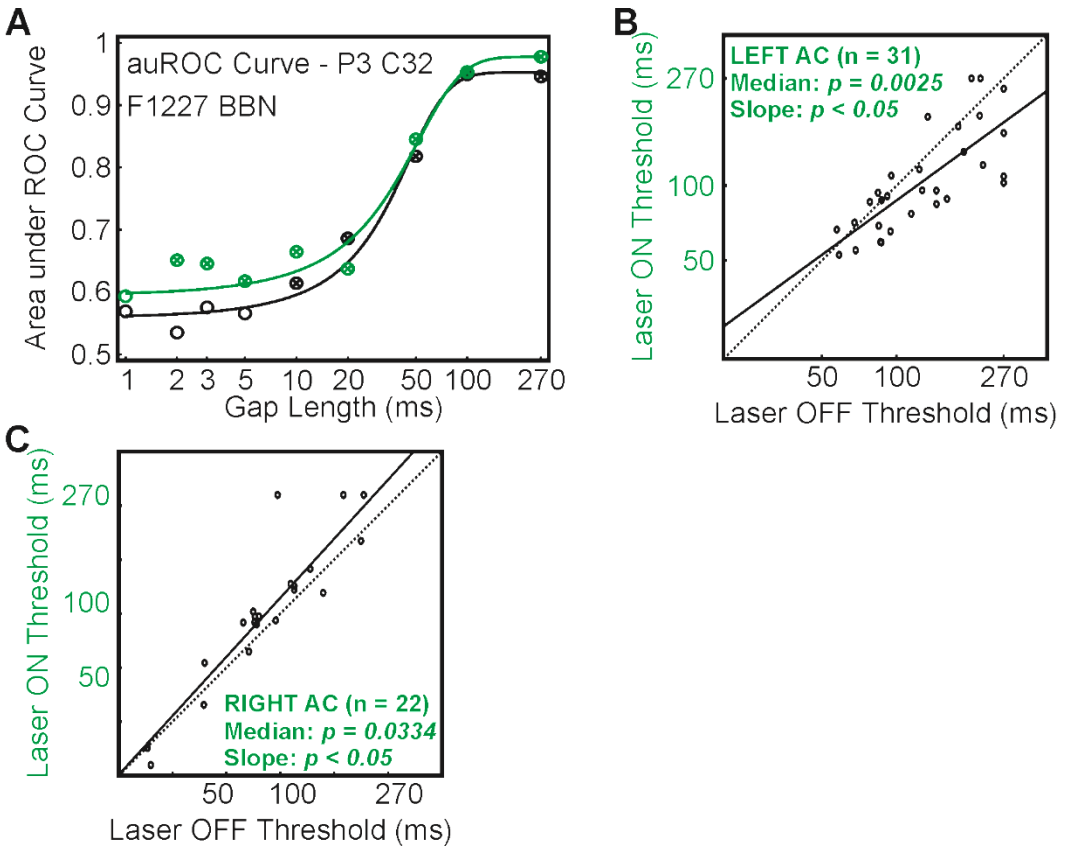

Figure 5-15: LEFT Laser Illumination, Gap-in-Noise ROC analysis. A) Example ROC analyses for a left AC neuron from F1227. Axes indicate area under the ROC curve (auROC) vs. gap-in-noise length (milliseconds). auROC values at each gap length are indicated by circles, with significant auROC values indicated by a cross through that circle. Curves were fitted using psignifit (see text). Thresholds calculated as gap length at auROC = 0.6915. Green = laser-ON; black = laser-OFF. B) auROC neurometric thresholds for left AC neurons (n = 31), during laser-ON (ordinate values) vs. laser-OFF (abscissa values). Solid line indicates linear fit through data (slope = 0.955, 95% CIs = 0.931 – 0.979). C) auROC neurometric thresholds for right AC neurons (n = 22). Solid line indicates linear fit through data (slope = 1.032, 95% CIs = 1.003 – 1.061).

5.2.3 Anatomical Identification of ArchT$^+$ Transfection

Following neurophysiological recordings in transfected animals, pAAV8-CAG-ArchT-GFP neuronal transfection was analysed using fluorescence and confocal microscopy (n = 3). Double immunohistochemical labelling against GFP and neuronal nuclear protein (NeuN) was applied to sections, which were mounted in medium containing DAPI (Fig.5-16).

In each AC, injection sites were centred primarily on A1, and identified by high regional concentrations of GFP$^+$ immunofluorescence, which were coincident, in size and location, with the number, location, and volume, of the viral injections described in Chapter 2 (Fig.5-16). At the injection sites specifically, double-labelling of anti-GFP and anti-NeuN was identifiable in a large number of cells, indicating that the transfected cells were predominantly neurons. Since two sub-pial depths were targeted for injection, we typically observed two distinct, but overlapping, regions of GFP$^+$ immunofluorescence that extended in parallel with cortical lamination. No retrogradely-labelled cells were found outside of targeted injection sites.

Contrastingly, GFP$^+$ fibres and terminal fields were found profusely in various regions of the central auditory system, mainly in non-primary AC fields, MGB, and IC (Fig.5-16). In AC, axon terminal fields were found in the posterior bank of EG, which comprises secondary AC fields PPF and PSF (Bizley et al., 2015). Descending corticothalamic fibres to auditory thalamus were observed to run from dorsomedial to ventrolateral, forming dense terminal fields, primarily within the ventral division of MGB, with minor projections also ending within the medial division. Finally, we identified axons of GFP$^+$ projection neurons within several

regions of IC: while predominantly localised dorsomedially within the dorsal cortex and central nucleus, labelled fibres and terminal fields could also be seen in layer 2 of the lateral nucleus, at lower density.

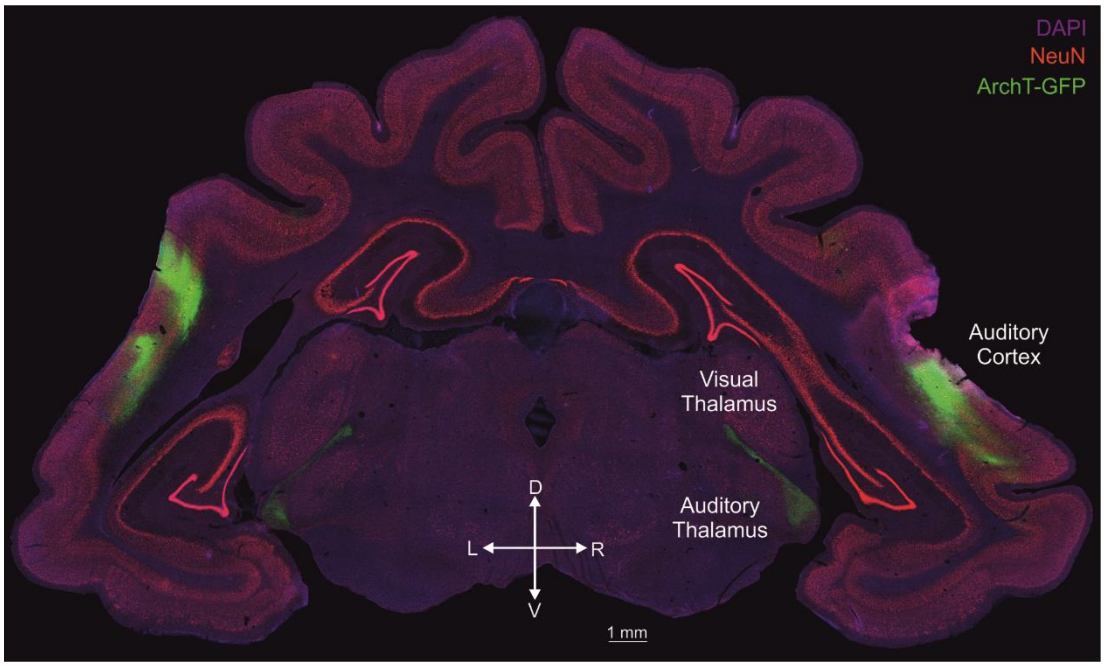

Figure 5-16: Immunohistochemical labelling of AAV-CAG-ArchT-GFP injection sites. Coronal section at the level of the auditory cortices from an injected animal (F1228). Purple = DAPI; red = anti-neuronal nuclear protein (NeuN); green = anti-Archaerhodopsin-T-Green Fluorescent Protein (ArchT-GFP). D = dorsal, V = ventral, L = Left, R = Right.

5.3 Discussion

In this chapter, the model of tinnitus-like changes developed in Chapter 4 was employed to explore the contribution of ferret primary AC to the behavioural shifts we observed following selective deafferentation. Through optogenetic suppression of AC during gap-detection behaviour, we isolated contralesional AC as a key locus for post-lesion changes in auditory processing. When we applied either a similar suppression of ipsilesional AC, or bilateral suppression to each AC simultaneously, few-to-no changes in behaviour developed, indicating the specificity of contralesional AC in the post-deafferentation adaptive/maladaptive process. To evaluate the optogenetic transfection paradigm, multiunit recordings were made in contralesional AC of a subset of behaviourally-tested animals, with and without laser illumination at the cortical surface. These experiments, alongside histological analysis, confirmed the efficacy of these injection sites, alongside the possibility for optogenetic suppression-mediated enhancement of temporal processing in AC neuronal ensembles.

Optogenetic suppression of the deafferented AC – perceptual effects and implications

Since the initial descriptions of optogenetic technologies by the Miesenböeck and Deisseroth groups (Zemelman et al., 2002, 2003; Boyden et al., 2005), they have aided numerous discoveries about the circuit basis underpinning perceptually-relevant neural computations. By optogenetically modifying a subpopulation of neurons, defined genetically and/or anatomically, their putative involvement in a behaviour's expression can be assessed (Grosenick et al., 2015). Typically, these experiments have been performed in rodents, and have focussed upon behaviours that are of a

stereotyped or reflexive nature, such as classical conditioning or avoidance paradigms (e.g. Tsai et al., 2009; Letzkus et al., 2011; Do-Monte et al., 2015; Marlin et al., 2015), and the cortical regions/microcircuits necessary for such behaviours (e.g. Weible et al., 2014a, 2014b; Li et al., 2015; Oka et al., 2015). Optogenetic disruption of simple behaviours has also been demonstrated in non-human primates (Gerits et al., 2012; Jazayeri et al., 2012).

The simplicity/stereotypy of these behaviours has facilitated the interpretation of the behavioural effects of optogenetic intervention, since each is unlikely to involve cognitive aspects related to operant task performance, such as attention and motivation. More recently, complex behaviours have been explored, with optogenetic effects ranging from the capacity to detect optogenetic stimulation of particular brain regions (Guo et al., 2015), to interrupting learned motor performance (Azim et al., 2014), or even enhancing sensory-guided behavioural judgements (Znamenskiy and Zador, 2013; Siegle and Wilson, 2014; Martins and Froemke, 2015).

Whereas the above studies reported homogeneous effects of optogenetic interventions on behaviour, our results were more diverse, with the behavioural effects of targeted AC inactivation ranging from heterogeneous both within and between animals (during contralesional suppression), to consistently inconsequential (during ipsilesional and bilateral suppression). Histological analysis confirmed the high density of transfection within all layers of AC bilaterally, with colocalisation of GFP^+ and $NeuN^+$ immunofluorescence indicating a largely neuronal population of cells expressing ArchT. These transfected cells projected, predictably, within non-

primary fields of AC (cf. Bizley et al., 2015, Fig.2, h – j), and within subcortical auditory regions including auditory thalamus and midbrain (cf. Bajo et al., 2007, Fig. 8). On the basis of commonality between our observed transfection distribution and these anatomical studies, AC optogenetic suppression was plausibly capable of modulating activity throughout much of the central auditory system (although confirmation would require additional neurophysiological experiments in other auditory regions).

While contralesional suppression clearly mediated substantial effects on behavioural activity, the within- and between-animal heterogeneity of these results may simply derive from the cognitively complex, operant task design, which probably relies on areas in addition to AC for aspects related to sensory-guided decision making (e.g. Znamenskiy and Zador, 2013; Raposo et al., 2014; Hanks et al., 2015; Xiong et al., 2015). Supposing that suppression of a primary sensory cortical region potentially disrupts the low-level encoding of stimulus parameters, enough residual information may conceivably be transmitted to allow for adequate, and even accurate, task engagement. Notably, AC suppression or removal are sufficient to mediate moderate-to-substantial interruptions to operant performance of auditory spatial (Nodal et al., 2010, 2012) and temporal tasks (Kelly et al., 1996), while neural activity in AC carries information about operant perceptual judgements (Bizley et al., 2013).

From the effects of contralesional A1/AAF suppression on temporal processing in animals with unilateral SG damage, we might conclude that AC integrity is necessary for our behavioural paradigm. Alternatively, disruptions to AC

computations that represent task-based contingencies, such as reward and decision biases, may impact upon more "cognitive" aspects of this behaviour, in addition to potentially affecting the encoding of the spectrotemporal features of sounds. Further clarification of the role of AC in temporal processing, as distinct from deafferentation-related plasticity, necessarily requires an investigation of the effects of optogenetic suppression on gap-detection in ferrets with normal hearing (see Chapter 6).

Therefore, a more likely contributory factor in the hemispheric differences that we observed is the putatively disrupted contralesional AC following hearing loss, which may be differentially expressed in animals with various degrees of post-lesion adaptation/maladaptation. Ours is not the first study to apply optogenetics to a model of pathological neuroplasticity, with work in an epilepsy model indicating the efficacy of closed-loop optogenetic disruption of thalamocortical discharge during electrographic and behavioural seizures (Paz et al., 2013); nor to attempt to remediate deafferentation-impaired (reflexive) behaviour by targeting cortical plasticity (Engineer et al., 2011). Yet to our knowledge, ours is the first attempt at an intervention in a neuroplastic pathology manifesting in conscious perception, evaluable only through cognitively complex behavioural performance. Thus, while our results were diverse, it is strikingly counterintuitive that cortical *inactivation* was selectively capable of *improving* discrimination performance: as a proof of concept, this surely is remarkable.

Physiological correlates of heterogeneous laser-mediated behavioural modulation

The inverse correlation between the behavioural effects of SG lesion and contralesional laser suppression indicates that, for temporal processing within

particular sound bandwidths, this optogenetic treatment interacts with the degree of post-lesion adaptation/maladaptation (post-lesion plasticity being putatively localised to contralesional AC). Evidence from animal studies (Robertson and Irvine, 1989; Rajan et al., 1993; Seki and Eggermont, 2002; Noreña et al., 2003), and from human patients (Lockwood et al., 1998; Weisz et al., 2007; van der Loo et al., 2009), suggests contralesional cortex may play a selective role in expressing post-deafferentation plasticity, even when ipsilesional AC remains unperturbed. Importantly, even in those ferrets that displayed laser-mediated enhancements/impairments during contralesional suppression, equivalent changes were not seen during bilateral suppression. It may be that, prior to bilateral illumination testing, the extensive behavioural training and laser exposure under each unilateral condition had normalised the ferrets to laser illumination, counteracting the efficacy of the suppression paradigm. That >96% of units displayed robust suppression of spiking during neurophysiological recordings, and that different animals with different behavioural profiles exhibited *identical* bilateral suppression outcomes, are evidence against such normalisation, however.

This unilateral/bilateral discrepancy, alongside that between the lateralised changes in behaviour and the absence of corresponding physiological evidence (Chapter 4), may be explicable in terms of microcircuit-specific, deafferentation-mediated changes. Whereas there are no such studies in the auditory system, long-term monitoring of dendritic spine dynamics by chronic imaging of rodent barrel cortex has been conducted following whisker trimming/removal. Such studies have demonstrated that the cortical neuroplastic recovery process is long-lasting and highly site-specific, depending on the nature and location of the peripheral lesion

(Margolis et al., 2012; Schubert et al., 2013), with layer II/III cells being particularly likely to display lesion-related neuroplasticity (Celikel et al., 2004; Feldman, 2009). Similar effects have been observed following monocular deprivation in adult animals, where the rate of ocular dominance shifts – albeit slow – nevertheless yields cortical layer-specific map plasticity in the representation of the remaining sources of visual input (Hofer et al., 2006).

By analogy, SG lesion-related neuroplasticity might also manifest specifically in supragranular cells, and be specifically localised to contralesional AC (correlated with the distribution of Arg3.1/Arc expression; Fig.4-29). Since our laser suppression was applied superficially – at the cortical surface – it may be that, under these circumstances, the location of post-lesion adaptive/maladaptive plasticity was inhibited preferentially, with deeper thalamo-recipient and corticofugal circuit structures, themselves necessary for effective, perceptually-salient temporal processing, enduring optogenetic suppression to a lesser degree, as possibly indicated by the range of negative contralesional z-scores (Fig.5-14). Inhibition of post-lesion plasticity in supragranular circuitry could therefore normalise cortical information processing to a state somewhat resembling that expressed prior to deafferentation (we do not argue that behaviour is remediated absolutely – rather, that the direction of change is indicative of an *incremental* normalisation). The absence of behavioural effects during ipsilesional illumination may derive from the more-or-less normal operation of some undefined infragranular "gap-detection" circuitry, which remains less affected by superficially-applied laser illumination.

Any cortical laminar dependence of auditory temporal processing remains unresolved, despite the cortical code representing acoustic temporal modulation being rather well-understood (Wang et al., 2008). Nevertheless, evidence does exist indicating functional differences between information representation between layers, particular infra- vs. supra-granular (Szymanski et al., 2011). Of note is the enhanced responsivity in infragranular neurons to slow temporal modulation, enabling these units to operate in an essentially low-pass manner (Atencio and Schreiner, 2010; Christianson et al., 2011). This filtering mode befits these cells to encoding the slow temporal modulation inherent within the type of gap-in-noise acoustic stimuli utilised here. This is not to imply that deafferentation-mediated plasticity is not expressed in infragranular layers, with the gain enhancement effects described in Chapter 4 somewhat reminiscent of the type of computation mediated by layer-6 neurons (Olsen et al., 2012; Bortone et al., 2014). Rather, the circuits critical for post-lesion perceptual adaptation are possibly localised superficially, or elsewhere via intracortical connectivity from these layers.

The utility of this locus-specific hypothesis is implied in the improvement in contralesional neurometric gap-detection thresholds observed during laser illumination (Fig.5-14). Despite the generalised suppressive effects of laser illumination (Figs.5-13, 5-14), neurons remained capable of encoding silent gaps as spike-rate elevations at the gap onset/offset, though in the context of ongoing spiking activity that is uncorrelated with salient features of the sound. This type of apparently uncorrelated activity, or noise correlation, is associated with trial-to-trial variability in stimulus coding efficacy (Faisal et al., 2008). Evidence has shown that reductions in noise correlation strength can enhance auditory-driven behavioural discrimination

performance (Downer et al., 2015). Computational and experimental work has also indicated that enhanced cortical suppression may be capable of mediating this desirable reduction in noise correlation strength, especially within AC (Stringer et al., 2015). Thus, laser suppression, in our hands, may be dually operating to diminish the dominance of post-lesion mal/adaptive plasticity, and intervening in processes responsible for generating systemic noise.

Our unilateral suppression paradigm simultaneously induced minor, but significant, neurometric impairments in contralateral (right) AC, which was not subject to direct laser illumination. These effects were probably mediated by interhemispheric projections, via the corpus callosum. Anatomically, we observed GFP-derived fluorescence in the callosum of injected ferrets, indicating the structural validity of this hypothesis. In a recent study of information transfer between rodent ACs via cortico-calloso-cortical projections – the highest density of which terminate in cortical layers II/III (Kelly and Wong, 1981; Code and Winer, 1986) – optogenetic tools were used to define the output targets to layer V pyramidal cells (Rock and Apicella, 2015). It was found that direct feedforward inhibition of corticocortical projection neurons is mediated through fast-spiking parvalbumin-positive (PV^+) interneurons. Interestingly, PV^+ interneurons are putatively responsible for adaptive gain modulation in sensory cortices (Bortone et al., 2014), and represent a suitable substrate for mediating functional suppression of noise correlation strength (Stringer et al., 2015), likely through ensemble entrainment and enhanced network connectivity (Hamilton et al., 2013). As such, contralesional suppression, while improving coding fidelity locally, might produce disinhibition-mediated contralateral network decorrelation, through loss of afferent drive to PV^+ interneurons. Conversely, and in

agreement with our behavioural results, bilateral suppression may indeed yield few changes to cortical processing, with each AC undergoing mutually destructive suppression and disinhibition – though crude, the mechanistic basis for this outcome is plausible.

Finally, we postulate that a similar network as was responsible for suppression-mediated modification of gap-detection is leveraged during post-laser residual effects in non-laser trials, termed Residual Suppression (RS), after the Residual Inhibition (RI) paradigm used to characterise tinnitus (Feldmann, 1971; Roberts, 2007). For each ferret in our study, RS was observed for the same sounds as were affected by within-trial suppression. By analogy, RI in tinnitus patients spectrally overlaps with sounds that are similar to their tinnitus and hearing loss (Roberts et al., 2008, 2012). Though mechanistically unclear, RI has been hypothesised to derive from enhanced feedforward inhibitory drive within those circuits that are specifically involved in generating the tinnitus-like percept, and which show evidence of abnormal hyperactivity/hypersynchrony (Chapter 4). In humans, this abnormal hyperactivity putatively manifests as increased power in the theta-to-delta range of the LFP (De Ridder et al., 2015). During a recent ECoG study, RI did indeed diminish power in this oscillation range, although not in A1 (Sedley et al., 2015), the target of our optogenetic paradigm. Nevertheless, it remains wholly conceivable that RS is operationally similar to RI, with both occurring through the involvement of corticofugal pathways that affect auditory perception: of note are projections to striatum (Znamenskiy and Zador, 2013) and IC (Bajo et al., 2010b), each of which is important in the generation of behaviourally-salient auditory percepts.

Chapter 6

Discussion and Future Directions

6.1 Overview

The mammalian auditory system is constantly confronted with the challenge of ensuring the stability of auditory perception in the face of dynamic spectrotemporal changes in sound properties. Throughout this thesis, we have been interested in gaining a better understanding of how the auditory system, and particularly the auditory cortex (AC), copes with changes in the periphery. Usually, these take the form of rapid environmental modulations, owing to changes in external environment and listening conditions. However, when confronted with sensory deafferentation, a raft of structural and functional reactions take place. Over a range of time frames, these changes impact the neural encoding of sounds whose

characteristic properties are simultaneously liable to evoke altered patterns of activity as a result of the peripheral trauma.

It is specifically these changes that we aimed to explore in this thesis, for several reasons. First, numerous studies have indicated that neuroplasticity following hearing loss might well be associated with the subject's capacity to adapt, perceptually and behaviourally, to their altered acoustic environment (Keuroghlian and Knudsen, 2007). By isolating key neural circuits involved in post-deafferentation reactivity, and identifying their relationship to behaviour, hearing loss therapy could be designed more rationally, beyond simply replacing the damaged sensory organ (an option that may be unavailable in some hereditary or extremely traumatic cases).

Second, recent interest has developed in subjective tinnitus, wherein the subject perceives a sound without any corresponding environmental source. As a root cause of tinnitus may be maladaptive – possibly homeostatic – neuroplasticity within the central auditory system, targeting these processes may provide treatment options, of which there are presently none.

Finally, it is possible – indeed likely – that the neuroplasticity mechanisms available to the brain to cope with these large-scale changes in sensory function are similar to those employed more conventionally during quotidian neural activity, though probably more subtly; therefore, to understand the mechanisms underpinning the deafferentation response may provide insight into brain processes in general.

6.2 Summary of Chapter Contents

Given these challenges, we set out to explore the perceptual and correlated neuroplastic changes that follow a rationally-designed partial hearing loss. This hearing loss – a partial, unilateral, selective lesion of the spiral ganglion (SG) – was modelled on the kinds of pathologies observed commonly among human hearing loss patients, and associated with the occasional development of tinnitus.

The methods we employed to understand these changes were behavioural testing of gap-in-noise detection capabilities in ferrets and humans; auditory brainstem response (ABR) measurements and analysis; multiunit neurophysiological recordings made in ferret AC; optogenetic implantation in the ferret AC; and histological analysis of the lesioned spiral ganglion (SG), and central auditory system neurochemistry and anatomy.

Gap-in-Noise Detection Behaviour in Ferrets and Humans

Having recognised the putative link, based on previously published work, between hearing loss and auditory temporal processing deficits, we aimed to design an experimental paradigm that would enable us to reliably test auditory temporal processing capabilities in ferrets, our experimental animal of choice. We trained ferrets under operant conditioning to report the gap-in-noise content of spectrally varying sound stimuli, which were designed to broadly sample the ferret's behavioural and physiological audiogram. We demonstrated that, when well-trained, ferrets display gap-detection sensitivity that varies with the frequency content and bandwidth of the acoustic carrier noise, displaying lower thresholds and better overall performance when the noise was of a high-frequency or

broadband nature, compared with sounds within the low-to-mid frequency range of the audiogram. Furthermore, by testing human subjects on an adapted version of the task, we demonstrated that ferrets and humans are statistically equivalent in their gap-in-noise stimulus sensitivity. This study allowed us to conclude that ferrets would be a good animal model for exploring temporal processing deficits in a clinically-relevant manner.

Behavioural and Physiological Effects of Lesioning the Ferret Spiral Ganglion – A Possible Model of Tinnitus?

After establishing the ferret as an effective behavioural model of auditory temporal processing, we next asked what effects a selective hearing loss would have on gap-detection behaviour, and whether we could find physiological and/or anatomical signs that would robustly correlate with not only the hearing loss, but also any perceptual changes that emerged. The hearing loss imposed was a unilateral lesion of the right SG in the cochlear basal coil, an insult that mediated a significant, selective reduction in the density of cell bodies within the SG.

The behavioural changes we observed were heterogeneous, with some animals displaying a capacity for improvement in their gap-detection performance, whereas others displayed temporal processing deficits of varying degrees. We found that this behavioural heterogeneity was well-correlated with features of the ABR generated even in the naïve auditory nerve (i.e. prior to the lesion), implying the existence of some underlying structural and/or functional disadvantage in some animals and their capacity to adapt to deafferentation. Similarly, we found evidence for a reactive hyperactivity/hypersynchrony in the AC of behaviourally impaired

animals, alongside lesion-mediated gain changes in the cortical encoding of sounds, compared with unlesioned controls. Surprisingly, no substantial evidence was found for deficits in the AC neurometric representation of gap-in-noise stimuli in behaviourally impaired animals, suggesting that behavioural abnormalities are unlikely to have emerged simply as a function of low-level changes to the encoding of temporally modulated acoustic stimuli.

These results together indicate that there are identifiable markers for trauma-related plasticity throughout the central auditory system, and that these markers may in some way be related to the perceptual changes experienced following hearing loss.

Optogenetic Silencing of the Ferret Primary Auditory Cortex

In this final chapter, we were interested in exploring a potential causal role of AC in mediating the adaptive/maladaptive effects on perception after SG lesion. To this end, in lesioned animals with and without behavioural deficits, we performed bilateral injections of the optogenetic actuator ArchT, enabling the laser-mediated suppression of AC spiking activity during gap-detection behaviour.

Optogenetic cortical suppression had a subtle effect on ferret gap-detection behaviour during contralesional AC suppression, following a trend predicted by our initial hypothesis. Specifically, where animals had displayed post-lesion adaptation, cortical suppression tended to impair their behaviour; by contrast, where animals were behaviourally worsened following the lesion, optogenetic suppression occasioned a selective improvement in detection performance. The physiological bases for these changes were explored by recording AC multiunit

activity while laser-illuminating the contralesional cortical surface. These experiments demonstrated the capacity of optogenetic suppression to diminish cortical noise, improving the signal-to-noise ratio of gap-in-noise stimulus encoding and enhancing neurometric temporal processing capabilities.

6.3 Ongoing Work

By the nature of its longitudinal design, and the amount of time required to collect behavioural data, there are aspects of this project that remain to be completed prior to our findings being submitted for publication. At present, we are completing the behavioural testing, under bilateral laser illumination, of one lesioned animal that had undergone optogenetic implantation. We expect the results to be in line with those reported for the five other animals whose data for bilateral illumination (under which no treatment effect was found) are reported in Chapter 5. This animal is one of three optogenetically implanted ferrets that will undergo neurophysiological recordings in the near future. These recordings will take the same format as those reported in Chapters 4 and 5.

The brains of these animals will be removed, *post mortem*, for anatomical analysis as described in Chapters 4 and 5, while their cochleae will be sent to the Furness Laboratory at Keele University for analysis of post-lesion SG cell density changes. It is also our intention, in collaboration with Prof Furness, to prepare some specimens for transmission electron microscopy, to investigate whether there occur ultrastructural changes in cochlear morphology following mechanical deafferentation.

Additional experimental progress will involve the collection of important control data, to strengthen the claims to be made upon submission for publication. As outlined in Table 2-1, one animal (F1411) has undergone unilateral optogenetic implantation in the left AC, using an inactive (ArchT-) viral construct (pAAV8-CAG-GFP); another animal (F1438) has undergone bilateral, pAAV8-CAG-ArchT-GFP

injections in both ACs. Neither of these animals underwent SG lesion surgery. Both were behaviourally tested prior to implantation, and are currently being tested to provide negative and positive control data, respectively, for the effects of AC silencing and laser illumination on gap-detection behaviour without hearing loss.

6.4 Future Directions

6.4.1 Behavioural Evaluation of Auditory Temporal Processing

In the present experiments, we utilized a 1-alternative forced choice (1-afc) categorization paradigm with (ferrets) or without (humans) feedback[1] as a means of testing gap-in-noise detection behavioural performance. With respect to the ferret task in particular, it has been shown previously that 2-afc approaches are highly effective in measuring psychometric task performance in similar though unrelated stimulus paradigms (e.g. Walker et al., 2009; Bizley et al., 2013).

It has been claimed that threshold testing necessitates negative conditioning to ensure optimality of response generation (Heffner and Heffner, 2014). The focus of our work here was to characterize gap-in-noise detection behaviour in ferrets in relation to humans, how this behaviour changes as a result of hearing loss, and whether remediation is possible by targeting the putatively offending site of neuroplasticity. Therefore, while the negative conditioning assertion may well be true, there is presently no pressing reason to explore this means of motivating task performance. Furthermore, the unlikelihood of being able to negatively condition humans suggests that, going forward, any task designed to test comparative psychophysical performance is better suited to using positive conditioning. It has been suggested that the mode of behavioural testing can determine the circuitry involved, with AC necessarily co-opted during positive conditioning (Masterton

[1] A choice made to maintain task difficulty in human subjects. We note however that for both ferrets and humans, task performance was motivated by reward (water, for ferrets, and monetary reimbursement, for humans. It is unlikely that any other permutation of these reward measures among our behavioural subjects would have improved motivation levels).

and Berkley, 1974). Since this brain region was focal in our investigation, it may be that our behavioural paradigm was in fact optimally suited to the task at hand.

The use of gap-detection to test auditory temporal processing has been highly successful in a number of species, not least due to its amenability to variation in constituent stimulus design factors, including duration, amplitude, gap length, and spectral content. In exploiting these effective – albeit simple – stimuli, there remains a large number of possible stimulus content permutations that could offer further insight into temporal perception. These options have included the use of spatially separated stimuli (Phillips et al., 1998), sinusoidally modulated stimuli (Henderson et al., 1984; Shailer and Moore, 1987), the use of background noise maskers to selectively occlude gap detection (Shailer and Moore, 1985; Carmichael et al., 2008), or the presentation of pre- and post-gap noise bursts with differing spectral content to stimulate across auditory channels (Phillips and Smith, 2004). The use of these paradigms may allow a more fine-grained examination of underlying perceptual changes associated with peripheral auditory deafferentation.

In a broader sense, the gap-in-noise detection paradigm employed may be criticised for lacking in ethological relevance, since the existence of structured white-noise stimuli is largely absent from the ferret's natural environment. An alternative may instead be to explore aspects of temporal processing that are probed using more "ferret-relevant" stimuli, such as playback of recorded ferret vocalisations. Indeed, a recent study conducted in the green tree frog confirms the potential for exploring ethologically appropriate auditory-driven behaviour using species-specific vocalisations (Höbel, 2014). As such, it may well be worth

considering the use of natural stimuli during behavioural testing to explore any differential processing mechanisms these may reveal.

6.4.2 The Presence of Tinnitus?

In spite of the relevance and adaptability of this behavioural paradigm in a variety of testing contexts, a quandary that remains unresolved is whether or not the animals in this study actually display evidence of tinnitus, or if the perceptual changes that we report are merely "tinnitus-like" in character. That is, do the behavioural differences we have described occasionally reflect an internal phantom acoustic percept in some animals? On the basis of our data taken together, the question remains open, indicating the necessity for future behavioural work focussed upon tinnitus specifically, as opposed to hearing loss-related temporal processing deficits, which represent a major clinical challenge regardless (Schmiedt, 2010; Dubno et al., 2013).

One potential solution might involve training animal subjects to detect silence, rather than an arbitrarily chosen acoustic stimulus, since it is the absence of silence that effectively characterises the tinnitus condition. This approach has reportedly yielded some success (Stolzberg et al., 2013), particularly compared with the problematic aspects of other more commonly-used behavioural paradigms (Eggermont, 2013; Lobarinas et al., 2013; Gold and Bajo, 2014; Hickox and Liberman, 2014). It is therefore appropriate to pursue alternative behavioural measures that better recapitulate the subjective experience of tinnitus. For reasons enumerated in Chapter 3, the ferret remains a highly versatile animal model that is potentially well-suited to this work in the future, particularly given its capacity for long-term

monitoring across multiple treatment conditions, as we have demonstrated here. Fundamentally, it is only by way of accurate behavioural assays that it will be possible to determine what separates tinnitus from other perceptual abnormalities that are possibly inducible by auditory deafferentation.

In a similar vein, strides have been made in human studies by way of correlating activity and functional connectivity in/between defined brain regions, with the perceptual experience of tinnitus (Elgoyhen et al., 2015; Zobay et al., 2015). In a recent case study, tinnitus perception, and its temporary suppression using acoustic residual inhibition (RI) techniques (Roberts, 2007; Roberts et al., 2008), were directly correlated with changes in network activity in a tinnitus sufferer implanted cortically with electrocorticography (ECoG) arrays for the treatment of refractory epilepsy (Sedley et al., 2015a). General clinical conclusions drawn from this study are likely to have limited value, owing to the highly abnormal temporal lobe activity of this epileptic patient; however, as a methodological approach it certainly indicates a way forward in animal work. Our laboratory is presently optimising procedures for the chronic recording of cortical single-unit activity in awake behaving ferrets (Bizley et al., 2013). Following SG lesion, there was an intriguing relationship between the heterogeneity of behavioural changes following deafferentation, and the neurophysiological changes reported in anaesthetised ferrets (see Chapter 4).. This relationship begs the question as to how AC activity changes over time in alert animals following the introduction of hearing loss, and how these changes might relate to the differential capacity of certain individuals to adapt to partial deafferentation, compared with those that fail to do so.

In this regard, the behaviourally impaired/unimpaired nature of different ferrets in our study indicates the existence of underlying differences in the functionality of the auditory system. On the basis of the ABR data presented here, we have been provided a glimpse of these differences, and have hypothesised the existence of anatomical heterogeneity at the level of the cochlea that may affect the capacity of a subject to cope with subsequent hearing loss. Further exploration of these differences, based on previously reported cochlear cytoarchitectural features (Fekete et al., 1984; Liberman, 1991, 1993; Tsuji and Liberman, 1997) is certainly warranted.

It is also known that the central auditory system possesses adaptive capabilities in the face of sporadic hearing loss, facilitating enhanced auditory scene analysis when allowed sufficient time for adaptation (Keating et al., 2013, 2015). This adaptation may fundamentally rely upon activity in the AC, including its corticocollicular connections (Bajo et al., 2010b; Nodal et al., 2010, 2012), and the likely influence of extra-cortically-derived neuromodulatory agents (Kamke et al., 2005; Leach et al., 2013; Froemke, 2014; Marlin et al., 2015; Martins and Froemke, 2015). It would thus be interesting to determine how these cortical and non-cortical circuits are differentially affected by deafferentation, and how they may impair/improve an animal's capacity to cope with a modified acoustic environment.

6.4.3 Perceptual Interventions: Opportunities for Amelioration?

In addition to exploring neuromodulatory influences on cortical plasticity, a starting point for future experiments is to further dissect the cortical circuitry specifically

responsible for mediating the behavioural heterogeneity seen during AC suppression. The promoter gene used in our construct to mediate ArchT expression was CAG, which was developed to yield high gene-product expression levels in all transfected cells (Niwa et al., 1991). Clearly, this precludes cell-type specificity during optogenetic silencing. In conceiving future work in the ferret, similar viral constructs that contain alternative promoter segments could be of great value, under otherwise identical experimental protocols. For example, the Thy1 promoter may allow optogenetic targeting of projection neurons in AC (Feng et al., 2000). Alternatively, the CaMKII promoter would enable specific transfection of excitatory cell types, an approach that we have successfully applied in our laboratory to explore the differential role of excitatory/inhibitory neurons in learning-related adaptation (Bajo et al., in preparation).

Optogenetic investigation using transgenic mouse lines may represent a useful avenue for exploring the roles of specific subpopulations of cells in adaptive/maladaptive plasticity. Using the cre-lox system for recombinant expression of optogenetic tools, Weible and colleagues have demonstrated distinct roles for parvalbumin- and somatostatin-positive inhibitory interneuron types in governing gap-prepulse inhibition of the acoustic startle reflex (GPIAS) (Weible et al., 2014). Though robust in mice, GPIAS displays rapid habituation in larger mammalian species (Gruner, 1989; Pilz and Leaton, 1999), and its role in revealing conscious perceptual features is unclear (Eggermont, 2013; Fournier and Hébert, 2013; Gold and Bajo, 2014). As such, much value could be gained from repeating those mouse experiments in an operant task like that described here and elsewhere (Radziwon et al., 2009; Gold et al., 2015). Additionally, the use of excitatory

optogenetic tools like channelrhodopsin-2 (Boyden et al., 2005) or Chronos (Klapoetke et al., 2014) for high-resolution excitation of these same cortical circuits would allow for the opposite hypotheses to be tested to those examined under ArchT-mediated suppression. These enhancement experiments would be necessary for understanding the origin of the behavioural heterogeneity reported here. Finally, the emergence of novel gene-editing technologies, based on bacterial defence mechanisms (e.g. CRISPR-Cas9), indicate a possible means by which transgenic ferrets could be utilised experimentally, in much the same capacity as mice (Sander and Joung, 2014); though very much in the future, experiments of this kind would allow site-specific exploration of neuroplastic mechanisms, while retaining the behavioural and translational superiority of the ferret.

The use of closed-loop optogenetic paradigms offers an approach to modifying neural activity in a feedback-dependent manner, adjusting the stimulation parameters according to simultaneously recorded neural activity states (Grosenick et al., 2015). This approach putatively lends itself to developing a better model of RI, which may depend upon oscillatory state transitions at defined sites within AC (Roberts, 2007; Sedley et al., 2015a). ECoG arrays used in rats have been successfully demonstrated in this regard (Stolzberg et al., 2013), and their adaptation to closed-loop use in ferrets would not represent a great technical challenge. Simultaneous coupling of recording arrays such as these, or those used previously in our laboratory (Bizley et al., 2013), with LED- or laser-based arrays for optogenetic intervention would be optimal. The gold standard approach would involve the use of optical arrays that allow depth-specific control of neural activity: whether incorporated as, for example, coupled LED-tetrode probes (Stark et al.,

2012) or multipoint-emitting optical fibres paired with extracellular Michigan-style probes (Pisanello et al., 2014), such experiments would be ideal for evaluating the layer-specific neuroplasticity hypothesis proposed in Chapter 5.

6.4.4 Relevance to Human Subjects and Patients

Although experiments in human subjects formed only a small component of this project, it was an important one, to verify the possible relevance of the behavioural paradigm used in ferrets to clinical progress in hearing loss and tinnitus. While the gap-detection experiments from Chapter 3 successfully demonstrated the value of the ferret as an experimental model, we have yet to determine how human subjects would perform under our behavioural paradigm when challenged by hearing loss of various forms. These data would offer insight into solving the current controversy about the use of temporal processing paradigms to characterise and objectively categorise tinnitus itself, as opposed to accompanying hearing loss or other perceptual disorders such as hyperacusis (Campolo et al., 2013; Eggermont, 2013; Fournier and Hébert, 2013; Hébert et al., 2013; Mehdizade Gilani et al., 2013; An et al., 2014; Boyen et al., 2015; Moon et al., 2015).

To this end, we are currently undertaking a study exploring gap-in-noise sensitivity in a selection of subjects. At present, we have collected a control dataset from a larger cohort (n = 12) of healthy, young listeners with clinically normal audiograms as part of a Final Honours School undergraduate project, co-supervised by the author. Aside from being tested on a broader range of sound frequencies and a larger number of silent gap lengths, listeners were subject to randomised trials during which stimuli were filtered to approximate the

audiological effects of sensorineural presbyacusis (conceived as a sloping low-pass filter, after Lee et al. (2005), & Dubno et al. (2013)). These data are presently being analysed. In future experiments, we will be recruiting sufferers of presbyacusis and tinnitus to attempt to disentangle the perceptual features of each condition.

While functional studies of human brain function have been highly successful in characterising the correlates of tinnitus and hearing loss with respect to changes in connectivity and signal power in different regions of the forebrain, there has been little effort to describe the neurochemical processes that may underlie these functional derangements. One hypothesis proposed by our work, and that of others (Chrostowski et al., 2011; Zeng, 2013; Eggermont and Tass, 2015; Noreña, 2015), suggests a role for modified excitatory/inhibitory balance in prescribed regions of the central auditory system, which may be correlated not only with the development of tinnitus, but more broadly with post-insult neuroplasticity. At the basic experimental level, it would be interesting to explore these possibilities in our animal model: functionally, changes in frequency response area inhibitory sideband activity following deafferentation have been appreciated for close to two decades (Rajan, 1998, 2001). With our present experimental setup, it may be possible to explore these features of neuronal spectrotemporal receptive fields (STRFs) by utilising dynamic random chord (DRC) stimuli during neurophysiological recordings (Linden et al., 2003). In addition to affording insight into the temporal dynamics of the excitatory/inhibitory subfields of neuronal responses, these stimuli may also be employed to investigate post-lesion changes in neuronal response gain (Rabinowitz et al., 2011, 2012), as postulated in Chapter 4.

Neural coding changes of these types imply correlated neurochemical changes that are associated with modulations in synaptic signalling. Recent studies at the University of Oxford Centre for the Functional MRI of the Brain (FMRIB) have utilised high-tesla magnetic resonance scanners for spectroscopic analysis of synaptic neurochemicals, including major neurotransmitters like GABA (γ-aminobutyric acid) (Stagg, 2014). This approach – magnetic resonance spectroscopy (MRS) – can be leveraged to explore the neurochemical underpinnings of structural and functional changes in brain states, putatively providing insight into neuroplastic modulation following learning or deafferentation (Stagg, 2014; Sampaio-Baptista et al., 2015). A recent study of this type has been published by Griffiths and colleagues, suggesting a lateralised reduction in GABA concentrations in right AC of tinnitus patients, irrespective of the lateralisation of the percept (Sedley et al., 2015b). Their study demonstrates the experimental potential of this approach, particularly if it were paired with objective psychophysical evaluation, as opposed to the self-reporting used therein. At present, we have undertaken pilot measurements of GABA concentration in AC of control subjects (n = 2), without acoustic stimulation; we hope to expand these data to include clinical patients, as above.

Moreover, interventional possibilities have been offered by technologies such as transcranial Direct Current Stimulation (tDCS), the effects of which may be monitored non-invasively using MRS approaches (Bachtiar et al., 2015). Caution is certainly necessary in applying neuromodulatory systems such as tDCS or deep brain stimulation (Krause and Kadosh, 2014; Sarkar et al., 2014; Smit et al., 2015). Nevertheless, the opportunity to test hypotheses regarding the functional role of

particular brain regions in tinnitus and hearing loss using potentially neuro-enhancing techniques (Krause and Kadosh, 2013) may offer therapeutic opportunities in sufferers of abnormal auditory function and tinnitus. Indeed, optogenetic technologies have been proposed for interventional clinical access (Chow and Boyden, 2013) – though they remain distant from surgical implementation, the current use of gene-targeted therapies mediated through AAV-based approaches suggests that clinical optogenetics holds promise in the future.

Ultimately, the findings from this thesis suggest not only possible interventional targets or foci of abnormal plasticity that may be related to tinnitus or the cognitive effects of hearing loss, but also opportunities for prevention. We have described the emergence of intriguing relationships between behavioural changes, baseline ABR differences stemming from the cochlea/auditory nerve, neurophysiological features in AC activity, and anatomical markers indicating specific sites of post-lesion plasticity. Together, these findings may imply that certain subjects – animal or human – may be fundamentally predisposed to experience substantial negative effects of hearing loss, largely in terms of their capacity to optimally adapt to their modified auditory environment. If this constellation of features is predictive for tinnitus, the clinical potential to reduce the risk of developing the condition in later life is certainly exciting.

Appendix

A. Gap-in-Noise Behaviour: Performance vs. Response Times

Percent-gap response data were pooled across sessions, and then segmented according to when the response was registered relative to the stimulus (rather than in absolute post-stimulus onset time): for gap stimuli, response segments were assigned as responses falling between the onset of the 3rd gap and before the onset of 4th gap, after the onset of the 4th gap and before the offset of the stimulus, or after the offset of the stimulus. Due to the low number of responses occurring before the onset of the 3rd gap, these trials were excluded. For no-gap stimuli, a similar approach was applied by segmenting the stimulus into equivalent response segments (3/5ths to 4/5ths through the stimulus; 4/5ths to 5/5ths through the stimulus; and after stimulus offset). Psychometric functions were generated for each of the three response segments using the algorithm described above.

As a means of testing the hypothesis that the ferret's decision criterion for response generation might be changing as a function of time, we evaluated the partial percent-gap psychometric functions for each animal, with responses segmented according to when, in the course of the stimulus, each response was registered. In theory, each stimulus type (defined according to the gap length) could be broken into equal segments, divided by the onset of each gap (and the onset/offset of the acoustic stimulus itself), thereby yielding a stimulus-normalised windowing approach to classifying responses. In practice, however, the vast majority (>99%) of responses were registered in one of three windows: between the onset of the third gap and the onset of the fourth gap (window 4); between the onset of the fourth gap and the offset of the stimulus (window 5); or between the offset of the stimulus and 6 seconds after stimulus onset (window 6). This latter window, while broader, represents the entirety of the post-stimulus period absent of acoustic stimulus that we analysed for response times, since all responses after 6 seconds were omitted. As such, we evaluated partial psychometric functions for each of these three windows for each of the stimuli presented (Fig.A-1).

As is evident from Fig.A-1, individual animals displayed significant shifts in their percent-gap psychometric functions during the course of the stimulus. In one example (F1226), trials performed later in time were associated with a higher proportion of "gap" responses for both gap and no-gap stimuli, yielding a corresponding increase in both hit and FA rates. While most animals responded in this fashion, one animal (F1228) displayed the inverse criterion shifts, with later responses displaying a clear rightward/no-gap bias. This case indicates that obvious animal-to-animal differences were present in the decision criterion placement, and

thus the behavioural task performance approach, as evidenced by the stimulus*ferret interaction described above. Nevertheless, across all stimuli, when each animal's responses were pooled and evaluated by binomial mixed-effects modelling, the effect of response window was highly significant in explaining the variance of the percent-gap values, even when accounting for animal identity and gap length (lme: 1 kHz NBN: $t = 10.92$; 4 kHz NBN: $t = 17.56$; 16 kHz NBN: $t = 18.44$; BBN: $t = 23.72$; $p < 0.0001$ in each case) (Fig.A-1). In particular, this effect was driven by highly significant differences (post-hoc Tukey, $p < 0.05$) between the responses in windows 4 and 5 for each stimulus, with a significant post-hoc effect also observed between windows 4 and 6 for 16 kHz NBN. The existence of these time-varying changes in the animal's decision criterion are possibly indicative of a number of factors, such as information acquisition as a function of time spent listening to the stimulus, allowing the animal to update its choice approach.

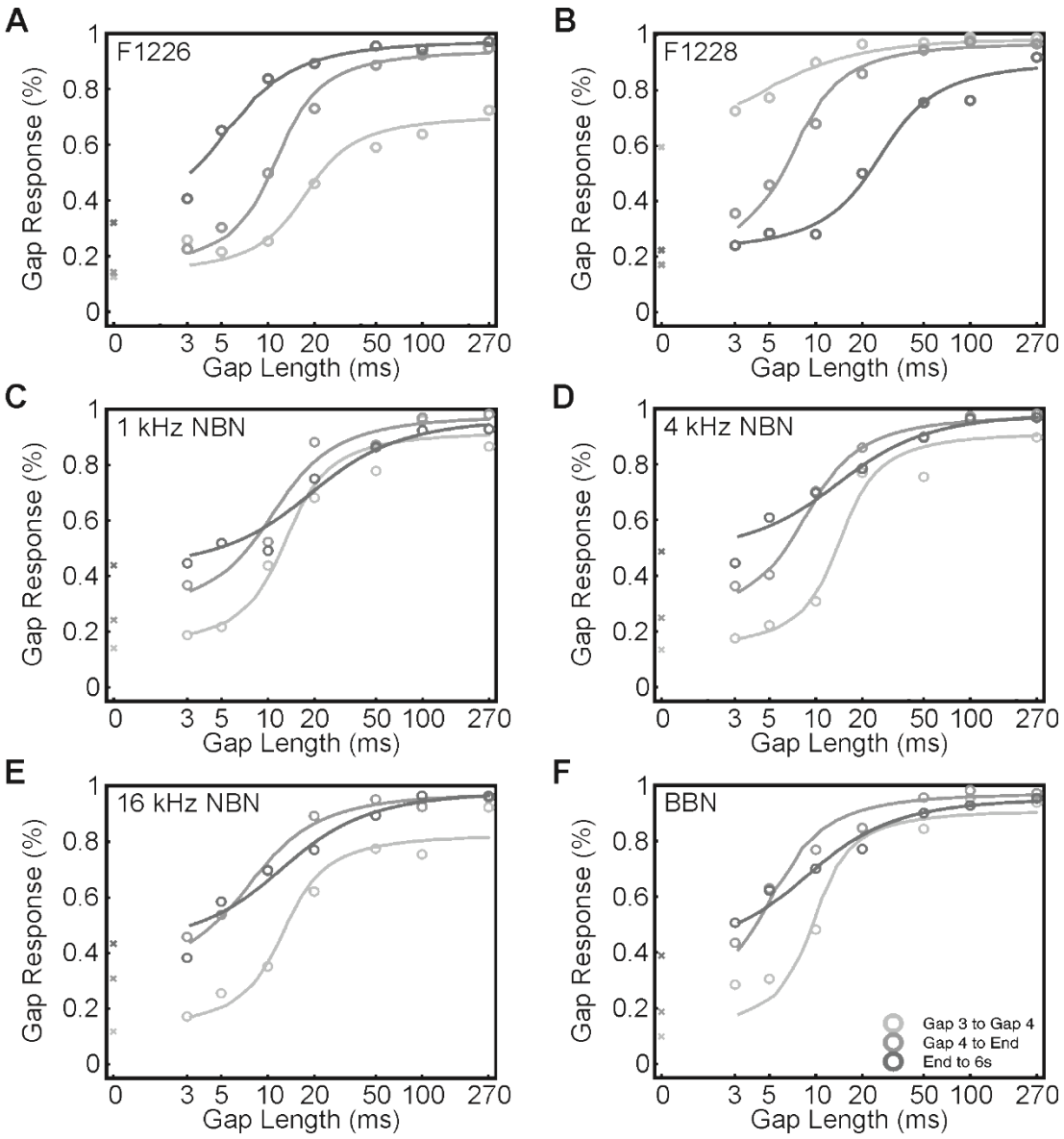

Figure A.1.: Psychometric functions of the proportion of "gap" responses (percent-gap) plotted as a function of gap-length (where no-gap is equivalent to gap length = 0); functions obtained as subsets of the original pooled datasets according to the time window during which the response was registered after the onset of the stimulus: between the onset of the third gap and the onset of the fourth gap (window 4; light grey); between the onset of the fourth gap and the offset of the stimulus (window 5; mid grey); between the offset of the stimulus and 6 seconds post-stimulus onset (window 6; dark grey). A, B) Example psychometrics functions for ferrets F1226 and F1228, representing all trials collapsed across stimulus type. In each case, stimulus periods **4 and 6 were significantly different at $p < 0.05$. C, D, E, F) Pooled psychometric functions across all animals, segregated according to stimulus type.**

Following the introduction of the SG lesion, by examining the relationship between response times and percent-gap scores, it emerged that animals integrated information over the course of the stimulus in a similar fashion, largely irrespective of detection performance. Specifically, during the stimulus presentation, the likelihood of generating a gap response was significantly higher following SG lesion (Fig.A-2). The correlated elevation in FA rates, however, yielded an overall reduction in detection sensitivity, suggesting that in general auditory temporal integration was impaired as a result of the SG lesion. Importantly, the absence of such differences for responses generated after the end of the acoustic stimulus suggests that information integration had concluded by this stage, and so that the animals' decision processes were no longer affected by the lesion.

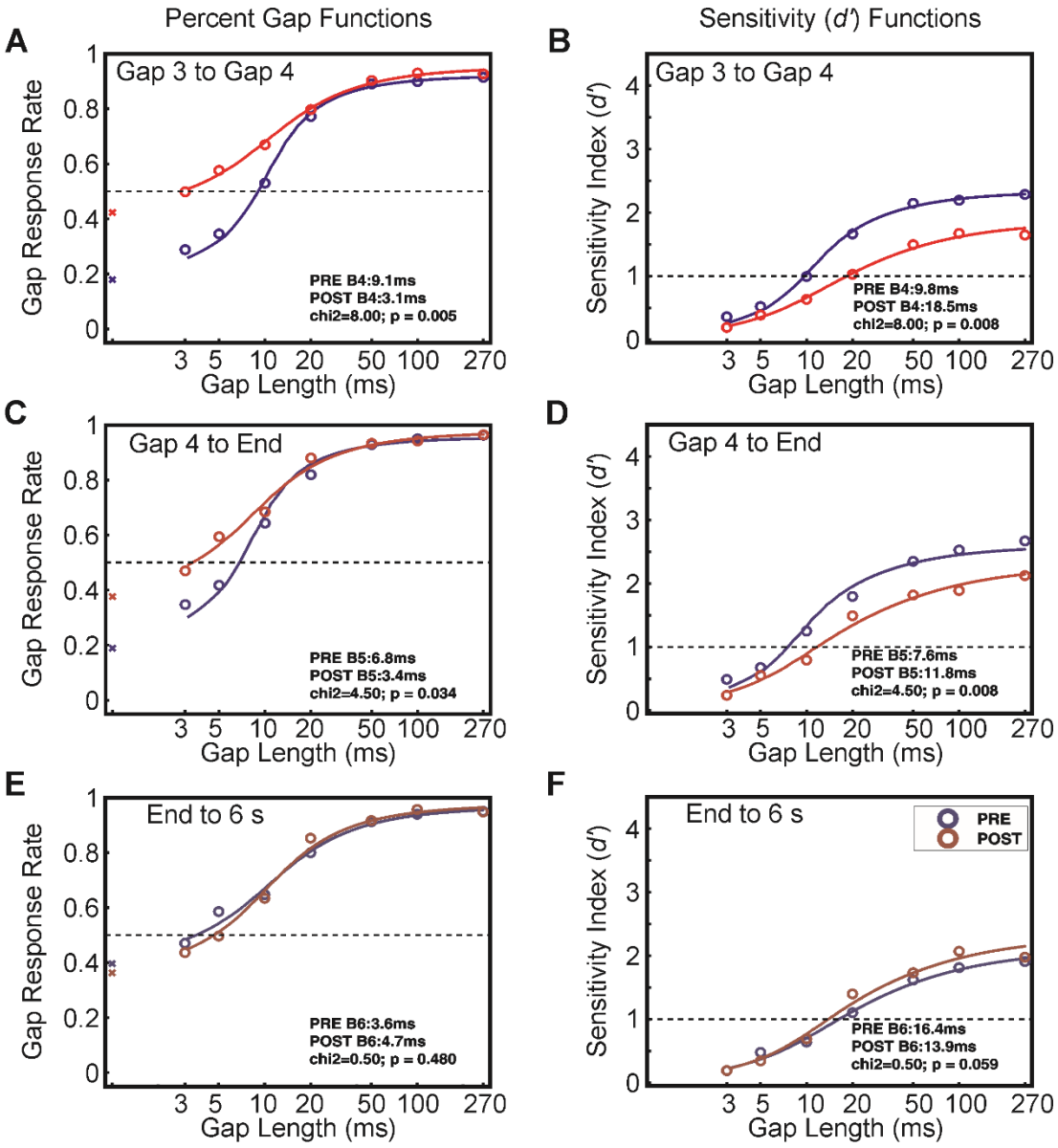

Figure A-2: Gap detection performance as a function of response time. Psychometric functions were fitted as right-weighted gumbel sigmoids to data from all animals. Pre-lesion = blue; postlesion = red. Left column = percent-gap performance; right column = d' sensitivity. In each panel, text describes pre- and post-lesion gap length at threshold (50% for percent gap; d' = 1 for sensitivity functions), and χ^2 and p values for pre- vs. post-lesion Friedman test. A, B) Responses made between the end of gap 3, and the start of gap 4. C, D) Responses made between the end of gap 4, and the offset of the acoustic stimulus. E, F) Responses made between the offset of the acoustic stimulus and 6 seconds after stimulus onset

References

Agrawal Y, Platz EA, Niparko JK (2008) Prevalence of hearing loss and differences by demographic characteristics among US adults: data from the National Health and Nutrition Examination Survey, 1999-2004. Arch Intern Med 168:1522–1530.

Ahlf S, Tziridis K, Korn S, Strohmeyer I, Schulze H (2012) Predisposition for and prevention of subjective tinnitus development. PLoS One 7:e44519.

Allen PD, Burkard RF, Ison JR, Walton JP (2003) Impaired gap encoding in aged mouse inferior colliculus at moderate but not high stimulus levels. Hear Res 186:17–29.

Allen PD, Virag TM, Ison JR (2002) Humans detect gaps in broadband noise according to effective gap duration without additional cues from abrupt envelope changes. J Acoust Soc Am 112:2967.

Allman BL, Keniston LP, Meredith MA (2009) Adult deafness induces somatosensory conversion of ferret auditory cortex. Proc Natl Acad Sci U S A 106:5925–5930.

Alves-Pinto A, Baudoux S, Palmer AR, Sumner CJ (2010) Forward masking estimated by signal detection theory analysis of neuronal responses in primary auditory cortex. J Assoc Res Otolaryngol 11:477–494.

Alves-Pinto A, Sollini J, Sumner CJ (2012) Signal detection in animal psychoacoustics: Analysis and simulation of sensory and decision-related influences. Neuroscience 220:215–227.

An Y, Jin SY, Yoon SW, Shim HJ (2014) The effects of unilateral tinnitus on auditory temporal resolution: gaps-in-noise performance. Korean J Audiol 18:119–125.

Asako M, Holt AG, Griffith RD, Buras ED, Altschuler R a (2005) Deafness-related decreases in glycine-immunoreactive labeling in the rat cochlear nucleus. J Neurosci Res 81:102–109.

Atencio CA, Schreiner CE (2010) Laminar Diversity of Dynamic Sound Processing in Cat Primary Auditory Cortex. J Neurophysiol 103:192–205.

Atiani S, David S V, Elgueda D, Locastro M, Radtke-Schuller S, Shamma SA, Fritz JB (2014) Emergent selectivity for task-relevant stimuli in higher-order auditory cortex. Neuron 82:486–499.

Axelsson A, Sandh A (1985) Tinnitus in noise-induced hearing loss. Br J Audiol 19:271–276.

Azim E, Jiang J, Alstermark B, Jessell TM (2014) Skilled reaching relies on a V2a propriospinal internal copy circuit. Nature.

Bachtiar V, Near J, Johansen-Berg H, Stagg CJ (2015) Modulation of GABA and resting state functional connectivity by transcranial direct current stimulation. Elife 10.7554.

Baguley D, McFerran D, Hall D (2013) Tinnitus. Lancet 382:1600–1607.

Bajo VM, King AJ (2012) Cortical modulation of auditory processing in the midbrain. Front Neural Circuits 6:114.

Bajo VM, Korn C, Reynolds K, Boyden ES, Nodal FR, King AJ (2013) Behavioural and neural effects of silencing the auditory cortex in adult ferrets using optogenetics. In: Society for Neuroscience Abstracts, pp 873–878.

Bajo VM, Nodal FR, Bizley JK, King AJ (2010a) The non-lemniscal auditory cortex in ferrets: convergence of corticotectal inputs in the superior colliculus. Front Neuroanat 4:18.

Bajo VM, Nodal FR, Bizley JK, Moore DR, King AJ (2007) The ferret auditory cortex: descending projections to the inferior colliculus. Cereb Cortex 17:475–491.

Bajo VM, Nodal FR, Moore DR, King AJ (2010b) The descending corticocollicular pathway mediates learning-induced auditory plasticity. Nat Neurosci 13:253–260.

Baldo P, Doree C, Molin P, McFerran D, Cecco S (2012) Antidepressants for patients with tinnitus. Cochrane database Syst Rev 9:CD003853.

Banay-Schwartz M, Lajtha a, Palkovits M (1989a) Changes with aging in the levels of amino acids in rat CNS structural elements. II. Taurine and small neutral amino acids. Neurochem Res 14:563–570.

Banay-Schwartz M, Lajtha A, Palkovits M (1989b) Changes with aging in the levels of amino acids in rat CNS structural elements. I. Glutamate and related amino acids. Neurochem Res 14:555–562.

Banks M, Smith P (2011) Thalamocortical Relations. In: The Auditory Cortex (Winer JA, Schreiner CE, eds), pp 73–98. New York: Springer New York.

Barsz K, Ison JR, Snell KB, Walton JP (2002) Behavioral and neural measures of auditory temporal acuity in aging humans and mice. Neurobiol Aging 23:565–578.

Bauch CD, Olsen WO, Pool AF (1996) ABR Indices. Am J Audiol 5:97.

Bauer CA, Brozoski TJ (2001) Assessing tinnitus and prospective tinnitus therapeutics using a psychophysical animal model. J Assoc Res Otolaryngol 2:54–64.

Béïque J, Na Y, Kuhl D, Worley PF, Huganir RL (2011) Arc-dependent synapse-specific homeostatic plasticity. Proc Natl Acad Sci U S A 108:816–821.

Bennett MH, Kertesz T, Perleth M, Yeung P, Lehm JP (2012) Hyperbaric oxygen for idiopathic sudden sensorineural hearing loss and tinnitus. Cochrane database Syst Rev 10:CD004739.

Berger JI, Coomber B (2015) Tinnitus-related changes in the inferior colliculus. Front Neurol 6:1–12.

Berger JI, Coomber B, Shackleton TM, Palmer AR, Wallace MN (2013) A novel behavioural approach to detecting tinnitus in the guinea pig. J Neurosci Methods 213:188–195.

Berger JI, Coomber B, Wells TT, Wallace MN, Palmer AR (2014) Changes in the response properties of inferior colliculus neurons relating to tinnitus. Front Neurol 5:203.

Bizley JK, Bajo VM, Nodal FR, King AJ (2015) Cortico-cortical connectivity within ferret auditory cortex. J Comp Neurol 00:n/a – n/a.

Bizley JK, Nodal FR, Nelken I, King AJ (2005) Functional organization of ferret auditory cortex. Cereb Cortex 15:1637–1653.

Bizley JK, Nodal FR, Parsons CH, King AJ (2007) Role of auditory cortex in sound localization in the midsagittal plane. J Neurophysiol 98:1763–1774.

Bizley JK, Walker KMM, Nodal FR, King AJ, Schnupp JWH (2013) Auditory cortex represents both pitch judgments and the corresponding acoustic cues. Curr Biol 23:620–625.

Bledsoe SC, Koehler S, Tucci DL, Zhou J, Le Prell C, Shore SE (2009) Ventral cochlear nucleus responses to contralateral sound are mediated by commissural and

olivocochlear pathways. J Neurophysiol 102:886–900.

Bortone DS, Olsen SR, Scanziani M (2014) Translaminar Inhibitory Cells Recruited by Layer 6 Corticothalamic Neurons Suppress Visual Cortex. Neuron:1–12.

Boyden ES, Zhang F, Bamberg E, Nagel G, Deisseroth K (2005) Millisecond-timescale, genetically targeted optical control of neural activity. Nat Neurosci 8:1263–1268.

Boyen K, Başkent D, van Dijk P (2015) The Gap Detection Test. Ear Hear:1.

Bramham CR, Alme MN, Bittins M, Kuipers SD, Nair RR, Pai B, Panja D, Schubert M, Soule J, Tiron A, Wibrand K (2010) The Arc of synaptic memory. Exp brain Res 200:125–140.

Brosch M, Schreiner CE (1999) Correlations between neural discharges are related to receptive field properties in cat primary auditory cortex. Eur J Neurosci 11:3517–3530.

Buchwald JS, Huang C (1975) Far-field acoustic response: origins in the cat. Science 189:382–384.

Buck L (1966) Reaction time as a measure of perceptual vigilance. Psychol Bull 65:291–304.

Buonomano D V, Merzenich MM (1998) Cortical plasticity: from synapses to maps. Annu Rev Neurosci 21:149–186.

Buran BN, Sarro EC, Manno F a. M, Kang R, Caras ML, Sanes DH (2014) A Sensitive Period for the Impact of Hearing Loss on Auditory Perception. J Neurosci 34:2276–2284.

Buran BN, Strenzke N, Neef A, Gundelfinger ED, Moser T, Liberman MC (2010) Onset coding is degraded in auditory nerve fibers from mutant mice lacking synaptic ribbons. J Neurosci 30:7587–7597.

Buras ED, Holt AG, Griffith RD, Asako M, Altschuler R a (2006) Changes in glycine immunoreactivity in the rat superior olivary complex following deafness. J Comp Neurol 494:179–189.

Busby PA, Clark GM (1999) Gap detection by early-deafened cochlear-implant subjects. J Acoust Soc Am 105:1841–1852.

Buunen TJ, van Valkenburg D a (1979) Auditory detection of a single gap in noise. J Acoust Soc Am 65:534–536.

Cai S, Ma W-LD, Young ED (2009) Encoding intensity in ventral cochlear nucleus following acoustic trauma: implications for loudness recruitment. J Assoc Res Otolaryngol 10:5–22.

Calford MB (2002) Dynamic representational plasticity in sensory cortex. Neuroscience 111:709–738.

Calford MB, Rajan R, Irvine DR (1993) Rapid changes in the frequency tuning of neurons in cat auditory cortex resulting from pure-tone-induced temporary threshold shift. Neuroscience 55:953–964.

Campolo J, Lobarinas E, Salvi R (2013) Does tinnitus "fill in" the silent gaps? Noise Health 15:398–405.

Carmichael ME, Hall SE, Phillips DP (2008) Ear and contralateral masker effects on auditory temporal gap detection thresholds. Hear Res 245:18–23.

Caspary DM, Ling L, Turner JG, Hughes LF (2008) Inhibitory neurotransmission, plasticity and aging in the mammalian central auditory system. J Exp Biol 211:1781–1791.

Celikel T, Szostak VA, Feldman DE (2004) Modulation of spike timing by sensory deprivation during induction of cortical map plasticity. Nat Neurosci 7:534–541.

Chen G, Lee C, Sandridge S a, Butler HM, Manzoor NF, Kaltenbach J a (2013) Behavioral evidence for possible simultaneous induction of hyperacusis and tinnitus following intense sound exposure. J Assoc Res Otolaryngol 14:413–424.

Cheung SW, Bonham BH, Schreiner CE, Godey B, Copenhaver D a (2009) Realignment of interaural cortical maps in asymmetric hearing loss. J Neurosci 29:7065–7078.

Chow BY, Boyden ES (2013) Optogenetics and Translational Medicine. Sci Transl Med 5:1–5.

Chow BY, Han X, Dobry AS, Qian X, Chuong AS, Li M, Henninger M a, Belfort GM, Lin Y, Monahan PE, Boyden ES (2010) High-performance genetically targetable optical neural silencing by light-driven proton pumps. Nature 463:98–102.

Christianson GB, Sahani M, Linden JF (2011) Depth-Dependent Temporal Response Properties in Core Auditory Cortex. J Neurosci 31:12837–12848.

Chrostowski M, Yang L, Wilson HR, Bruce IC, Becker S (2011) Can homeostatic plasticity in deafferented primary auditory cortex lead to travelling waves of excitation? J Comput Neurosci 30:279–299.

Code RA, Winer JA (1986) Columnar organization and reciprocity of commissural connections in cat primary auditory cortex (AI). Hear Res 23:205–222.

Cohen GM, Park JC, Grasso JS (1990) Comparison of demyelination and neural degeneration in spiral and Scarpa's ganglia of C57BL/6 mice. J Electron Microsc Tech

15:165–172.

Coomber B, Berger JI, Kowalkowski VL, Shackleton TM, Palmer AR, Wallace MN (2014) Neural changes accompanying tinnitus following unilateral acoustic trauma in the guinea pig. Eur J Neurosci 40:2427–2441.

Coomber B, Kowalkowski VL, Berger JI, Palmer AR, Wallace MN (2015) Modulating Central Gain in Tinnitus: Changes in Nitric Oxide Synthase in the Ventral Cochlear Nucleus. Front Neurol 6:1–12.

Coote EJ, Rees a (2008) The distribution of nitric oxide synthase in the inferior colliculus of guinea pig. Neuroscience 154:218–225.

Dallos P, Harris D (1978) Properties of auditory nerve responses in absence of outer hair cells. J Neurophysiol 41:365–383.

Dazert S, Feldman ML, Keithley EM (1996) Cochlear spiral ganglion cell degeneration in wild-caught mice as a function of age. Hear Res 100:101–106.

De Ridder D, Joos K, Vanneste S (2014) The enigma of the tinnitus-free dream state in a Bayesian world. Neural Plast 2014.

De Ridder D, Vanneste S (2014) Auditory Cortex Stimulation Might be Efficacious in a Subgroup of Tinnitus Patients. Brain Stimul 7:917–918.

De Ridder D, Vanneste S, Langguth B, Llinas R (2015) Thalamocortical dysrhythmia : a theoretical update in tinnitus. Front Neurol 6.

de Villers-Sidani E, Alzghoul L, Zhou X, Simpson KL, Lin RCS, Merzenich MM (2010) Recovery of functional and structural age-related changes in the rat primary auditory cortex with operant training. Proc Natl Acad Sci U S A 107:13900–13905.

DeFilippo CL, Snell KB (1986) Detection of a temporal gap in low-frequency narrow-band signals by normal-hearing and hearing-impaired listeners. J Acoust Soc Am 80:1354–1358.

Dehmel S, Eisinger D, Shore SE (2012a) Gap prepulse inhibition and auditory brainstem-evoked potentials as objective measures for tinnitus in guinea pigs. Front Syst Neurosci 6:42.

Dehmel S, Pradhan S, Koehler S, Bledsoe S, Shore S (2012b) Noise overexposure alters long-term somatosensory-auditory processing in the dorsal cochlear nucleus--possible basis for tinnitus-related hyperactivity? J Neurosci 32:1660–1671.

Dolan TR, Ades HW, Bredberg G, Neff WD (1975) Inner ear damage and hearing loss after exposure to tones of high intensity. Acta Otolaryngol 80:343–352.

Do-Monte FH, Quinones-Laracuente K, Quirk GJ (2015) A temporal shift in the

circuits mediating retrieval of fear memory. Nature 519:460–463.

Don M, Kwong B, Tanaka C, Brackmann D, Nelson R (2005) The stacked ABR: a sensitive and specific screening tool for detecting small acoustic tumors. Audiol Neurootol 10:274–290.

Dong S, Mulders WH a M, Rodger J, Robertson D (2009) Changes in neuronal activity and gene expression in guinea-pig auditory brainstem after unilateral partial hearing loss. Neuroscience 159:1164–1174.

Dooling RJ, Zoloth SR, Baylis JR (1978) Auditory sensitivity, equal loudness, temporal resolving power, and vocalizations in the house finch (Carpodacus mexicanus). J Comp Physiol Psychol 92:867–876.

Doron NN, LeDoux JE (1999) Organization of Projections to the Lateral Amygdala From Auditory and Visual. J Comp Neurol 412:383–409.

Downer JD, Niwa M, Sutter ML (2015) Task Engagement Selectively Modulates Neural Correlations in Primary Auditory Cortex. J Neurosci 35:7565–7574.

Druga R, Syka J (1993) NADPH-diaphorase activity in the central auditory structures of the rat. Neuroreport 4:999–1002.

Dubno JR, Eckert M a., Lee FS, Matthews LJ, Schmiedt R a. (2013) Classifying human audiometric phenotypes of age-related hearing loss from animal models. JARO - J Assoc Res Otolaryngol 14:687–701.

Eddins D a, Hall JW, Grose JH (1992) The detection of temporal gaps as a function of frequency region and absolute noise bandwidth. J Acoust Soc Am 91:1069–1077.

Eggermont JJ (1999) Neural correlates of gap detection in three auditory cortical fields in the Cat. J Neurophysiol 81:2570–2581.

Eggermont JJ (2013) Hearing loss, hyperacusis, or tinnitus: what is modeled in animal research? Hear Res 295:140–149.

Eggermont JJ, Roberts LE (2004) The neuroscience of tinnitus. Trends Neurosci 27:676–682.

Eggermont JJ, Tass P a. (2015) Maladaptive Neural Synchrony in Tinnitus: Origin and Restoration. Front Neurol 6:1–17.

Elgoyhen AB, Langguth B, Ridder D De, Vanneste S (2015) Tinnitus: perspectives from human neuroimaging. Nat Rev Neurosci 16:632–642.

Elliott DN, Stein L, Farrison MJ (1960) Determination of Absolute-Intensity Thresholds and Frequency-Difference Thresholds in Cats. J Acoust Soc Am 32:380.

Engineer ND, Riley JR, Seale JD, Vrana W a, Shetake J a, Sudanagunta SP, Borland MS, Kilgard MP (2011) Reversing pathological neural activity using targeted plasticity. Nature 470:101–104.

Engle JR, Recanzone GH (2012) Characterizing spatial tuning functions of neurons in the auditory cortex of young and aged monkeys: a new perspective on old data. Front Aging Neurosci 4:36.

Engle JR, Tinling S, Recanzone GH (2013) Age-related hearing loss in rhesus monkeys is correlated with cochlear histopathologies. PLoS One 8:e55092.

Evans EF, Palmer AR (1980) Relationship Between the Dynamic Range of Cochlear Nerve Fibres and Their Spontaneous Activity. Exp brain Res 118:115–118.

Faisal AA, Selen LPJ, Wolpert DM (2008) Noise in the nervous system. Nat Rev Neurosci 9:292–303.

Fame RM, Macdonald JL, Macklis JD (2011) Development, specification, and diversity of callosal projection neurons. Trends Neurosci 34:41–50.

Fekete DM, Rouiller EM, Liberman MC, Ryugo DK (1984) The Central Projections of Intracellularly Labeled Auditory Nerve Fibers in Cats. J Comp Neurol 229:432–450.

Feldman DE (2009) Synaptic mechanisms for plasticity in neocortex. Annu Rev Neurosci 32:33–55.

Feldmann H (1971) Homolateral and contralateral masking of tinnitus by noise-bands and by pure tones. Audiology 10:138–144.

Feng G, Mellor RH, Bernstein M, Keller-Peck C, Nguyen QT, Wallace M, Nerbonne JM, Lichtman JW, Sanes JR (2000) Imaging Neuronal Subsets in Transgenic Mice Expressing Multiple Spectral Variants of GFP. Neuron 28:41–51.

Feng J, Bendiske J, Morest DK (2012) Degeneration in the ventral cochlear nucleus after severe noise damage in mice. J Neurosci Res 90:831–841.

Fenno L, Yizhar O, Deisseroth K (2011) The development and application of optogenetics. Annu Rev Neurosci 34:389–412.

Finlayson PG, Kaltenbach J a (2009) Alterations in the spontaneous discharge patterns of single units in the dorsal cochlear nucleus following intense sound exposure. Hear Res 256:104–117.

Fitzgibbons PJ (1983) Temporal gap detection in noise as a function of frequency, bandwidth, and level. J Acoust Soc Am 74:67–72.

Fitzgibbons PJ (1984) Temporal gap resolution in narrow-band noises with center frequencies from 6000-14000 Hz. J Acoust Soc Am 75:566–569.

Fitzgibbons PJ, Gordon-Salant S (1987) Temporal gap resolution in listeners with high-frequency sensorineural hearing loss. J Acoust Soc Am 81:133–137.

Flores EN, Duggan A, Liberman MC, Garcı J, Flores EN, Duggan A, Madathany T, Kumar G, Hogan AK, Ma FG, Seal RP, Edwards RH (2015) A Non-canonical Pathway from Cochlea to Brain Signals Tissue-Damaging Noise. Curr Biol 25:606–612.

Formby C, Gerber MJ, Sherlock LP, Magder LS (1998) Evidence for an across-frequency, between-channel process in asymptotic monaural temporal gap detection. J Acoust Soc Am 103:3554–3560.

Fournier P, Hébert S (2013) Gap detection deficits in humans with tinnitus as assessed with the acoustic startle paradigm: does tinnitus fill in the gap? Hear Res 295:16–23.

Frisina RD (2001) Subcortical neural coding mechanisms for auditory temporal processing. Hear Res 158:1–27.

Fritz J, Shamma S, Elhilali M, Klein D (2003) Rapid task-related plasticity of spectrotemporal receptive fields in primary auditory cortex. Nat Neurosci 6:1216–1223.

Fritz JB, David S V, Radtke-Schuller S, Yin P, Shamma S a (2010) Adaptive, behaviorally gated, persistent encoding of task-relevant auditory information in ferret frontal cortex. Nat Neurosci 13:1011–1019.

Froemke RC (2014) Plasticity of Cortical Excitatory-Inhibitory Balance. Annu Rev Neurosci 38:150421150146009.

Froemke RC, Martins ARO (2011) Spectrotemporal dynamics of auditory cortical synaptic receptive field plasticity. Hear Res 279:149–161.

Fründ I, Haenel NV, Wichmann FA (2011) Inference for psychometric functions in the presence of nonstationary behavior. J Vis 11:1–19.

Fryatt AG, Mulheran M, Egerton J, Gunthorpe MJ, Grubb BD (2011) Ototrauma induces sodium channel plasticity in auditory afferent neurons. Mol Cell Neurosci 48:51–61.

Furman AC, Kujawa SG, Liberman MC (2013) Noise-induced cochlear neuropathy is selective for fibers with low spontaneous rates. J Neurophysiol 110:577–586.

Gao M, Sossa K, Song L, Errington L, Cummings L, Hwang H, Kuhl D, Worley P, Lee H (2010) A specific requirement of Arc/Arg3.1 for visual experience-induced homeostatic synaptic plasticity in mouse primary visual cortex. J Neurosci 30:7168–7178.

Gerits A, Farivar R, Rosen BR, Wald LL, Boyden ES, Vanduffel W (2012)

Optogenetically induced behavioral and functional network changes in primates. Curr Biol 22:1722–1726.

Giraudi D, Salvi R, Henderson D, Hamernik R (1980) Gap detection by the chinchilla. J Acoust Soc Am 68:802–806.

Giraudi-Perry DM, Salvi RJ, Henderson D (1982) Gap detection in hearing-impaired chinchillas. J Acoust Soc Am 72:1387–1393.

Godfrey D a, Godfrey M a, Ding D-L, Chen K, Salvi RJ (2005) Amino acid concentrations in chinchilla cochlear nucleus at different times after carboplatin treatment. Hear Res 206:64–73.

Godfrey D a, Jin Y-M, Liu X, Godfrey M a (2014) Effects of cochlear ablation on amino acid levels in the rat cochlear nucleus and superior olive. Hear Res 309:44–54.

Gold JR, Bajo VM (2014) Insult-induced adaptive plasticity of the auditory system. Front Neurosci 8:1–31.

Gold JR, Nodal FR, Peters F, King AJ, Bajo VM (2015) Auditory gap-in-noise detection behavior in ferrets and humans. Behav Neurosci 129:473–490.

Gold JR, Peters F, Nodal FR, King AJ, Bajo VM (2013) Towards a new animal model of tinnitus: gap detection behaviour in adult ferrets. In: 7th International TRI Tinnitus Conference. Valencia.

Gośdon-Salant S, Fitzgibbons PJ (1993) Temporal factors and speech recognition performance in young and elderly listeners. J Speech Hear Res 36:1276–1285.

Gradinaru V, Zhang F, Ramakrishnan C, Mattis J, Prakash R, Diester I, Goshen I, Thompson KR, Deisseroth K (2010) Molecular and cellular approaches for diversifying and extending optogenetics. Cell 141:154–165.

Granzow M, Riedel H, Kollmeier B (2001) Single-sweep-based methods to improve the quality of auditory brain stem responses Part I : Optimized linear filtering. ZEITSCHRIFT FUR Audiol 40:32–44.

Gray DT, Engle JR, Recanzone GH (2014) Age-related neurochemical changes in the rhesus macaque superior olivary complex. J Comp Neurol 522:573–591.

Grosenick L, Marshel JH, Deisseroth K (2015) Closed-Loop and Activity-Guided Optogenetic Control. Neuron 86:106–139.

Gruner J a (1989) Comparison of vestibular and auditory startle responses in the rat and cat. J Neurosci Methods 27:13–23.

Gu JW, Herrmann BS, Levine R a, Melcher JR (2012) Brainstem auditory evoked potentials suggest a role for the ventral cochlear nucleus in tinnitus. J Assoc Res

Otolaryngol 13:819–833.

Guitton MJ, Caston J, Ruel J, Johnson RM, Pujol R, Puel J-L (2003) Salicylate induces tinnitus through activation of cochlear NMDA receptors. J Neurosci 23:3944–3952.

Guo W, Hight AE, Chen JX, Klapoetke NC, Hancock KE, Shinn-Cunningham BG, Boyden ES, Lee DJ, Polley DB (2015) Hearing the light: neural and perceptual encoding of optogenetic stimulation in the central auditory pathway. Sci Rep 5:10319.

Hamann I, Gleich O, Klump GM, Kittel MC, Strutz J (2004) Age-dependent changes of gap detection in the Mongolian gerbil (Meriones unguiculatus). J Assoc Res Otolaryngol 5:49–57.

Hamilton LS, Sohl-Dickstein J, Huth AG, Carels VM, Deisseroth K, Bao S (2013) Optogenetic Activation of an Inhibitory Network Enhances Feedforward Functional Connectivity in Auditory Cortex. Neuron 80:1066–1076.

Han X, Chow BY, Zhou H, Klapoetke NC, Chuong A, Rajimehr R, Yang A, Baratta M V, Winkle J, Desimone R, Boyden ES (2011) A high-light sensitivity optical neural silencer: development and application to optogenetic control of non-human primate cortex. Front Syst Neurosci 5:18.

Hanks TD, Kopec CD, Brunton BW, Duan C a, Erlich JC, Brody CD (2015) Distinct relationships of parietal and prefrontal cortices to evidence accumulation. Nature.

Hardingham N, Dachtler J, Fox K (2013) The role of nitric oxide in pre-synaptic plasticity and homeostasis. Front Cell Neurosci 7:1–19.

Harris KC, Eckert M a, Ahlstrom JB, Dubno JR (2010) Age-related differences in gap detection: effects of task difficulty and cognitive ability. Hear Res 264:21–29.

Harris KD, Shepherd GMG (2015) The neocortical circuit: themes and variations. Nat Neurosci 18:170–181.

Hartley DEH, Vongpaisal T, Xu J, Shepherd RK, King AJ, Isaiah A (2010) Bilateral cochlear implantation in the ferret: a novel animal model for behavioral studies. J Neurosci Methods 190:214–228.

Hausser M (2014) Optogenetics: the age of light. Nat Methods 11:1012–1014.

Hawkins JE, Johnsson LG, Stebbins WC, Moody DB, Coombs SL (1976) Hearing loss and cochlear pathology in monkeys after noise exposure. Acta Otolaryngol 81:337–343.

He NJ, Horwitz a R, Dubno JR, Mills JH (1999) Psychometric functions for gap detection in noise measured from young and aged subjects. J Acoust Soc Am 106:966–978.

Hébert S, Fournier P, Noreña A (2013) The auditory sensitivity is increased in tinnitus ears. J Neurosci 33:2356–2364.

Heffner HE, Harrington I a (2002) Tinnitus in hamsters following exposure to intense sound. Hear Res 170:83–95.

Heffner HE, Heffner RS (2014) The Behavioral Study of Mammalian Hearing. In: Perspectives on Auditory Research - Springer Handbook of Auditory Research, Vol. 50 (Popper AN, Fay RR, eds), pp 269–285. Springer New York.

Henderson D, Salvi R, Pavek G, Hamernik R (1984) Amplitude modulation thresholds in chinchillas with high-frequency hearing loss. J Acoust Soc Am 75:1177–1183.

Hernandez VH, Gehrt A, Reuter K, Jing Z, Jeschke M, Schulz AM, Hoch G, Bartels M, Vogt G, Garnham CW, Yawo H, Fukazawa Y, Augustine GJ, Bamberg E, Kügler S, Salditt T, De Hoz L, Strenzke N, Moser T (2014) Optogenetic stimulation of the auditory pathway. J Clin Invest 124:1114–1129.

Hickox AE, Liberman MC (2014) Is noise-induced cochlear neuropathy key to the generation of hyperacusis or tinnitus? J Neurophysiol 111:552–564.

Hildebrandt H, Hoffmann N a, Illing R-B (2011) Synaptic reorganization in the adult rat's ventral cochlear nucleus following its total sensory deafferentation. PLoS One 6:e23686.

Hilton MP, Zimmermann EF, Hunt WT (2013) Ginkgo biloba for tinnitus. Cochrane database Syst Rev 3:CD003852.

Hoare DJ, Edmondson-Jones M, Sereda M, Akeroyd MA, Hall D (2014) Amplification with hearing aids for patients with tinnitus and co-existing hearing loss. Cochrane database Syst Rev 1:CD010151.

Höbel G (2014) Effect of temporal and spectral noise features on gap detection behavior by calling green treefrogs. Behav Processes 108:43–49.

Hobson J, Chisholm E, El Refaie A (2012) Sound therapy (masking) in the management of tinnitus in adults. Cochrane database Syst Rev 11:CD006371.

Hoekstra C El, Rynja SP, van Zanten GA, Rovers MM (2011) Anticonvulsants for tinnitus. Cochrane database Syst Rev:CD007960.

Hofer SB, Mrsic-Flogel TD, Bonhoeffer T, Hubener M (2006) Lifelong learning: ocular dominance plasticity in mouse visual cortex. Curr Opin Neurobiol 16:451–459.

Holt AG, Bissig D, Mirza N, Rajah G, Berkowitz B (2010) Evidence of key tinnitus-related brain regions documented by a unique combination of manganese-enhanced

MRI and acoustic startle reflex testing. PLoS One 5:e14260.

Horwitz AR, Ahlstrom JB, Dubno JR (2011) Level-dependent changes in detection of temporal gaps in noise markers by adults with normal and impaired hearing. J Acoust Soc Am 130:2928.

Hughes LF, Turner JG, Parrish JL, Caspary DM (2010) Processing of broadband stimuli across A1 layers in young and aged rats. Hear Res 264:79–85.

Huh Y, Kim C, Lee W, Kim J, Ahn H (1997) Age-related change in the neuropeptide Y and NADPH-diaphorase-positive neurons in the cerebral cortex and striatum of aged rats. Neurosci Lett 223:157–160.

Huh Y, Lee W, Cho J, Ahn H (1998) Regional changes of NADPH-diaphorase and neuropeptide Y neurons in the cerebral cortex of aged Fischer 344 rats. Neurosci Lett 247:79–82.

Huh Y, Park DC, Yeo SG, Il CCHA (2008) Evidence for increased NADPH-diaphorase-positive neurons in the central auditory system of the aged rat. Acta Otolaryngol:648–653.

Irvine DRF (2007) Auditory cortical plasticity: does it provide evidence for cognitive processing in the auditory cortex? Hear Res 229:158–170.

Irvine DRF, Rajan R, Smith S (2003) Effects of restricted cochlear lesions in adult cats on the frequency organization of the inferior colliculus. J Comp Neurol 467:354–374.

Isaiah A, Vongpaisal T, King AJ, Hartley DEH (2014) Multisensory Training Improves Auditory Spatial Processing following Bilateral Cochlear Implantation. J Neurosci 34:11119–11130.

Ison JR, Allen PD, Rivoli PJ, Moore JT (2005) The behavioral response of mice to gaps in noise depends on its spectral components and its bandwidth. J Acoust Soc Am 117:3944.

Ison JR, O'Connor K, Bowen GP, Bocirnea A (1991) Temporal resolution of gaps in noise by the rat is lost with functional decortication. Behav Neurosci 105:33–40.

Izquierdo M a, Gutiérrez-Conde PM, Merchán M a, Malmierca MS (2008) Non-plastic reorganization of frequency coding in the inferior colliculus of the rat following noise-induced hearing loss. Neuroscience 154:355–369.

Jain R, Shore S (2006) External inferior colliculus integrates trigeminal and acoustic information : Unit responses to trigeminal nucleus and acoustic stimulation in the guinea pig. Neurosci Lett 395:71–75.

Jakkamsetti V, Tsai N-P, Gross C, Molinaro G, Collins K a, Nicoletti F, Wang KH,

Osten P, Bassell GJ, Gibson JR, Huber KM (2013) Experience-Induced Arc/Arg3.1 Primes CA1 Pyramidal Neurons for Metabotropic Glutamate Receptor-Dependent Long-Term Synaptic Depression. Neuron 80:72–79.

Jastreboff PJ, Brennan JF, Coleman JK, Sasaki CT (1988) Phantom auditory sensation in rats: an animal model for tinnitus. Behav Neurosci 102:811–822.

Jastreboff PJ, Sasaki CT (1986) Salicylate-induced changes in spontaneous activity of single units in the inferior colliculus of the guinea pig. J Acoust Soc Am 80:1384–1391.

Jazayeri M, Lindbloom-Brown Z, Horwitz GD (2012) Saccadic eye movements evoked by optogenetic activation of primate V1. Nat Neurosci 15:1368–1370.

Juarez-Salinas DL, Engle JR, Navarro XO, Recanzone GH (2010) Hierarchical and serial processing in the spatial auditory cortical pathway is degraded by natural aging. J Neurosci 30:14795–14804.

Jun-ichi M, Satoshi T, Kimi A, Fumi T, Akira T, Kiyoshi T, Ken-ichi Y (1989) Expression vector system based on the chicken β-actin promoter directs efficient production of interleukin-5. Gene 79:269–277.

Kakigi A, Hirakawa H, Harel N, Mount RJ, Harrison R V (2000) Tonotopic mapping in auditory cortex of the adult chinchilla with amikacin-induced cochlear lesions. Audiology 39:153–160.

Kaltenbach J a (2011) Tinnitus: Models and mechanisms. Hear Res 276:52–60.

Kaltenbach J a, Afman CE (2000) Hyperactivity in the dorsal cochlear nucleus after intense sound exposure and its resemblance to tone-evoked activity: a physiological model for tinnitus. Hear Res 140:165–172.

Kamke MR, Brown M, Irvine DRF (2003) Plasticity in the tonotopic organization of the medial geniculate body in adult cats following restricted unilateral cochlear lesions. J Comp Neurol 459:355–367.

Kamke MR, Brown M, Irvine DRF (2005) Basal forebrain cholinergic input is not essential for lesion-induced plasticity in mature auditory cortex. Neuron 48:675–686.

Keating P, Dahmen JC, King AJ (2013) Context-specific reweighting of auditory spatial cues following altered experience during development. Curr Biol 23:1291–1299.

Keating P, Dahmen JC, King AJ (2015) Complementary adaptive processes contribute to the developmental plasticity of spatial hearing. Nat Neurosci:1–6.

Keating P, Nodal FR, King AJ (2014) Behavioural sensitivity to binaural spatial cues in ferrets: evidence for plasticity in the duplex theory of sound localization. Eur J

Neurosci 39:197–206.

Keithley EM, Feldman ML (1979) Spiral ganglion cell counts in an age-graded series of rat cochleas. J Comp Neurol 188:429–442.

Kelly JB, Judge PW (1994) Binaural organization of primary auditory cortex in the ferret (Mustela putorius). J Neurophysiol 71:904–913.

Kelly JB, Judge PW, Phillips DP (1986a) Representation of the cochlea in primary auditory cortex of the ferret (Mustela putorius). Hear Res 24:111–115.

Kelly JB, Kavanagh GL, Dalton JC (1986b) Hearing in the ferret (Mustela putorius): thresholds for pure tone detection. Hear Res 24:269–275.

Kelly JB, Rooney BJ, Phillips DP (1996) Effects of bilateral auditory cortical lesions on gap-detection thresholds in the ferret (Mustela putorius). Behav Neurosci 110:542–550.

Kelly JP, Wong D (1981) LAMINAR CONNECTIONS OF THE CAT'S AUDITORY CORTEX. Brain Res 212:1–15.

Keuroghlian AS, Knudsen EI (2007) Adaptive auditory plasticity in developing and adult animals. Prog Neurobiol 82:109–121.

Kiang NY, Liberman MC, Levine RA (1975) Auditory-nerve activity in cats exposed to ototoxic drugs and high-intensity sounds. Ann Otol Rhinol Laryngol 85:752–768.

Kilgard MP (2012) Harnessing plasticity to understand learning and treat disease. Trends Neurosci 35:715–722.

King AJ (2004) The superior colliculus. Curr Biol 14:R335–R338.

King AJ, Bajo VM, Bizley JK, Campbell R a a, Nodal FR, Schulz AL, Schnupp JWH (2007) Physiological and behavioral studies of spatial coding in the auditory cortex. Hear Res 229:106–115.

King AJ, Dahmen JC, Keating P, Leach ND, Nodal FR, Bajo VM (2011) Neural circuits underlying adaptation and learning in the perception of auditory space. Neurosci Biobehav Rev 35:2129–2139.

Kirby AE, Middlebrooks JC (2010) Auditory temporal acuity probed with cochlear implant stimulation and cortical recording. J Neurophysiol 103:531–542.

Klapoetke NC et al. (2014) Independent optical excitation of distinct neural populations. Nat Methods 11:338–346.

Klump GM, Maier EH (1989) Gap detection in the starling (Sturnus vulgaris). J Comp Physiol A 164:531–538.

Knipper M, Van Dijk P, Nunes I, Rüttiger L, Zimmermann U (2013) Advances in the neurobiology of hearing disorders: recent developments regarding the basis of tinnitus and hyperacusis. Prog Neurobiol 111:17–33.

Koehler SD, Shore SE (2013a) Stimulus Timing-Dependent Plasticity in Dorsal Cochlear Nucleus Is Altered in Tinnitus. J Neurosci 33:19647–19656.

Koehler SD, Shore SE (2013b) Stimulus-timing dependent multisensory plasticity in the guinea pig dorsal cochlear nucleus. PLoS One 8:e59828.

Koerber KC, Pfeiffer RR, Warr WB, Kiang NY (1966) Spontaneous spike discharges from single units in the cochlear nucleus after destruction of the cochlea. Exp Neurol 16:119–130.

Korb E, Wilkinson CL, Delgado RN, Lovero KL, Finkbeiner S (2013) Arc in the nucleus regulates PML-dependent GluA1 transcription and homeostatic plasticity. Nat Neurosci 16:874–883.

Kral A, Sharma A (2012) Developmental neuroplasticity after cochlear implantation. Trends Neurosci 35:111–122.

Krause B, Kadosh RC (2013) Can transcranial electrical stimulation improve learning difficulties in atypical brain development ? A future possibility for cognitive training. Dev Cogn Neurosci 6:176–194.

Krause B, Kadosh RC (2014) Not all brains are created equal: the relevance of individual differences in responsiveness to transcranial electrical stimulation. Front Syst Neurosci 8:1–12.

Kuhl PK, Miller JD (1978) Speech perception by the chinchilla: identification function for synthetic VOT stimuli. J Acoust Soc Am 63:905–917.

Kujawa SG, Liberman MC (2006) Acceleration of age-related hearing loss by early noise exposure: evidence of a misspent youth. J Neurosci 26:2115–2123.

Kujawa SG, Liberman MC (2009) Adding insult to injury: cochlear nerve degeneration after "temporary" noise-induced hearing loss. J Neurosci 29:14077–14085.

Lacouture Y, Cousineau D (2008) How to use MATLAB to fit the ex-Gaussian and other probability functions to a distribution of response times. Tutor Quant Methods Psychol 4:35–45.

Langers DRM, de Kleine E, van Dijk P (2012) Tinnitus does not require macroscopic tonotopic map reorganization. Front Syst Neurosci 6:2.

Langguth B, Kreuzer PM, Kleinjung T, De Ridder D (2013) Tinnitus: causes and clinical management. Lancet Neurol 12:920–930.

Leach ND, Nodal FR, Cordery PM, King AJ, Bajo VM (2013) Cortical cholinergic input is required for normal auditory perception and experience-dependent plasticity in adult ferrets. J Neurosci 33:6659–6671.

Leaver AM, Renier L, Chevillet M a, Morgan S, Kim HJ, Rauschecker JP (2011) Dysregulation of limbic and auditory networks in tinnitus. Neuron 69:33–43.

Lee F-S, Matthews LJ, Dubno JR, Mills JH (2005) Longitudinal study of pure-tone thresholds in older persons. Ear Hear 26:1–11.

Lee HJ, Wallani T, Mendelson JR (2002) Temporal processing speed in the inferior colliculus of young and aged rats. Hear Res 174:64–74.

Lee J, Cho Y, Huh Y, Cha C Il, Yeo SG (2008) Effect of nitric oxide on auditory cortical neurons of aged rats. Neurosci Lett 447:37–41.

Leigh-Paffenroth ED, Elangovan S (2011) Temporal Processing in Low-Frequency Channels: Effects of Age and Hearing Loss in Middle-Aged Listeners. J Am Acad Audiol 22:393–404.

Lemus L, Hernández A, Romo R (2009) Neural codes for perceptual discrimination of acoustic flutter in the primate auditory cortex. Proc Natl Acad Sci U S A 106:9471–9476.

Letzkus JJ, Wolff SBE, Meyer EMM, Tovote P, Courtin J, Herry C, Luthi A (2011) A disinhibitory microcircuit for associative fear learning in the auditory cortex. Nature 480:331–335.

Lewis JE, Stephens SDG, McKenna LM (1994) Tinnitus and suicide. Clin Otolaryngol allied Sci 19:50–54.

Li N, Chen T, Guo Z V, Gerfen CR, Svoboda K (2015) A motor cortex circuit for motor planning and movement. Nature 519:51–56.

Liberman MC (1982) Single-neuron labeling in the cat auditory nerve. Science 216:1239–1241.

Liberman MC (1991) Central Projections of Auditory-Nerve Fibers of Differing Spontaneous Rate . I . Anteroventral Cochlear Nucleus. J Comp Neurol 313:240–258.

Liberman MC (1993) Central Projections of Auditory Nerve Fibers of Differing Spontaneous Rate , II : Posteroventral and Dorsal Cochlear Nuclei. J Comp Neurol 327:17–36.

Lin HW, Furman AC, Kujawa SG, Liberman MC (2011) Primary neural degeneration in the Guinea pig cochlea after reversible noise-induced threshold shift. J Assoc Res Otolaryngol 12:605–616.

Linden JF, Liu RC, Sahani M, Schreiner CE, Merzenich MM (2003) Spectrotemporal structure of receptive fields in areas AI and AAF of mouse auditory cortex. J Neurophysiol 90:2660–2675.

Lisker L, Abramson A (1964) A cross-language study of voicing in initial stops - acoustical measurements. Word - J Int Linguist Assoc 20:384–422.

Liu K, Jiang X, Shi C, Shi L, Yang B, Shi L, Xu Y, Yang W, Yang S (2013) Cochlear Inner Hair Cell Ribbon Synapse is the Primary Target of Ototoxic Aminoglycoside Stimuli. Mol Neurobiol 48:647–654.

Llano D a, Turner JG, Caspary DM (2012) Diminished cortical inhibition in an aging mouse model of chronic tinnitus. J Neurosci 32:16141–16148.

Lobarinas E, Hayes SH, Allman BL (2013a) The gap-startle paradigm for tinnitus screening in animal models: limitations and optimization. Hear Res 295:150–160.

Lobarinas E, Salvi R, Ding D (2013b) Insensitivity of the audiogram to carboplatin induced inner hair cell loss in chinchillas. Hear Res 302:113–120.

Lockwood AH, Salvi RJ, Coad ML, Towsley ML, Wack DS, Murphy BW (1998) The functional neuroanatomy of tinnitus: Evidence for limbic system links and neural plasticity. Neurology 50:114–120.

Longenecker RJ, Galazyuk a. V (2012) Methodological optimization of tinnitus assessment using prepulse inhibition of the acoustic startle reflex. Brain Res 1485:54–62.

Lowe AS, Walton JP (2015) Alterations in Peripheral and Central Components of the Auditory Brainstem Response: A Neural Assay of Tinnitus. PLoS One 10:e0117228.

Luce RD, Green DM (1972) A neural timing theory for response times and the psychophysics of intensity. Psychol Rev 79:14–57.

Ma L, Micheyl C, Yin P, Oxenham AJ, Shamma SA (2010) Behavioral measures of auditory streaming in ferrets (Mustela putorius). J Comp Psychol 124:317–330.

Ma W-LD, Hidaka H, May BJ (2006) Spontaneous activity in the inferior colliculus of CBA/J mice after manipulations that induce tinnitus. Hear Res 212:9–21.

Macmillan NA, Creelman CD (2005) Detection Theory: A User's Guide.

Magri C, Whittingstall K, Singh V, Logothetis NK, Panzeri S (2009) A toolbox for the fast information analysis of multiple-site LFP, EEG and spike train recordings. BMC Neurosci 10:81.

Mahlke C, Wallhäusser-Franke E (2004) Evidence for tinnitus-related plasticity in the auditory and limbic system, demonstrated by arg3.1 and c-fos immunocytochemistry.

Hear Res 195:17–34.

Maison SF, Usubuchi H, Liberman MC (2013) Efferent feedback minimizes cochlear neuropathy from moderate noise exposure. J Neurosci 33:5542–5552.

Makin TR, Scholz J, Filippini N, Henderson Slater D, Tracey I, Johansen-Berg H (2013) Phantom pain is associated with preserved structure and function in the former hand area. Nat Commun 4:1570.

Manzoor NF, Gao Y, Licari F, Kaltenbach J a (2013) Comparison and contrast of noise-induced hyperactivity in the dorsal cochlear nucleus and inferior colliculus. Hear Res 295:114–123.

Manzoor NF, Licari FG, Klapchar M, Elkin RL, Gao Y, Chen G, Kaltenbach J a (2012) Noise-induced hyperactivity in the inferior colliculus: its relationship with hyperactivity in the dorsal cochlear nucleus. J Neurophysiol 108:976–988.

Margolis DJ, Lütcke H, Schulz K, Haiss F, Weber B, Kügler S, Hasan MT, Helmchen F (2012) Reorganization of cortical population activity imaged throughout long-term sensory deprivation. Nat Neurosci 15:1539–1546.

Marlin BJ, Mitre M, James a D, Chao M V, Froemke RC (2015) Oxytocin enables maternal behaviour by balancing cortical inhibition. Nature.

Martinez-Devesa P, Perera R, Theodoulou M, Waddell A (2010) Cognitive behavioural therapy for tinnitus. Cochrane database Syst Rev:CD005233.

Martins ARO, Froemke RC (2015) Coordinated forms of noradrenergic plasticity in the locus coeruleus and primary auditory cortex. Nat Neurosci 18:1483–1492.

Masterton RB, Berkley MA (1974) BRAIN FUNCTION: Changing Ideas on the Role of Sensory, Motor, and Association Cortex in Behavior. Annu Rev Psychol 25:277–312.

McAlpine D, Martin RL, Mossop JE, Moore DR (1997) Response properties of neurons in the inferior colliculus of the monaurally deafened ferret to acoustic stimulation of the intact ear. J Neurophysiol 78:767–779.

Mehdizade Gilani V, Ruzbahani M, Mahdi P, Amali A, Nilforush Khoshk MH, Sameni J, Karimi Yazdi A, Emami H (2013) Temporal processing evaluation in tinnitus patients: results on analysis of gap in noise and duration pattern test. Iran J Otorhinolaryngol 25:221–226.

Melcher JR, Guinan JJ, Knudson IM, Kiang NY (1996a) Generators of the brainstem auditory evoked potential in cat. II. Correlating lesion sites with waveform changes. Hear Res 93:28–51.

Melcher JR, Kiang NY (1996) Generators of the brainstem auditory evoked potential in cat. III: Identified cell populations. Hear Res 93:52–71.

Melcher JR, Knudson IM, Fullerton BC, Guinan JJ, Norris BE, Kiang NY (1996b) Generators of the brainstem auditory evoked potential in cat. I. An experimental approach to their identification. Hear Res 93:1–27.

Meng Z, Liu S, Zheng Y, Phillips JS (2011) Repetitive transcranial magnetic stimulation for tinnitus. Cochrane database Syst Rev:CD007946.

Meredith M a, Keniston LP, Allman BL (2012) Multisensory dysfunction accompanies crossmodal plasticity following adult hearing impairment. Neuroscience 214:136–148.

Middleton JW, Kiritani T, Pedersen C, Turner JG, Shepherd GMG, Tzounopoulos T (2011) Mice with behavioral evidence of tinnitus exhibit dorsal cochlear nucleus hyperactivity because of decreased GABAergic inhibition. Proc Natl Acad Sci U S A 108:7601–7606.

Milbrandt JC, Albin RL, Caspary DM (1994) Age-related decrease in GABAB receptor binding in the Fischer 344 rat inferior colliculus. Neurobiol Aging 15:699–703.

Moon IJ, Won XJH, Kang HW, Kim XDH, An Y, Shim XHJ (2015) Influence of Tinnitus on Auditory Spectral and Temporal Resolution and Speech Perception in Tinnitus Patients. J Neurosci 35:14260–14269.

Moore BCJ, Vickers D a., Mehta A (2012) The effects of age on temporal fine structure sensitivity in monaural and binaural conditions. Int J Audiol 51:715–721.

Moore DR (1993) Auditory brainstem responses in ferrets following unilateral cochlear removal. Hear Res 68:28–34.

Moore DR, France SJ, McAlpine D, Mossop JE, Versnel H (1997) Plasticity of inferior colliculus and auditory cortex following unilateral deafening in adult ferrets. In: Acoustical Signal Processing in the Central Auditory System (Syka J, ed), pp 489–499. New York: Plenum.

Morey a L, Carlile S (1990) Auditory brainstem of the ferret: maturation of the brainstem auditory evoked response. Brain Res Dev Brain Res 52:279–288.

Mühler R, von Specht H, Specht H (1999) Sorted averaging--principle and application to auditory brainstem responses. Scand Audiol 28:145–149.

Mühlnickel W, Elbert T, Taub E, Flor H (1998) Reorganization of auditory cortex in tinnitus. Proc Natl Acad Sci U S A 95:10340–10343.

Mukherjea D, Rybak LP, Sheehan KE, Kaur T, Ramkumar V, Jajoo S, Sheth S (2011)

The design and screening of drugs to prevent acquired sensorineural hearing loss. Expert Opin Drug Discov 6:491–505.

Mulders WH a M, Ding D, Salvi R, Robertson D (2011) Relationship between auditory thresholds, central spontaneous activity, and hair cell loss after acoustic trauma. J Comp Neurol 519:2637–2647.

Mulders WH a M, Robertson D (2009) Hyperactivity in the auditory midbrain after acoustic trauma: dependence on cochlear activity. Neuroscience 164:733–746.

Mulders WH a M, Robertson D (2011) Progressive centralization of midbrain hyperactivity after acoustic trauma. Neuroscience 192:753–760.

Mulders WH a M, Seluakumaran K, Robertson D (2010) Efferent pathways modulate hyperactivity in inferior colliculus. J Neurosci 30:9578–9587.

Müller U, Barr-Gillespie PG (2015) New treatment options for hearing loss. Nat Rev Drug Discov 14:346–365.

Nagel G, Szellas T, Huhn W, Kateriya S, Adeishvili N, Berthold P, Ollig D, Hegemann P, Bamberg E (2003) Channelrhodopsin-2, a directly light-gated cation-selective membrane channel. Proc Natl Acad Sci U S A 100:13940–13945.

Neff WD (1947) The effects of partial section of the auditory nerve. J Comp Physiol Psychol 40:203–215.

Nelken I, Bizley JK, Nodal FR, Ahmed B, Schnupp JWH, King AJ (2004) Large-scale organization of ferret auditory cortex revealed using continuous acquisition of intrinsic optical signals. J Neurophysiol 92:2574–2588.

Nienhuys TG, Clark GM (1978) Frequency discrimination following the selective destruction of cochlear inner and outer hair cells. Science 199:1356–1357.

Niskar a. S, Kieszak SM, Holmes a. E, Esteban E, Rubin C, Brody DJ (2001) Estimated Prevalence of Noise-Induced Hearing Threshold Shifts Among Children 6 to 19 Years of Age: The Third National Health and Nutrition Examination Survey, 1988-1994, United States. Pediatrics 108:40–43.

Niwa H, Yamamura K, Miyazaki J (1991) Efficient selection for high-expression transfectants with a novel eukaryotic vector. Gene 108:193–199.

Nodal FR, Bajo VM, King AJ (2012) Plasticity of spatial hearing: behavioural effects of cortical inactivation. J Physiol 590:3965–3986.

Nodal FR, Bajo VM, Parsons CH, Schnupp JW, King a J (2008) Sound localization behavior in ferrets: comparison of acoustic orientation and approach-to-target responses. Neuroscience 154:397–408.

Nodal FR, Kacelnik O, Bajo VM, Bizley JK, Moore DR, King AJ (2010) Lesions of the auditory cortex impair azimuthal sound localization and its recalibration in ferrets. J Neurophysiol 103:1209–1225.

Nodal FR, King AJ (2014) Hearing and Auditory Function in Ferrets. In: Biology and Diseases of the Ferret, 3rd ed. (Fox JG, Marini RP, eds), pp 685–710. Wiley-Blackwell.

Nondahl DM, Cruickshanks KJ, Huang G-H, Klein BEK, Klein R, Nieto FJ, Tweed TS (2011) Tinnitus and its risk factors in the Beaver Dam offspring study. Int J Audiol 50:313–320.

Nondahl DM, Cruickshanks KJ, Wiley TL, Klein BEK, Klein R, Chappell R, Tweed TS (2010) The ten-year incidence of tinnitus among older adults. Int J Audiol 49:580–585.

Noreña AJ (2015) Revisiting the cochlear and central mechanisms of tinnitus and therapeutic approaches. Audiol Neurootol 20 Suppl 1:53–59.

Noreña AJ, Eggermont JJ (2003) Changes in spontaneous neural activity immediately after an acoustic trauma: implications for neural correlates of tinnitus. Hear Res 183:137–153.

Noreña AJ, Eggermont JJ (2006) Enriched acoustic environment after noise trauma abolishes neural signs of tinnitus. Neuroreport 17:559–563.

Noreña AJ, Farley BJ (2013) Tinnitus-related neural activity: theories of generation, propagation, and centralization. Hear Res 295:161–171.

Noreña AJ, Tomita M, Eggermont JJ (2003) Neural changes in cat auditory cortex after a transient pure-tone trauma. J Neurophysiol 90:2387–2401.

Oertel D, Young ED (2004) What's a cerebellar circuit doing in the auditory system? Trends Neurosci 27:104–110.

Ohlemiller KK (2004) Age-related hearing loss: the status of Schuknecht's typology. Curr Opin Otolaryngol Head Neck Surg 12:439–443.

Oka Y, Ye M, Zuker CS (2015) Thirst driving and suppressing signals encoded by distinct neural populations in the brain. Nature 520:349–352.

Okanoya K, Dooling RJ (1990) Detection of gaps in noise by budgerigars (Melopsittacus undulatus) and zebra finches (Poephila guttata). Hear Res 50:185–192.

Olsen SR, Bortone DS, Adesnik H, Scanziani M (2012) Gain control by layer six in cortical circuits of vision. Nature 483:47–52.

Ouda L, Nwabueze-Ogbo FC, Druga R, Syka J (2003) NADPH-diaphorase-positive neurons in the auditory cortex of young and old rats. Neuroreport 14:363–366.

Ouda L, Syka J (2012) Immunocytochemical profiles of inferior colliculus neurons in the rat and their changes with aging. Front Neural Circuits 6:68.

Oxenham a J (2000) Influence of spatial and temporal coding on auditory gap detection. J Acoust Soc Am 107:2215–2223.

Palmer AR, King AJ (1982) The representation of auditory space in the mammalian superior colliculus. Nature 299:248–249.

Panzeri S, Treves A (1996) Analytical estimates of limited sampling biases in different information measures. Network 7:87–107.

Parthasarathy A, Bartlett EL (2011) Age-related auditory deficits in temporal processing in F-344 rats. Neuroscience 192:619–630.

Parthasarathy A, Cunningham P a, Bartlett EL (2010) Age-related differences in auditory processing as assessed by amplitude-modulation following responses in quiet and in noise. Front Aging Neurosci 2:152.

Paz JT, Davidson TJ, Frechette ES, Delord B, Parada I, Peng K, Deisseroth K, Huguenard JR (2013) Closed-loop optogenetic control of thalamus as a tool for interrupting seizures after cortical injury. Nat Neurosci 16:64–70.

Penner MJ (1977) Detection of temporal gaps in noise as a measure of the decay of auditory sensation. J Acoust Soc Am 61:552–557.

Perkel DH, Gerstein GL, Moore GP (1967) Neuronal spike trains and stochastic point processes. II. Simultaneous spike trains. Biophys J 7:419–440.

Petkov CI, O'Connor KN, Sutter ML (2007) Encoding of illusory continuity in primary auditory cortex. Neuron 54:153–165.

Phillips D., Hall S., Boehnke S. (2002) Central auditory onset responses, and temporal asymmetries in auditory perception. Hear Res 167:192–205.

Phillips DP, Hall SE (2000) Independence of frequency channels in auditory temporal gap detection. J Acoust Soc Am 108:2957–2963.

Phillips DP, Hall SE, Harrington I a, Taylor TL (1998) "Central" auditory gap detection: a spatial case. J Acoust Soc Am 103:2064–2068.

Phillips DP, Judge PW, Kelly JB (1988) Primary auditory cortex in the ferret (Mustela putorius): neural response properties and topographic organization. Brain Res 443:281–294.

Phillips DP, Smith JC (2004) Correlations among within-channel and between-channel auditory gap-detection thresholds in normal listeners. Perception 33:371–378.

Phillips DP, Taylor TL, Hall SE, Carr MM, Mossop JE (1997) Detection of silent intervals between noises activating different perceptual channels: some properties of "central" auditory gap detection. J Acoust Soc Am 101:3694–3705.

Phillips JS, McFerran D (2010) Tinnitus Retraining Therapy (TRT) for tinnitus. Cochrane database Syst Rev:CD007330.

Piazza S, Abitbol M, Gnirs K, Huynh M, Cauzinille L (2014a) Prevalence of deafness and association with coat variations in client-owned ferrets. J Am Vet Med Assoc 244:1047–1052.

Piazza S, Huynh M, Cauzinille L (2014b) Brainstem auditory-evoked response (BAER) in client-owned pet ferrets with normal hearing. Vet Rec.

Pienkowski M, Eggermont JJ (2011) Cortical tonotopic map plasticity and behavior. Neurosci Biobehav Rev 35:2117–2128.

Pilz PKD, Leaton RN (1999) Short-term and long-term habituation of the acoustic startle response as a function of stimulus rise time in rats. PSYCHOBIOLOGY 27:402–414.

Pisanello F, Sileo L, Oldenburg IA, Pisanello M, Martiradonna L, Assad JA, Sabatini BL, Vittorio M De (2014) NeuroResource Multipoint-Emitting Optical Fibers for Spatially Addressable In Vivo Optogenetics. Neuron 82:1245–1254.

Plomp R (1964) Rate of Decay of Auditory Sensation. J Acoust Soc Am 36.

Potashner SJ, Suneja SK, Benson CG (2000) Altered glycinergic synaptic activities in guinea pig brain stem auditory nuclei after unilateral cochlear ablation. Hear Res 147:125–136.

Puel JL, Ruel J, Gervais d'Aldin C, Pujol R (1998) Excitotoxicity and repair of cochlear synapses after noise-trauma induced hearing loss. Neuroreport 9:2109–2114.

Pujol R, Puel JL (1999) Excitotoxicity, synaptic repair, and functional recovery in the mammalian cochlea: a review of recent findings. Ann N Y Acad Sci 884:249–254.

Qiu C, Salvi R, Ding D, Burkard R (2000) Inner hair cell loss leads to enhanced response amplitudes in auditory cortex of unanesthetized chinchillas: evidence for increased system gain. Hear Res 139:153–171.

Rabinowitz NC, Willmore BDB, Schnupp JWH, King AJ (2011) Contrast gain control in auditory cortex. Neuron 70:1178–1191.

Rabinowitz NC, Willmore BDB, Schnupp JWH, King AJ (2012) Spectrotemporal contrast kernels for neurons in primary auditory cortex. J Neurosci 32:11271–11284.

Radziwon KE, June KM, Stolzberg DJ, Xu-Friedman MA, Salvi RJ, Dent ML (2009)

Behaviorally measured audiograms and gap detection thresholds in CBA/CaJ mice. J Comp Physiol A Neuroethol Sens Neural Behav Physiol 195:961–969.

Rahne T, von Specht H, Mühler R (2008) Sorted averaging-application to auditory event-related responses. J Neurosci Methods 172:74–78.

Raimondo J V, Kay L, Ellender TJ, Akerman CJ (2012) Optogenetic silencing strategies differ in their effects on inhibitory synaptic transmission. Nat Neurosci 15:1102–1104.

Rajan R (1998) Receptor organ damage causes loss of cortical surround inhibition without topographic map plasticity. Nat Neurosci 1:138–143.

Rajan R (2001) Plasticity of excitation and inhibition in the receptive field of primary auditory cortical neurons after limited receptor organ damage. Cereb Cortex 11:171–182.

Rajan R, Irvine DR (1998) Absence of plasticity of the frequency map in dorsal cochlear nucleus of adult cats after unilateral partial cochlear lesions. J Comp Neurol 399:35–46.

Rajan R, Irvine DR, Wise LZ, Heil P (1993) Effect of unilateral partial cochlear lesions in adult cats on the representation of lesioned and unlesioned cochleas in primary auditory cortex. J Comp Neurol 338:17–49.

Raposo D, Kaufman MT, Churchland AK (2014) A category-free neural population supports evolving demands during decision-making. Nat Neurosci 17:1784–1792.

Rauschecker JP, Maudoux A, May, Ploner M (2015) Frontostriatal gating of tinnitus and chronic pain. Trends Cogn Sci 19:567–578.

Recanzone GH, Engle JR, Juarez-Salinas DL (2011) Spatial and temporal processing of single auditory cortical neurons and populations of neurons in the macaque monkey. Hear Res 271:115–122.

Reed A, Riley J, Carraway R, Carrasco A, Perez C, Jakkamsetti V, Kilgard MP (2011) Cortical map plasticity improves learning but is not necessary for improved performance. Neuron 70:121–131.

Reed CM, Braida LD, Zurek PM (2009) Review article: review of the literature on temporal resolution in listeners with cochlear hearing impairment: a critical assessment of the role of suprathreshold deficits. Trends Amplif 13:4–43.

Richardson BD, Brozoski TJ, Ling LL, Caspary DM (2012) Targeting inhibitory neurotransmission in tinnitus. Brain Res 1485:77–87.

Riedel H, Granzow M, Kollmeier B (2001) Single-sweep-based methods to improve the quality of auditory brain stem responses Part II: Averaging methods.

ZEITSCHRIFT FUR Audiol 40:62–85.

Roberts LE (2007) Residual inhibition. Prog Brain Res 166:487–495.

Roberts LE, Bosnyak DJ, Thompson DC (2012) Neural plasticity expressed in central auditory structures with and without tinnitus. Front Syst Neurosci 6:40.

Roberts LE, Eggermont JJ, Caspary DM, Shore SE, Melcher JR, Kaltenbach J a (2010) Ringing ears: the neuroscience of tinnitus. J Neurosci 30:14972–14979.

Roberts LE, Husain FT, Eggermont JJ (2013) Role of attention in the generation and modulation of tinnitus. Neurosci Biobehav Rev 37:1754–1773.

Roberts LE, Moffat G, Baumann M, Ward LM, Bosnyak DJ (2008) Residual inhibition functions overlap tinnitus spectra and the region of auditory threshold shift. J Assoc Res Otolaryngol 9:417–435.

Robertson D, Bester C, Vogler D, Mulders WH a M (2013) Spontaneous hyperactivity in the auditory midbrain: relationship to afferent input. Hear Res 295:124–129.

Robertson D, Irvine DR (1989) Plasticity of frequency organization in auditory cortex of guinea pigs with partial unilateral deafness. J Comp Neurol 282:456–471.

Rock C, Apicella AJ (2015) Callosal Projections Drive Neuronal-Specific Responses in the Mouse Auditory Cortex. J Neurosci 35:6703–6713.

Rouiller EM, Welker E (1991) Morphology of corticothalamic terminals arising from the auditory cortex of the rat: A Phaseolus vulgaris-leucoagglutinin (PHA-L) tracing study. Hear Res 56:179–190.

Rüttiger L, Ciuffani J, Zenner H-P, Knipper M (2003) A behavioral paradigm to judge acute sodium salicylate-induced sound experience in rats: a new approach for an animal model on tinnitus. Hear Res 180:39–50.

Rüttiger L, Singer W, Panford-Walsh R, Matsumoto M, Lee SC, Zuccotti A, Zimmermann U, Jaumann M, Rohbock K, Xiong H, Knipper M (2013) The reduced cochlear output and the failure to adapt the central auditory response causes tinnitus in noise exposed rats. PLoS One 8:e57247.

Ryan A, Dallos P (1975) Effect of absence of cochlear outer hair cells on behavioural auditory threshold. Nature 253:44–46.

Ryan A, Dallos P, McGee T (1979) Psychophysical tuning curves and auditory thresholds after hair cell damage in the chinchilla. J Acoust Soc Am 66:370–378.

Rybalko N, Syka J (2005) Effect of noise exposure on gap detection in rats. Hear Res 200:63–72.

Salloum RH, Yurosko C, Santiago L, Sandridge SA, Kaltenbach JA (2014) Induction of Enhanced Acoustic Startle Response by Noise Exposure : Dependence on Exposure Conditions and Testing Parameters and Possible Relevance to Hyperacusis. PLoS One 9:1–11.

Salthouse TA, Hedden T (2002) Interpreting reaction time measures in between-group comparisons. J Clin Exp Neuropsychol 24:858–872.

Saltzman IJ, Garner WR (1948) Reaction time as a measure of span of attention. J Psychol 25:227–241.

Salvi RJ, Arehole S (1985) Gap detection in chinchillas with temporary high-frequency hearing loss. J Acoust Soc Am 77:1173–1177.

Salvi RJ, Wang J, Ding D (2000) Auditory plasticity and hyperactivity following cochlear damage. Hear Res 147:261–274.

Samelli AG, Schochat E (2008) The gaps-in-noise test: gap detection thresholds in normal-hearing young adults. Int J Audiol 47:238–245.

Sametsky E a., Turner JG, Larsen D, Ling L, Caspary DM (2015) Enhanced GABAA-Mediated Tonic Inhibition in Auditory Thalamus of Rats with Behavioral Evidence of Tinnitus. J Neurosci 35:9369–9380.

Sampaio-Baptista C, Filippini N, Stagg CJ, Near J, Scholz J, Johansen-Berg H (2015) Changes in functional connectivity and GABA levels with long-term motor learning. Neuroimage 106:15–20.

Sanchez-Zuriaga D, Marti-Gutierrez N, Angeles Perez De La Cruz M, Rosa Peris-Sanchis M (2007) Age-Related Changes of NADPH-Diaphorase-Positive Neurons in the Rat Inferior Colliculus and Auditory Cortex. Microsc Res Tech 1059:1051–1059.

Sander JD, Joung JK (2014) CRISPR-Cas systems for editing, regulating and targeting genomes. Nat Biotechnol 32:347–355.

Sarkar A, Dowker A, Kadosh RC (2014) Cognitive Enhancement or Cognitive Cost : Trait-Specific Outcomes of Brain Stimulation in the Case of Mathematics Anxiety. J Neurosci 34:16605–16610.

Schaette R, McAlpine D (2011) Tinnitus with a normal audiogram: physiological evidence for hidden hearing loss and computational model. J Neurosci 31:13452–13457.

Schmid LM, Rosa MG, Calford MB, Ambler JS (1996) Visuotopic reorganization in the primary visual cortex of adult cats following monocular and binocular retinal lesions. Cereb Cortex 6:388–405.

Schmiedt R a, Mills JH, Boettcher F a (1996) Age-related loss of activity of auditory-nerve fibers. J Neurophysiol 76:2799–2803.

Schmiedt RA (2010) The Aging Auditory System (Gordon-Salant S, Frisina RD, Popper AN, Fay RR, eds). New York, NY: Springer New York.

Schneider BA, Hamstra SJ (1999) Gap detection thresholds as a function of tonal duration for younger and older listeners. J Acoust Soc Am 106:371–380.

Schneider BA, Pichora-Fuller MK, Kowalchuk D, Lamb M (1994) Gap detection and the precedence effect in young and old adults. J Acoust Soc Am 95:980–991.

Schneider DM, Nelson A, Mooney R (2014) A synaptic and circuit basis for corollary discharge in the auditory cortex. Nature 513:189–194.

Schnupp JWH, Nelken I, King AJ (2011) Auditory Neuroscience - Making Sense of Sound. MIT Press.

Schreiber BE, Agrup C, Haskard DO, Luxon LM (2010) Sudden sensorineural hearing loss. Lancet 375:1203–1211.

Schubert V, Lebrecht D, Holtmaat A (2013) Peripheral Deafferentation-Driven Functional Somatosensory Map Shifts Are Associated with Local, Not Large-Scale Dendritic Structural Plasticity. J Neurosci 33:9474–9487.

Schuknecht HF (1964) FURTHER OBSERVATIONS ON THE PATHOLOGY OF PRESBYCUSIS. Arch Otolaryngol 80:369–382.

Schuknecht HF, Gacek MR (1993) Cochlear pathology in presbycusis. Ann Otol Rhinol Laryngol 102:1–16.

Schuknecht HF, Woellner RC (1953) Hearing losses following partial section of the cochlear nerve. Laryngoscope 63:441–465.

Schuknecht HF, Woellner RC (1955) An experimental and clinical study of deafness from lesions of the cochlear nerve. J Laryngol Otol 69:75–97.

Schwaber MK, Garraghty PE, Kaas JH (1993) Neuroplasticity of the adult primate auditory cortex following cochlear hearing loss. Am J Otol 14:252–258.

Sederholm F, Swedberg MDB (2013) Establishment of auditory discrimination and detection of tinnitus induced by salicylic acid and intense tone exposure in the rat. Brain Res 1510:48–62.

Sedley W, Gander PE, Kumar S, Oya H, Kovach CK, Nourski KV, Kawasaki H, Howard MA, Griffiths TD (2015a) Intracranial Mapping of a Cortical Tinnitus System using Residual Inhibition. Curr Biol:1–7.

Sedley W, Parikh J, Edden RAE, Tait V, Blamire A, Griffiths TD (2015b) Human Auditory Cortex Neurochemistry Reflects the Presence and Severity of Tinnitus. J Neurosci 35:14822–14828.

Seki S, Eggermont JJ (2002) Changes in cat primary auditory cortex after minor-to-moderate pure-tone induced hearing loss. Hear Res 173:172–186.

Seki S, Eggermont JJ (2003) Changes in spontaneous firing rate and neural synchrony in cat primary auditory cortex after localized tone-induced hearing loss. Hear Res 180:28–38.

Selters WA, Brackmann DE (1977) Acoustic tumor detection with brain stem electric response audiometry. Arch Otolaryngol 103:181–187.

Sergeyenko Y, Lall K, Liberman MC, Kujawa SG (2013) Age-related cochlear synaptopathy: an early-onset contributor to auditory functional decline. J Neurosci 33:13686–13694.

Shailer MJ, Moore BC (1983) Gap detection as a function of frequency, bandwidth, and level. J Acoust Soc Am 74:467–473.

Shailer MJ, Moore BC (1985) Detection of temporal gaps in bandlimited noise: effects of variations in bandwidth and signal-to-masker ratio. J Acoust Soc Am 77:635–639.

Shailer MJ, Moore BC (1987) Gap detection and the auditory filter: phase effects using sinusoidal stimuli. J Acoust Soc Am 81:1110–1117.

Shepherd JD, Rumbaugh G, Wu J, Chowdhury S, Plath N, Kuhl D, Huganir RL, Worley PF (2006) Arc/Arg3.1 mediates homeostatic synaptic scaling of AMPA receptors. Neuron 52:475–484.

Shimano T, Fyk-Kolodziej B, Mirza N, Asako M, Tomoda K, Bledsoe S, Pan ZH, Molitor S, Holt a. G (2013) Assessment of the AAV-mediated expression of channelrhodopsin-2 and halorhodopsin in brainstem neurons mediating auditory signaling. Brain Res 1511:138–152.

Shore SE, Koehler S, Oldakowski M, Hughes LF, Syed S (2008) Dorsal cochlear nucleus responses to somatosensory stimulation are enhanced after noise-induced hearing loss. Eur J Neurosci 27:155–168.

Shore SE, Zhou J (2006) Somatosensory influence on the cochlear nucleus and beyond. Hear Res 217:90–99.

Siegle JH, Wilson MA (2014) Enhancement of encoding and retrieval functions through theta phase-specific manipulation of hippocampus. Elife 3:1–18.

Singer W, Zuccotti A, Jaumann M, Lee SC, Panford-Walsh R, Xiong H, Zimmermann

U, Franz C, Geisler H-S, Köpschall I, Rohbock K, Varakina K, Verpoorten S, Reinbothe T, Schimmang T, Rüttiger L, Knipper M (2013) Noise-induced inner hair cell ribbon loss disturbs central arc mobilization: a novel molecular paradigm for understanding tinnitus. Mol Neurobiol 47:261–279.

Sinnott JM, Adams FS (1987) Differences in human and monkey sensitivity to acoustic cues underlying voicing contrasts. J Acoust Soc Am 82:1539–1547.

Skottun BC, Shackleton TM, Arnott RH, Palmer a R (2001) The ability of inferior colliculus neurons to signal differences in interaural delay. Proc Natl Acad Sci U S A 98:14050–14054.

Smit JV, Janssen MLF, Schulze H, Jahanshahi a., Van Overbeeke JJ, Temel Y, Stokroos RJ (2015) Deep brain stimulation in tinnitus: Current and future perspectives. Brain Res 1608:51–65.

Snell KB, Frisina DR (2000) Relationships among age-related differences in gap detection and word recognition. J Acoust Soc Am 107:1615–1626.

Snell KB, Hu HL (1999) The effect of temporal placement on gap detectability. J Acoust Soc Am 106:3571–3577.

Snell KB, Ison JR, Frisina DR (1994) The effects of signal frequency and absolute bandwidth on gap detection in noise. J Acoust Soc Am 96:1458–1464.

Snyder RL, Bonham BH, Sinex DG (2008) Acute changes in frequency responses of inferior colliculus central nucleus (ICC) neurons following progressively enlarged restricted spiral ganglion lesions. Hear Res 246:59–78.

Snyder RL, Sinex DG (2002) Immediate changes in tuning of inferior colliculus neurons following acute lesions of cat spiral ganglion. J Neurophysiol 87:434–452.

Snyder RL, Sinex DG, McGee JD, Walsh EW (2000) Acute spiral ganglion lesions change the tuning and tonotopic organization of cat inferior colliculus neurons. Hear Res 147:200–220.

Spongr VP, Boettcher F a, Saunders SS, Salvi RJ (1992) Effects of noise and salicylate on hair cell loss in the chinchilla cochlea. Arch Otolaryngol Head Neck Surg 118:157–164.

Stagg CJ (2014) Magnetic Resonance Spectroscopy as a tool to study the role of GABA in motor-cortical plasticity. Neuroimage 86:19–27.

Stamataki S, Francis HW, Lehar M, May BJ, Ryugo DK (2006) Synaptic alterations at inner hair cells precede spiral ganglion cell loss in aging C57BL/6J mice. Hear Res 221:104–118.

Stark E, Koos T, Buzsáki G (2012) Diode probes for spatiotemporal optical control of multiple neurons in freely moving animals. J Neurophysiol 108:349–363.

Stolzberg D, Hayes SH, Kashanian N, Radziwon K, Salvi RJ, Allman BL (2013) A novel behavioral assay for the assessment of acute tinnitus in rats optimized for simultaneous recording of oscillatory neural activity. J Neurosci Methods 219:224–232.

Stringer C, Pachitariu XM, Hildebrandt KJ, Bartho P, Harris KD, Linden JF, Latham PE, Lesica NA, Sahani M (2015) Changes in inhibition explain variability in cortical activity and its role in sensory representations. In: Society for Neuroscience Abstracts.

Sumner CJ, Palmer AR (2012) Auditory nerve fibre responses in the ferret. Eur J Neurosci 36:2428–2439.

Suneja SK, Benson CG, Potashner SJ (1998a) Glycine receptors in adult guinea pig brain stem auditory nuclei: regulation after unilateral cochlear ablation. Exp Neurol 154:473–488.

Suneja SK, Potashner SJ, Benson CG (1998b) Plastic changes in glycine and GABA release and uptake in adult brain stem auditory nuclei after unilateral middle ear ossicle removal and cochlear ablation. Exp Neurol 151:273–288.

Suta D, Rybalko N, Pelánová J, Popelář J, Syka J (2011) Age-related changes in auditory temporal processing in the rat. Exp Gerontol 46:739–746.

Sutter ML, Schreiner CE (1991) Physiology and topography of neurons with multipeaked tuning curves in cat primary auditory cortex. J Neurophysiol 65:1207–1226.

Syka J (2002) Plastic changes in the central auditory system after hearing loss, restoration of function, and during learning. Physiol Rev 82:601–636.

Syka J, Rybalko N, Mazelová J, Druga R (2002) Gap detection threshold in the rat before and after auditory cortex ablation. Hear Res 172:151–159.

Szymanski FD, Rabinowitz NC, Magri C, Panzeri S, Schnupp JWH (2011) The Laminar and Temporal Structure of Stimulus Information in the Phase of Field Potentials of Auditory Cortex. J Neurosci 31:15787–15801.

Taberner AM, Liberman MC (2005) Response properties of single auditory nerve fibers in the mouse. J Neurophysiol 93:557–569.

Takahashi H, Yokota R, Funamizu A, Kose H, Kanzaki R (2011) Learning-stage-dependent, field-specific, map plasticity in the rat auditory cortex during appetitive operant conditioning. Neuroscience 199:243–258.

Tan J, Rüttiger L, Panford-Walsh R, Singer W, Schulze H, Kilian SB, Hadjab S, Zimmermann U, Köpschall I, Rohbock K, Knipper M (2007) Tinnitus behavior and hearing function correlate with the reciprocal expression patterns of BDNF and Arg3.1/arc in auditory neurons following acoustic trauma. Neuroscience 145:715–726.

Threlkeld SW, Penley SC, Rosen GD, Fitch RH (2008) Detection of silent gaps in white noise following cortical deactivation in rats. Neuroreport 19:893–898.

Tolnai S, Litovsky RY, King AJ (2014) The precedence effect and its buildup and breakdown in ferrets and humans. J Acoust Soc Am 135:1406–1418.

Tomita M, Noreña AJ, Eggermont JJ (2004) Effects of an acute acoustic trauma on the representation of a voice onset time continuum in cat primary auditory cortex. Hear Res 193:39–50.

Tsai HC, Zhang F, Adamantidis A, Stuber GD, Bonci A, de Lecea L, Deisseroth K (2009) Phasic firing in dopaminergic neurons is sufficient for behavioral conditioning. Science 324:1080–1084.

Tsuji J, Liberman MC (1997) Intracellular Labeling of Auditory Nerve Fibers in Guinea Pig : Central and Peripheral Projections. J Comp Neurol 202:188–202.

Turner JG, Brozoski TJ, Bauer C a, Parrish JL, Myers K, Hughes LF, Caspary DM (2006) Gap detection deficits in rats with tinnitus: a potential novel screening tool. Behav Neurosci 120:188–195.

Turner JG, Larsen D, Hughes L, Moechars D, Shore S (2012) Time course of tinnitus development following noise exposure in mice. J Neurosci Res 90:1480–1488.

Tzounopoulos T, Kim Y, Oertel D, Trussell LO (2004) Cell-specific, spike timing-dependent plasticities in the dorsal cochlear nucleus. Nat Neurosci 7:719–725.

Unger JW, Lange W (1992) NADPH-diaphorase-positive cell populations in the human amygdala and temporal cortex: neuroanatomy, peptidergic characteristics and aspects of aging and Alzheimer ' s disease. Acta Neuropathol 83:636–646.

van der Loo E, Gais S, Congedo M, Vanneste S, Plazier M, Menovsky T, Van de Heyning P, De Ridder D (2009) Tinnitus intensity dependent gamma oscillations of the contralateral auditory cortex. PLoS One 4:e7396.

Viana LM, O'Malley JT, Burgess BJ, Jones DD, Oliveira C a. CP, Santos F, Merchant SN, Liberman LD, Liberman MC (2015) Cochlear neuropathy in human presbycusis: Confocal analysis of hidden hearing loss in post-mortem tissue. Hear Res 327:78–88.

Viemeister NF (2014) Temporal Processing: Observations on the Psychophysics and

Modeling of Temporal Integration and Temporal Resolution. In: Perspectives on Auditory Research (Popper AN, Fay RR, eds), pp 601–610. Springer New York.

Vogler DP, Robertson D, Mulders WH a M (2011) Hyperactivity in the ventral cochlear nucleus after cochlear trauma. J Neurosci 31:6639–6645.

Vogler DP, Robertson D, Mulders WH a M (2014) Hyperactivity following unilateral hearing loss in characterised cells in the inferior colliculus. Neuroscience 265:28–36.

Wada SI, Starr A (1983) Generation of auditory brain stem responses (ABRs). III. Effects of lesions of the superior olive, lateral lemniscus and inferior colliculus on the ABR in guinea pig. Electroencephalogr Clin Neurophysiol 56:352–366.

Wagner E, Klump GM, Hamann I (2003) Gap detection in Mongolian gerbils (Meriones unguiculatus). Hear Res 176:11–16.

Walker KMM, Bizley JK, King AJ, Schnupp JWH (2011) Multiplexed and robust representations of sound features in auditory cortex. J Neurosci 31:14565–14576.

Walker KMM, Schnupp JWH, Hart-Schnupp SMB, King AJ, Bizley JK (2009) Pitch discrimination by ferrets for simple and complex sounds. J Acoust Soc Am 126:1321–1335.

Wallace MN, Harper MS (1997) Callosal connections of the ferret primary auditory cortex. Exp brain Res 116:367–374.

Wallace MN, Roeda D, Harper MS (1997) Deoxyglucose uptake in the ferret auditory cortex. Exp brain Res 117:488–500.

Wallhäusser-Franke E, Mahlke C, Oliva R, Braun S, Wenz G, Langner G (2003) Expression of c-fos in auditory and non-auditory brain regions of the gerbil after manipulations that induce tinnitus. Exp Brain Res 153:649–654.

Walton JP (2010) Timing is everything: temporal processing deficits in the aged auditory brainstem. Hear Res 264:63–69.

Walton JP, Frisina RD, O'Neill WE (1998) Age-related alteration in processing of temporal sound features in the auditory midbrain of the CBA mouse. J Neurosci 18:2764–2776.

Walton JP, Simon H, Frisina RD (2002) Age-related alterations in the neural coding of envelope periodicities. J Neurophysiol 88:565–578.

Wan I, Pokora O, Chiu T, Lansky P, Poon PW (2015) Altered intensity coding in the salicylate-overdose animal model of tinnitus. Biosystems.

Wang H, Brozoski TJ, Turner JG, Ling L, Parrish JL, Hughes LF, Caspary DM (2009) Plasticity at glycinergic synapses in dorsal cochlear nucleus of rats with behavioral

evidence of tinnitus. Neuroscience 164:747–759.

Wang J, Powers NL, Hofstetter P, Trautwein P, Ding D, Salvi R (1997) Effects of selective inner hair cell loss on auditory nerve fiber threshold, tuning and spontaneous and driven discharge rate. Hear Res 107:67–82.

Wang X, Lu T, Bendor D, Bartlett E (2008) Neural coding of temporal information in auditory thalamus and cortex. Neuroscience 157:484–493.

Wayne R V, Johnsrude IS (2015) A review of causal mechanisms underlying the link between age-related hearing loss and cognitive decline. Ageing Res Rev 23:154–166.

Weible AP, Liu C, Niell CM, Wehr M (2014a) Auditory cortex is required for fear potentiation of gap detection. J Neurosci 34:15437–15445.

Weible AP, Moore AK, Liu C, DeBlander L, Wu H, Kentros C, Wehr M (2014b) Perceptual gap detection is mediated by gap termination responses in auditory cortex. Curr Biol 24:1447–1455.

Weisz N, Müller S, Schlee W, Dohrmann K, Hartmann T, Elbert T (2007) The neural code of auditory phantom perception. J Neurosci 27:1479–1484.

White J a, Burgess BJ, Hall RD, Nadol JB (2000) Pattern of degeneration of the spiral ganglion cell and its processes in the C57BL/6J mouse. Hear Res 141:12–18.

Willott JF, Parham K, Hunter KP (1988) Response properties of inferior colliculus neurons in young and very old CBA/J mice. Hear Res 37:1–14.

Xiong Q, Znamenskiy P, Zador AM (2015) Selective corticostriatal plasticity during acquisition of an auditory discrimination task. Nature.

Yang G, Lobarinas E, Zhang L, Turner JG, Stolzberg D, Salvi R, Sun W (2007) Salicylate induced tinnitus: behavioral measures and neural activity in auditory cortex of awake rats. Hear Res 226:244–253.

Yang G, Pan F, Gan W (2009) Stably maintained dendritic spines are associated with lifelong memories. Nature 462:920–924.

Yang S, Su W, Bao S (2012) Long-term, but not transient, threshold shifts alter the morphology and increase the excitability of cortical pyramidal neurons. J Neurophysiol 108:1567–1574.

Yang S, Weiner BD, Zhang LS, Cho S-J, Bao S (2011) Homeostatic plasticity drives tinnitus perception in an animal model. Proc Natl Acad Sci U S A 108:14974–14979.

Yeomans JS, Frankland PW (1995) The acoustic startle reflex: neurons and connections. Brain Res Brain Res Rev 21:301–314.

Yin P, Fritz JB, Shamma S a (2010) Do ferrets perceive relative pitch? J Acoust Soc Am 127:1673–1680.

Yin S-K, Feng Y-M, Chen Z-N, Wang J (2008) The effect of noise-induced sloping high-frequency hearing loss on the gap-response in the inferior colliculus and auditory cortex of guinea pigs. Hear Res 239:126–140.

Ying S, Futter M, Rosenblum K, Webber MJ, Hunt SP, Bliss TVP, Bramham CR (2002) Brain-derived neurotrophic factor induces long-term potentiation in intact adult hippocampus: requirement for ERK activation coupled to CREB and upregulation of Arc synthesis. J Neurosci 22:1532–1540.

Yizhar O, Fenno LE, Davidson TJ, Mogri M, Deisseroth K (2011) Optogenetics in neural systems. Neuron 71:9–34.

Young ED, Nelken I, Conley RA (1995) Somatosensory Effects on Neurons in Dorsal Cochlear Nucleus. J Neurophysiol 73:764–765.

Zacharek MA, Kaltenbach JA, Mathog TA, Zhang J (2002) Effects of cochlear ablation on noise induced hyperactivity in the hamster dorsal cochlear nucleus: implications for the origin of noise induced tinnitus. Hear Res 172:137–143.

Zemelman B V, Lee GA, Ng M, Miesenbo G (2002) Selective Photostimulation of Genetically ChARGed Neurons. Neuron 33:15–22.

Zemelman B V, Nesnas N, Lee GA, Miesenbock G (2003) Photochemical gating of heterologous ion channels: Remote control over genetically designated populations of neurons. Proc Natl Acad Sci 100:1352–1357.

Zeng C, Nannapaneni N, Zhou J, Hughes LF, Shore S (2009) Cochlear damage changes the distribution of vesicular glutamate transporters associated with auditory and nonauditory inputs to the cochlear nucleus. J Neurosci 29:4210–4217.

Zeng C, Yang Z, Shreve L, Bledsoe S, Shore S (2012) Somatosensory projections to cochlear nucleus are upregulated after unilateral deafness. J Neurosci 32:15791–15801.

Zeng F-G (2013) An active loudness model suggesting tinnitus as increased central noise and hyperacusis as increased nonlinear gain. Hear Res 295:172–179.

Zhang F, Wang L-P, Brauner M, Liewald JF, Kay K, Watzke N, Wood PG, Bamberg E, Nagel G, Gottschalk A, Deisseroth K (2007) Multimodal fast optical interrogation of neural circuitry. Nature 446:633–639.

Zhang JS, Kaltenbach JA, Godfrey DA, Wang J (2006) Origin of hyperactivity in the hamster dorsal cochlear nucleus following intense sound exposure. J Neurosci Res 84:819–831.

Zhou J, Nannapaneni N, Shore S (2007) Vessicular glutamate transporters 1 and 2 are differentially associated with auditory nerve and spinal trigeminal inputs to the cochlear nucleus. J Comp Neurol 500:777–787.

Znamenskiy P, Zador AM (2013) Corticostriatal neurons in auditory cortex drive decisions during auditory discrimination. Nature 497:482–485.

Zobay O, Palmer AR, Hall D a., Sereda M, Adjamian P (2015) Source Space Estimation of Oscillatory Power and Brain Connectivity in Tinnitus. PLoS One 10:e0120123.